

Progressive Collapse of Reinforced Concrete Flat Slab Structures

Justin Russell, MEng (Hons)

Thesis submitted to The University of Nottingham
for the degree of Doctor of Philosophy

July 2015

Abstract

In 1968 a relatively small gas explosion on the 18th floor of the Ronan Point tower building resulted in the partial collapse of the structure. This event highlighted that progressive collapse may occur to structures under an accidental loading event. Other events, including the bombing of the Murrah federal building in 1993 in Oklahoma, have resulted in the common design requirement that a structure be capable of surviving the removal of a load bearing element. This approach, often referred to as the sudden column loss scenario, effectively ignores the cause of the damage and focuses on the structure's response afterwards. The refinement of the analysis varies, with options to include the nonlinear and dynamic behaviours associated with extreme events, or to use simplified linear and static models with factors included to account for the full behaviour.

Previous research into progressive collapse has highlighted that providing ductility in the connections, and avoiding brittle failures, is important in ensuring the structure maintains integrity after a column loss event. However, the majority of this work has been focused on the behaviour of steel and Reinforced Concrete (RC) frame structures. As flat slab construction is a popular method for many structures, due to the flexibility it offers for layouts and its low storey heights, it is an important to consider flat slab behaviour in more detail. Furthermore, slab elements behave differently to frame structures due to the Alternative Load Paths (ALPs) that can develop after a column loss via two-dimensional bending mechanisms. Additionally, punching shear failure is a known issue due to the thin section depths.

This work addresses the issue of the response of RC flat slab structures after a sudden column loss. As previous case studies have demonstrated that brittle failures may lead to progressive collapse of such structures, a complete understanding of the response is required. The nonlinear behaviour of a slab structure, due to both material and geometric factors, is investigated to determine the additional capacity available beyond the usual design limits. Additionally, the dynamic factors involved, primarily due to inertial effects, are also considered. To achieve this, experimental and numerical stud-

ies were conducted. A series of 1/3 scale models of slab substructures were constructed to replicate column loss events. Two types of tests were conducted, a static push down test with a support removed and a sudden dynamic column removal case. Displacements, strains and support reactions were recorded throughout, along with cracking patterns. For the dynamic tests a high speed camera was used to obtain the deflection response in the short time period after removal and to observe the formation of cracks. Comparisons between the two cases allowed determination of the dynamic effects on the response of the system. The experimental programme was then replicated using a Finite Element (FE) model. The results taken from the experimental case were used to validate the material and modelling assumptions made during the numerical simulations. This validated model was finally used to investigate a wider range of variables and assess the response of typical structural arrangements, with particular focus on the nonlinear and dynamic factors involved after a sudden column loss.

The experimental and numeral investigations demonstrated that after the loss of a column, flat slab structures can maintain integrity due to a change in the load paths away from the removal location. Although in some cases a large amount of flexural damage to the concrete and reinforcement occurred, such effects did not lead to complete failure. However, during the experimental programme some punching shear failures occurred, usually at the corner column locations. From the numerical analysis, shear forces of over twice the fully supported condition occurred as a result of removing a column, which may exceed the designed capacity. Comparisons between a static and dynamic analysis provides information into a suitable Dynamic Amplification Factor (DAF) for use with simplified modelling approaches. Based on the range of structures considered, the maximum increase in deflections as a result of a sudden removal was 1.62 times the static case, this is less than the commonly used factor of 2.0. Additionally, this factor reduces as the nonlinearity increases due to further damage, with a smallest DAF calculated at 1.39. This factor can be reduced further if the column is not removed instantaneously. Finally, the material strengthening effect, due to high strain rates, was considered with the conclusion that as such effects only make a limited increase in the capacity of the slab and may be conservatively ignored.

In conclusion, RC flat slab structures are capable of resisting progressive collapse after the loss of a column. This is primarily due to their ability to develop ALPs. However, while flexural damage is usually fairly minimal, progressive punching shear failure is a critical design condition as it may result in a complete collapse. Furthermore, the inertial effects involved after a sudden removal can increase the damage sustained, although current design methods may be over conservative.

Acknowledgements

I would firstly like to thank my supervisor, Dr. John Owen, for his guidance, support and insights as I have conducted this work. His instruction and example into how to conduct engineering research has shaped the priorities I have in carrying out my own work. I would also like to thank Dr. Iman Hajirasouliha for his supervision and the time he spent with me developing the focus of the work, especially for the early part of this project.

My thanks also go out to the civil engineering technical team, in particular Nigel Rook and Gary Davies, for their skill and helpfulness during the experimental programme of this work. Their pro-active approach to preparing the samples and equipment made the process run smoothly. I am also very grateful for the assistance they provided in regularly moving all the sand bags required for the experiment.

I would like to acknowledge the Early Career Research and Knowledge Transfer grant awarded by the University of Nottingham to Dr. Hajirasouliha that funded the experimental aspects of the project. Additionally, I am grateful for access to the University of Nottingham High Performance Computing Facility, on which the bulk of the simulations were run.

I am incredibly grateful for all the support I am received from my friends and family during this period. In particular, to my parents for their interest in this project even if they haven't fully understood what I've been doing. Finally, I would like to express the greatest thanks to my wife, Michelle, whose encouragements have spurred me on and who also undertook the task of proofreading this document.

Contents

Abstract	i
Acknowledgements	ii
Contents	iv
List of Figures	ix
List of Tables	xvii
1 Introduction	1
1.1 Background	1
1.2 Problem statement	1
1.3 Aim and objectives	2
1.3.1 Hypothesis	2
1.3.2 Aim	2
1.3.3 Objectives	2
1.4 Methodology	3
1.5 Scope and structure	4
2 Background and Literature Review	6
2.1 Definition of key terms	6
2.2 Historical case studies	7
2.2.1 Ronan Point	8
2.2.2 Oklahoma City bombing	8

CONTENTS

2.2.3	Sampoong Department Store	10
2.2.4	Pipers Row Car Park	10
2.2.5	World Trade Center Attack	10
2.2.6	Other collapses due to punching shear	12
2.3	Progressive collapse design requirements	12
2.3.1	Design approaches	12
2.3.2	European and British standards	14
2.3.3	United States standards	16
2.4	Previous research into progressive collapse	16
2.4.1	Design considerations	17
2.4.2	Column loss idealisation	18
2.4.3	Structural consideration of progressive collapse	19
2.4.4	Tests on real structures	25
2.4.5	Dynamic effects	26
2.5	Previous research into concrete slabs	28
2.5.1	Failure modes	28
2.5.2	Geometric nonlinearity	30
2.6	Summary	33
3	Experimental Testing	34
3.1	Introduction to experimental work	34
3.1.1	Aim and objectives	34
3.1.2	Methodology	35
3.2	Description of experimental programme	36
3.2.1	Design of experiment	36
3.2.2	Variables considered	37
3.2.3	Experimental set up	38
3.2.4	Instrumentation	40
3.3	Results	43
3.3.1	Corner column loss	48

3.3.2	Penultimate column loss	58
3.3.3	Continuous slab	73
3.4	Discussion of experimental results	79
3.4.1	Force redistribution	79
3.4.2	Flexural damage	81
3.4.3	Shear cracking	81
3.4.4	Whole slab behaviour	82
3.4.5	Dynamic effects	83
3.5	Summary	84
4	Finite Element Model of Floor Slab	86
4.1	Introduction to the finite element model	86
4.1.1	Justification of the use of the finite element method	86
4.2	Requirements and description for model	87
4.2.1	Numerical solver	87
4.2.2	Geometry of the model	89
4.2.3	Modelling of the concrete slab	89
4.2.4	Modelling of the steel reinforcement	90
4.2.5	Modelling the support conditions	90
4.2.6	Modelling the load	91
4.2.7	Modelling the nonlinear effects	93
4.3	Material models	94
4.3.1	Nonlinear material model for concrete	94
4.3.2	Nonlinear material model for steel	101
4.4	Model checks	102
4.4.1	Mesh sensitivity	102
4.4.2	Quasi-static loading	103
4.4.3	Artificial strain energy in the concrete elements	106
4.4.4	Over-closures on the spherical bearings	108
4.5	Summary	110

5	Validation of the Finite Element Model	111
5.1	Introduction and overview	111
5.2	Validation of Finite Element model against experimental results	112
5.2.1	Force redistribution	113
5.2.2	Displacements from static tests	116
5.2.3	Displacements from dynamic tests	120
5.2.4	Flexural damage	125
5.2.5	Frequency analysis	133
5.3	Summary	135
6	Parameter Study on Different Floor Variables	138
6.1	Introduction to parameter study	138
6.2	Description of multi-bay floor model	139
6.2.1	Design of the model	139
6.2.2	Details of the FE model	142
6.3	Parameters varied for the study	144
6.3.1	Span to depth ratio	144
6.3.2	Concrete strength	145
6.3.3	Removal location	146
6.3.4	Removal time	146
6.3.5	Dynamic Increase Factor for concrete	146
6.4	Outputs monitored during analysis	147
6.4.1	Displacement values	147
6.4.2	Reaction forces	147
6.4.3	Steel strain rates	148
6.4.4	Tensile damage to the concrete	148
6.4.5	Fundamental frequencies	149
6.5	Numerical results and discussion	149
6.5.1	Static results	149
6.5.2	Dynamic results	172

CONTENTS

6.5.3	Static to dynamic comparison	183
6.5.4	Influence of strain rate effects	189
6.6	Summary	194
7	Conclusions and Further Work	197
7.1	Overview of the thesis	197
7.2	Conclusions	200
7.3	Further Work	201
	References	202
	Appendices	214
A	Experiment Design Calculations	214
A.1	Model slab details	214
A.2	Moment calculations	214
A.3	Reinforcement calculations	216
A.4	Shear checks	216
A.5	Scaling comparison	218

List of Figures

2.1	Ronan Point after a partial collapse caused by a gas explosion. Photograph from The Daily Telegraph, 1968	8
2.2	Murrah Federal Building in Oklahoma City after the bomb attack in 1995. Note the progression of damage vertically and horizontally. Photograph credit to Associated Press, Bill Waugh, 1995	9
2.3	Pipers Row car park after the progressive punching shear failures. Image from Health and Safety Executive funded report	11
2.4	Collapse of WTC tower 2 after the 9/11 terrorist attacks. Note the vertical failure progression due to the pancaking mechanism	12
2.5	Example of tying elements in a structure to improve redundancy. Reproduced from IStructE (2010).	14
2.6	Photographs of flat plate corner panels after overloading. Reproduced from Mitchell and Cook (1984)	20
2.7	Experimental test for axially restrained beams under a column loss scenario (Su et al., 2009)	21
2.8	Static push down test of an RC frame under a column loss scenario (Yi et al., 2008)	22
2.9	Experimental tests for column column removal (Qian and Li, 2012) . . .	23
2.10	Reproduction of Malvar and Ross (1998)'s review of strain rate tests . . .	27
2.11	Flat slab failing in punching shear with integrity reinforcement. Reproduced from Ruiz et al. (2013)	30
2.12	Saito et al. (1995)'s experimental impact tests on RC slabs	31
2.13	Testing and analysis of an RC slab (Foster et al., 2004)	32

LIST OF FIGURES

2.14	Compressive arching action in laterally restrained reinforced concrete slab (Zheng et al., 2008)	33
3.1	Details of test setup showing slab sizes, reinforcement layouts and support locations	39
3.2	Diagram showing the process of removing the temporary support for dynamic tests	40
3.3	a) Photograph of slab PC-D before dynamic testing, note the visual targets; b) Cameras for visual monitoring	43
3.4	Support reactions as sand/gravel bags are applied - Tests C-D (a) and C-S (b)	45
3.5	Images from the High Speed Camera (HSC) for test C-D, with 6.8kN/m^2 of loading, to estimate column removal time	46
3.6	Locations of Linear Variable Differential Transformers (LVDTs) and visual targets (D), strain gauges (S) and grid markings for tests C-S and C-D	48
3.7	Distribution of forces to supports - Test C-S	49
3.8	Mean change in distribution of forces to each support after corner column loss - Tests C-S and C-D	50
3.9	Annotated flexural cracks after corner column loss	52
3.10	Load against normalised displacements - Test C-S	53
3.11	Normalised strain against position for top reinforcement bars - Test C-S	54
3.12	Normalised displacement against time after column removal at different positions and loading - Test C-D	55
3.13	Power spectral density of displacement following corner column loss at different load levels - Test C-D	56
3.14	Short-Time Fourier Transform (STFT) for displacements at column removal location for 7.7kN/m^2 - Test C-D. Magenta and green lines show 3.54Hz and 4.21Hz respectively	57
3.15	Maximum strain rates against time. Also showing changes to peak strains. Test C-D	59
3.16	Final state of corner removal case after shear failure - Test C-D	60

LIST OF FIGURES

3.17	Locations of LVDTs and visual targets (D), strain gauges (S) and grid markings for penultimate removal conditions - Continuous (C) and Reduced (R)	60
3.18	Distribution of forces to supports - Tests PC-S and PR-S	61
3.19	Load against normalised displacement for PC-S and PR-S	62
3.20	Normalised strain against position for bottom reinforcement bars	64
3.21	Displacement against time for PC-D at 5.6kN/m^2	66
3.22	Power spectral density of displacement following corner column loss at different positions for 5.7kN/m^2 - Test PC-D	66
3.23	Failure of slab PR-D captured from the High Speed Camera - a) Flexural cracking; b) Shear crack	67
3.24	Displacement against time for PR-D, position D1 at 5.7kN/m^2	68
3.25	Maximum strain rates against time. Also showing changes to peak strains - Test PC-D	70
3.26	Maximum strain rates against time at 5.7kN/m^2 . Also showing changes to peak strains and the point that a shear crack forms - Test PR-D	70
3.27	Annotated bottom surface flexural cracks and reinforcement after penultimate column loss	71
3.28	Test M-D loaded before sudden column removal	72
3.29	Locations of LVDTs and visual targets (D) and grid markings for middle column removal condition - Test M-D	72
3.30	Distribution of forces to supports during static loading - Test M-D	74
3.31	Mean change in distribution of forces to each support after corner column loss - Test M-D	75
3.32	Displacements against time at the removal location (D1) for different loadings - Test M-D	76
3.33	Displacements against time at different positions and loading - Test M-D	77
3.34	Power density spectrums for displacement following corner column loss at different loadings - Test M-D	78
3.35	STFT for displacements at column removal location for 3.1kN/m^2 - Test M-D. Magenta and green lines show 13.4Hz and 16.4Hz respectively	78
3.36	Annotated underside cracking pattern for continuous slab - Test M-D	80

LIST OF FIGURES

4.1	Rendering of the spherical bearings and plate used as permanent supports for the slab	91
4.2	A schematic representation of the increase in total load and the removal of a support during dynamic tests	93
4.3	Yield surface in plane stress for the Concrete Damaged Plasticity (CDP) model. Reproduced from the Abaqus user manual (Simulia, 2010)	96
4.4	Uniaxial compressive model for concrete	97
4.5	Uniaxial tensile model for concrete	98
4.6	Compressive and tensile damage indices for concrete	99
4.7	Uniaxial stress-strain relationship for reinforcement steel for compression and tension	102
4.8	Effect of mesh refinement on Finite Element Analysis (FEA) predictions for test C-S. Experimental results are also shown with solid lines.	104
4.9	Ratio of kinetic and internal energies during quasi-static loading for corner removal tests	107
4.10	Diagram demonstrating the hour glassing issue leading to bending deformation without straining	108
4.11	Internal and artificial strain energy for concrete elements during test C-S	109
5.1	Distribution of forces to each support as loading increases - Test C-S. Solid line is numerical model, +’s the experimental results	114
5.2	Distribution of forces to each support as loading increases - Test PR-S. Solid line is numerical model, +’s the experimental results	114
5.3	Mean change in distribution of forces to each support after column loss. Comparing experimental tests C-S and C-D for the FE model.	115
5.4	Reaction forces against time after column loss for each support. Also showing the peak displacement against time - Test C-D	117
5.5	PSD of support reactions following corner column loss. Also showing PSD for the peak displacement - Test C-D	118
5.6	Percentage change in reaction forces to each support against time due to a dynamic column loss - Test M-D	119
5.7	Normalised displacement against load for test comparing experimental results to the FE - Test C-S	120

LIST OF FIGURES

5.8	Normalised displacement against load comparing experimental results to the FE - Test PR-S	121
5.9	Normalised displacement against time for test at different locations and loadings. Experimental results (solid lines) and FE (dashed lines) are shown - Test C-D	122
5.10	Displacements against time for different support removal times. Experimental results are shown as well - Test C-D	124
5.11	Displacements against time at different locations comparing comparing experimental results (solid lines) to the FE (dashed lines) - Test M-D . . .	126
5.12	Maximum strain rate in the steel against time from FE model. Also showing the peak displacement against time - Test M-D	127
5.13	Location of tensile plastic strain regions in the concrete elements at 5.4kN/m ² of loading for test C-S	129
5.14	Location of tensile plastic strain regions in the concrete elements at 7.8kN/m ² of loading for test C-S	130
5.15	Normalised strain against against position for the top steel. FE (dashed lines) and experiment results (solid lines) are shown for different loadings - Test C-S	131
5.16	Plastic deformation for the bottom steel in tests PC-S and PR-S at different loadings	132
5.17	Predicted mode shapes for test C-D	136
5.18	Predicted mode shapes for test M-D	137
6.1	Graphical rendering of the multi-bay floor model	139
6.2	Plan and elevation of floor slab for parameter study showing dimension labels, key column locations and grid markings	140
6.3	Example of the top flexural steel layout for the model with column positions marked	141
6.4	Normalised displacement after corner column removal	151
6.5	Displacement ductility factor, μ_δ , after corner column removal	152
6.6	Normalised displacement against static loading for different span to depth ratios. Internal column removal	154

LIST OF FIGURES

6.7	Normalised displacement at different locations against static loading. Corner column removed with different span to depth ratios	156
6.8	Normalised displacement at different locations against static loading for different column loss scenarios	157
6.9	Normalised displacement against static loading for different column loss scenarios	159
6.10	Normalised displacement against static loading for concrete strengths. Corner and internal column removal. $L_{eff}/t=19.4$	163
6.11	Location of tensile plastic strain regions in the concrete elements after corner column (A1) removal	164
6.12	Location of tensile plastic strain regions in the concrete elements after internal column (B2) removal	166
6.13	Location of tensile plastic strain regions in the concrete elements after penultimate column (A2) removal	167
6.14	Location of tensile plastic strain regions in the concrete elements after two column (A1/A2) removal	168
6.15	Change in column reaction forces due to static load increases for differ- ent span to depth ratios. Corner column removal	170
6.16	Change in column reaction forces due to static load increases. Corner column removal. $L_{eff}/t=19.4$	170
6.17	Change in column reaction forces due to static load increases. Internal column removal. $L_{eff}/t=19.4$	171
6.18	Change in column reaction forces due to static load increases. Penulti- mate column removal. $L_{eff}/t=19.4$	171
6.19	Change in column reaction forces due to static load increases. Two col- umn removal. $L_{eff}/t=19.4$	172
6.20	Normalised displacement against time for different span to depth ratios	174
6.21	Normalised displacement against time for different column loss scenar- ios. $L_{eff}/t = 19.4$	176
6.22	Normalised displacement against time for different removal times	177
6.23	Change in column reaction forces against time. Corner column removal. $L_{eff}/t=19.4$	178

LIST OF FIGURES

6.24	Change in column reaction forces against time. Internal column removal. $L_{eff}/t=19.4$	179
6.25	Change in column reaction forces against time. Penultimate column re- moval. $L_{eff}/t=19.4$	180
6.26	Change in column reaction forces against time. Two column removal. $L_{eff}/t=19.4$	181
6.27	Change in column reaction forces against time for different removal times. Corner column removal. $L_{eff}/t=19.4$	181
6.28	Change in column reaction forces against time for different removal times. Internal column removal. $L_{eff}/t=19.4$	182
6.29	Maximum increase in column reaction forces compared to the fully sup- ported condition. Corner column removal.	183
6.30	Maximum increase in column reaction forces compared to the fully sup- ported condition. Internal column removal.	184
6.31	Maximum increase in column reaction forces compared to the fully sup- ported condition. Penultimate column removal.	184
6.32	Maximum increase in column reaction forces compared to the fully sup- ported condition. Two column removal.	185
6.33	Maximum change in column reaction forces against time for different column loss scenarios. $L_{eff}/t=19.4$	185
6.34	DAF from displacement values for different span to depth ratios	186
6.35	DAF from reaction forces for different span to depth ratios	188
6.36	Reduction in DAF from displacement values due to column removal time	189
6.37	Maximum steel strain rate against time after corner column loss for dif- ferent models. Also showing peak displacements against time.	190
6.38	Maximum steel strain rate against time after corner column loss for dif- ferent concrete strengths for model with L_{eff}/t of 19.4	191
6.39	Maximum steel strain rate against time after corner column loss for model with L_{eff}/t of 15.4	192
6.40	Normalised displacement against time after corner column loss compar- ing effect of applying a Dynamic Increase Factor (DIF)	193
6.41	Maximum steel strain rate against time after an internal column loss for model	195

LIST OF FIGURES

A.1	Equivalent Bending Moment Diagram for Long direction under Ultimate Limit State (ULS) loading	215
A.2	Equivalent Bending Moment Diagram for Short direction under ULS loading	215
A.3	Summary and comparison of slab prototype and model design	219

List of Tables

2.1	Examples of different design approaches	15
3.1	Slab IDs for each test and corresponding variables	37
3.2	Summary of the loading levels conducted for dynamic removal tests . .	38
3.3	Concrete material properties from test samples	41
3.4	Reinforcement material properties from tensile tests	41
3.5	Estimated column removal times for each test	46
3.6	Summary of test results giving details of shear failures	47
3.7	Fraction of force to each support as total load increases - Test C-S	50
3.8	Results from dynamic removal - Test C-D	56
3.9	Comparison of stiffnesses after cracking - Test P-S	63
3.10	Results from dynamic removal - Test PC-D	67
3.11	Results from dynamic removal - Test M-D	76
4.1	Concrete Damage Plasticity inputs	96
4.2	Results from mesh sensitivity parameter study - Test C-S	105
4.3	Summary of adjustments made due to node over-closures between sur- faces	110
5.1	Summary of all FE models including the variables that were compared to the experimental results	112
5.2	Comparison of the frequencies from a modal analyses and the dominant frequency seen in the experimental and FE results - Test C-D	133
5.3	Comparison of the frequencies from a modal analyses and the dominant frequency seen in the experimental and FE results - Test M-D	133

LIST OF TABLES

6.1	Values for the varied dimensions in Figure 6.2	140
6.2	Values for the fixed dimensions in Figure 6.2	140
6.3	Span length and slab thickness for each model	145
6.4	Summary of static deflections - Corner removal	153
6.5	Summary of static deflections - Internal removal	153
6.6	Summary of static deflections - All column removal locations	160
6.7	Displacement ductility factor, μ_δ , at different loadings for all column re- moval locations	161
6.8	Summary of static deflections for different concrete strengths, $L_{eff}/t=19.4$	162
6.9	Summary of static reaction forces at remaining columns	173
6.10	Summary of dynamic displacements	175
6.11	Summary of dynamic values from the displacement response	175

Introduction

This chapter introduces the topic of this thesis and provides some justification for its relevancy. It then summarises the project aims and objectives. It also outlines the methodology used for investigating the issues raised, as well as the structure and scope for this project.

1.1 Background

Ever since the explosion at the Ronan Point tower building in 1968, due to a relatively small gas explosion, consideration has been given to understanding the mechanisms involved in its partial collapse. This led to common design recommendations that structures should maintain integrity even if an element is damaged or destroyed. Other catastrophic incidents have since occurred, including the bombing of a federal building in Oklahoma City in 1995, the collapse of the Sampson department store in South Korea, 1995, and the terrorist attacks on the World Trade Center in 2001, leading to their collapse. These events, where a local damaging event leads to further failures, are typically referred to as progressive collapses. Accurate consideration of these events is often difficult due nature of the damaging event, possibility involving explosions, sudden impacts, fire or natural hazards. Furthermore, such cases are likely to be beyond the structure's design conditions and so involve more complicated modelling and assessment techniques.

1.2 Problem statement

Catastrophic failures of structures, due to progressive failure, have occurred, therefore highlighting the need to design against such events. Extensive research has been

conducted into steel and RC frame structures, however, the response of flat slabs to accidental or malicious events is not fully understood. RC flat slab construction is a popular form around the world due to its design flexibility and low storey heights, therefore many structures may be at risk of progressive collapse. These structural forms have alternative load paths which can protect such structures after the loss of a key element, but the capacity of these can be difficult to assess due to the nonlinear material and geometric factors. Additionally, the sudden removal of a structural element is a dynamic event, and so such factors must be included to obtain accurate indication into the response.

1.3 Aim and objectives

1.3.1 Hypothesis

It is postulated that RC flat slab structures may undergo progressive failure after a sudden column loss, and that nonlinear and dynamic effects are important in assessing this potential.

1.3.2 Aim

The aim of this project is to investigate the behaviour of flat slab structures after a sudden column loss event. The extent of damage, and the influence of dynamic effects and nonlinear capacity will be examined to consider their roles in assessing the potential for progressive failures. Different structural configurations will also be investigated.

1.3.3 Objectives

To achieve the above aim the following objectives will be completed:

- Develop a numerical model to simulate a column loss event for an RC flat slab structure.
- Conduct a series of experimental tests on a scaled substructure of a flat slab, comparing static incremental loading, to a dynamic column removal case. Column loss location and reinforcement layout will also be considered.
- Validate the numerical model against the results from the experimental tests.

- Analyse a range of structural layouts and designs under a sudden column loss scenario considering different geometric, design and modelling variables.
- Use the results of the parametric study to identify key factors influencing the potential for progressive collapse.

1.4 Methodology

In general, two options are used for the study of the behaviour of structures during extreme loading conditions; computer simulations or experimental testing. Of these, the most common is to rely on numerical modelling based on the Finite Element Method (FEM). This has the advantage of being cheaper and quicker to conduct than experimental work, it can also consider a large range of parameters and conditions more effectively. However the results are highly dependant on the input variables, such as the material model used, and therefore a firm understanding of all the effects involved is needed to get reliable results. On the other hand, experimental testing can provide valuable results if conducted well. Two types of test are common and can be described by their size. There are large scale tests which consider the full behaviour of the entire structure, or localised testing which isolates a single section of the structure to investigate. Whilst full scale tests can provide results that completely replicate real events, they are expensive and often limited in the range of conditions that can be considered within one test programme. Alternatively, local element testing is cheaper and more efficient and so can give more flexibility for the range of issues that can be studied. However, issues such as the boundary conditions and loading arrangements need to be designed carefully to ensure they reflect realistic situations. Additionally, experimental results can complement analytical work by providing information on the material behaviour as well as validating the results from the numerical models.

For this a project a combination of both numerical modelling, using the FEM, and experimental testing will be conducted to fulfil the aim in Section 1.3.

Full scale testing is impractical for this project, and therefore simplified tests will be conducted to focus on the key issues. The most significant aspect is the dynamic behaviour of concrete slabs immediately after a column loss scenario. By limiting the test to a small section of the structure, it allows detailed consideration to be made efficiently of all the aspects of interest, such as material failure. The results can then be compared against numerical simulations and extended to cover all building arrangements.

The computer simulations also allow a large range of parameters to be considered in

detail. Comparisons can be made between different layouts, material properties, loading configurations and initiating events. By considering a broad range of situations, generalised rules can be formed to improve the resilience of all common flat slab structures. Furthermore, numerical analysis can provide detailed results for the behaviour of a large structure, at all locations, and at every time interval, during the analysis. While care needs to be taken in ensuring these results accurately reflect real behaviours, they can give an important insight into the damage experienced by the structure which would be impractical, or impossible, to obtain via other methods.

1.5 Scope and structure

This project is focused on investigating the response of flat slab structures after the common sudden column loss design scenario. To obtain realistic results, nonlinear material and geometric effects will be included, and their significance discussed. Similarly, the influence of dynamic effects shall be considered. Additionally, geometric and design variables will also be investigated to determine their influence on the response of a structure after a column loss. The sudden column loss event does not consider any particular initiating event, therefore the only effects considered on the structure shall be as a result of the loss, i.e. the effects of a blast, or other damaging events, to the surrounding elements are beyond the scope of this project. Only RC flat slab structures, with conventional steel reinforcement bars are investigated. Furthermore, as primarily the vertical loading and response are of interest, no consideration is given to lateral restraint options.

The issue of progressive collapse is described fully in Chapter 2 by providing relevant historical case studies. Key previous research, analysing the mechanisms and behaviour of structures undergoing such events, is also presented and summarised along with common design methodologies. A selection of research regarding the behaviour of slab elements is also discussed.

Chapter 3 presents the description, results and discussion from the experimental programme conducted on scaled slab elements simulating column loss. As mentioned in the project objectives in Section 1.3.3, these results are primarily used to validate a numerical model.

Chapter 4 introduces the details for the numerical model, describing the approach and the material and modelling parameters used. A preliminary check is also conducted to ensure the model is suitable.

Chapter 5 then validates this model by replicating the experimental programme and compares the two sets of results.

The validated numerical model is then used for a parameter study in Chapter 6, investigating the key variables that influence the response of a structure after a column loss event, and its potential for progressive failure or collapse.

The findings and main conclusions are finally presented in Chapter 7, along with a brief description of the next steps for research in this area.

Background and Literature Review

This chapter gives the details of a selection of key structural failures which have influenced the consideration for progressive collapse. A review of the design approaches, guidelines, and requirements, currently used around the world is presented. Finally an in-depth overview is given of the state of the art for progressive collapse testing and analysis, along with research into the behaviour of Reinforced Concrete (RC) slab elements and structures.

2.1 Definition of key terms

To avoid ambiguity, the following definitions will be used for the key terms.

Progressive failure:

A condition where the damage or failure of one element results in the failure of another.

Broadly this can be split into horizontal and vertical cases. The former may be caused by surrounding members becoming overloaded, after the loss of an element. Alternatively, vertical failures may occur if one element, possibly an entire floor, falls and lands on a lower element. The additional load, combined with the dynamic impact, causes that element to fail as well, and the failure propagates vertically leading to a pancaking effect. However, the failures may be arrested, and the damage remain localised, with only a few surrounding elements failing.

Progressive collapse:

A condition where the collapse commences with the failure of one or a few structural components and then progresses over successive other compo-

nents (Starossek, 2009).

Technically a subsection of the previous case, in this instance the progressive failure mechanism is not arrested and results in the collapse of the structure, or a significant part of it.

Disproportionate collapse:

An event where a comparatively minor event results in the collapse of a major part, or even the whole, of a structure.

Whilst often used interchangeably with progressive collapse, the term typically refers to the extent of damage with relation to the cause, while the previous definition describes the mechanism. The designers' challenge is to consider an acceptable level of damage for a particular initiating event.

Accidental design scenario:

A design situation involving exceptional conditions of the structure or its exposure, including fire, explosion, impact or local failure (EN 1990, 2002)

Such events have a low probability of occurring beyond what might be expected during usual design life.

Flat slab construction:

A form of structure in which a Reinforced Concrete (RC) slab is supported directly on columns, without the use of beams or girders. Column capitals or drop panels may be used.

Note that the term 'flat plate' used by some writers is considered interchangeable with flat slab throughout this document.

2.2 Historical case studies

As is common in engineering, the issue of progressive collapse of structures arose after the high-profile, and unexpected, failure of a number of buildings. This highlighted that catastrophic failure, due to a relatively minor action, could occur and present a risk to human life and economic investment. The key events that have shaped the work in this area are described below.



Figure 2.1: Ronan Point after a partial collapse caused by a gas explosion. Photograph from The Daily Telegraph, 1968

2.2.1 Ronan Point

Interest started in 1968 when a 22 storey precast apartment tower building known as Ronan Point in East London partly collapsed only 3 months into its service life. The collapse was shocking to the engineering community as it was initiated by a relatively small gas explosion on the 18th floor, which removed external structural panels. With this loss of robustness, the floors above collapsed resulting in the failure of lower floors, due to the impact loading of the debris. Figure 2.1 shows the result of this event. From this, concern arose about the possibility of small, or local, damage to a structural member leading to a large level of damage to the global structure, including total failure of all elements. This type of event became known as disproportionate collapse. This highlighted the importance of considering robustness in design (Pearson and Delatte, 2005; Bussell and Jones, 2010).

2.2.2 Oklahoma City bombing

The next major event occurred on April 19th, 1995, in Oklahoma City. Unlike Ronan Point, which was the result of an accidental gas explosion, this was a malicious and planned attack involving a large truck bomb placed outside the main entrance of the Murrah Federal Building. The explosives were estimated to be equivalent to 1,800 kg of TNT and located approximately 4m from an external column (Osteraas, 2006).



Figure 2.2: Murrah Federal Building in Oklahoma City after the bomb attack in 1995. Note the progression of damage vertically and horizontally. Photograph credit to Associated Press, Bill Waugh, 1995

The main structure included a 9 storey, traditionally reinforced concrete frame with shear walls around elevator cores to provide lateral stability. However, in order to achieve the required architectural form at ground level, the external columns were not continuous, but rather a transfer beam was placed at the 2nd floor, and only every other column continued to ground. The blast from the bomb destroyed one of these columns and damaged (potentially destroying) at least 2 others. Without these supports the transfer beam was now spanning far beyond its design limit, leading to its collapse. The failure of this element resulted in the failure of all the beams above it. The collapse then also progressed horizontally as the structure lost integrity, this continued until brittle failure occurred, due to discontinuous reinforcement detailing, arresting the progression. Figure 2.2 shows the extent of the damage.

In total approximately 42% of the floor area was destroyed killing 168 people. Similar to the Ronan Point disaster, a relatively small initiating event led to a disproportionately large failure which could have been prevented had the structure contained sufficient redundancy to carry its gravity loads whilst in a damaged state (Hayes et al., 2005).

Further investigations have been made by Byfield and Paramasivam (2012). They demonstrate that the size of the explosion would still have destroyed closer spaced

columns, and the use of a glazed façade and open plan spaces, reduced the structural redundancy and provided no alternative load paths. Thus they concluded that the structural flaw was not the use, or design, of the transfer beam.

2.2.3 Sampoong Department Store

The Sampoong Department Store in Seoul, South Korea, was a 5 storey RC structure that collapsed catastrophically on the 29th June, 1995, killing 502 people and injuring 937. The store was a flat slab construction and was only in its 5th year of service when the entire structure pancaked down. Inspections after the event identified that a number of factors contributed to the failure, primarily overloading of the upper floors due to changes in use, and reduction in column cross-sections. Additionally, poor construction quality was noted which reduced the capacity. These effects led to punching shear failure around the 5th floor columns that progressed throughout the level.

It should, however, also be noted that poor maintenance and management of the building meant that warning signs of structural distress were ignored prior to the collapse that could have prevented the disaster (Gardner et al., 2002; Park, 2012).

2.2.4 Pipers Row Car Park

In 1997 another incidence of progressive collapse, due to punching shear also occurred. In this case it was the Pipers Row car park in Wolverhampton, UK. During the night of the 20th March a shear failure around one column on the top floor led to a progressive failure of 7 adjacent columns and the collapse of a 120 tonne section, as can be seen in Figure 2.3. As the structure was not in use, its only loading was its own self weight. As no one was present at the time there were no deaths or injuries.

Prior to the collapse, investigations had revealed significant construction issues, and high levels of degradation of the concrete, with recommendation for remedial action to be taken. However, before this work could take place, corrosion of reinforcement led to a local failure which progressed through the floor. The failure was arrested by a lack of continuity in the slab's reinforcement which prevented the entire level collapsing and potentially triggering a collapse of every level (Wood, 2003; Whittle, 2013).

2.2.5 World Trade Center Attack

On September 11th, 2001, the world was shocked when two commercial aeroplanes were hijacked and crashed into the two World Trade Center (WTC) towers as shown in



Figure 2.3: Pipers Row car park after the progressive punching shear failures.
Image from Health and Safety Executive funded report

Figure 2.4. Each building was 110 storeys and built to withstand extreme conditions, including hurricane force winds, sabotage of external columns and collision from a medium size aircraft. As evidence of its structural robustness, a previous bomb explosion in 1993, whilst destroying multiple levels of basement, failed to put the building at risk (Ramabhushanam and Marjorie, 1994).

After the aircraft impact both towers stood for around an hour, however the explosion damage, combined with the long fires, weakened the steel beams, and then the columns, until they buckled. Once collapse had been initiated the dynamic impact of each floor led to progressive failure of all columns and the complete destruction of both towers (Bazant et al., 2008).

Whilst the result was catastrophic with over 2800 people killed, it may not be accurate to refer to this collapse as disproportionate due to the extreme nature of the attack.

The significance of this event, combined with the high death toll, has led to many researchers investigating the event. The mechanics behind the two main towers, along with buildings 5 and 7 which also collapsed, is now well understood and these structures are possibly the most studied in history (Newland and Cebon, 2002; Usmani et al., 2003; Corley, 2004; Karim and Fatt, 2005; Bazant and Verdure, 2007; Flint et al., 2007; LaMalva et al., 2009).



Figure 2.4: Collapse of WTC tower 2 after the 9/11 terrorist attacks. Note the vertical failure progression due to the pancaking mechanism

2.2.6 Other collapses due to punching shear

Punching shear is often the most critical failure condition for flat slab structures and can lead to a progressive collapse of the structure. This has been demonstrated with the collapse of 2000 Commonwealth Avenue, Massachusetts (1971), Skyline Plaza apartment building, Virginia (1973) and Harbour Clay condominium building, Florida (1981). In all these cases failure occurred during construction, and later investigations revealed significant failings in complying with design codes, along with a lack of project oversight and contractors not following the specified design. However, while these tragedies could have been prevented at the time, they all started with a local shear failure that resulted in extensive damage and this collapse mechanism is still a concern (Feld and Carper, 1997; King and Delatte, 2004; Schellhammer et al., 2013).

2.3 Progressive collapse design requirements

2.3.1 Design approaches

Methodologies for preventing accidental or unlikely considerations on a structure, which may potentially lead to unsatisfactory conditions (whether collapse, partial collapse or loss of serviceability), typically fall into two areas, direct and indirect design.

Direct design attempts to consider the potential hazards and ensure the structure is

suitably protected against the effects of them. This is most suitable where a realistic threat can be identified and quantified. Such examples include vehicle impacts, accidental or malicious explosions, or natural hazards such as flooding, high winds, avalanche, or earthquakes. However, in order to conduct a direct design against these actions a likely force, or force profile, is required as well as identification of which elements may be affected. Additionally, accurate impact or blast analysis requires experience and significant computational time making it unsuitable for anything other than structures that are at a high risk of attack or accidental explosions, for example government buildings or certain industrial structures.

Indirect design approaches simplify the early considerations by removing explicit actions and replacing them with a generic case that seeks to represent a large range of possible events. The most common of these is the sudden column loss scenario. In this a structural element, usually a column or wall section, is removed and the remaining structure assessed. Completely ignoring the initiating event and considering only its potential effect, i.e. the loss of a load bearing element, greatly reduces the computational effort required. However, the sudden and complete removal of an element represents the worst case scenario, and may predict higher total damage than a true case. Furthermore, real structures never experience a clean removal of a single element and no consideration is given to the surrounding features experiencing damage due to the hypothetical event.

For each of these approaches, two further design methods can be used; local resistance or Alternative Load Path (ALP). Local resistance methods seek to strengthen elements that are deemed to be critical so that they will not fail due to the initial action, and will continue to support the entire structure. This could be achieved by structural means, e.g. more reinforcement, stronger sections etc., or non-structural techniques, e.g. barriers to protect the area from vehicles. This method may end up being expensive if a large number of elements are oversized to protect against an unlikely event. Additionally, the structure may remain vulnerable to an event larger than originally designed, as no explicit consideration is given for the structural response if the element does fail.

Alternatively, the ALP method allows the original element to fail but aims to prevent further damage by utilising additional capacity from both the materials and the geometry. If a full analysis of the damaged structure is conducted, the potential for progressive failures can be determined, and therefore designed against, however this is time consuming. Assumptions can be made about the behaviour of a structure to simplify the analysis, and minimum reinforcement provisions or ductility requirements can ensure the structure maintains integrity and does not experience disproportionate

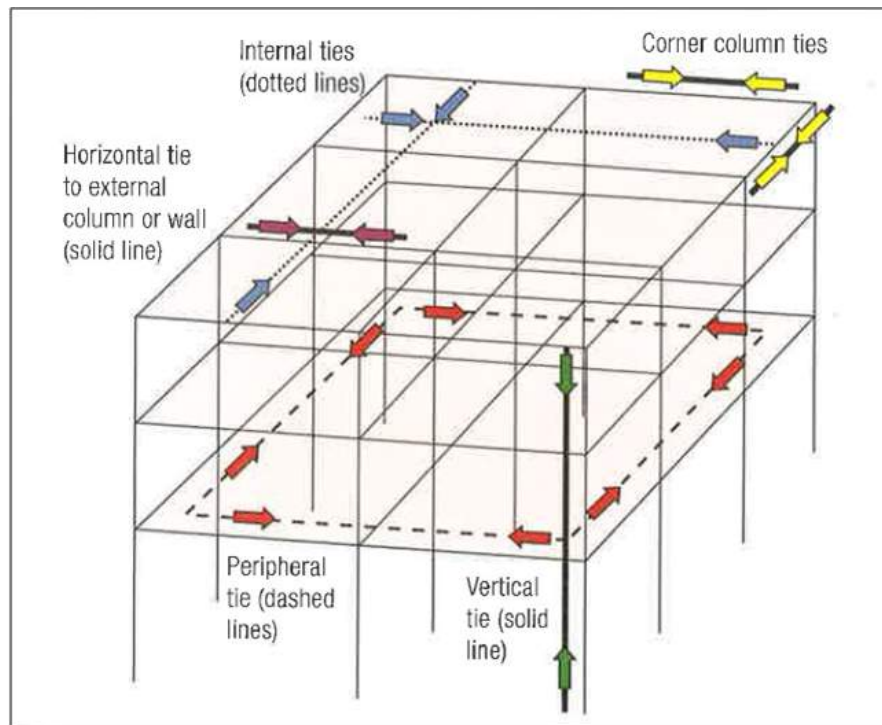


Figure 2.5: Example of tying elements in a structure to improve redundancy.
Reproduced from IStructE (2010).

damage. Commonly the redundancy in the structure is improved with the use of tying elements. These are intended to allow the structure to utilise ALPs and avoid collapse. Figure 2.5 provides an example of the locations for tying elements for a structure. This approach is very useful for structures with a low likelihood of an initiating event. However, as the actual demand and capacity of tying elements is not checked, there is still potential for unexpected progressive failures. Furthermore, a well tied structure may aid progressive collapse as a larger part of the structure is influenced by a local event (Starossek, 2009). As an example of the opposite of this effect, the progression of failure was prevented on Pipers Row car park (Section 2.2.4) because the reinforcement was non-continuous, not because it maintained integrity.

Examples of the approaches are given in Table 2.1.

2.3.2 European and British standards

Since the collapse of Ronan Point national design codes have included sections, or guidelines, to protect structures from this mode of failure. The first of these were the British code requirements in 1970 as a direct result of the investigation into Ronan Point (Pearson and Delatte, 2005); the updated form of which are still in use. The current

Table 2.1: Examples of different design approaches

Approach	Action	Examples
Direct	Local Resistance	Strengthening walls for a predicted size bomb
	ALP	Conduct analysis of full structure after column loss due to a blast
Indirect	Local Resistance	Strengthen elements against a generic force
	ALP	Provide tying elements to maintain structural integrity after a column loss

Structural Eurocode specifications state that as a basic requirement:

A structure shall be designed and executed in such a way that it will not be damaged by events such as explosion, impact, and the consequences of human errors, to an extent disproportionate to the original cause (EN 1990, 2002).

The UK Building Regulations Approved Document A (2006), and the Structural Eurocode EN 1991-1-7 (2006), classifies structures according to their size and use. The guidelines are based on a prescriptive approach that aims to ensure the structure has sufficient redundancy by providing continual reinforcement and specifying minimum strength requirements. It specifies that structures up to class 2B, typically structures under 15 floors, must include appropriate tying elements, see Figure 2.5. Alternatively, the direct design approach may be used. Here an element, e.g. column, beam or length of wall, is removed and a simple analysis conducted on the rest of the structure. If more than 15% of the floor area, or 70m², is at risk of collapse then the element is designated as key and then must be designed to withstand a static pressure of 34 kN/m². This uses an indirect local resistance method, and the value is derived from the size of the accidental gas explosion at Ronan Point.

Additionally, Class 3 structures, i.e. structures larger than 15 storeys, grandstands accommodating more than 5000 spectators, or buildings containing hazardous substances and/or processes have the additional requirement:

A systematic risk assessment of the building should be undertaken taking into account all the normal hazards that may reasonably be foreseen,

together with any abnormal hazards (Approved Document A, 2006).

2.3.3 United States standards

Similar to the European requirements the ASCE 7-05 Guidelines state:

...buildings and structural systems shall possess general structural integrity, which is the quality of being able to sustain local damage with the structure as a whole remaining stable and not being damaged to an extent disproportionate to the original local damage. (ASCE, 2006)

The guidelines used in the USA for Federal and Government buildings arose from the Oklahoma bombing. Under this approach modelling requirements are specified for a column loss scenario, i.e. a key element is removed, and the entire structure analysed to determine if surrounding elements can create suitable alternative load paths. The General Service Administration (GSA) provides different options for the level of analysis conducted which allow the inclusion of nonlinear or dynamic effects. These have different safety factors assigned, depending on the complexity of the simulations. However, it recommends a simple linear static analysis using the following load combination

$$2.0(1.2DL + 0.5LL) \quad (2.3.1)$$

where the DL and LL are the Dead Load and Live Loads respectively, and includes a reduction factor for the Live Load. This also includes a force Dynamic Amplification Factor (DAF) of 2 to compensate for the static approach (GSA, 2013).

Finally, the Department of Defence (DoD, 2009) also have a series of requirements for military buildings depending on the level of hazard. These range from prescriptive requirements of minimum tie forces to specifications for load factors, and combinations for nonlinear static and dynamic analysis.

Whilst full nonlinear dynamic analysis should create less conservative designs, care needs to be taken in the assumptions required for modelling. Furthermore, material failure is a complex issue that can be time-consuming to model and understand (Mohamed, 2006; Marjanishvili and Agnew, 2006).

2.4 Previous research into progressive collapse

This section provides an overview of the previous research into progressive collapse. It highlights the common approaches used, key results that have influenced the field,

and the limitations of the work.

2.4.1 Design considerations

When considering prevention of disproportionate collapse at the design stage, the concept of robustness is often used. Starossek (2009) defines this as "...insensitivity to local failure". Baker et al. (2008) also lists the common definitions, from a number of fields, before highlighting that for structural robustness, design codes such as EN 1990 (2002) do not quantify robustness in a manner that is helpful for an engineer considering different options.

The concept of robustness is usually related to the redundancy of a structure, or its ability to undergo ductile deformations. Beeby (1999) made a suggestion that to avoid brittle failures, an energy absorption criteria should be required for a structure, which could also be expressed as a specified ductility or deformation. Bertero and Bertero (1999) propose that the robustness of a structure can be determined by a push over analysis, and the number of plastic hinges that form.

Several authors have also sought to quantify redundancy, usually by means of an index (Pandey and Barai, 1997). For example Husain and Tsopelas (2004) suggested Equation 2.4.1, where, S_u is the ultimate strength or the maximum resistance, and S_{nr} is the strength of the same structural system, as if it was non-redundant. The authors note that the value varies as a function of the structure's geometry, and the ductility of the members, allowing the index to be used to aid the design choice.

$$r_s = \frac{S_u}{S_{nr}} \quad (2.4.1)$$

Yagob et al. (2009) gives an overview of different design approaches and code requirements for typical reinforced concrete buildings concluding that whilst "...they might somehow produce buildings of acceptable safety, much research is still needed. This is especially the case for improving the overall structural response of existing RC buildings to local failure...".

The different analysis approaches (i.e. inclusion of nonlinearities or time history / dynamic effects) have been considered by Marjanishvili (2004) and Menchell et al. (2009) for steel and RC frames respectively. As they expected, the simpler methods produce more conservative results. They recommend conducting multiple analyses of increasing complexity, until a safe and efficient result is demonstrated.

Non-standard structural forms have also been investigated. Irregular shapes, or un-

usual bracing systems, need to be considered carefully as they may lack the usual robustness found in conventional design. Alternatively, they may have unexpected ALPs which decrease the potential for progressive failures. Therefore, more extensive analysis should be conducted for these types of structures (Kim and Lee, 2010; Kim and Hong, 2011; Patel and Joshi, 2012; Kim and Kong, 2013; Kim and Jung, 2013).

2.4.2 Column loss idealisation

As described in Section 2.3, the sudden column loss scenario is a common design tool. For such analysis, a load bearing element is removed instantaneously from the structure without directly applying any damage or loss of capacity to other elements and the remaining structure is assessed for failure.

Studies have been conducted to consider the suitability, and limitations, of the sudden column loss scenario. Sharma et al. (2012) conducted dynamic analyses of RC columns to evaluate both the shear demand caused by a vehicle impact, and the dynamic shear capacity. Their work improved the determination of the potential that a column might be destroyed. The effect of an explosion on RC structures, and whether it will lead to a column loss event, depends strongly on the reinforcement detailing. Furthermore, seismic strengthening techniques have been shown to increase the residual column capacity (Bao and Li, 2010). Jayasooriya et al. (2011) modelled the effect of explosions on an RC frame structure and concluded that both the details of the local damage to elements, and a global analysis are required in evaluating the response of the structure.

Gudmundsson and Izzuddin (2012) investigated the suitability of the sudden column loss scenario for multi-storey steel frame structures under blast loading. They highlighted that its event independent nature makes it useful for progressive collapse assessments, where a full nonlinear dynamic analysis for blast conditions would be unfeasible. It was also concluded that it offers an upper bound on the maximum dynamic floor deformations, when excluding shear failures, and therefore may lead to conservative results. As the results of a column loss can still be complicated, further simplifications have been suggested (Pujol and Smith-Pardo, 2009), by conducting a linear static analysis and setting limits for forces and ductilities.

While the column loss event is recognised to be an over simplified scenario, its easy application to any structure makes it a good benchmark to consider the potential for progressive collapse.

2.4.3 Structural consideration of progressive collapse

Any structure in an accidental load condition, such as a column loss, is likely to be stressed beyond its elastic limits. Since after this point, all materials exhibit either ductile plastic deformations, or a brittle reduction in strength, the potential for progressive failures is strongly dependant on the post-peak material behaviour. If there is a ductile strain-hardening, as common with steel, the structure may still be able to reach a new equilibrium despite its damage. Alternatively, brittle materials, or ones with tension-softening, are more likely to fail and lead to a complete collapse.

Geometric nonlinearity may also play a role during such events. Catenary action, that is beam elements resisting vertical loads by their axial capacity as well as by bending, has been shown to play an important role in preventing progressive collapse in frame structures (Byfield and Paramasivam, 2007; Valipour and Foster, 2010; Yang and Tan, 2013). These effects only occur at high deflections, once the element is deformed beyond its elastic limit (Abruzzo et al., 2006). For RC beams, this is dependent on the reinforcement maintaining integrity and allowing ductile deformations and rotations (Bao et al., 2013). However, Kim and Yu (2012) considered the effect of multi-storey structures (as opposed to sub-assemblages) and concluded that the effect is less significant due to the more flexible boundary conditions for the beams.

Membrane action in slabs at high deflections, a 2-dimensional equivalent of catenary action, can also provide additional capacity to resist progressive failures. This mechanism will be discussed further in Section 2.5.2.

One of the first works to really consider progressive collapse was by Hawkins and Mitchell (1979) and Mitchell and Cook (1984). Their work focused on the experimental response of flat slabs to extreme loading events. Here they recognised the need to "design and detail slabs such that they are able to develop secondary load carrying mechanisms after initial failures have occurred". Their testing involved overloading a typical flat slab-column frame and measuring deflections as well as considering failure modes and patterns. They also compared different boundary conditions, and loading patterns, to see in what situations slabs can produce membrane action. Figure 2.6 shows photographs of some of their slabs after testing. They identified the risk of punching shear around internal columns, but also highlighted that the provision of continuous reinforcement allows the formation of tensile membranes which increase the capacity of the slab. However, these tests were based on static loading conditions and did not include the effects of a sudden column loss.

Sasani and Kropelnicki (2008) carried out detailed experimental work of RC beams

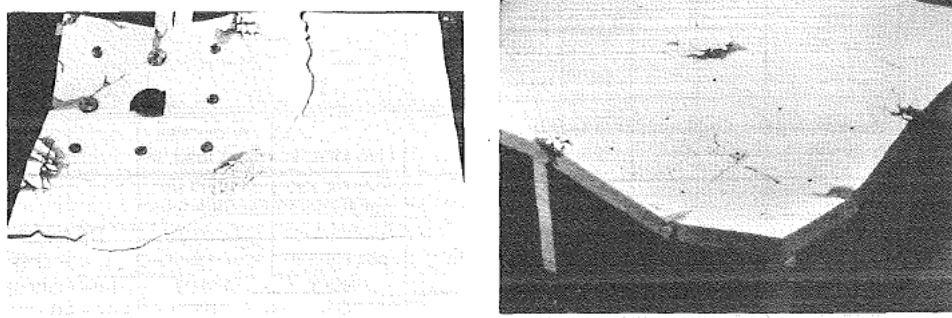


Figure 2.6: Photographs of flat plate corner panels after overloading. Reproduced from Mitchell and Cook (1984)

considering a sudden column loss situation. In particular they attempted to calculate, and model, the catenary action that develops in beams at high deflections. They constructed a 3/8th scale frame and forced displacement at a location without a column at the 1st floor. They also ran Finite Element Analysis (FEA) simulations to compare the predicted capacity of the beam. Their testing demonstrated that the structure could still carry high loads in a deformed state, but excessive cracking occurs at joints, and midspan, as reinforcement yields. Furthermore, whilst their simulation could accurately consider the first stage of loading, the relationship broke down after the bottom bars fractured, whilst the test showed the top bars could still carry load by tensile catenary action. Forces in the column above the location of the removed column reduced to zero within 5–15ms.

Further detailed testing has been done for RC frame structures. This has included consideration of boundary conditions present for axially-restrained beams which allows compressive arching to form (Su et al., 2009). It was also demonstrated that even under high speed loading, the effect can still develop; the experimental set up is shown in Figure 2.7. Similarly Yi et al. (2008) tested 4 bay by 3 storey frames, under an internal column loss situation. Whilst their results suggested that the structure might collapse, they concluded that for a full building, with more floors and contribution from the floor slab, it would be able to hold its own weight in a damaged state. The static push down test is shown in Figure 2.8. They also conducted further work on a flat slab section, (Yi et al., 2014). Again these tests were limited to quasi-static due to the difficulty in instrumenting, and recording, dynamic data for a very short duration. This work highlighted that side and corner spans are more vulnerable to column loss, and identified punching shear and rupturing of reinforcement to be the critical failure mechanism. Additionally, they applied yield-line analysis to their slab but concluded that the membrane actions involved result in higher capacity than estimated with such

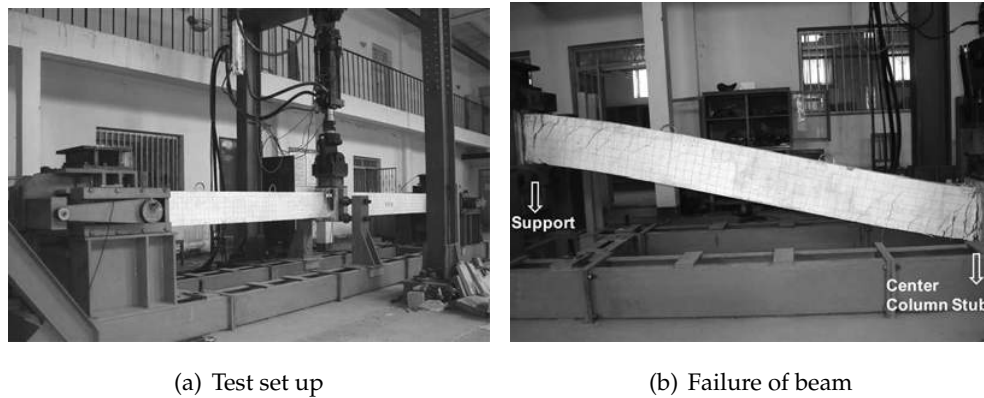


Figure 2.7: Experimental test for axially restrained beams under a column loss scenario (Su et al., 2009)

methods.

Iribarren et al. (2011) modelled RC frames numerically under a column loss scenario. They concluded that the reinforcement ratio and the column removal time were very significant in the extent of damage, and potential for progressive failures, as was the inclusion of a strain-rate dependant material model for the steel bars. However, their model did not include the tensile capacity of the concrete, or the contributions from a structural slab. Therefore, the true capacities are likely to be higher.

Work conducted by Yap and Li (2011) and Choi and Kim (2011) on beam-column substructures with a column loss scenario, confirmed that shear failures were dominant, and independent of transverse reinforcement ratios. They also highlighted the importance of secondary effects, such as catenary action, when modelling these conditions.

A recent experiential programme into the behaviour of RC beam-column substructures has allowed verification of the failure modes experienced for various beam designs (Qian and Li, 2013). The authors considered different transverse reinforcement ratios, type of design detailing, i.e. nonseismic or seismic, and beam span aspect ratios. Both shear failures and plastic hinges were observed, and Vierendeel action was identified as the major load redistribution mechanism. That is, after a column loss the surrounding beam-column connections transfer and resist bending moments. The influence of dynamic removal was then investigated, along with similar findings to other static tests, they demonstrated a sudden column loss can be suitably recreated experimentally (Kai and Li, 2012). Next, comparisons were made to beam-column systems including a slab (Qian and Li, 2012). Here they gave the conclusion that ignoring the slab's contribution is extremely conservative with a 40.7-63.0% increase in capacity reported. The inclusion of drop panels further increases the capacity of a flat slab after a column loss, due to the higher shear resistance (Qian and Li, 2013). Figure 2.9 shows their experimen-



Figure 2.8: Static push down test of an RC frame under a column loss scenario
(Yi et al., 2008)

tal set up and testing with Figure 2.9(a) demonstrating the failure experienced after a corner column loss, and Figure 2.9(b) showing the set up for a test including the slab effects.

Kokot et al. (2012) conducted quasi-static experiments, and dynamic modelling, of RC frame structures with slabs. Their investigations demonstrated that no progressive collapse occurred due to the ductile ALPs utilising additional capacity from plastic hinges in the beams.

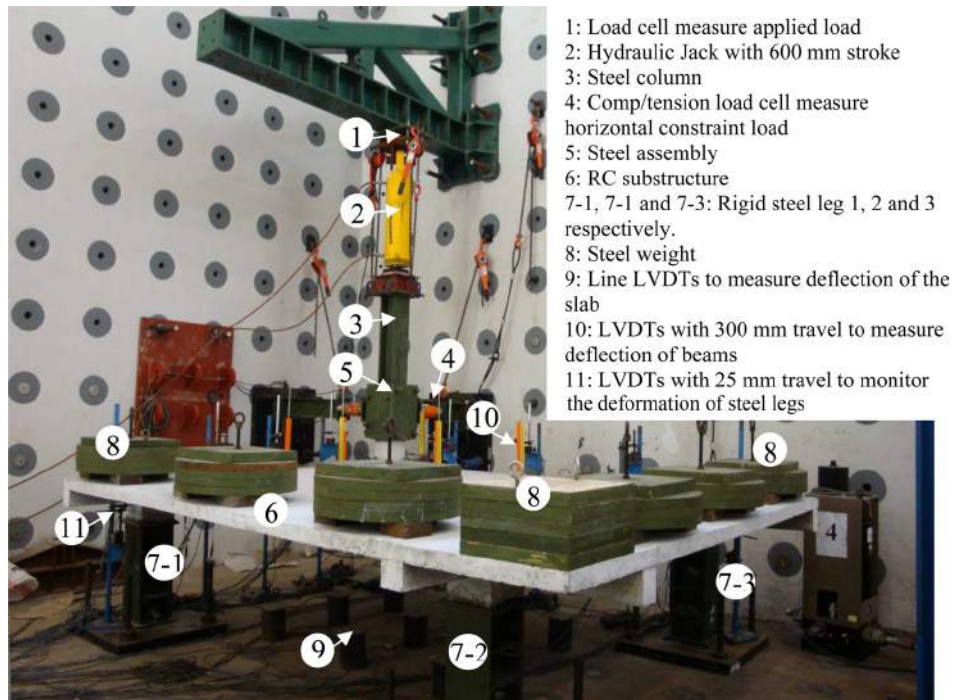
Investigations into steel frames and composite slabs have been conducted by Izzuddin et al. (2007, 2008) and Vlassis et al. (2008), typically using a nonlinear pseudo-static approach applied to a substructure. Their main conclusions are that the ductility of composite joints are the critical aspect, and that the robustness can be improved by additional reinforcement in those locations. Vlassis et al. (2009) also considered the effect of a floor impact in steel structures, concluding the ability of a structure to arrest impact is related to the ductility of the connections.

Fire in multi-storey structures has the potential to start a progressive collapse, see Section 2.2.5, and this has been especially considered for car parks (Fang et al., 2012, 2013), and steel structures (Flint et al., 2007; Fang et al., 2011). The authors identify that steel column buckling, due to the fire, is the most likely initiating event and that the ductility of the joints is critical in preventing progressive failures.

Consideration has also been given to the influence that masonry infill panels exhibit



(a) Failure of beam-column substructure



(b) Set up for beam-column with a slab

Figure 2.9: Experimental tests for column column removal (Qian and Li, 2012)

in providing additional resistance to progressive collapse. Smith et al. (2010) in their study of damage done by bombs in World War 2 attributed the rarity of progressive failures to the ability of the panelling to redistribute loads from the damaged area.

Sasani and Sagioglu (2008) in their study into the collapse of a real RC frame structure (Hotel San Diego) identified bi-directional Vierendeel action, combined with resistance from the infill walls, as the major mechanism for redistribution of forces. A further study was then done without the infill walls which led to an increase in vertical deflection by a factor of nearly 2.4. However, the system still resisted progressive collapse despite formation of flexural cracks.

Numerical analysis into the influence of both interior, and external, brick partitions demonstrates the size, location and existence of openings can change the Demand to Capacity Ratio (DCR) after a column loss. It was also noted that they often increase the collapse resistance, with a decrease in ductility. This means the failure mechanism of the structure can change from a moment failure to a shear collapse (Tsai and Lin, 2009; Tsai and Huang, 2013; Farazman et al., 2013).

Probabilistic approaches to progressive collapse assessment have also been made. However as Bennett (1988) notes, "...little statistical data exists at present in such areas as magnitudes and frequencies of abnormal loads, redistribution of loads after component failures, and the behavior of damaged structures". Additionally, as large portion of the structure contributes to its potential for progressive failure, detailed information is required on the structural form to make meaningful predictions. Despite this further investigations have been successful, Izzuddin et al. (2012) and Le and Xue (2014) have demonstrated that by including the uncertainties in material properties, and the loading, the probability of different levels of damage can be calculated after a column loss event.

Finally, many authors have considered the seismic capacity of RC frames. In particular Chen et al. (2012) considered the damage sustained by non-seismically designed columns. This case is similar to much analysis work done for progressive collapse since few buildings are explicitly designed for the extreme loadings and deformations caused by low probability events. They recognised that non ductile behaviour was common, in particular shear failures. This type of mechanism can be very serious, resulting in progressive failures leading to a sudden, and catastrophic, failure of the entire structure. Also tests by Laskar et al. (2009) on a two-storey RC frame investigated its push over behaviour while monitoring with Structural Health Monitoring (SHM) techniques. Whilst not a typical progressive collapse scenario, their numerical work identified well the plastic hinges that formed and could lead to progressive failure.

2.4.4 Tests on real structures

Work has been done to simulate an actual progressive collapse of a structure, by applying a damaging event to a building already scheduled for demolition. In 2007, Sasani et al. (2007), explosively removed a column of the University of Arkansas Medical Center dormitory. This was a 10-storey reinforced concrete building with one-way slabs supported on beams. An interesting observation is that the large axial stiffness of the columns, leads to almost identical vertical movement of different floors. They show experimentally and analytically, that the axial compressive forces in the columns above the removed column reduce rapidly, and then the floors move almost together, with slightly smaller values for the upper floors. For the experimental test no live load was present in the structure, however it still resisted progressive failure even when this load was reapplied during numerical modelling.

Further tests on the Hotel San Diego (Sasani, 2008) with the sudden removal of two columns demonstrated the Vierendeel, or frame action, of the beams and columns was the main mechanism for the redistribution of loads, with the hollow clay tile infill walls assisting by providing constraint to the beams. The structure did not meet current reinforcement integrity requirements, however, relatively small deflections were observed ($<6.4\text{mm}$) and collapse did not occur. The authors attribute this to the three dimensional response of the structure and its redundancy (Sasani and Sagioglu, 2008).

The 20 storey Baptist Memorial Hospital was scheduled for demolition and presented a further opportunity for Sasani and Sagioglu (2010) to explosively remove a column. In this case, the structure did not fail progressively and little damage was observed away from removal area. The results also led to the conclusions that the behaviour of the whole structure is important in resisting progressive failure, and that taller structures are not necessarily more susceptible to collapse.

Similarly the response of the 11-storey Crowne Plaza Hotel, after a significant damaging event, was considered (Sasani et al., 2011). Here 4 columns and 2 beams were explosively removed, however this only led to a maximum permanent vertical displacement of 56mm. The analytical study into this revealed the importance of the flexural-axial response of the 2nd floor deep beams. The authors also note that the steel bars at the location of the explosions were not completely removed, as in other experiments, thereby potentially reducing the maximum damage experienced.

2.4.5 Dynamic effects

As has been highlighted from previous case studies and research, column loss and progressive collapse is a dynamic event. This influences the response of a structure in two ways; an inertial effect that increases the peak forces and deflections in the structure, and a strain rate effect that changes the properties of the material. The critical aspects behind these issues, and the studies that consider them, are summarised in this section.

Force amplification

Due to the inertial effects, once a structural element is moving an external force is required to bring it back to equilibrium. This results in higher peak deflections than would be experienced under a static, or quasi-static, loading condition. The increase in force, resulting in an increase of deflections, is referred to as the Dynamic Amplification Factor (DAF). For a linearly elastic material there is a direct relationship between force and displacement, and with the further assumptions of instantaneous application of force and no damping results in a DAF of 2.0.

This effect was demonstrated with a simple experimental system by Pretlove et al. (1991). They confirmed the prediction that a structure can be statically safe but dynamically unsafe. Ruth et al. (2006) considered the factors that influence the DAF, for a range of structures, and concluded that whilst the factor varies based on structural properties, a value of 1.5 is adequate for steel structures; this could be even lower for concrete. Also the DAF for three-dimensional models were generally higher than the two-dimensional cases. They did however highlight that this is only valid in cases where damage beyond serviceability requirements is permitted, and therefore may not be suitable for critical facilities.

Further numerical investigations of the DAF, for both steel and RC frames under sudden column loss, including nonlinear effects have been conducted (Tsai and Lin, 2009; McKay et al., 2012). It has been demonstrated that the DAF varies significantly based on the structural details, with values of 1.2 to 1.8 for steel, and 1.05–1.75 for concrete, with lower values at higher rotations. Naji and Irani (2012) also observed the influence of ductility and catenary action on the amplification factor. An experiential test on an RC beam (Yu et al., 2014) gave an upper bound of 1.86. However, as the column was removed with an explosion, damage occurred to the surrounding structure, therefore the dynamic response may have been higher than from a standard column loss scenario, limiting the application of this value. The DAF for flat slabs construction has also been experimentally measured at between 1.13–1.23, however this is based on limited data,

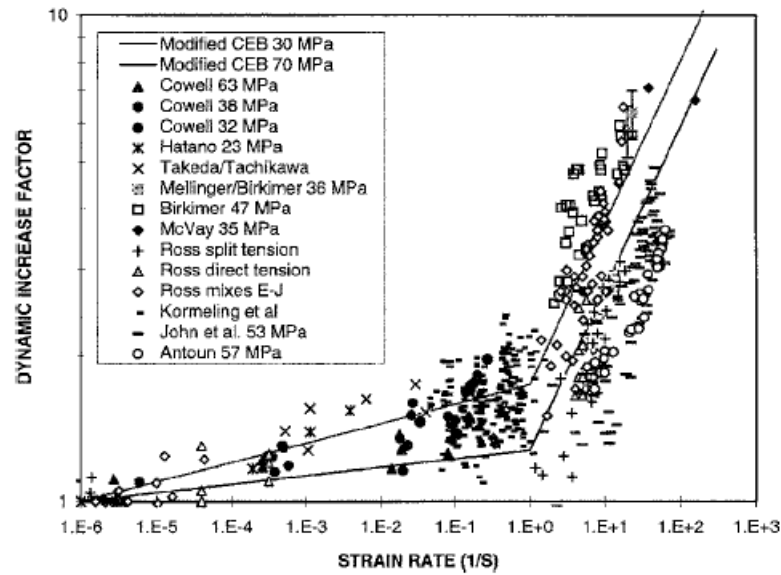


Figure 2.10: Reproduction of Malvar and Ross (1998)'s review of strain rate tests

and parameters, and requires further investigation (Qian and Li, 2013).

In their numerical study of steel frames under a sudden column loss, Ali et al. (2014) suggested that the DAF can be determined from a nonlinear static analysis, followed by an assessment of the structure's ductility and energy equilibrium, however it is uncertain how easy this may be to apply more generally.

Material strength increase

Nearly all materials exhibit different material properties with different rates of loading. Primarily this affects the modulus of elasticity, peak compressive and tensile strengths, and post peak behaviour. Typically, for RC structures, the most critical of these is the increase in yield stress for the reinforcement and cracking stress for concrete. This is referred to as the Dynamic Increase Factor (DIF). Malvar and Ross (1998) give a comprehensive review of many concrete tensile tests, at various strain-rates. The results indicate that the tensile DIF is dependant on the material properties of the concrete, as well as the rate of loading. They also observed that strain rate effects become suddenly more critical after 1s^{-1} , see Figure 2.10.

Similar to this, the current Model Code, (CEB-fib, 2012), recommends the two phase model, with the change at 10s^{-1} , shown in Equation 2.4.2.

$$(f_t/f_{ts}) = \begin{cases} \left(\frac{\dot{\epsilon}_{ct}}{\dot{\epsilon}_{ct0}}\right)^{0.018} & \text{for } \dot{\epsilon}_{ct} \leq 10s^{-1} \\ 0.0062 \left(\frac{\dot{\epsilon}_{ct}}{\dot{\epsilon}_{ct0}}\right)^{1/3} & \text{for } \dot{\epsilon}_{ct} > 10s^{-1} \end{cases} \quad (2.4.2)$$

where

f_t/f_{ts} = the concrete tensile DIF at $\dot{\epsilon}$

$\dot{\epsilon}_{ct}$ = the concrete tensile strain rate

$\dot{\epsilon}_{ct0} = 10^{-6}s^{-1}$ (static strain rate)

However, Wu et al. (2012) and Chen et al. (2013) have investigated the influence of the testing method on tensile concrete DIF, and observed different responses for splitting tests, direct tension, and four-point flexural bending, with the former being more sensitive to strain rate effects. Therefore, since most strain-rate models are based on indirect splitting tests, it is uncertain as to how well they replicate actual constitutive relationships.

In their experimental investigation of RC beams under a sudden column loss, Yu et al. (2014) measured strain rates of between 10^{-2} to $10^{-1}/s$, and suggested that this only gives a small increase in material strength and can be conservatively ignored.

2.5 Previous research into concrete slabs

2.5.1 Failure modes

In order to conduct detailed analysis into the potential for collapse of a structure, the causes of failure mechanisms need to be understood and suitably modelled. For reinforced concrete slabs this can be challenging due to the range of mechanisms involved. Abbasi et al. (1992) reviews the possible failure modes and highlights the differences between flexural and shear failure. They also investigate the influence of the reinforcement ratio on the type of cracks forming, and conclude for typical, medium reinforcement levels, there is a strong interaction between flexural and shear failure. Additionally, Choi and Kim (2012) studied the change in bending moment redistribution of flat slabs and concluded that it is directly affected by the ratio of shear and flexural strength.

Cracking is an inherent issue for concrete due to its low tensile capacity and brittle nature. Under extreme loading conditions cracking is inevitable, leading to a change in

the stiffness and performance of the element. Therefore suitable cracked concrete models are vital for any numerical analysis. Two approaches are common, either a smeared crack or a discrete crack. Naturally the latter is more computationally intensive and difficult to implement, due to challenges in identifying the orientation of principle stresses (Wang and Teng, 2007). Regardless, any method must be able to consider the reduction in stiffness, and change in neutral axis experienced, during excessive cracking (Foster and Marti, 2003; Marzouk et al., 2010). The available options will be introduced and discussed in more detail in Chapter 4 while describing the Finite Element (FE) model.

Most theoretical methods considering the behaviour of slab elements incorporate some form of layered approach. Here a suitable plate model, such as Classical Lamination Plate Theory (CLPT) or First-Order Shear Deformation Plate Theory (FSDT) is applied to each layer to achieve material and geometric nonlinearity (Reddy, 2004). Many authors have applied these techniques, though there are still issues in incorporating both shear and flexural behaviour at high displacements (Phuvoravan and Sotelino, 2005; Agbossou and Mougou, 2006; Zhang et al., 2007a,b; Wang and Teng, 2008).

Punching shear failure is recognised as being a major risk to flat slab structures due to its sudden and brittle nature (Muttoni, 2008). For this reason many authors have considered possible modelling approaches to determine shear forces and capacity (Loo and Guan, 1997; Vollum et al., 2010). A recent parametric study of punching shear in slabs by Mamede et al. (2013) confirmed that a nonlinear 3D FEA using '8-node brick elements' can suitably predict the shear capacity. As expected, they concluded that increasing reinforcement ratios, concrete strength, slab thickness or column size increases the capacity, though may also lead to more brittle failures. Additionally, comparisons of different shear reinforcement systems and strengthening techniques have been made, such as the work by Broms (2007) and Koppitz et al. (2013). They have concluded that top reinforcement is often not efficient in preventing punching shear, as insufficiently anchored rebars can rip out of the concrete. The post-punching behaviour of RC slabs has been investigated by a number of authors (Faria et al., 2012; Ruiz et al., 2013; Mirzaei and Sasani, 2013). In general, the inclusion of 'integrity' reinforcement, that is reinforcement not required for flexural strength under normal design conditions but provides ties between sections (see Figure 2.11), can provide further shear capacity via dowel action.

Saito et al. (1995) tested concrete slabs under static, and high speed loading, to simulate impact. Figure 2.12(a) shows the apparatus set up, while Figure 2.12(b) shows the comparison of loading rate on the mode of failure. For all tests, bending deformation occurred to begin with, before the slab failed due to punching shear. Interestingly, the

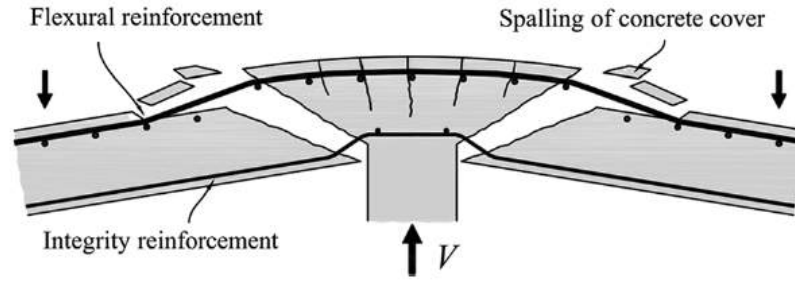


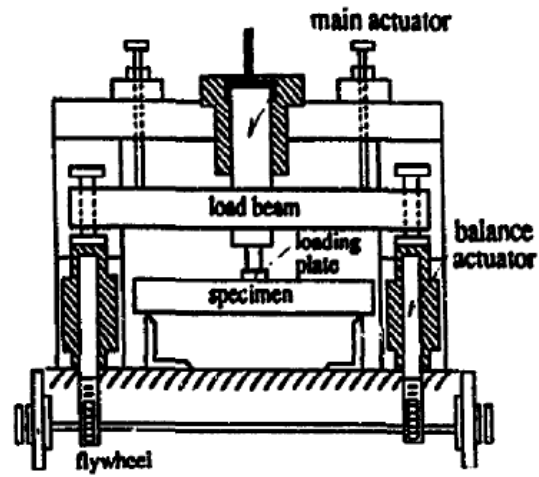
Figure 2.11: Flat slab failing in punching shear with integrity reinforcement.
Reproduced from Ruiz et al. (2013)

loaded side showed no cracking apart from the hole punched out at failure while the tension side produced large radial cracks for all tests. Other tests have been conducted to consider this further, with the DIF associated with high loading rates resulting in higher strength but a more brittle performance (Zineddin and Krauthammer, 2007). Trivedi and Singh (2013) conducted FEA comparisons of these tests with 3D solid elements, and nonlinear material properties, with good agreement to the experimental tests. The computed strain rates were of an order between 10^{-4} and 10^{-2}s^{-1} , with associated concrete tensile DIF of between 1.5 and 1.75. However, they report no significant change in the output when including such effects, and conclude it is not significant for this problem.

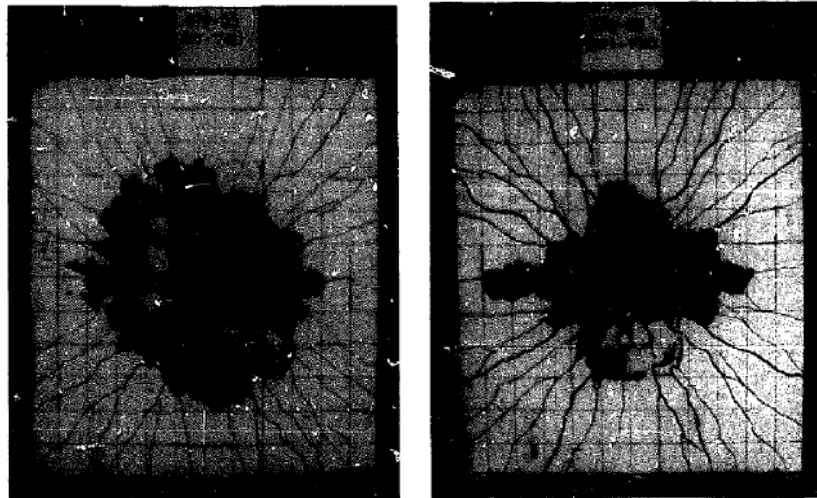
2.5.2 Geometric nonlinearity

Geometric nonlinearity of slab elements is known to change their response at high deformations. The formation of tensile membranes, with a compressive ring, can increase the capacity of a slab. This is only possible with the right boundary conditions for the slab, the ability of the reinforcement to undergo ductile yielding, and requires the concrete to not undergo a brittle in tension failure (Bailey, 2001).

Foster et al. (2004) loaded 15 RC slabs to high deflections (3 times the slab thickness) using the equipment shown in Figure 2.13(a). From this they could identify areas of tension and compression in the slab, see Figure 2.13(b). The tests were limited in their application by the small scale of the slabs, but all the tested slabs showed a load-carrying capacity greater than the design capacity using the yield-line theory. By also comparing smooth and deformed wire reinforcement, they observed that if the steel does not debond from the concrete during cracking, then it may fracture and reduce the membrane effect.



(a) Loading apparatus



(b) Failure of flat slab for static (Left) and high speed (Right) loadings

Figure 2.12: Saito et al. (1995)'s experimental impact tests on RC slabs

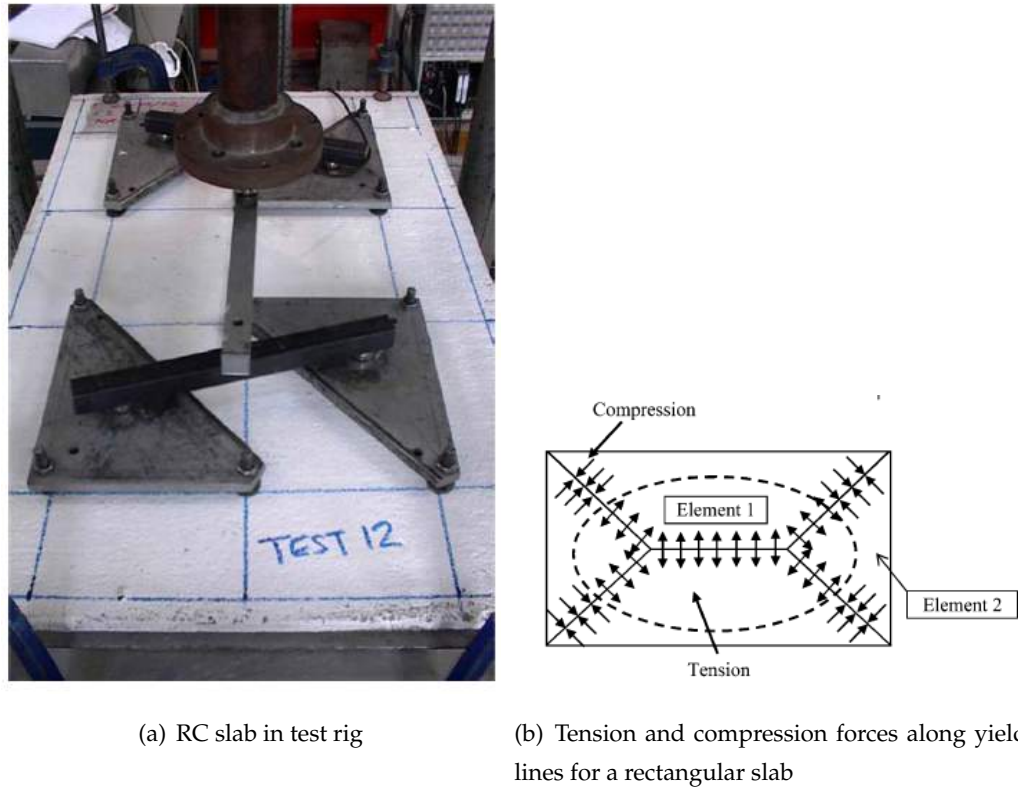


Figure 2.13: Testing and analysis of an RC slab (Foster et al., 2004)

The majority of high deflection RC slab tests have been conducted under fire conditions (Izzuddin and Elghazouli, 2004; Elghazouli and Izzuddin, 2004; Dong and Zhu, 2011). These have, again, highlighted the effect tensile membrane has on maintaining the slab's integrity, allowing higher capacities than from a yield-line analysis.

As has been mentioned, ductility is an important issue in activating the full capacity of a slab at high loadings. Polak (2005) highlights this and identifies the need for adequate punching shear reinforcement to prevent brittle, and sudden shear failures, and to allow the flexural reinforcement to yield.

Das and Morley (2005) made experimental investigations into compressive membrane action in restrained slabs, which revealed the additional stiffness provided by the geometric nonlinearity. At a displacement of 5% of the double span length, twice the flexural capacity was observed for beam-slab sections (Dat and Hai, 2013). The authors note the need for further experimental tests to validate the failure mechanisms.

Other authors have considered the effect of Compressive Arching Action (CAA) in restrained slabs (Das and Morley, 2005; Zheng et al., 2008). These papers, have demonstrated that once cracking starts to occur in a laterally restrained slab, then a compressive arch can form provided displacements are still small as shown in Figure 2.14.

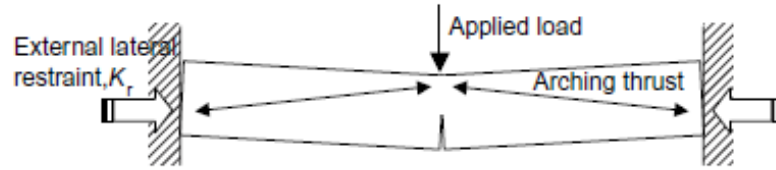


Figure 2.14: Compressive arching action in laterally restrained reinforced concrete slab (Zheng et al., 2008)

2.6 Summary

From the extensive study of the issues effecting progressive collapse over the last 35 years which have been reviewed above, a few broad factors can be identified.

Whilst usually rare, the past structural failures have demonstrated that progressive failures can occur, and should be considered at the design stage to prevent disproportionate collapses. Numerous researchers have identified that ductility in the structure, and especially in the connections, is key to preventing progressive collapse. However, flat slab construction is susceptible to brittle failure mechanisms, predominantly by punching shear, which may cause progressive failures. RC structures also exhibit non-linear behaviour after damage, both materially and geometrically, which can increase their capacity beyond normal design limits. Additionally, elements such as masonry infill walls, or slab elements, can increase the robustness of a structure and allow the formation of ALPs which may allow the structure to survive severe local damaging events.

Progressive collapse is always a dynamic event. The majority of initiating events occur in a short time span, and result in significant motion to the surrounding elements. Therefore the influence of inertial effects must be included in some form during an analysis. Additionally, other related effects may be important, including material strengthening due to high strain-rates.

From considering the case studies, and the key research papers, it is clear that not only is progressive collapse of RC flat slab structures a potential issue, there is currently a lack of experimental and numerical information regarding their response after a sudden column loss. In particular, the influence of dynamic effects and the Dynamic Amplification Factor (DAF) is uncertain, as well as the full capacity of such elements including their nonlinear behaviour. This project seeks to address these points with experimental tests and parametric numerical analysis.

Experimental Testing

As highlighted in the previous chapter, there is a lack of information about the progressive collapse of Reinforced Concrete (RC) flat slab structures. This chapter describes the experimental tests conducted on seven scaled RC flat slab substructures replicating a column loss event.

It gives details of the approach, and instrumentation used, along with the results and a discussion of their significance for the entire project.

3.1 Introduction to experimental work

As described in Section 1.3 one of the objectives of this project is:

Conduct a series of experiential tests on a scaled substructure of a flat slab comparing static incremental loading to a dynamic column removal case. Column loss location and reinforcement layout will also be considered.

This chapter addresses this objective and describes the experimental programme conducted and highlights the results that will be relevant to complete other project objectives.

3.1.1 Aim and objectives

The aim of these tests is to provide information to validate the assumptions and results from numerical models of sudden column loss and to provide evidence for the susceptibility of flat slab structures to progressive failure.

In order to achieve the above aim, the following objectives will to be completed:

- Construct a series of scale RC flat slab subsections representing typical design
- Measure the support reactions, deflections, strains and cracking of a flat slab under static loading for different column removal positions and reinforcement layouts
- Measure the support reactions, deflections, strains and cracking of slabs during a sudden dynamic column removal scenario
- Use measurements obtained to determine the changes in response due to dynamic column removal compared to a static case
- Obtain data of the damage profile under a column loss scenario to validate modelling assumptions for Finite Element Analysis (FEA).
- Observe common or likely failure modes associated with progressive collapse of flat slabs

3.1.2 Methodology

With structural testing there often is a compromise between the difficulties in constructing and testing on full sized elements and the challenges of creating suitable scaled versions that still accurately represent the full scale behaviour. For this experimental programme, slab elements at 1/3 scale were chosen to make efficient use of the materials, equipment and space available. Below this ratio, Reinforced Concrete's composite behaviour can start to change for several reasons. The aggregate used for the concrete can not always be scaled suitably. To achieve the small reinforcement areas very thin steel bars (or possibly wires) may be required which exhibit different tensile and compressive behaviours to usual reinforcement. Finally, the bond between the concrete and steel may not represent full scale conditions due to the low level of concrete cover.

As the primary aim of these tests is to validate numerical models, certain assumptions have been made that do not represent a typical structure but are simpler to model. The most significant of these is the boundary conditions and support design. A true continuous flat slab structure provides vertical, horizontal and rotational restraint to the slab, however, it can be difficult to achieve and monitor such effects on a substructure. For example, a slab-column connection cannot be considered to be truly fixed or pinned. Therefore to avoid these uncertainties when replicating the system with Finite Elements (FEs) the supports were designed as pinned, free to rotate in any direction.

No horizontal restraint was applied to the supports, apart from that provided by friction between the concrete surface and the steel support.

The loading system also needs to be carefully considered. Previous research has suggested that upper floors do not significantly transfer vertical loading to the column loss location (Sasani et al., 2007). Therefore the only loading that needs to be included is the Uniformly Distributed Load (UDL) on the floor elements. This was achieved by placing sand and gravel bags across the surface until the required load was reached. For the static tests this created a load control system, rather than the displacement controlled often used by other authors conducting experimental investigations into slab elements (see Section 2.5). While a displacement control does give a better force-displacement profile of an element, especially during the nonlinear phase after a local force maximum, applying a dead load represents the loading conditions for a real structure. It is also easier to ensure that loading is applied uniformly across the surface without local concentrations of force with an imposed dead load. Furthermore, for the dynamic tests, displacement controlled methods such as with a hydraulic actuator may not maintain the constant load during the short time period after removal, nor will they replicate the required additional mass.

Finally, the space available for specimens meant that samples were limited to only one bay in width. This meant that all removal locations were at an external position. While the influence of more of the structure can be considered with an internal location, edge columns are more exposed to accidental actions and represent a typical area of concern.

3.2 Description of experimental programme

3.2.1 Design of experiment

The tested scaled models were designed to have an equivalent Demand to Capacity Ratio (DCR) as a full size prototype based on the method presented by Kai and Li (2012). For third scale tests, span and depth values were reduced by factor of 3, UDL by 1 and reinforcement areas by 3. This also maintained the same reinforcement ratio, ρ , between the prototype and the scaled version. Design loads and reinforcement quantities were calculated according to Eurocodes EN 1990 (2002), EN 1991-1 (2002) and EN 1992 (2004). The full calculations and comparison to the prototype are given in Appendix A.

Table 3.1: Slab IDs for each test and corresponding variables

Slab ID	No. of bays	Removal Position	Reinforcement	Test Type
C-S	2x1	Corner		Static
C-D	2x1	Corner		Dynamic
PC-S	2x1	Penultimate	Continuous	Static
PC-D	2x1	Penultimate	Continuous	Dynamic
PR-S	2x1	Penultimate	Reduced	Static
PR-D	2x1	Penultimate	Reduced	Dynamic
M-D	4x1	Middle		Dynamic

3.2.2 Variables considered

This section describes the three key variables investigated in this experimental programme. Table 3.1 also provides each test ID and its arrangement.

Loading and support removal condition

Two loading and support removal conditions were considered; an increase in static loading and a sudden dynamic column removal. Under the static case, the slab was placed on the supports and the column at the position under investigation was removed. A uniform load was then applied across the entire sample and the response monitored. Under the dynamic removal, an identically designed slab cast at the same time as the static, was loaded whilst fully supported. Once the required UDL was achieved, the chosen support was removed dynamically and the system allowed to deform and either come to rest or undergo total failure. Static and Dynamic tests are designated with S or D in their ID respectively.

Column location

Three column loss locations were tested. The first type, corner removal (designated with C for test IDs) allowed investigation into the edge conditions with a continuous support in one direction.

Tests P-S and P-D removed the middle column in a two bay system, this in effect replicated a penultimate (P) column loss on either side.

Finally, the middle (M) condition with a 4x1 bay system provided a continuous slab over both adjacent supports, replicating removal of an external column at the middle

Table 3.2: Summary of the loading levels conducted for dynamic removal tests

	Slab ID			
	C-D	PC-D	PR-D	M-D
Loads tested (kN/m ²)	3.0	2.5	2.3	3.1 ^b
	6.8	5.6	5.7	6.7
	7.7 ^a			8.5

^aAfter the final dynamic test a large load was applied over the removed corner to cause complete failure.

^bA static test was also conducted on this sample with loading between 2.1 and 4.4kN/m².

of a longer structure. This test was only done as a dynamic removal.

Figure 3.1 shows the location of the removed support for each test.

Reinforcement layout

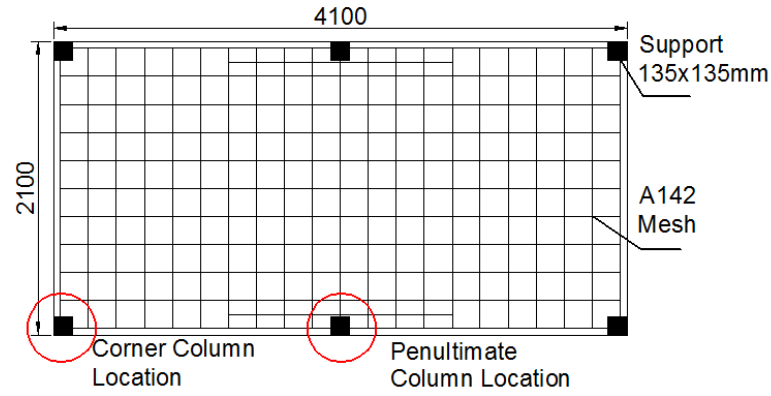
Additionally, tests P-S and P-D were repeated without having continuous bottom reinforcement through the removed column. This represents a common approach of only providing tension steel where required for normal usage and allows the additional capacity the bottom steel provides in this location to be determined. The two cases are designated as PC for Penultimate removal with Continuous reinforcement and PR for the equivalent case with Reduced steel.

Loading level

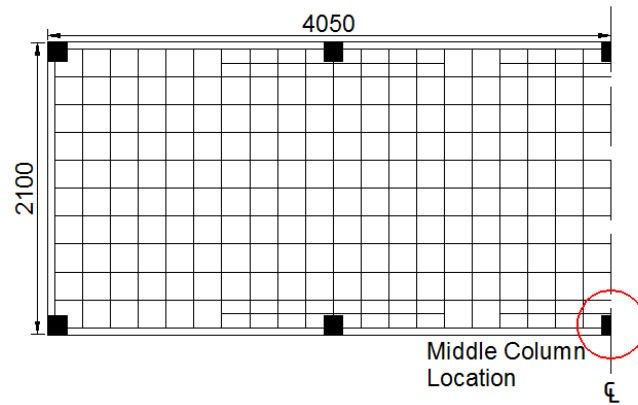
During the dynamic removal conditions, the tests were repeated with different levels of loading on the same slab sample. A summary of the total UDLs for each test is given in Table 3.2. By testing at different applied load the changes in dynamic response of the slab due to increased mass and the damage can be observed. The lower levels of load were tested first to minimise the effect of damage for further tests.

3.2.3 Experimental set up

For the first three series of tests, a 2x1 bay subsection of a flat slab structure was constructed. The specimens were 4100mm x 2100mm in plan with a thickness of 80mm. Each sample included two A142 meshes providing 6mm bars at 200mm spacing for both top and bottom reinforcement. Additional 6mm bars were added over internal



(a) Corner and penultimate removal conditions



(b) Middle removal condition

Figure 3.1: Details of test setup showing slab sizes, reinforcement layouts and support locations

supports to meet requirements for the hogging moment. No shear reinforcement was included as the concrete alone provided enough capacity for a fully supported condition. This set up was used to replicate a corner (C) or penultimate (P) column loss as shown in Figure 3.1(a).

The middle (M) column removal case used a 4x1 bay system, constructed in the same manner, with a total length of 8100mm (Figure 3.1(b)).

Supports were 135mm square steel plates, 25mm thick, on spherical bearings to allow rotations. For the dynamic tests, a temporary support that could be quickly removed was constructed. The design was based on a vertical steel bar between two plates. The bottom plate rested on a load cell and steel rollers to allow the support to move easily. The removal process used is shown in Figure 3.2. During the pre-loading period, the support needed to remain securely in place. Therefore, chocks were placed to prevent lateral movement and a clamp placed around the bar to ensure it remained upright; see

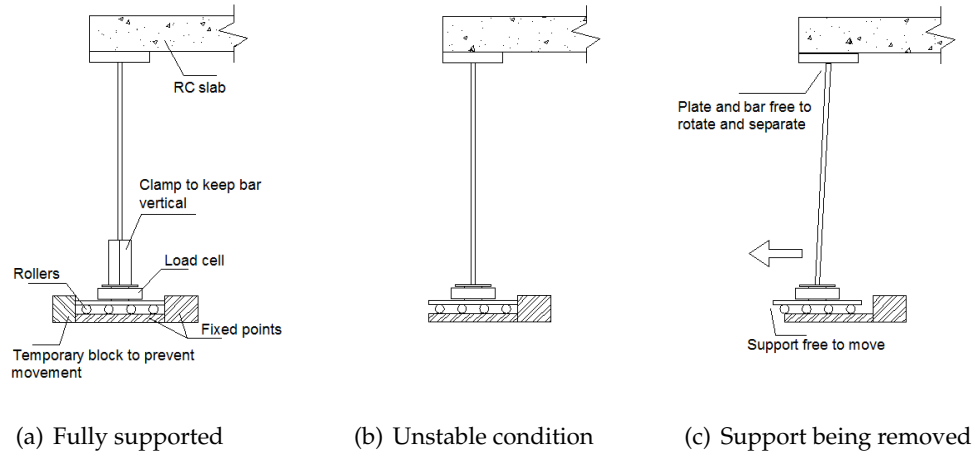


Figure 3.2: Diagram showing the process of removing the temporary support for dynamic tests

Figure 3.2(a) for details. Once the required loading was reached, and the area cleared, the temporary supports and clamps were removed to create an unstable condition (Figure 3.2(b)). Finally, the rope attached to the bar was pulled sharply, causing the support base to move and the bar to disengage with the slab, as in Figure 3.2(c).

Samples were taken from each batch of concrete, these were used to obtain the 28 day compressive cube strength. On the day of testing further cube tests were conducted, along with cylinder splitting tests to obtain estimates for the tensile strength. Specimen details for each test are given in Table 3.3, note that test M-D was conducted before 28 days. Concrete batches 1–3 had a 28 day target cube strength of 30MPa, batch 4 was designed to reach this in 14 days. Unused sections of the steel reinforcement were also tested to determine their tensile properties. A summary of these samples is given in Table 3.4 providing the average Young's Modulus (E), 0.2% proof stress ($\sigma_{0.2}$), the ultimate tensile stress (σ_{max}) and the percent elongation at fracture.

3.2.4 Instrumentation

Under each support, a load cell was positioned to measure vertical reactions. During the test set up phase, these were used to ensure the slab was balanced correctly on the multiple supports. The summation of all support reaction forces also allowed calculation of the applied UDL. For the static tests a recording was taken for a fully supported condition, under the slab's self weight, and measurements taken for every load increment afterwards. This provides information on the redistribution of forces

Table 3.3: Concrete material properties from test samples

Concrete Batch	28 Day Cube Strength (MPa)	Slab ID	Test Day Cube Strength (MPa)	Indirect Tensile Splitting (MPa)
1	25.6 <i>S.D.</i> 2.0	C-S	26.6	— ^a
			<i>S.D.</i> 1.0	
		C-D	26.7	2.18
			<i>S.D.</i> 1.8	<i>S.D.</i> 0.18
2	29.8 <i>S.D.</i> 0.3	PC-S	33.9	2.71
			<i>S.D.</i> 1.5	<i>S.D.</i> 0.43
		PC-D	37.1	2.79
			<i>S.D.</i> 0.9	<i>S.D.</i> 0.10
3	28.1 <i>S.D.</i> 0.8	PR-S	33.8	2.92
			<i>S.D.</i> 1.5	<i>S.D.</i> 0.03
		PR-D	35.2	2.46
			<i>S.D.</i> 0.3	<i>S.D.</i> 0.23
4	32.0 <i>S.D.</i> 1.0	M-D	30.0 ^b	2.95
			<i>S.D.</i> 0.8	<i>S.D.</i> 0.14

^aNo cylinder samples were tested at this time.

^bTest was conducted before 28 days.

Table 3.4: Reinforcement material properties from tensile tests

Sample Number	E (GPa)	$\sigma_{0.2}$ (MPa)	σ_{max} (MPa)	Elongation at fracture (%)
1	198.5	671	700.8	1.69
2	199.7	660	683.8	1.37
3	198.7	669	685.7	0.62 ^a
4	198.1	645	675.9	1.38
5	200.8	679	707.9	1.48
Average	199.1	665	690.8	1.48
<i>Standard Deviation</i>	<i>1.1</i>	<i>13.0</i>	<i>13.1</i>	<i>0.15</i>

^aThis sample failed unexpectedly due to poor a steel sample; its fracture strain is not included in the average.

to the supports after a column loss event and as a result of damage to the slab. For dynamic tests, reaction values were recorded whilst the slab was fully supported and loaded. This allowed determination of the total load applied and ensured the dead loads were placed evenly to create a UDL. The data loggers were unable to measure dynamic readings from the load cells and so, once the slab had come to rest, reaction values were recorded to determine change in final force distributions. The calibration was checked before each test, to a precision of 50N per load cell, leading to total uncertainties of 0.25, 0.30, 0.45 and 0.5kN of the total measured load for configurations using 5, 6, 9 and 10 load cells respectively.

To measure vertical deflections, Linear Variable Differential Transformers (LVDTs) were placed around the underside of the slab. At each static load increment readings were taken for at least 5 seconds and the values averaged over the time period. During dynamic tests the LVDTs were sampled at 250Hz whilst the support was removed to give the displacement-time profiles until the slab reached a static equilibrium. This sampling frequency was chosen as it was high enough to detect the responses of interest and to avoid aliasing issues when analysing the signal, but also it was not so fast as to cause excessive file sizes for the output which would limit the period of recording.

Use of Digital Image Correlation (DIC) techniques allowed deflections at a number of points across the sample to be monitored without contact. This is especially useful in the area around the column loss location where deflections will be highest and the potential for sudden collapse may risk damaging a LVDT or other contact based sensor placed under the slab; dead loads on the top surface prevent placing sensors above the test, see Figure 3.3(a). Camera footage combined with video gauge software (Imetrum Ltd, 2014) determined the static deflections at clearly defined targets for each load increment. For the dynamic tests a Phantom v12.1 High Speed Camera (HSC) was utilised to capture the behaviour in the short time period after the column removal (Figure 3.3(b)). By recording at 2500 frames per second (fps) with an exposure of $300\mu s$ and a resolution of 1280x800 pixels, the images were later processed with the DIC software to obtain deflection readings. Based on the size of the visual targets, distance of the camera and processing software used, an accuracy of $\pm 0.1mm$ was achieved. The high speed footage was also used to identify crack propagation.

Each test, with the exception of M-D, included a number of strain gauges to provide information regarding the distribution of stress after a column loss. Primarily these were attached to the steel reinforcement and were used to identify when yielding occurred. The penultimate removal location tests also included some gauges attached to the top surface of the concrete, directly above the removed support, to detect evidence



Figure 3.3: a) Photograph of slab PC-D before dynamic testing, note the visual targets; b) Cameras for visual monitoring

of concrete crushing. Measurements were taken with the same data logger and in the same manner as the LVDTs.

Cracks on the sides or under surface of the concrete were noted as they occurred and their position and the level of loading recorded. At the end of each test, the sample was cleared of the dead weights and the positions of cracks on the top surface were also marked. The slab was then tilted up to near vertical and the top and bottom surfaces photographed to record the final cracking patterns.

3.3 Results

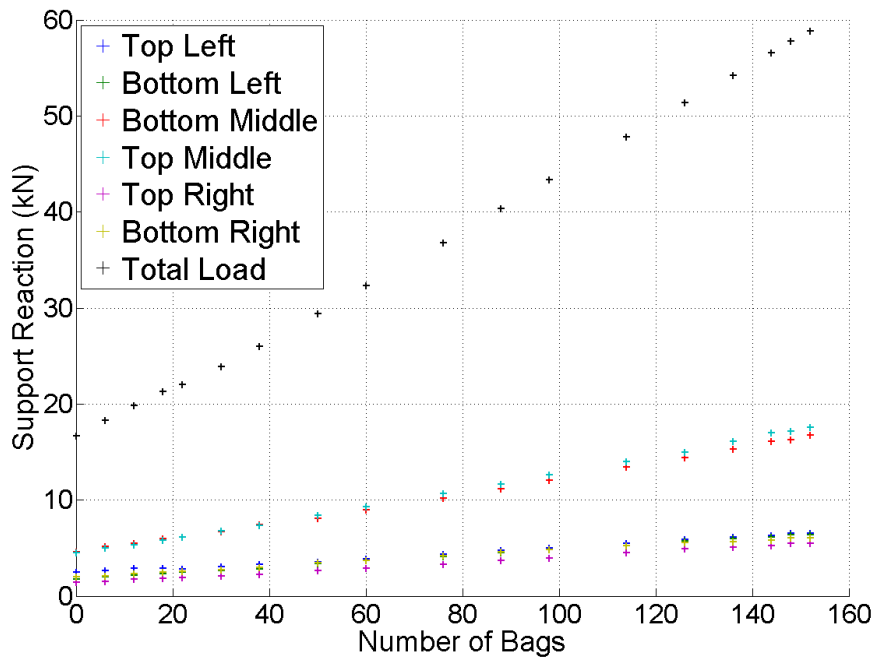
For both the static and dynamic tests, an imposed load was slowly added to the slab's surface by means of sand and gravel bags. Each bag had a nominal mass of 25kg and the position of each bag was arranged to ensure the sample had a UDL whenever data was recorded, as well as preventing significant uneven loading between measurements. The increase in load to each support as bags were placed is shown in Figure 3.4 from the corner column loss tests. The pre-loading period for the dynamic test to create the required UDL before column removal is plotted in Figure 3.4(a). The lin-

ear relationship, $R^2 > 0.995$, demonstrates that throughout the test the distribution of the imposed loads to each support remained constant. Additionally, note the similar values for the corner locations (Top Left, Bottom Left, Top Right and Bottom Right) and the two middle positions indicating the slab was balanced correctly. For the static test (C-S), with one support removed, the increases in forces are given in Figure 3.4(b). Again, the constant gradient with R^2 values between 0.927 and 0.999 demonstrates the loading was placed evenly. The same layout of bags was applied for each test and all gave similar responses, therefore these figures are not repeated for each case.

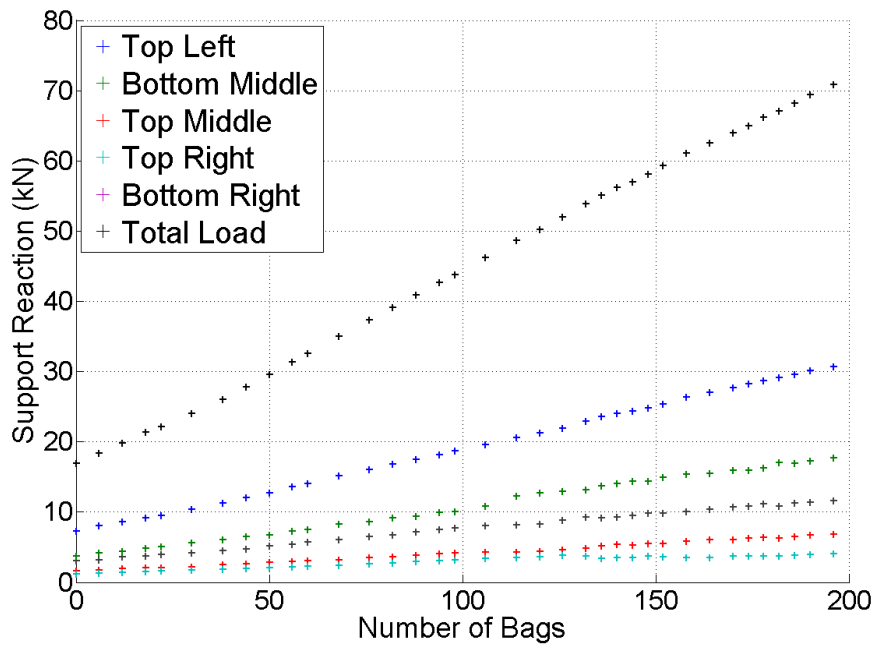
For the dynamic removal tests, the high speed footage was analysed to estimate the time taken for the support to be removed (see Figure 3.5). The small size and lack of contrast of the temporary support meant the DIC software could not provide accurate tracking. Therefore removal time was taken to be the period between the rope attached to the support becoming taught with the bar starting to move (Figure 3.5(a)) and the moment that either the bar was clearly disengaged with the support plate, or the plate was no longer in contact with the slab (Figure 3.5(b)). Due to the subjective nature of this approach, estimations were repeated to give a range of uncertainty. However, this method is likely to overestimate the removal time, as it does not take account of the condition where the support plate and slab remain in contact, moving vertically at the same rate whilst not transferring forces. A summary of removal times for each test is given in Table 3.5.

Additionally, the HSC footage allowed the response of the dead loads to be observed after the support was removed. As the bags were loose and not attached to the slab surface a sudden, large motion could cause the bags to separate and not remain in contact. This would then change the response of the slab, firstly its mass and loading would be temporarily different and secondly, the bags would apply an impact load when they regained contact. From considering the available recordings, no evidence of separation between slab and the load was seen. One exception to this however was test PR-D, after the support was removed a shear crack formed resulting in a second sudden drop in the slab. As this occurred, the bags around this area could be seen to move at a different rate to the slab deck.

Table 3.6 on page 47 provides a summary of all seven tests. It describes the maximum loading and deflection achieved, whether shear failure occurred and if this led to further failures.

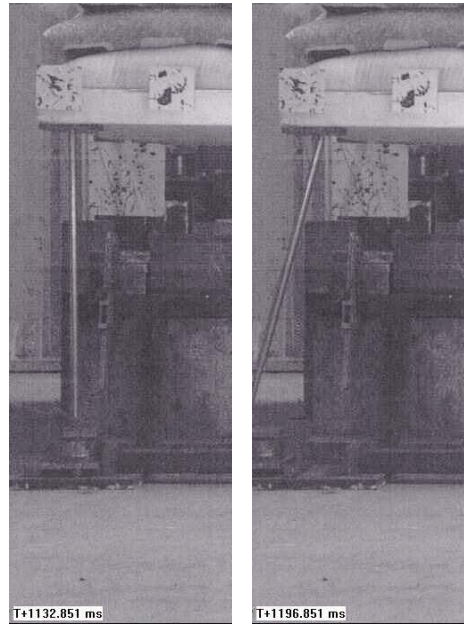


(a) Dynamic test - pre loading



(b) Static test

Figure 3.4: Support reactions as sand/gravel bags are applied - Tests C-D (a) and C-S (b)



(a) Fully supported (b) Column removed

Figure 3.5: Images from the HSC for test C-D, with 6.8kN/m^2 of loading, to estimate column removal time**Table 3.5:** Estimated column removal times for each test

Slab ID	Loading Level (kN/m^2)	Estimated time (ms)	Uncertainty (ms)
C-D	3.0	53.2	± 10
	6.8	57.0	± 13.4
	7.7	50	± 17.6
PC-D	2.5	40	± 10
	5.6	50	± 10
PR-D	2.3	52.5	± 22.5
	5.7	39	± 18.2
M-D	3.1	33.7	± 13.9
	6.7	49.2	± 11.6
	8.5	42.6	± 3
Average		46.7	

Table 3.6: Summary of test results giving details of shear failures

Slab ID	Max loading (kN/m ²)	Max displacement (δ /slab depth)	Shear failure	Loading type at failure	Initial location	Further failure
C-S	8.2	1.08	No			
C-D	>7.7	1.54	Yes	Static push down ^a	Back left corner	Bottom middle
PC-S	6.4	2.23	No			
PC-D	6.8	1.71	Yes	Static ^b	Front left corner	
PR-S	6.7	1.67	Yes	Static	Front left corner	Front right corner
PR-D	5.7	2.12	Yes	Dynamic	Front right corner	Front left corner
M-D	9.2	0.74	No			

^a After the final dynamic test a large load was applied over the removed corner to cause complete failure.

^b After the final dynamic test, loading changed to a static UDL.

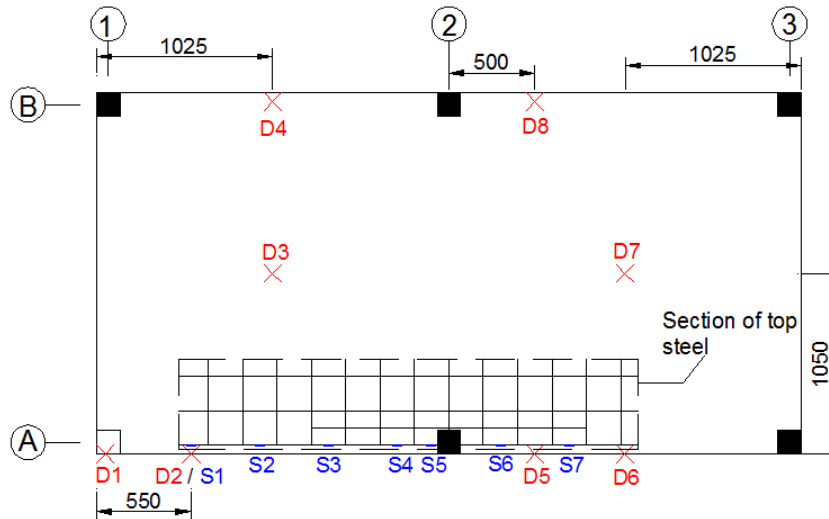


Figure 3.6: Locations of LVDTs and visual targets (D), strain gauges (S) and grid markings for tests C-S and C-D

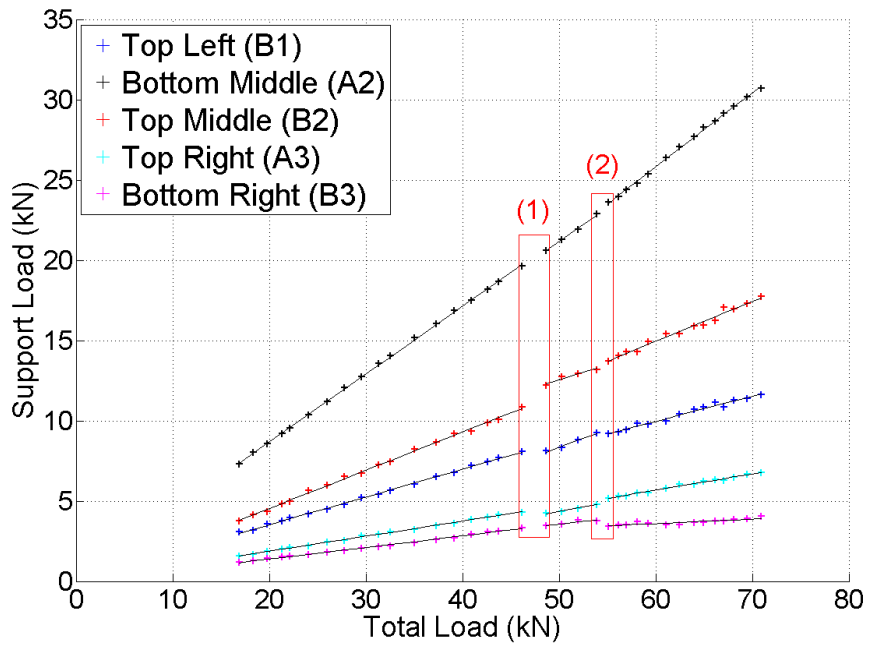
3.3.1 Corner column loss

Figure 3.6 provides the location of the presented monitoring points for tests C-S and C-D. This includes displacement readings (designated with D) taken from both LVDTs and camera footage, usable strain gauges data (designated with S) and the grid reference system to identify support locations and their associated load cell readings.

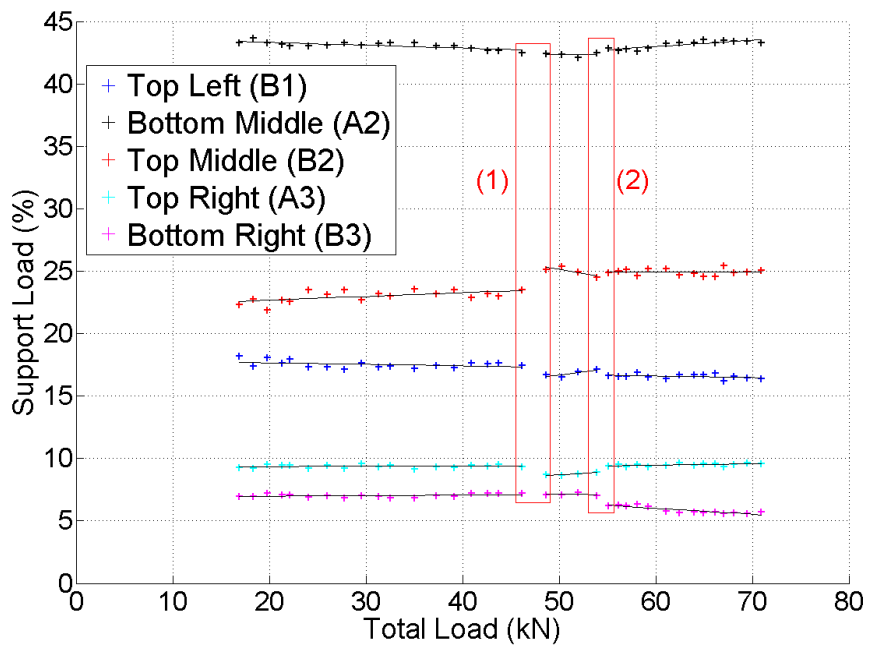
The results from the two tests conducted on the corner removal slabs, static and dynamic, are presented separately below.

Static loading test

Figure 3.7(a) shows the vertical reactions at the supports during the corner static test (C-S). As was expected, the reaction forces increased linearly by increasing the total load in the elastic range, with a goodness of fit above 0.996. However, beyond 46.2kN total load (5.4kN/m^2) there was a change in response (Label 1) until approximately 55kN (6.4kN/m^2), coinciding with the formation of cracks across the slab. Past this phase (Label 2) there is another linear response, though with a larger deviation from the trend line. From the changes in gradient for the two phases, presented in Table 3.7, along with relative distribution of forces to each support given in Figure 3.7(b), it is noted that the relative demand stays fairly constant in the elastic and final ranges. Between labels 1 and 2 there is again a noticeable change whilst redistribution occurs. However, considering the full range demonstrates that the total deviation from the linear relation is not great.



(a) Vertical reaction to each support

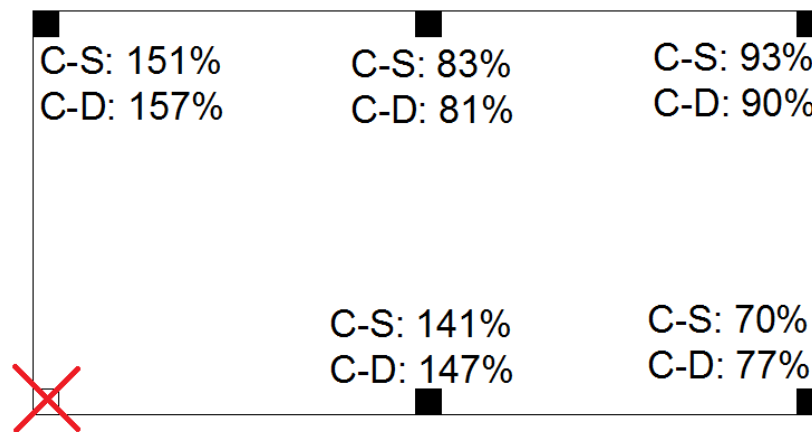


(b) Percent of total load to each support

Figure 3.7: Distribution of forces to supports - Test C-S

Table 3.7: Fraction of force to each support as total load increases - Test C-S

Position	Gradient from Figure 3.7(a) (kN/kN)			Relative change
	Full range	16–46 kN	55–71 kN	
Top Left (B1)	0.159	0.173	0.157	-0.09
R^2	0.998	0.998	0.982	
Bottom Middle (A2)	0.432	0.424	0.463	0.10
R^2	0.999	1.000	0.998	
Top Middle (B2)	0.262	0.237	0.249	0.05
R^2	0.997	0.998	0.985	
Top Right (B3)	0.051	0.072	0.029	-0.60
R^2	0.931	0.996	0.714	
Bottom Right (A3)	0.095	0.094	0.102	0.08
R^2	0.994	0.998	0.987	

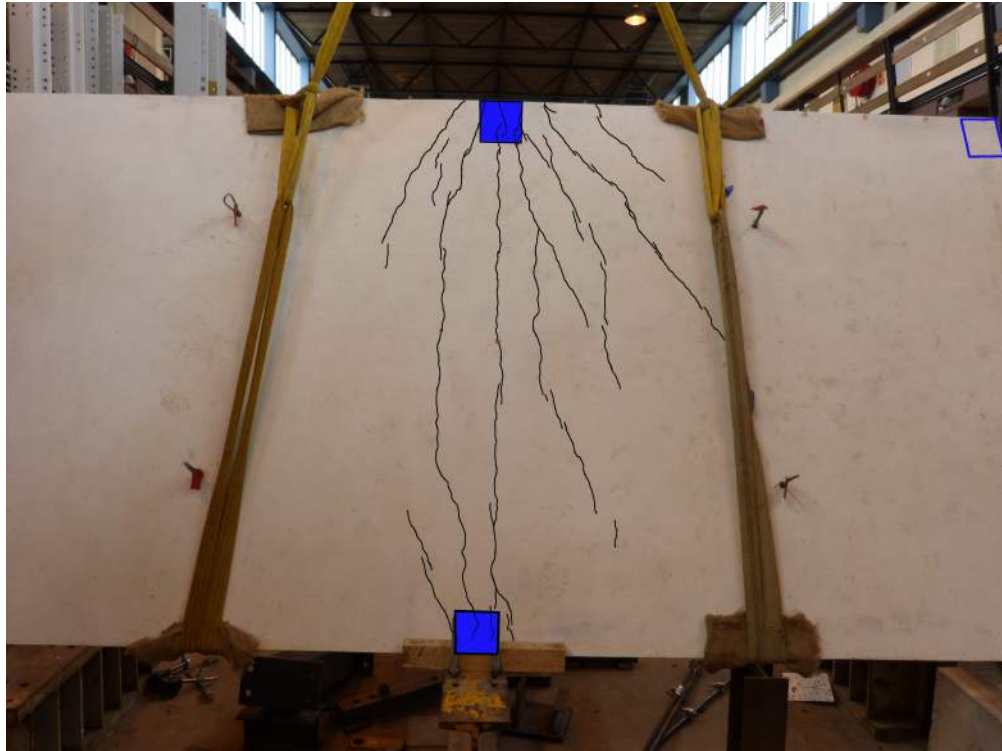
**Figure 3.8:** Mean change in distribution of forces to each support after corner column loss - Tests C-S and C-D

Comparison between the averaged reaction forces for fully supported and damaged conditions, see Figure 3.8, indicates that the two orthogonally adjacent supports experience a 41-57% increase in their vertical reaction while all other supports had a decrease in demand. It should be noted that C-S and C-D showed similar ratios, indicating dynamic removal did not change the final distribution of reaction forces.

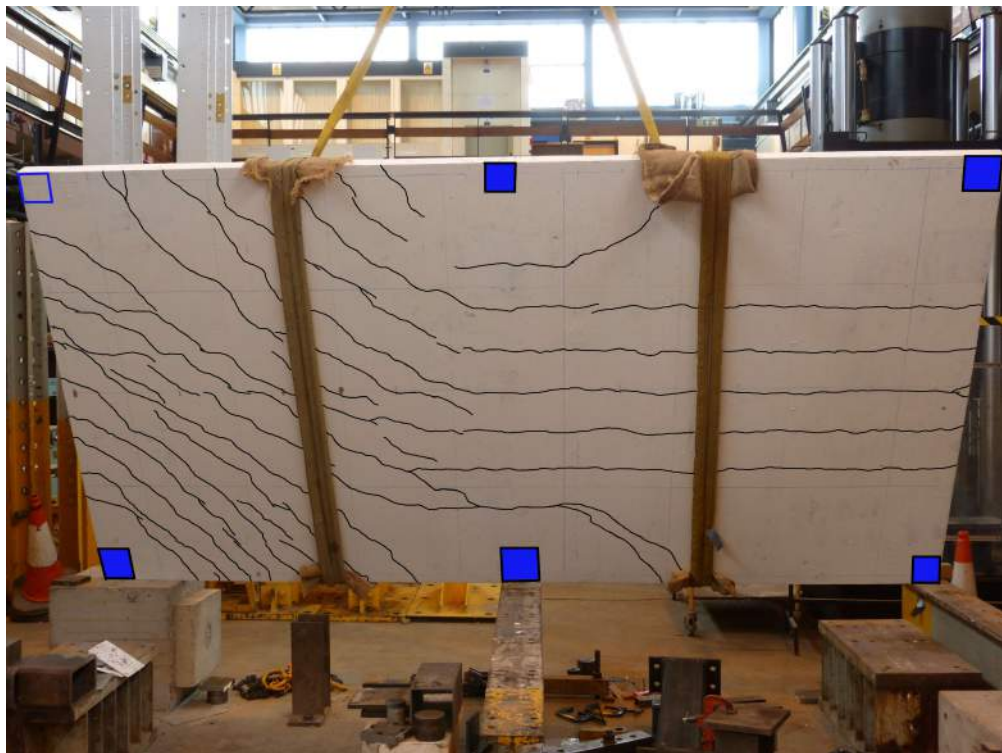
At higher levels of loading significant flexural cracks formed due to the large increase in hogging moments in both tests; this was primarily on the top surface (Figure 3.9(a)). Sagging flexural cracks also formed on the underside as the slab now spanned diagonally between the two supports nearest the removed location (Figure 3.9(b)). The location of permanent supports (solid boxes) and the removed support (outline) are annotated in this figure.

The normalised deflections (displacement/slab depth) against load in the damaged bay area (Figure 3.10(a)) show an initial linear response. However after 4.6kN/m^2 , flexural cracks started to form resulting in a decrease in stiffness to around 57% of the initial value. At 6.0kN/m^2 , when the peak displacement equalled 0.19 times the slab depth, there was a discontinuity due to significant cracking over the adjacent support along with yielding of the reinforcement. At this point there was an increase in displacements across the entire sample, with the maximum exceeding half the slab depth. After this, there was a brief stiffening phase before a final softening with a relative stiffness of 6% of the elastic range. The slab continued to carry additional load until the test was aborted at 8.2kN/m^2 . In the adjacent bay shown in Figure 3.10(b), once damage occurred there was a jump in response observed in the middle (point D7, Figure 3.6) due to the flexural sagging cracks in that area. The high deflections in the damaged area also led to a relative uplift due to the large rotation around the central support (point D5). The discontinuous response corresponds to the changes in reaction forces seen in Figure 3.7, as discussed in the previous section.

The strain data in Figure 3.11 provides a further understanding of the damage profile. Strain readings have been adjusted against the fully loaded condition under the slab's own self weight and normalised against the yield strain. Below 4.1kN/m^2 , strains on the steel over the central column were relatively low. However, after the formation of flexural cracking, the top reinforcement strains increased significantly and, as further displacement occurred, there was a peak in strain on the damaged side of the support. As loading increased there was local yielding of the reinforcement in this area, while other areas stayed minimal.

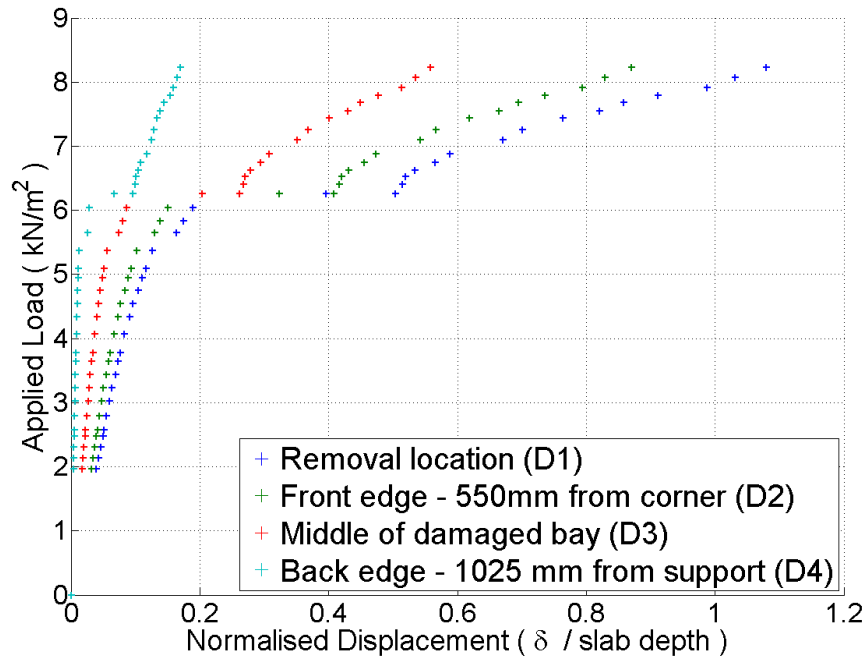


(a) Top surface

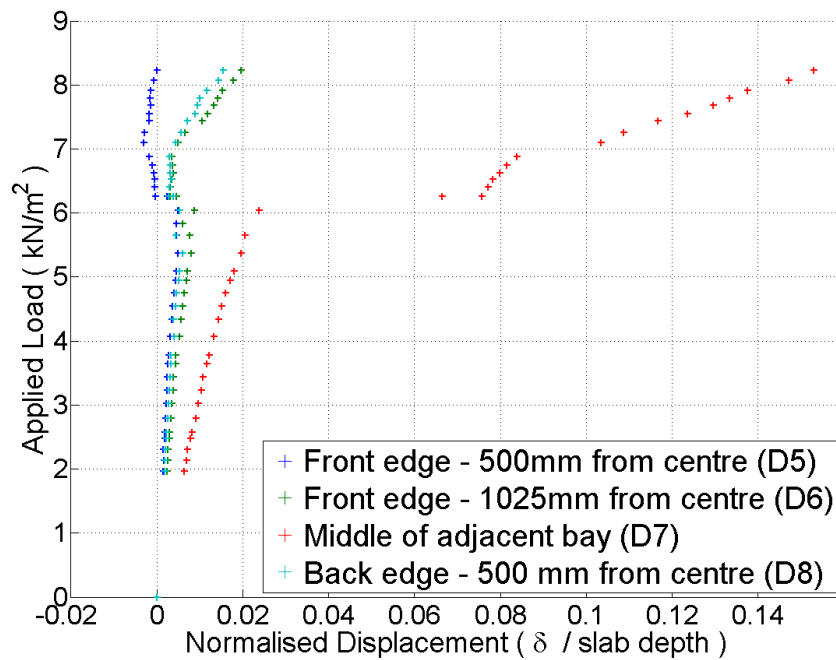


(b) Bottom surface

Figure 3.9: Annotated flexural cracks after corner column loss



(a) Displacements in the damaged bay



(b) Displacements in the adjacent bay

Figure 3.10: Load against normalised displacements - Test C-S

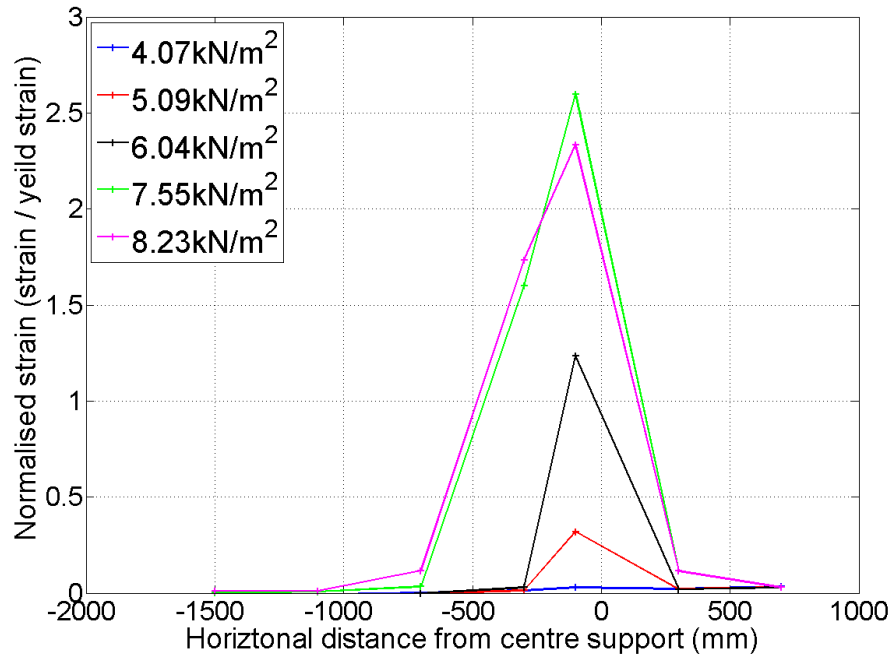


Figure 3.11: Normalised strain against position for top reinforcement bars - Test C-S

Dynamic removal test

The normalised displacements for dynamic removal at three different levels of loading are plotted in Figure 3.12 for the removal location and the middle of the adjacent bay (Points D1 and D7 in Figure 3.6). The frequency spectrum from a Fourier transform is also given in Figure 3.13 for each of the load cases. Peak displacements, damped natural frequency and damping ratio results for these tests are compared in Table 3.8.

At 3.0 kN/m^2 the structure was within the elastic range resulting in small deflections (7% and 5% of slab depth for peak and final displacements respectively). The low total mass resulted in a higher frequency response, while as no damage occurred, there was little dissipation of the energy. The low damping ratio ($\zeta = 0.01$) caused the system to take several seconds to return to equilibrium. The specimen was then reset back to starting position and the load increased to 6.8 kN/m^2 , just within the plastic region from the static condition. Much higher deflections, peaking at almost 60% of the slab depth, were measured. Low levels of cracking were observed which resulted in a higher energy dissipation and a larger damping ratio ($\zeta = 0.24$); overall damage was not extensive. For the final case the load was increased to 7.7 kN/m^2 and the test repeated. Figure 3.13 shows the power density spectrum of displacement following a corner column loss at different load levels. The results indicate for the slab in the

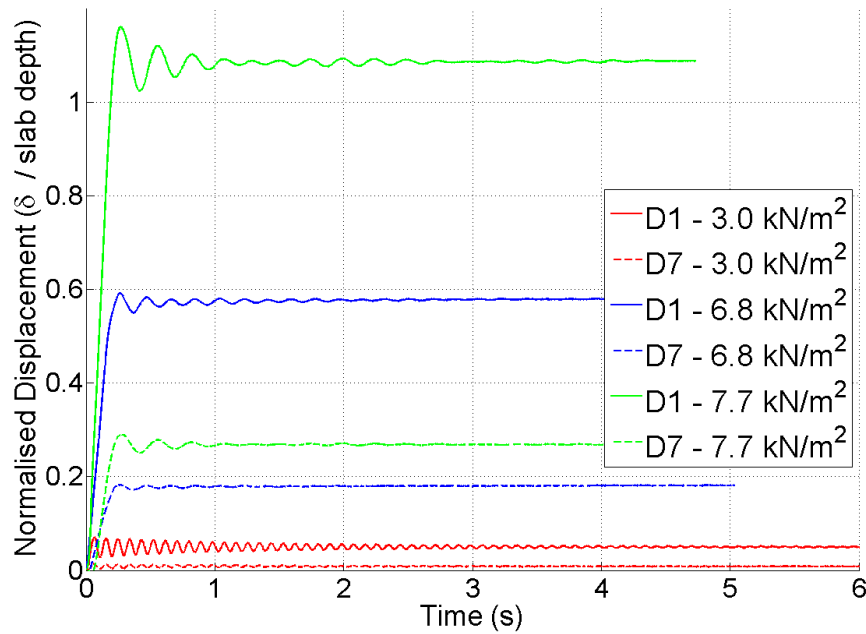


Figure 3.12: Normalised displacement against time after column removal at different positions and loading - Test C-D

plastic region (i.e. 7.7 kN/m^2), the large deflections and resulting damage created a different response to the single dominant frequency peaks seen before. In this case, peak deflections exceeded 110% of the slab depth but did not lead to complete failure.

Within the elastic range the amplitude between the first peak and first dip is 60.7% of the maximum displacement, indicating the structure returns relatively close to its starting state. Once permanent damage occurs both these ratios drop considerably as seen in Table 3.8.

A Short-Time Fourier Transform (STFT) of the signal was conducted for the highest loading case and the distribution of power with frequency and time is given in Figure 3.14. The two frequencies detected from the standard Fourier transform are also plotted. The contours suggest there is a change in frequency response during the test. Up to around 1 second the lower frequency dominates, however, this quickly decays and is replaced with the 4.21Hz response. The cracking and damage that occurred during the 6.8 kN/m^2 test may have resulted in the relative reduction in damping ratio observed at 7.7 kN/m^2 (Table 3.8) and been a factor in the two frequency response. Additionally, the large drop in the slab after support removal may have caused a slight separation between the bags and the slab surface. This would reduce the mass slightly for the first oscillation and therefore lead to a lower frequency which is then corrected as the am-

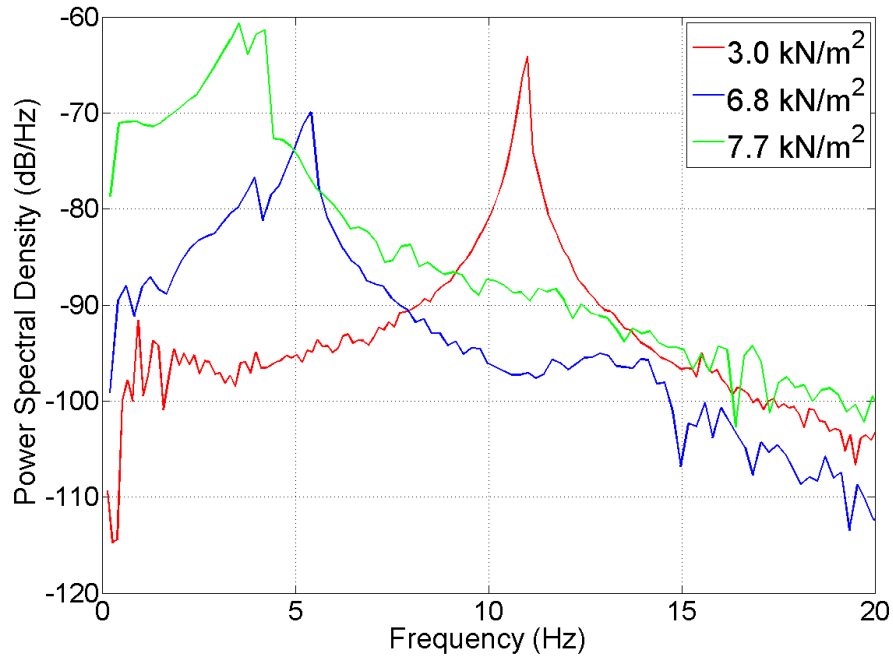


Figure 3.13: Power spectral density of displacement following corner column loss at different load levels - Test C-D

plitude of motion drops and the loading bags move in contact with the slab. However, this effect is still very small and should not influence the results significantly.

The strain data collected during a dynamic removal also allowed estimation of the strain rates, $\dot{\varepsilon}(t)$, occurring at those positions on the steel bars. This was calculated with Equation 3.3.1 where $\varepsilon(t)$ is the strain at time t and t_p is the sampling period of the data equal to 4ms.

$$\dot{\varepsilon}(t) = \frac{\varepsilon(t + t_p) - \varepsilon(t - t_p)}{2t_p} \quad (3.3.1)$$

Table 3.8: Results from dynamic removal - Test C-D

Loading (kN/m ²)	3.0	6.8	7.7
Normalised Peak	0.07	0.59	1.16
Amplitude / Peak (%)	60.7	7.36	11.91
Peak / Final Displacement	1.42	1.02	1.07
Damped Natural Frequency (Hz)	11.0	5.41	3.54/4.21
Damping Ratio	0.01	0.24	0.123

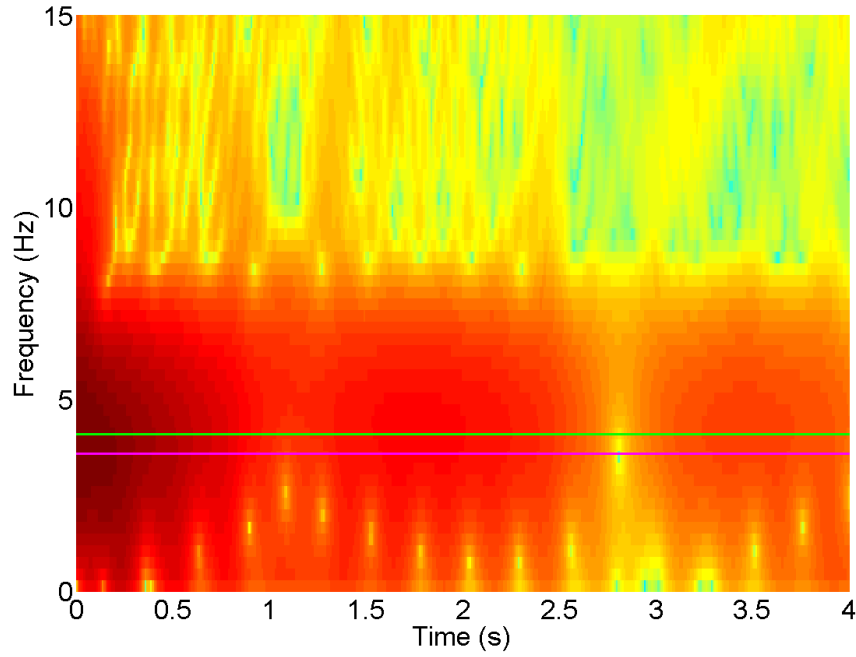


Figure 3.14: STFT for displacements at column removal location for 7.7kN/m² - Test C-D. Magenta and green lines show 3.54Hz and 4.21Hz respectively

The tensile strain rates against time for the top steel are presented in Figure 3.15 for the three loading levels. Each graph shows the maximum strain rate that occurred at any monitored position, at each time step, according to Equation 3.3.2. Here i is the index of a strain gauge and n is the total number of gauges monitored.

$$\dot{\epsilon}_{max}(t) = \max_{i=1}^n \dot{\epsilon}_i(t) : \text{for each } t \quad (3.3.2)$$

Strain gauge S5, positioned next to the central support, see Figure 3.6, experienced the highest strain demand with the quickest rate in each loading level. As this hides the condition at other locations, a second line is plotted excluding this sensor. Additionally, the key strain data with time, adjusted against the strain readings at the fully support condition, is also plotted on the second vertical axis to allow further comparisons.

In Figure 3.15(a), the elastic case, most the sensors on the top steel show very low levels of strain rates, with only sensor S5 showing a strong peak. However, it is clear that the peak strain occurs a period of time after the peak strain rate. This is significant in considering the influence of strain rate effects in increasing the material tensile capacity during sudden column losses and will be discussed further in the next chapter. At 6.8kN/m² of loading, shown in Figure 3.15(b), a similar pattern is seen, however there

is still a reasonable peak at other locations. Overall, high strain rates are observed here with a maximum rate of 0.153s^{-1} occurring just before the maximum strain. The change in maximum strain from the fully loaded to final case suggests that the steel has yielded in this area; this may explain the localised high strain rate and also affect the final results.

The final loading case presented in Figure 3.15(c) shows a different response. While the largest strain rate again comes from sensor S5 (next to the central support), the rates and change in strains are smaller than the previous case. This is most likely due to the plastic deformations that occurred. Of further interest is sensor S3, see Figure 3.6, for its location. As this position was previously closer to the middle of the span, it was under a compressive condition and then changed to a tensile state due to the column loss. This change demonstrated itself by a delay in response before the large tensile deformations occurred leading to large permanent strains. The peak rates were 0.031 and 0.034s^{-1} .

Finally the sample was loaded to failure, which occurred due to punching shear at the two adjacent supports as shown in Figure 3.16.

3.3.2 Penultimate column loss

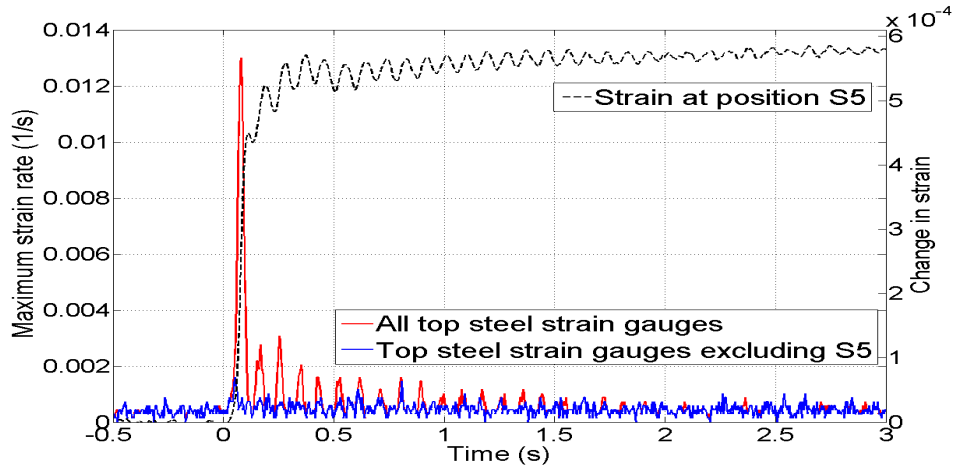
The results from the Penultimate removal tests are presented in this section. Both the continuous and reduced reinforcement cases are treated together to allow a direct comparison to be made. The locations of the relevant instrumentation and grid markings are given in Figure 3.17.

Static loading test

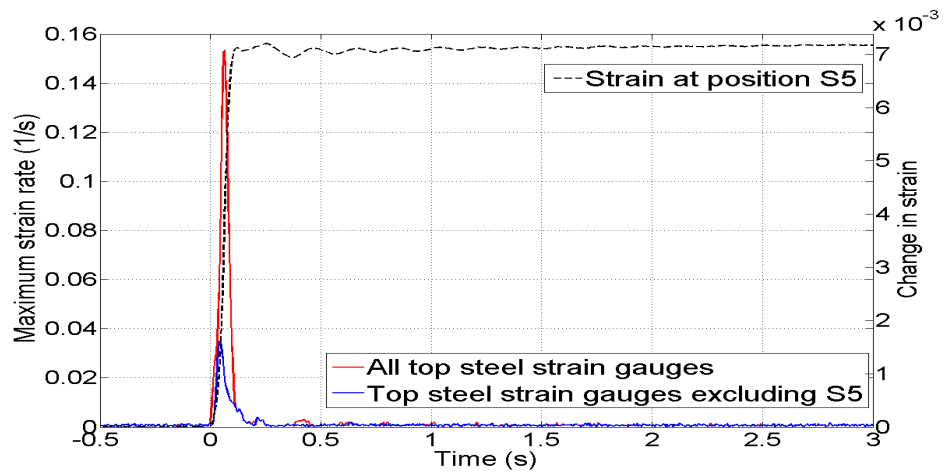
The load increase to each support, for the two Penultimate removal cases with static loading, are shown in Figure 3.18(a). Similar responses are observed for the two conditions with nearly all points showing a simple linear response at low loading at equivalent rates. The back middle support takes the highest proportion of loading, followed by the front corners.

Flexural cracking occurred at 35kN and 30kN of total load, for PC-S and PR-S respectively, which was followed by a period of redistribution of reaction forces across the samples until approximately 45kN, between labels (1) and (2). After this stage the distribution remains reasonably constant until failure.

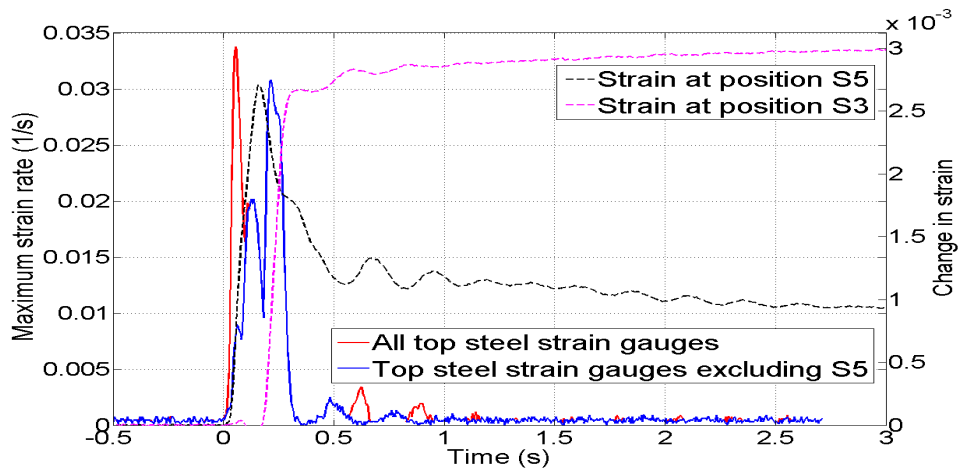
The primary change in support reaction distribution occurred due to uplift at the back



(a) 3.0 kN/m² loading



(b) 6.8 kN/m² loading



(c) 7.7 kN/m² loading

Figure 3.15: Maximum strain rates against time. Also showing changes to peak strains. Test C-D



Figure 3.16: Final state of corner removal case after shear failure - Test C-D

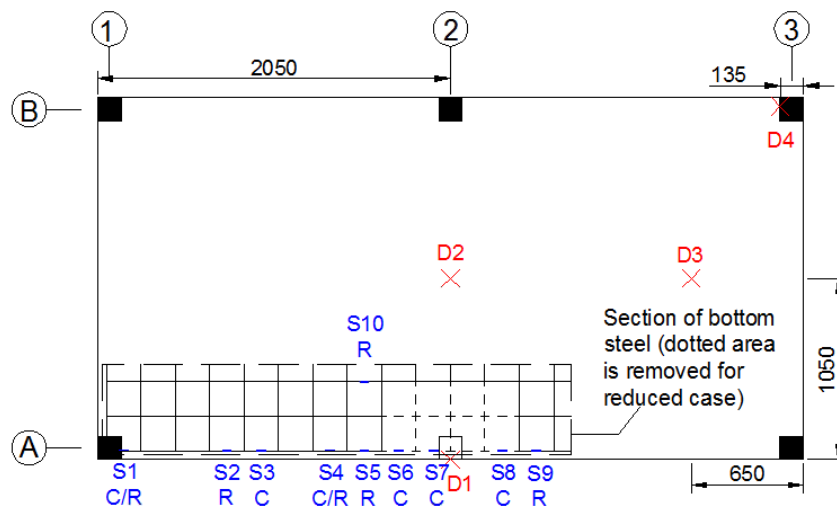
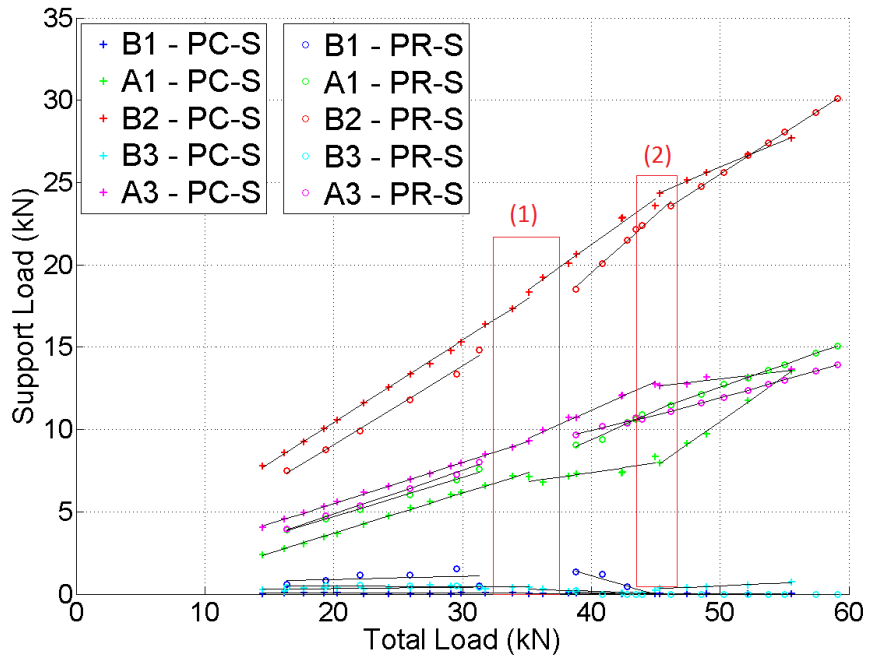
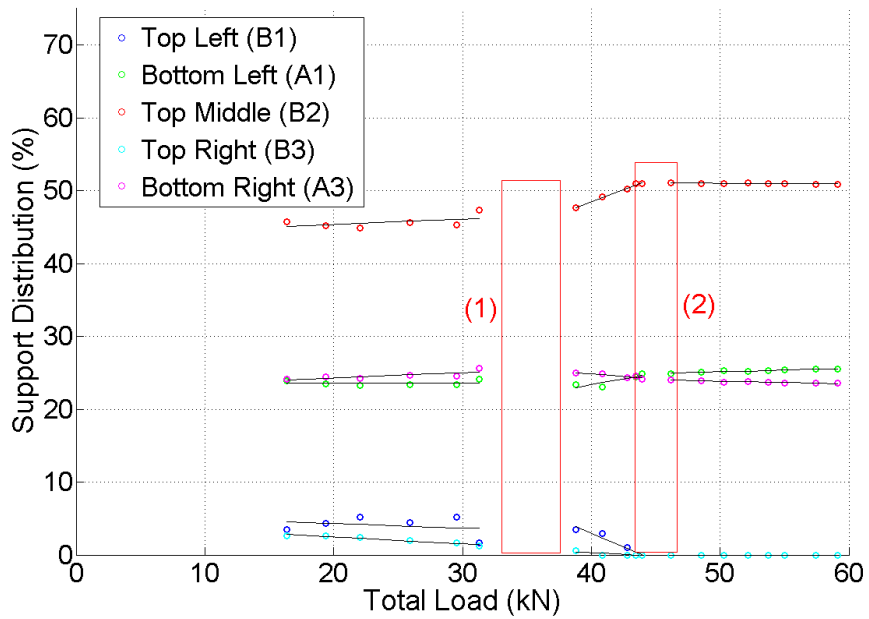


Figure 3.17: Locations of LVDTs and visual targets (D), strain gauges (S) and grid markings for penultimate removal conditions - Continuous (C) and Reduced (R)



(a) Vertical reaction to each support - Tests PC-S and PR-S



(b) Percent of total load to each support - Test PR-S

Figure 3.18: Distribution of forces to supports - Tests PC-S and PR-S

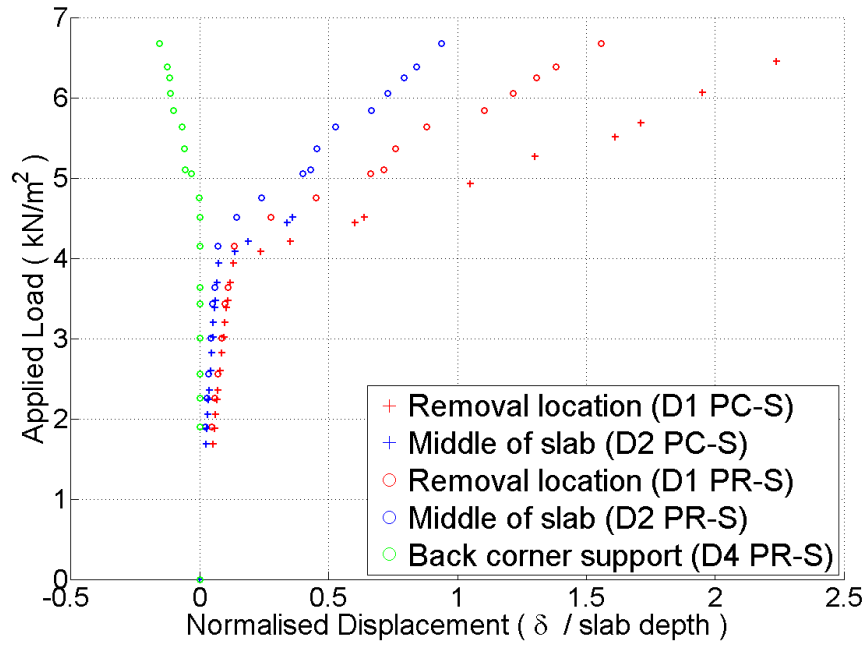


Figure 3.19: Load against normalised displacement for PC-S and PR-S

two corners, as a result of the large deflections in the middle. Therefore, the little load they were carrying was taken by the other supports, primarily the back middle (see Figure 3.18(b)).

The load in position A1 in PC-S shows a more dramatic change. This was due to the load cell rotating at higher deflections, an issue that was corrected for other tests and does not indicate a change in loading on the support.

Deflections of PC-S and PR-S are given in Figure 3.19 for the positions identified in Figure 3.17. It is clear that there is linear response across all parts of the slab before cracking occurs. Additionally, the initial stiffness of the two reinforcement cases are identical. Both cases start to crack at similar points, with a slight reduction in stiffness observed after 3.4 kN/m^2 . This corresponds to a peak normalised displacement of 0.1. However, after peak displacement of 0.13 times the depth, there is a significant reduction in stiffness due to more extensive flexural cracking. Table 3.9 compares the relative stiffnesses at each position between the initial state and the post cracking response. As a result of the damage, the stiffness at all the locations is less than 5% of the elastic range. Additionally, the R^2 values demonstrate that the post cracking range still shows a strong linear relationship. However, the results also demonstrate the uplift effect experienced at the back support after 5 kN/m^2 (point D3 in Figure 3.17). This effect coincides with an apparent change in the displacement response for test PR-S, indicating

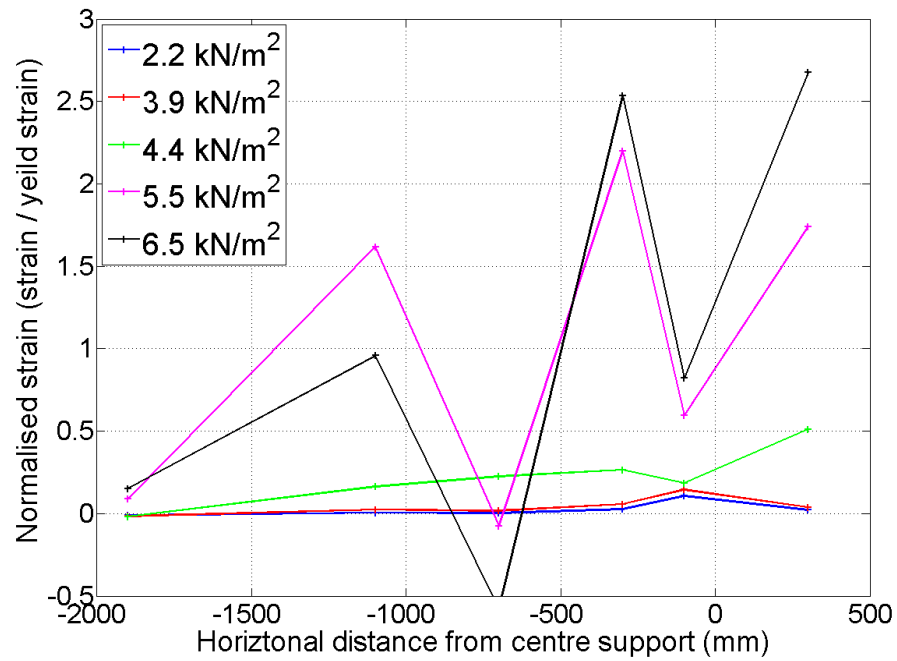
Table 3.9: Comparison of stiffnesses after cracking - Test P-S

Test	Position	Stiffness ratio (%)	Post cracking R^2
PC-S	D1	3.6	0.993
	D2	2.9	0.990
PR-S	D1	4.9	0.991
	D2	4.2	0.991

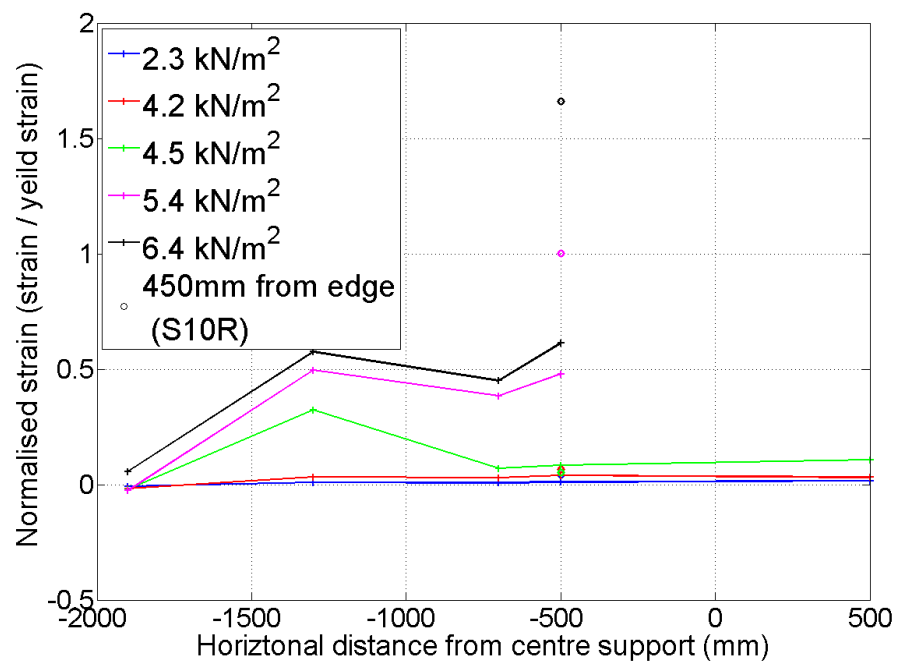
that the linear model may not be the most suitable, despite the high coefficient given in Table 3.9.

Test PR-S experienced a sudden shear crack of the front left support at 6.7kN/m^2 . As soon as this occurred, the second front corner support also failed by shear (see Table 3.6). The rotation of the load cells, and therefore support conditions, for the continuous reinforcement test resulted in the higher deflections whilst not inducing the usual shear stresses that would accompany a partially restrained support and therefore did not lead to shear failure.

Figure 3.20 shows the strain profiles of the bottom reinforcement bars for tests PC-S and PR-S. The location of the strain gauges are shown in Figure 3.17. For the continuous reinforcement case, the middle area ($\pm 500\text{mm}$ from the removed column) has the highest stress when the loading is less than 4.5kN/m^2 (see Figure 3.20(a)). However, once cracking starts, there is a significant change in the stress distribution and yielding occurs across much of the length of the monitored bar. The drops in values can be explained by local variation in stress due to the effect of concrete de-bonding around the steel. Removing the central bottom flexural steel from the column location ($\pm 400\text{mm}$ from the centre) results in a different response (see Figure 3.20(b)). Note that beyond 4.5kN/m^2 the strain gauge at 500mm (gauge S9R) failed and its values have been removed. Due to the non-continuous state of the reinforcement, smaller stress was observed at equivalent loading and positions; none of these steel bars yielded. However, an extra position at -500mm horizontal distance and 450mm away from the edge (gauge S10R), is shown (marked with o's). This sensor was on the first bar that is continuous along the length and did yield. Strain gauges on the top surface of the concrete, along with visual inspections, demonstrated that the concrete never crushed.



(a) Continuous reinforcement - Test PC-S



(b) Reduced reinforcement - Test PR-S

Figure 3.20: Normalised strain against position for bottom reinforcement bars

Dynamic removal test

Under the dynamic condition, for test PC-D, the deflections against time at 3 locations for a UDL of 5.6kN/m^2 are shown in Figure 3.21. At the removal location there is a strong peak in deflection, followed by a low frequency oscillation, until it quickly finds an equilibrium state. Also under this condition, the back corner support experienced uplift, emphasizing further the change in distribution of loading to each support as a result of the column loss. However, this uplift did allow the slab to rotate inwards and experience higher deflections than would have occurred had the supports been restrained. This indicates that two mechanisms control the deformations, a pivoting effect causing the rotation and the formation of hinges at the damaged locations. This can be seen further with the monitoring point in the middle of the bay (point D3 in Figure 3.17). This position is in between the two areas of opposite movement (points D1 and D4) and is slower to respond to the column removal, as initially the majority of the deflection is a result of the rotating effect. As damage starts to occur, beyond peak deflections of around 0.1 times the depth, then point D3 also experiences downward deflection, although shows almost no oscillating motion and reaches its final position quicker than the other points.

After the support has been lost, the removal location and the back support oscillate at frequencies of 3.29 and 3.52Hz respectively. However, as the back support position becomes free it also vibrates at twice the primary frequency, as visible in Figure 3.22. Note the broad peaks in the frequency spectrum indicating the high damping ratio and dissipation of energy due to damage. As a result of the damage experienced, mainly due to sagging cracking on the underside, there are large deflections, with a peak value of 1.49 times the slab depth

The different loading cases, shown in Table 3.10, indicate that although 2.5kN/m^2 was within the elastic range for the static condition, there is evidence that the slab has now experienced damage. The values of damped natural frequency and amplitude to peak ratio are noticeably lower than were observed in the other tests (Tables 3.8 and 3.11). Additionally the damping ratio and normalized peak are higher than would have otherwise been expected if damage had not occurred due to the inertial effects taking the material past its elastic limit. However, the dynamic factors are still much less significant with higher loading (5.7kN/m^2).

The HSC captured the formation of cracks for the reduced reinforcement condition under dynamic removal with 5.7kN/m^2 of loading and this is shown in Figure 3.23. An extensive flexural crack initially occurred due to the lack of tensile reinforcement.

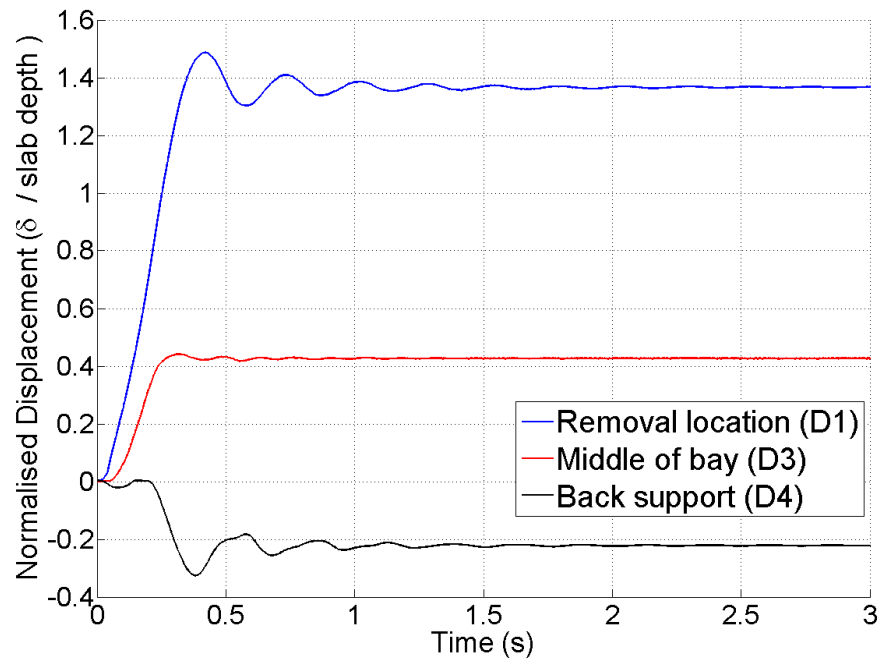


Figure 3.21: Displacement against time for PC-D at 5.6kN/m²

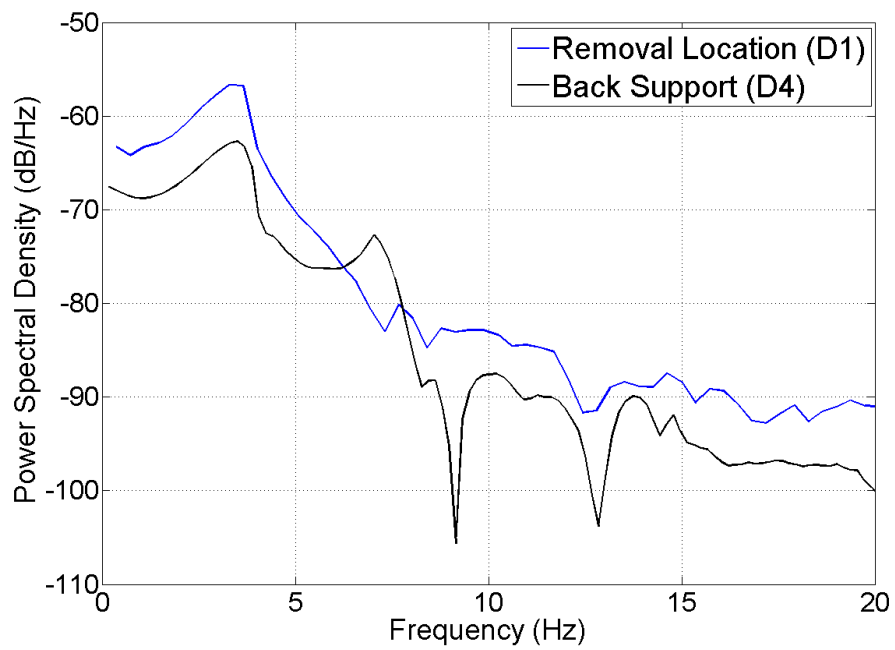


Figure 3.22: Power spectral density of displacement following corner column loss at different positions for 5.7kN/m² - Test PC-D

Table 3.10: Results from dynamic removal - Test PC-D

Loading (kN/m ²)	2.5	5.6
Normalised Peak	0.14	1.49
Amplitude / Peak (%)	44.3	12.36
Peak / Final Displacement	1.46	1.09
Damped Natural Frequency (Hz)	5.92	3.29
Damping Ratio	0.147	0.160



Figure 3.23: Failure of slab PR-D captured from the High Speed Camera - a) Flexural cracking; b) Shear crack

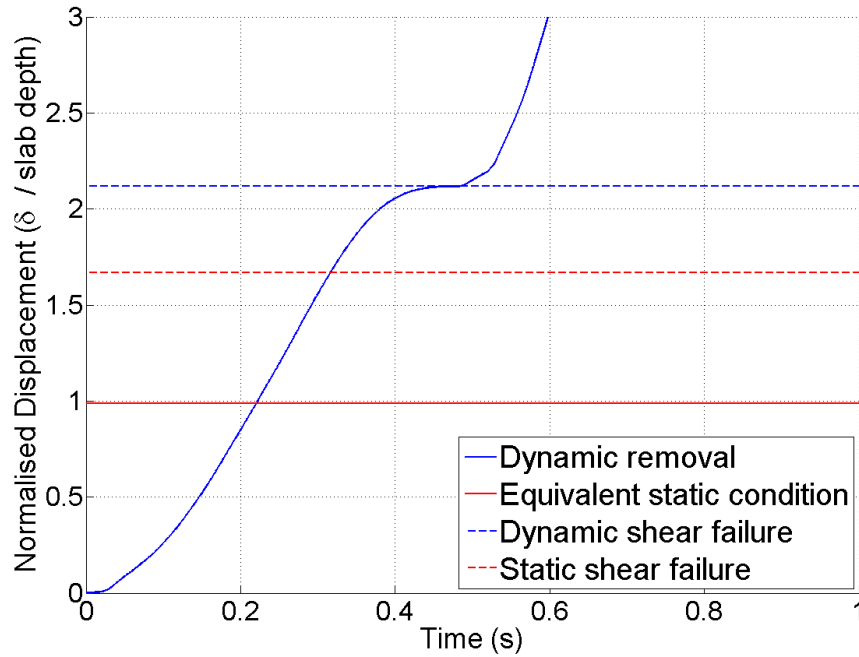


Figure 3.24: Displacement against time for PR-D, position D1 at 5.7kN/m^2

Then a final shear crack formed leading to complete shear failure, see Figure 3.23(a) and (b) respectively.

The normalised deflections with time for this test are plotted in Figure 3.24, along with the static case at equivalent loading, to demonstrate the increase in deflections experienced due to the dynamic effects. In the dynamic case there was a peak displacement of 2.12 times the slab depth, before the shear crack formed at 0.47 seconds. After this point the slab accelerated quickly downwards, as shown by the line continuing off the top of the graph. Comparing the results to the static test gives a dynamic displacement amplification ratio of 2.14 between the temporary maximum value at 0.47s and the static displacement at an equivalent loading. However, extrapolating beyond values from the static force displacement line (Figure 3.19) gives an equivalent force Dynamic Amplification Factor (DAF) of only 1.35, based on the assumption shear failure does not occur. The reduction in stiffness caused by the flexural damage may have caused the much higher deflections observed. Furthermore, the maximum vertical reaction at adjacent supports occurs as the slab reaches a temporary static condition at its maximum deflection. This delays the shear crack forming and potentially allows higher deflections to be reached. For further comparisons, details of shear failures are given in Table 3.6.

Considering the strain rate data for the two tests, shown in Figures 3.25 and 3.26,

demonstrates that fairly high strain rates occur after sudden column loss at the higher loadings, in the order of $0.2\text{--}0.3\text{s}^{-1}$. However, as was seen in the corner loss case, the peak strain, and therefore highest stress, in the material occurs after the maximum strain rate. Additionally at this point, the rate is often close to its minimum as the sample is at a temporary rest position between oscillations. Test PC-D in Figure 3.25 shows that the strain rates in the elastic test are relatively small, around 0.02s^{-1} . Furthermore, most the monitored points also had small strain rates even at the higher loading. However, strain gauge S3, see Figure 3.17, does show much higher values. This is to be expected from comparing to the static case in Figure 3.20(a) as that location clearly undergoes yielding. Of further interest is strain gauge S7, which was positioned at the support that was removed. This location quickly switches from a compressive, hogging state, to a sagging, tensile condition, which explains its quick strain rate immediately after removal. However, as further damage occurs across the slab this area becomes less critical.

Figure 3.26, showing strain rate data from test PR-D, gives a comparison between maximum strain rates and maximum strain. Additionally, the vertical line indicates the time at which the shear crack formed. Considering the two strain positions it can be seen that the sample had reached its maximum deflection and stress and was about to continue its oscillation when the slab failed due to shear. In this period, the strain rates were very low at all points across the slab.

The flexural cracks on the underside of the test specimens are shown in Figure 3.27. Permanent supports (solid boxes) and the removed support (outline) are shown. In both cases there are primary cracks spanning perpendicular to the new support arrangement. A section of the bottom reinforcement mesh is also annotated so that the orthogonal cracks in the middle area that follow the steel positions can be seen. This is especially pronounced in PC-D, while the diagonal cracks reach right to the centre line for the reduced case (PR-D). Also it is shown in Figure 3.27(b) that the cracks were non-continuous at the column loss location, and propagated around the edge of the column area following the reinforcement lines, rather than exploiting the lack of tensile reinforcement in the central area (c.f. Figure 3.27(a)). However these cracks were wider and deeper than other locations and tests. For all penultimate removal tests, there was only minimal hogging cracking on the top side running down the centre line, which was followed by shear failures on, one or both, of the front corner supports (see Table 3.6).

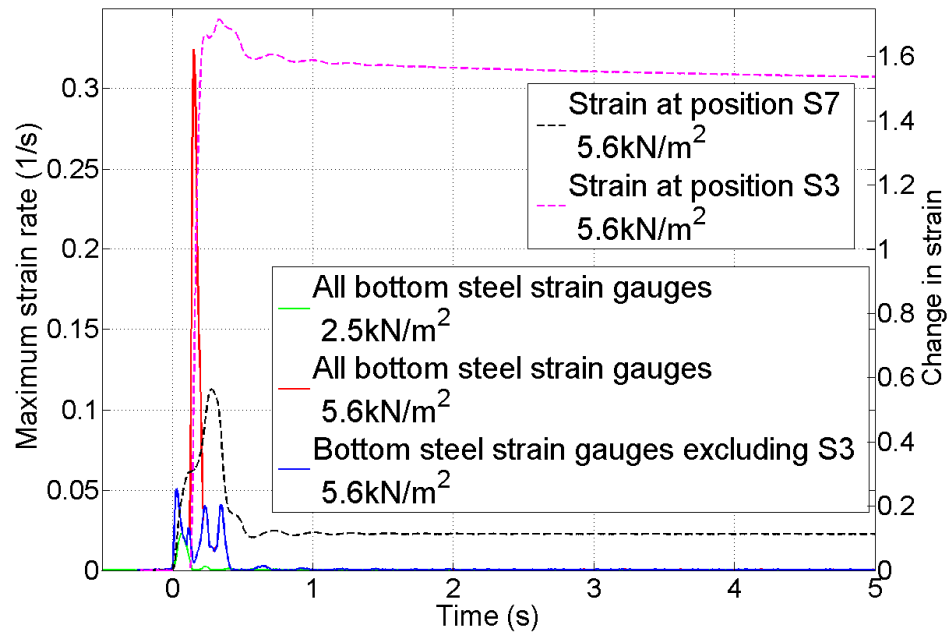


Figure 3.25: Maximum strain rates against time. Also showing changes to peak strains - Test PC-D

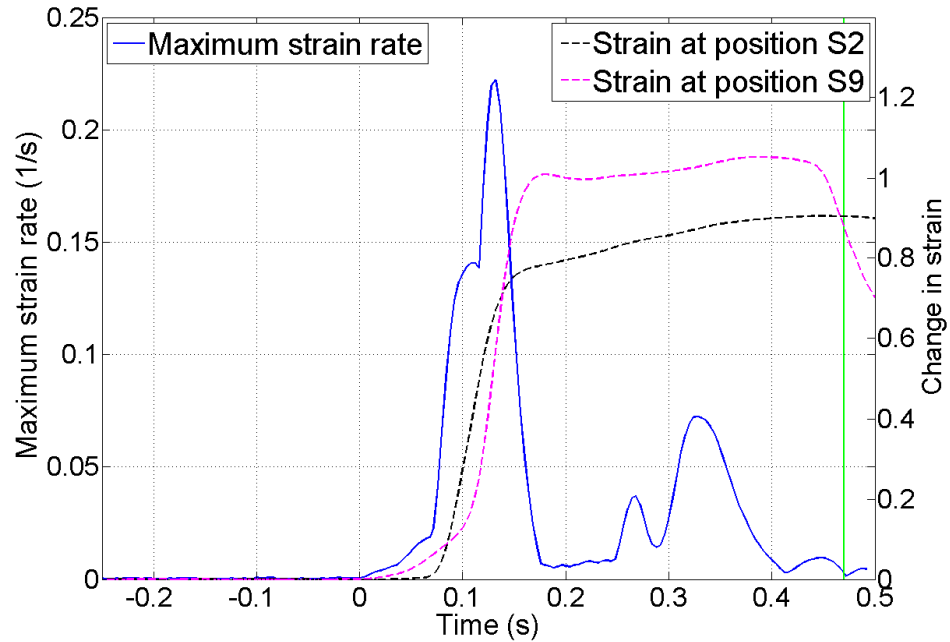
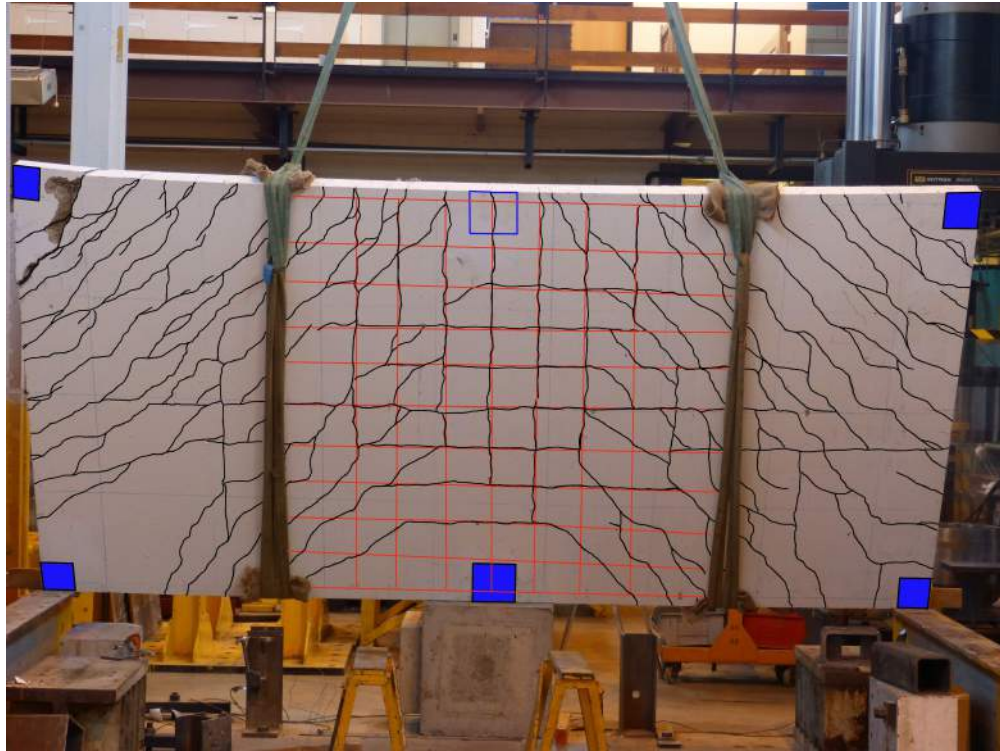
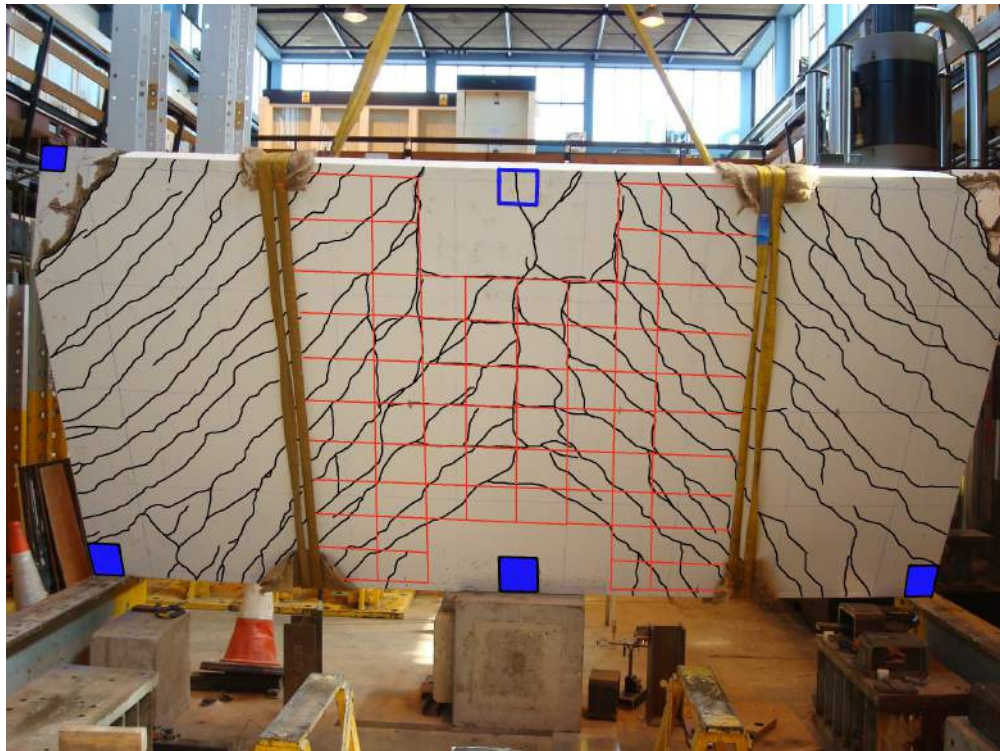


Figure 3.26: Maximum strain rates against time at 5.7kN/m². Also showing changes to peak strains and the point that a shear crack forms - Test PR-D



(a) Continuous reinforcement - Test PC-D



(b) Reduced reinforcement - Test PR-D

Figure 3.27: Annotated bottom surface flexural cracks and reinforcement after penultimate column loss



Figure 3.28: Test M-D loaded before sudden column removal

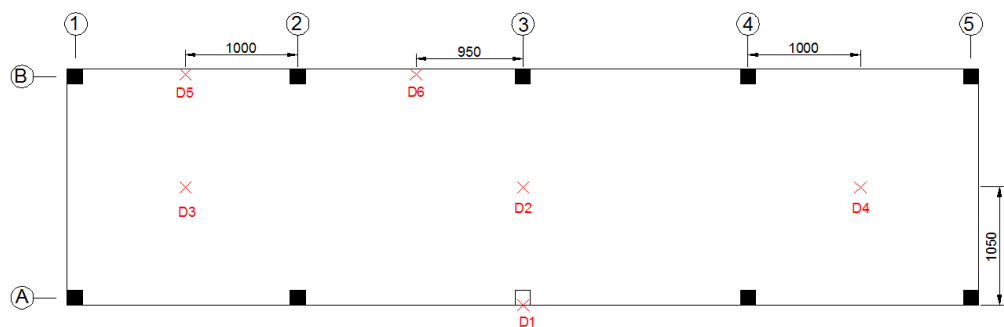


Figure 3.29: Locations of LVDTs and visual targets (D) and grid markings for middle column removal condition - Test M-D

3.3.3 Continuous slab

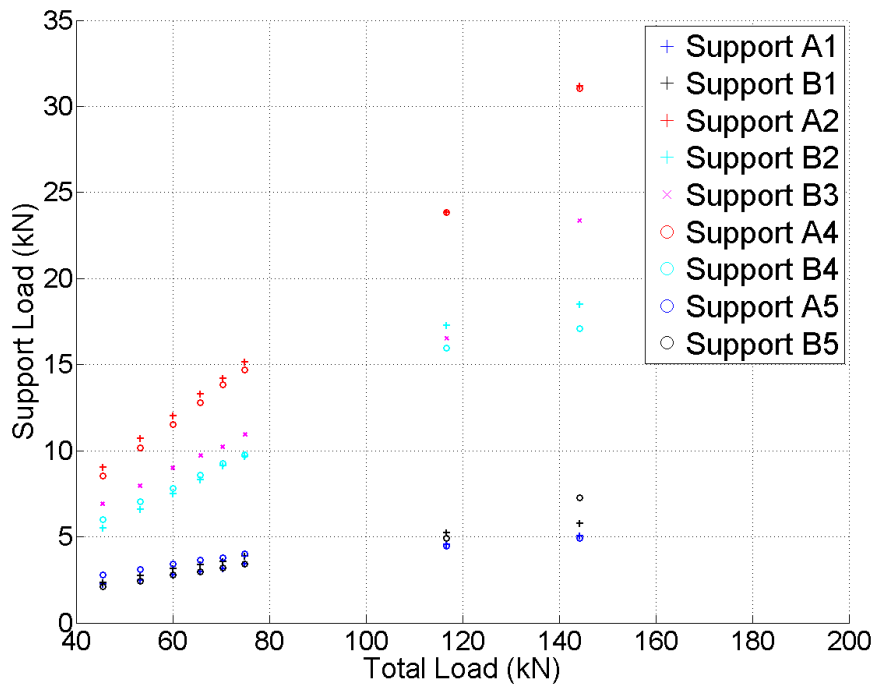
Figure 3.28 shows a photograph of test M-D, loaded and ready for testing. Although this slab was primarily used for dynamic tests, see Table 3.2, static loading with middle support removed was also conducted within the elastic range and the reaction forces recorded. Additionally, after a dynamic removal tests, values from the load cells were also taken once the slab had reached static equilibrium. Grid locations for the load cells and the locations of displacement monitoring points are provided in Figure 3.29

Figure 3.30(a) shows the load carried by each of the 9 remaining supports at different loadings. It can be seen that equivalent positions either side of the middle show very similar values (compare +’s with o’s), therefore these were averaged and converted to a percentage of total load (Figure 3.30(b)). Within the elastic range, i.e. below 80kN (4.7kN/m^2) there is a strong linear trend, however the ratio does not remain constant. Note also, that the increased number of load cells, along with the difficulties associated with loading the larger surface area, reduces the combined accuracy of the measurements. The final points, after dynamic removal, clearly do not lie on the same line, indicating the damage sustained has changed the distribution of loading.

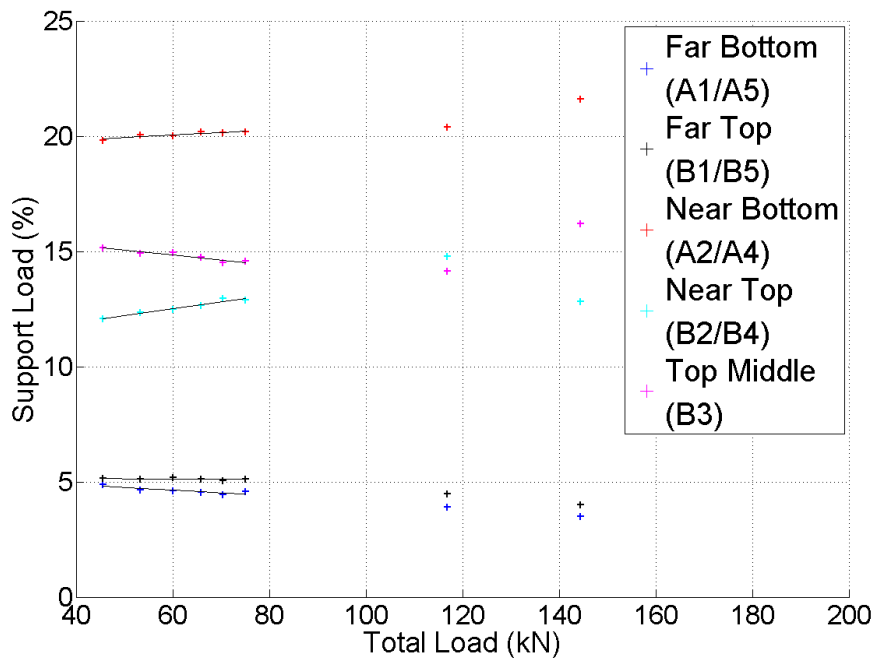
The averaged change in support reactions from fully supported to the removed case are shown in Figure 3.31 from the test values in the elastic range. Similar to the previous tests, the highest proportion of additional load is placed on the immediately adjacent supports whilst the supports further away have a relative reduction in vertical reaction force.

Dynamic removal tests were conducted at different loadings and normalised deflections were calculated using images captured from the HSC. Figure 3.32 compares displacement at the removal location in test M-D for different load levels. In general these results shows the same behaviour as the previous tests, though there is a significant reduction in the normalised displacements as the sample is stiffer due to the continuous slab. Comparing the key results given in Table 3.11 with the equivalent loading for the corner removal case (Table 3.8), gives a reduction of 55% for the peak displacement in elastic cases. Additionally, at the next loading level ($6.8/6.9\text{kN/m}^2$), the continuous slab’s peak displacement was only 0.09 times the slab depth, compared to 0.59 in test C-D. This difference is partially due to the naturally stiffer response of the continuous slab, which is then emphasised further as a higher load is also required to cause damage and the associated reduction in stiffness.

At lower levels of load, the bays adjacent to the damaged area experienced a slight uplift, as shown by the negative displacements in Figure 3.33(a), due to the slab rotating



(a) Vertical reaction to each support



(b) Percentage of total load to each support, averaged between symmetrical positions

Figure 3.30: Distribution of forces to supports during static loading - Test M-D

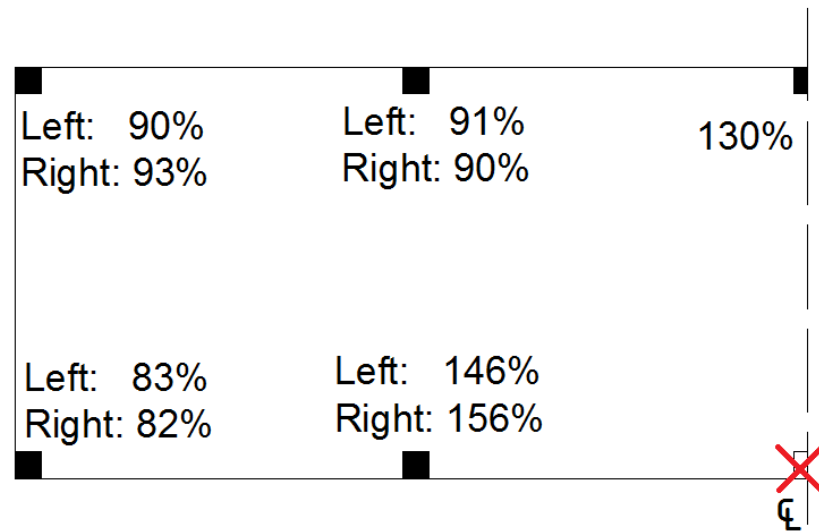


Figure 3.31: Mean change in distribution of forces to each support after corner column loss - Test M-D

inwards towards the removed support. Also note the three monitored points on the adjacent bay (D3, D4 and D5, see Figure 3.29) move by identical amounts, although this is at the limit of the accuracy of the sensors. Initially after the column was removed in the 8.5kN/m^2 test there was a brief uplift in the adjacent bay (Label (A) in Figure 3.33(b)). However, the damage sustained across the slab resulted in a final downward trend for most locations. Positions D3 and D4 are at symmetrical positions (see Figure 3.29) and therefore should have the same motion. Whilst they start similarly, and experience the same uplift values, their final conditions are different. However, this difference is less than 0.01 times the slab depth, or 1mm, and therefore is not an indication of the slab loading or damage becoming uneven.

Cracking of both the top and bottom surfaces of the concrete led to large plastic deformations and the drift observed in Figures 3.32 and 3.33. However, collapse due to total flexural failure did not seem likely and shear cracks did not form at the level of loading applied (see Table 3.6).

Figure 3.34 shows the power density spectra for different loading levels, calculated from HSC footage of the column removal location. The results demonstrate that as the load is increased, there is a decrease in the frequency of oscillation due to the higher mass and the lower stiffness caused by damage. All three cases also show another, noisier, frequency response at around 16Hz. The STFT taken of the 3.1kN/m^2 case is plotted in Figure 3.35, and the higher frequency can be seen to be an intermittent signal. However, this response was not detected from the LVDT sensors. Therefore this effect

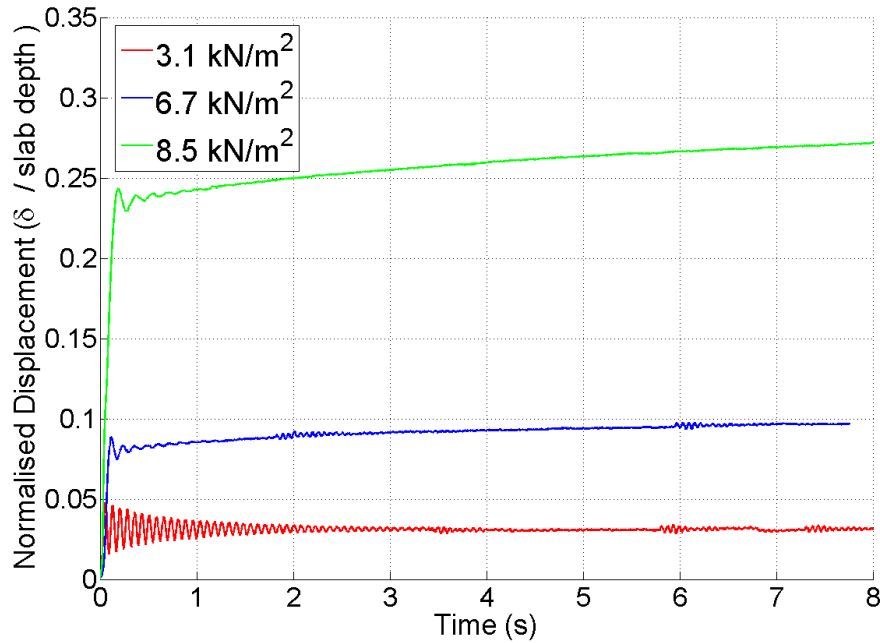


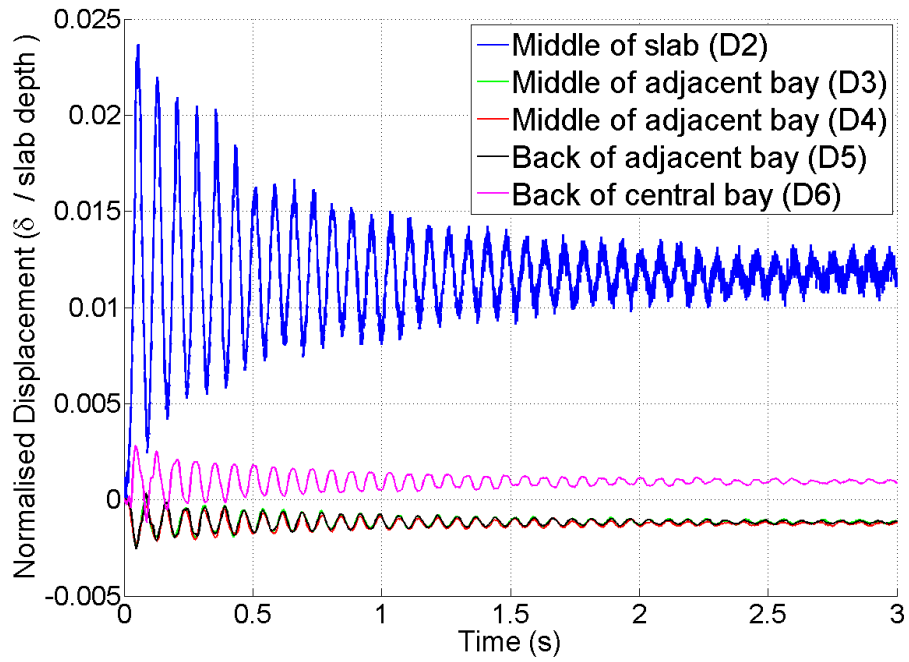
Figure 3.32: Displacements against time at the removal location (D1) for different loadings - Test M-D

is independent of the main slab oscillations and was most likely caused by vibrations from other equipment operating nearby affecting the camera. The key dynamic results, shown in Table 3.11, again demonstrate that in the elastic range (i.e. 3.1 kN/m^2) there is a higher frequency response and a small damping ratio. Furthermore, there is a high peak to final displacement ratio of 1.54, highlighting the influence of inertial effects on a lightly loaded slab. At higher loadings, with more mass, the oscillations are smaller, in relative terms, and are damped out quicker, causing the lower amplitude behind the dominant frequency (see Figure 3.34).

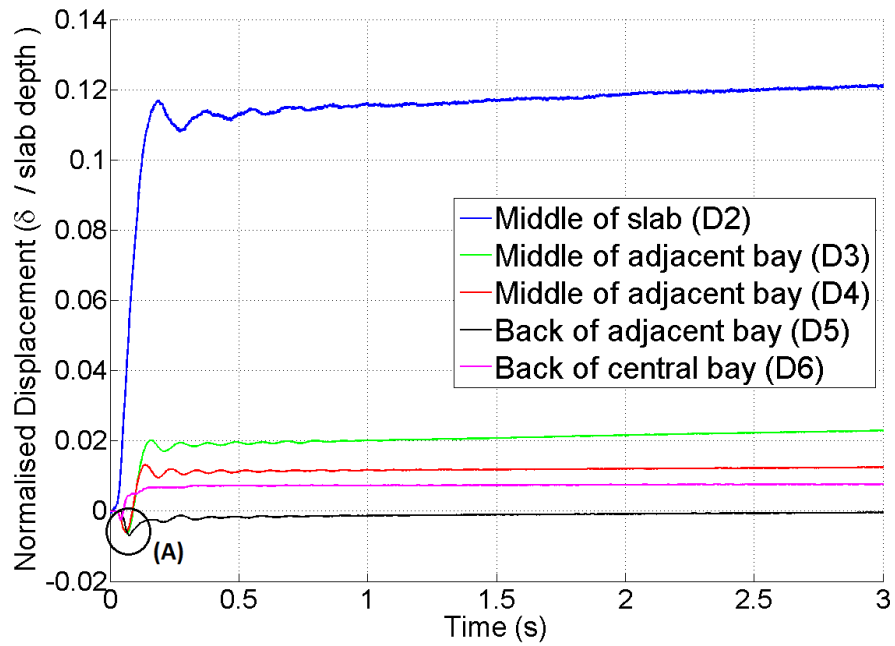
Figure 3.36 shows a photograph of the underside of slab M-D after the test was com-

Table 3.11: Results from dynamic removal - Test M-D

Loading (kN/m^2)	3.1	6.9	8.5
Normalised Peak	0.05	0.09	0.24
Amplitude / Peak (%)	67.31	15.98	5.82
Peak / Final Displacement	1.54	<0.92	<0.90
Damped Natural Frequency (Hz)	13.4	8.55	6.00
Damping Ratio	0.017	0.219	0.204



(a) 3.1kN/m² loading test



(b) 8.5kN/m² loading test

Figure 3.33: Displacements against time at different positions and loading - Test M-D

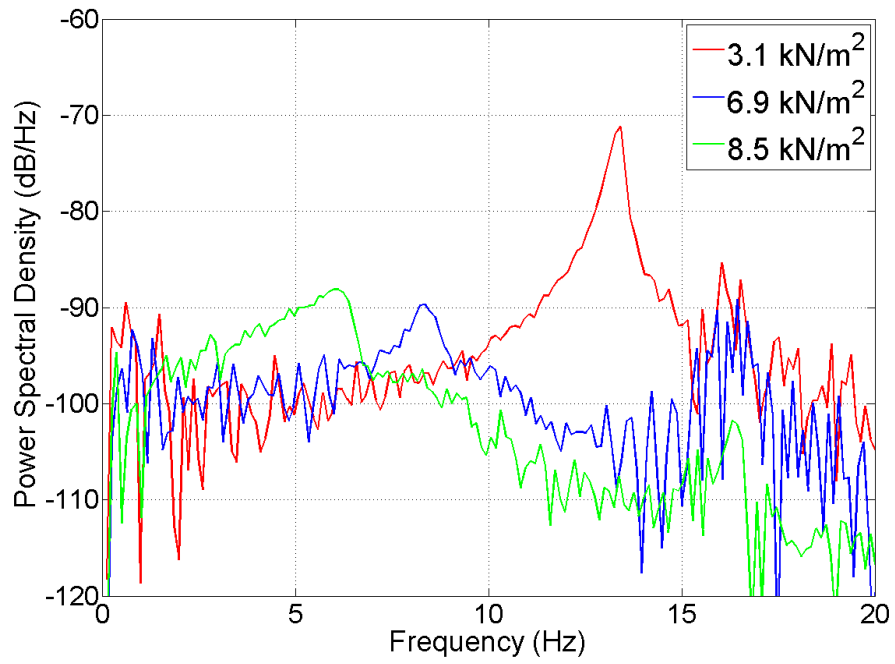


Figure 3.34: Power density spectra for displacement following corner column loss at different loadings - Test M-D

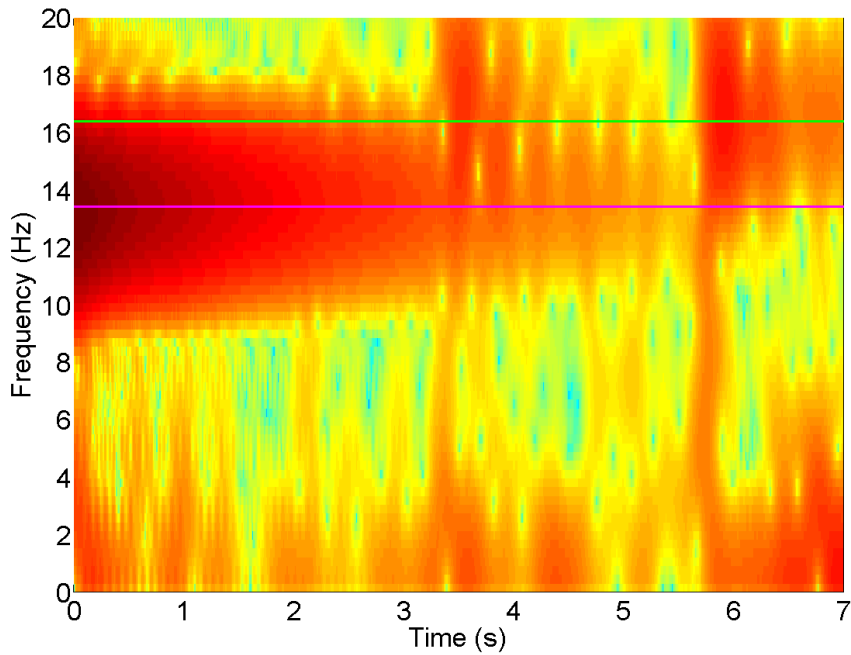


Figure 3.35: STFT for displacements at column removal location for 3.1kN/m² - Test M-D. Magenta and green lines show 13.4Hz and 16.4Hz respectively

pleted with the cracks annotated. The primary cracking pattern is shown in black. In this specimen the two-way spanning nature of a slab structure after a column loss is clearly shown by the diagonal cracks. The red lines are secondary flexural cracks that follow the reinforcement lines. These cracks were more extensive than expected as the slab was not continuous in both directions. The top cracking due to the increased hogging moments over the adjacent supports was almost identical to the corner removal case shown previously in Figure 3.9. These cracks follow the same pattern as seen in Figure 3.27, though are less extensive due to the smaller deflections and the influence of adjacent bays. This suggests that the stress distributions for smaller subsections after a column removal are similar to those of the larger area and therefore useful indications into the response of a complete floor slab can be gained from a simplified subsection.

3.4 Discussion of experimental results

These tests sought to simulate the effect of a column loss on a flat slab system. The measured reactions forces indicate that each slab was balanced suitably at the start of each test and the loading applied evenly across its surface. Analysis of the high speed footage, presented in Table 3.5, shows that the support was, typically, completely removed within 50ms. Whilst this is slower than a true instantaneous column loss scenario, or the duration of an explosion which is commonly within a few milliseconds (Cormie et al., 2009; Byfield and Paramasivam, 2012), similar removal rates were achieved for all tests allowing comparisons to be made, and so the results still emphasise the influence of a sudden removal. Additionally, dynamic effects will be even more significant with a quicker removal scenario.

3.4.1 Force redistribution

The reaction force distribution and the cracking patterns shown in Figures 3.8, 3.9, 3.18, 3.27, 3.31 and 3.36 give a good indication into the change in load paths that a damaged slab experiences. The test observations indicate that the bending profile becomes truly two-dimensional, with new spans primarily acting diagonally between the nearest supports. The change in spanning arrangement means that the supports closest to the removal location carry the loads that were previously taken from the lost support and a higher proportion of the load on the alternate bay, as shown by the decrease in forces at the further locations in Figures 3.8 and 3.31. This increase of potentially more than 50% may therefore exceed the shear capacity of the slab and lead to a catastrophic failure. Furthermore, simple techniques for analysing moment distributions for flat

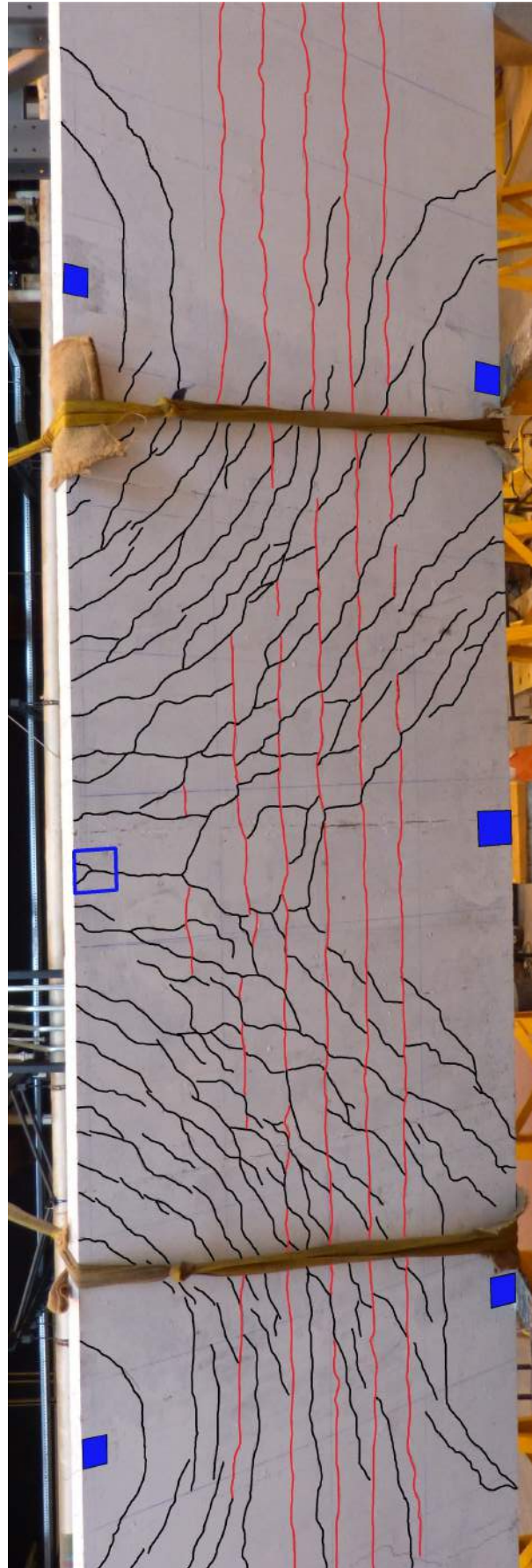


Figure 3.36: Annotated underside cracking pattern for continuous slab - Test M-D

slabs, such as the equivalent frame method, can not be applied after a column loss. Therefore other methods are required for assessing structures for progressive collapse.

As flexural damage occurred, a change in the distribution of forces to each support was observed. As large rotations occurred at the supports, there was a local reduction in stiffness due to concrete cracking; this changes the effective spans and results in a different reaction forces. In general however, the deviation from a linear model for support load against total load was not great, and the restraint provided by continuous slabs and columns will make these effects less significant. Therefore, static conditions with small loading may provide suitable information to predict the final demand on the supports.

3.4.2 Flexural damage

All the conducted tests demonstrated that flexural damage is an issue for flat slab structures as significant cracks formed on both top and bottom surfaces, which reduced the stiffness of the slab. After a column loss event the new spanning arrangement results in a moment demand, both hogging over supports and sagging in the spans, that exceeds the traditional design case.

The damage profiles, and results from the two penultimate cases, suggest that the inclusion of continuous reinforcement through a column location does change the distribution of stresses around the removal location, however, there is not a significant difference in ultimate capacity. This is due to the change in load paths away from the removed column. The static tests show that even after cracking has occurred in the concrete, along with yielding of the reinforcement, the structure can maintain its integrity and show a ductile behaviour. This is partly due to the strain hardening in the steel reinforcement providing additionally capacity. Additionally, geometric nonlinearity also contributes to capacity as the slab forms a tensile membrane at higher deflections, typically when the peak displacement exceeds half the slab depth.

3.4.3 Shear cracking

Flat slab systems are known to be vulnerable to brittle shear failure. All the tests in which complete failure was experienced, described in Table 3.6, occurred due to punching shear. This initially occurred at the corner location, before potentially progressing to other supports. The additional demand placed at these locations when a neighbouring column is lost, combined with their small shear perimeter, makes them vulnerable to progressive failures.

As these tests emphasise that brittle mechanisms need to be avoided, increasing punching shear capacity and ensuring surrounding supports have sufficient ductility can therefore prevent progressive collapse. Furthermore, while it seems that continuous bottom reinforcement through a column may not be significant for flexural capacity, previous research has demonstrated its efficiency in increasing the post-punching shear capacity of the surrounding supports (Mirzaei and Sasani, 2013). Therefore, its inclusion will aid in preventing progressive shear failures.

3.4.4 Whole slab behaviour

Slab elements are capable of spanning efficiently in two directions, therefore Alternative Load Paths (ALPs) will exist after a column loss event. This provides a high level of redundancy to the structure and reduces the potential for progressive collapse. These tests demonstrated that slab elements designed to current standards do provide the flexural capacity required for the new load spans, however, they also highlighted the risk that brittle failure mechanisms, such as punching shear, can cause. In general, provided suitable account is taken for the increase in shear demands after a column loss, flat slab structures are robust and resist progressive failures after a local damaging event (Starossek, 2009).

Furthermore, the global response of the surrounding structure plays a key role of flat slab structures, as loads are redistributed due to the damage in the slab elements. As the slab deflected vertically at the column loss location two behaviours were observed. The first was a rotational motion as the slab pivots around a diagonal axis located between the orthogonally adjacent supports. This can cause a relative uplift in areas away from the column removal point, especially in the adjacent bays, and also causes the reduction in reaction forces mentioned previously in Section 3.4.1. The adjacent bays also act to counterbalance the damaged area leading to lower peak deflections. For this effect to form, the slab must maintain its stiffness and therefore dominates in the low loading tests within the elastic range.

The alternative occurs as flexural damage, either hogging or sagging, causes hinges to form resulting in a reduction in stiffness and further deflections. The continuous slab condition in tests C-S, C-D and M-D allowed formation of plastic hinges over the adjacent supports, which also dissipated energy from the system. However, in some cases, plastic deformations continued after the test, as shown by peak to final displacement ratios less than 1. This means that the maximum stresses in the structure may not occur during the initial dynamic motion, and could potentially lead to a later collapse.

Typically, both behaviours occurred, with a rotational effect firstly causing the main deflections and associated uplift. If the slab then deformed enough and cracking occurred, then the reduction in stiffness across the entire area resulted in downward deflections at all points.

The continuous slab tests demonstrated the expected result that the larger structure is stiffer than the simplified substructure due to the influence of the adjacent bays and support conditions. Therefore such arrangements experience less damage after a column loss. As the aim of these tests was to investigate the general behaviour of slab elements, to back up more detailed numerical modelling, the inclusion of simple supports and non-fixed edges is not viewed to be an issue. Realistic structural arrangements, including the restraint provided by columns and the effect of multi-bay slab elements, will be considered in Chapter 6.

3.4.5 Dynamic effects

The dynamic effects involved in suddenly removing a support can play a significant role in the structural performance of the flat slab structures. At low levels of loading, within the elastic limits, there is typically a strong peak in deflections followed by higher frequency oscillations until the slab returns to rest after 3 or 4 seconds. At larger levels of loading, the additional mass increases reduces the natural frequency. Additionally, the higher inertial effect leads to a higher peak and more damage than from a static equivalent, which reduces the structural stiffness and lowers the natural frequency further. The damage also dissipates energy from the system, via crack formation and plastic deformations of the steel, resulting in a frequency response with a broader spectrum peak, which is damped out within a second or two.

Furthermore, after a sudden removal, forces are not redistributed to surrounding support instantaneously, with the peak demand occurring as the structure comes to a temporary rest position between oscillations. Therefore, under a dynamic condition, significant flexural damage may occur before a potential shear failure. However, under static loading, shear forces are immediately applied at the supports, therefore these locations may fail with less flexural damage than the dynamic case.

In design codes a factor of 2.0 is often applied to the loading around the damaged area during a static analysis to account for dynamic effects (GSA, 2013). This is based on the behaviour of a linear elastic system with no damping and instantaneous removal, and theoretically represents the worst case scenario. However, as all real structures experience some level of damping, it is clear this amplification factor does not reflect a

realistic condition. Furthermore, after cracking occurs in the slab there is a reduction in its stiffness creating a nonlinear response. Therefore, at common levels of loading, there is not a direct relationship between the load applied and the level of displacement or damage.

The rate of the straining of the steel reinforcement from all the tests indicates that the maximum strain rate is less than 0.35s^{-1} . However this only occurs at very localised points which were undergoing significant plastic deformations already. Generally the strain rates in the steel were much less than this. Furthermore, while quick strain rates do change the material properties, most significantly increasing concrete's tensile capacity, the results demonstrate that at the time of high strains, and therefore stresses, the strain rate is fairly low. This suggests that the Dynamic Increase Factor (DIF) for concrete may not be critical in providing additional flexural capacity.

3.5 Summary

This chapter described the details for the experimental programme. As has been noted, the primary purpose of these tests is to validate the numerical model presented in Chapter 4. However, the tests themselves provide important information of the behaviour of slab elements under various column loss scenarios. The sudden column loss scenario was replicated on scaled substructures of a flat slab structure. While the behaviour of such systems is known to depend on the restraint and influence of the surrounding elements, as was seen in these tests with continuous slab conditions over supports, the test set up provided useful information into the key performance parameters.

Whilst true instantaneous column removal could not be achieved with the methods used, significant differences to the equivalent static cases were still observed. The effect of removal time on the response a full structure will be considered numerically in Chapter 6.

For the dynamic tests the High Speed Camera (HSC) combined with Digital Image Correlation (DIC) techniques provided detailed information into the response of the slab after a column loss. In particular the displacement-time profile at multiple points could be observed to determine peak deflections and conduct frequency analysis. Additionally, crack propagation could be observed with particular interest in the formation of shear cracks.

The tests demonstrated that the material and geometric nonlinearities occurring at high

deflections provides additional capacity beyond the elastic limit. As the peak deflections reached between 0.1 and 0.15 times the slab depth, cracking of the concrete resulted in a significant reduction in the stiffness. However, the two-dimensional nature of flat slab structures allows ALPs to form after the removal of a support, demonstrating that such structural forms have a large level of redundancy. Flexural cracking and yielding of steel reinforcement occurred, which was quite extensive in places, in both sagging and hogging moment areas. As they enter the nonlinear range, there is also a change in the response of the system. Force distributions change and the damage alters the dynamic response of the system. Therefore a suitable concrete cracking model will be presented in Chapter 4 for use with the Finite Element Analysis (FEA), along with description of a nonlinear steel constitutive law. However, for these tests, ultimate failure did not occur due to the moment demand, and all observed failures were due to punching shear, usually at corner locations. Progressive shear failures also occurred in three tests.

The column loss event is inherently dynamic, with the level of loading changing the response of the system. This is partly due to the increase in mass changing the natural frequency, along with the sustained damage. When damage occurs, the dissipation of energy affects the peak displacement and level of damping. Additionally, a peak increase in displacements of 50% more than the static case was observed during elastic tests due to inertial effects. This may therefore cause damage to a structure near its limit, however, this effect is less pronounced as the structure experiences permanent damage. Additionally, consideration of the nonlinear relationship between force and displacement after cracking occurs may suggest that the common design recommendations of a load increase of 2.0 is conservative.

Data from these tests, especially the change in distribution of forces after a column loss, the deflected profile and damaged areas due to cracking and reinforcement yielding, will be compared to an equivalent numerical model in Chapter 5. The tests also provide information into what key aspects which will be considered parametrically in Chapter 6.

Finite Element Model of Floor Slab

This chapter introduces the background and details of the numerical model for column loss of flat slabs. Finite Element Analysis (FEA) is used to replicate the experimental programme discussed. The details for the model, including nonlinear material laws, are presented and explained. Additionally, preliminary investigations are conducted to check the suitability of the model.

4.1 Introduction to the finite element model

A parameter study was conducted numerically using a Finite Element (FE) model in order to conduct further investigations into the behaviour of flat slab structures after a column loss event, beyond the experimental programme. The details for that model and a justification for the assumptions made are presented in this chapter.

4.1.1 Justification of the use of the finite element method

The results presented in the previous chapter, from experimental investigations, demonstrate that flat slab structures have complicated behaviour during a sudden column loss event. The change in load paths involves the two-dimensional nature of the slab. The new load spans act, primarily, between the two closest remaining supports, resulting in a span length acting diagonally across the section, rather than the previous orthogonal arrangement. For this reason, analysis techniques such as the equivalent frame method commonly used to analyse slab structures cannot be applied for such situations. As the change in demand in certain locations leads to extensive concrete cracking, along with yielding of reinforcement, these nonlinear effects must be included to gain a useful prediction of the response of a structure. Use of yield line theory has been attempted by some authors to estimate the capacity of slab elements under extreme loading, however

they concluded that geometric nonlinearity in the form of membrane action results in a higher capacity than predicted (Foster et al., 2004; Dong and Zhu, 2011; Yi et al., 2014). More advanced formulations could be utilised, however, these rely on accurately predicting the position and orientation of plastic regions and the correct influence of membrane action, both tensile and compressive, due to the horizontal in plane restraint.

Alternatively, FEA has demonstrated its ability to consider complicated loading scenarios, with the material and geometric nonlinearities, that Reinforced Concrete (RC) flat slabs experience during column loss events, as well as the dynamic effects involved (Miyamoto et al., 1991; Jayasooriya et al., 2011; Li and Hao, 2013; Trivedi and Singh, 2013; Keyvani et al., 2014). A well created finite element model can replicate the response of a large structure to an extreme event and provide information on the damage sustained and the potential for progressive failures. Additionally, the flexibility available for changing both the geometry and the material properties of an FE model makes it highly suitable for conducting a parameter study to investigate the influence of various factors. However, numerical models often experience convergence issues, especially during nonlinear analysis, therefore care must be taken when constructing a model and checking the results to ensure the solution is reasonable. A large FE model may also require long computational times and large amounts of memory, which may be beyond the resources available for some investigations. Furthermore, numerical models are highly dependent on their input values and the modelling techniques used, and so need to be validated. Provided these aspects are understood when creating a model, and interpreting the results, FEA is still a useful method. Due to the limitations of other methods, and the advantages FEA presents, FE models shall be used to conduct further investigations.

4.2 Requirements and description for model

In order to replicate the experimental tests conducted in the previous chapter, a number of aspects must be accurately considered. This section highlights the approach and details used to achieve a suitable model.

4.2.1 Numerical solver

For the main simulations Abaqus/Explicit from Simulia (2010) was used. The integrations of the required equations of motions were solved with a central difference algorithm and the element properties converted into a lumped mass matrix. Explicit

formulations have three advantages over the implicit approaches for these types of problems. Firstly, they are more efficient at modelling highly nonlinear effects without the convergence issues that often affect implicit formulation; as significant material nonlinearity was observed during the experimental programme this was an important consideration. Secondly, as no stiffness matrix is required, the memory and computational demands of a large model are reduced. This allows large, detailed models to be considered in a reasonable time frame. Finally, explicit models are inherently based on dynamic equilibrium, rather than static, making them more suitable for simulations involving changes in loading within a short time period. As the critical tests involve sudden dynamic column removal leading to large deformations, an explicit analysis approach was chosen. Abaqus/Explicit can still consider static loading by applying small load increments to create a quasi-static condition, this is covered in more detail in Section 4.4.2.

For problems involving material softening, a strong mesh dependency can arise. As the mesh is refined the energy dissipated decreases. Abaqus reduces this issue by introducing a characteristic length, based on the element geometry and formulation. The stress-strain relationship is then converted to a stress-displacement relation. With this approach the formulation ensures that the correct amount of energy is dissipated and greatly reduces the mesh dependency. The characteristic length is taken as a typical length of a line across an element for a first-order element and half of the same typical length for a second-order element. This definition is required as the direction of softening is not known in advance and so the approach typically gives good results for any direction, however, some mesh dependency remains for elements with high aspect ratios (Simulia, 2010).

With explicit solvers, any residual forces after a time step are propagated as stress waves between elements. Therefore, a bounded solution requires the time increment to be less than the stable time increment based on the element wave speed. The stable time increment, Δt_{stable} , for an element is calculated from Equation 4.2.1:

$$\Delta t_{stable} = \frac{L^e}{c_d} \quad (4.2.1)$$

where L^e is the characteristic element length and c_d is the dilational wave speed, related to the Young's modulus, E , and material density, ρ , and is given by Equation 4.2.2.

$$c_d = \sqrt{\frac{E}{\rho}} \quad (4.2.2)$$

Therefore, it can be seen that decreasing the element length, increasing the elastic

stiffness or decreasing the density will all result in a smaller stable time increment and therefore require a longer analysis time. Abaqus/Explicit automatically calculates Δt_{stable} for each element at the start of the analysis and then applies a suitable time step. This value may be updated during the analysis if required.

4.2.2 Geometry of the model

The geometry of the model was based on the design case for the experimental slabs. Therefore, for corner and penultimate removal tests, the concrete deck was 4.1m by 2.1m and the middle removal case used a 8.1m by 2.1m. All slabs were 80mm deep. Other geometric details, e.g. reinforcement positions and support designs, also matched the experimental case.

4.2.3 Modelling of the concrete slab

Solid, 8 node, brick elements (C3N8R) were used for the concrete sections of the model. The entire slab was treated as one section, matching how it was cast, and material properties were homogeneous throughout. The elements used a linear shape function, and reduced integration was specified, i.e. only one integration point per element. Fully integrated elements, along with being more computationally demanding, may exhibit shear locking under certain conditions. Under pure bending the first order shape function may not represent the correct shape of the deformed element. This causes a shear deformation at the integration point, therefore the strain energy is not entirely controlled by the bending deformation. This effect can lead to overly stiff sections and therefore wrong stresses and displacements. Second order shape functions can reduce this issue, however require longer analysis times. Alternatively, elements with a reduced number of integration points do not experience less shear locking problems, but are prone to hour-glassing effects. As Abaqus includes methods to control issues with hour-glassing by introducing an artificial strain, the improved speed in simulation makes this option the most suitable. Details on hour-glassing, along with checks to ensure it is not an issue for these models, is presented in Section 4.4. A mesh sensitivity study was also conducted to identify the optimum number and size of the concrete elements.

4.2.4 Modelling of the steel reinforcement

The steel reinforcement was modelled with beam elements with a circular cross section, diameter of 6mm. The nonlinear material properties are described below in Section 4.3.2. Each beam element contained two nodes and used a linear shape formulation, element ID B31. The bond between the steel bars and the concrete was achieved by using Abaqus's embedded region feature, which constrains the translational degree of freedom for the reinforcement beam nodes to the interpolated values of the corresponding degrees of freedom of the surrounding concrete nodes (Simulia, 2010). This represents the fully bonded condition that occurs with deformed bars and well compacted, non cracked, concrete. Additionally, full bond is assumed along the entire anchorage length. Whilst this may potentially overestimate the capacity provided by the steel in these regions, since no bar pull out was observed during the tests, this simplification should be adequate. At higher levels of stress, localised debonding will occur as the concrete cracks, resulting in a non-uniform distribution of stresses along the reinforcement. This effect can be complicated, and computationally demanding to model accurately for a large structure, and is not included for these simulations. Although this may lead to differences in the localised response of some elements, its effect on the whole system is less significant as the majority of the steel will remain fully bonded.

4.2.5 Modelling the support conditions

For the experimental programme, the slabs were supported on steel plates. These were placed on steel spherical bearings and then on load cells. The support plate provided a stiff area to distribute loading and reduce stress concentrations, while the bearings allowed free rotations for all axes. The plates were modelled as solid elements with elastic material properties (Young's Modulus and Poisson's Ratio of 210GPa and 0.3 respectively) and according to the experimental geometry, i.e. 135x135x25mm. The two halves of the bearing were modelled separately with solid elements, again according to the used geometry. For both the plate and the bearings, 4 node linear tetrahedron elements (C3D4) were used as these avoid the issues of hour-glassing previously mentioned, and provide a better interaction surface for the bearings. This is covered further in Section 4.4.4. Fixed boundary conditions in the three translational directions were applied to the bases of the bearings to restrain the model and measure reaction forces. A rendering of the three parts is shown in Figure 4.1. For the dynamic removal tests, a steel plate was placed at the location under investigation as before. However, since during the experimental tests a simple steel bar was used to support the position in-

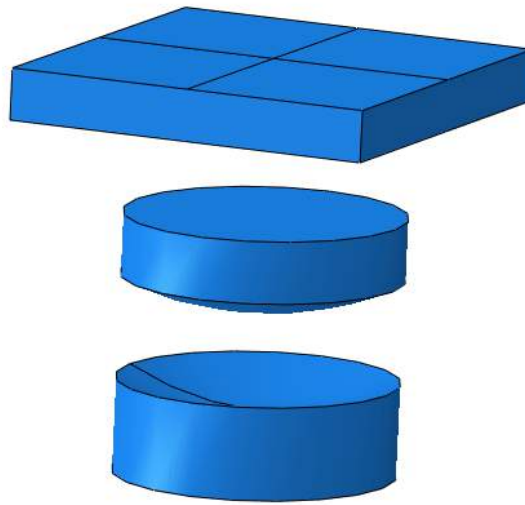


Figure 4.1: Rendering of the spherical bearings and plate used as permanent supports for the slab

stead of a bearing, see Figure 3.5 in the previous chapter, this plate was held by a single fixed node restrained only vertically in the centre of the plate.

Interaction between the sections was modelled with a hard contact, i.e. no penetration of the surfaces. For the concrete to steel boundary a coefficient of friction of 0.4 was applied, and between the steel bearings 0.01 was used to account for the smooth, greased surfaces. Separation was allowed at all interfaces.

By modelling the supports in this manner, a close representation of the experimental condition could be achieved. While the use of additional elements, and interaction definitions, does increase the computational time for each simulation, the rotational behaviour is captured better than a simple pinned boundary condition, as the centre of rotation matches the experimental set up. Additionally, the frictional dissipation of energy is important during the dynamic removal test and this method includes this effect.

4.2.6 Modelling the load

The effect of the sandbags used to load the experimental tests was replicated in two ways for the numerical models. During static loading tests, a uniform pressure was applied to the top surface of the concrete slab elements, acting vertically downwards. This pressure was ramped linearly, from zero to its full value, over the course of the

loading period, See Section 4.4.2 on page 103 for details on ensuring a quasi-static loading rate. Additionally, a non-structural mass was also applied to the concrete elements to account of the increased mass of system due to the dead load; this was applied in full from the start of the analysis. While during static tests, the inertial effects should not be significant, the influence of the mass helps to create a quasi-static state. Additionally, explicit analyses require a minimum time increment to obtain a stable solution, which is inversely related to the square root of the mass matrix. Therefore, including a higher mass value decreases the stable time increment, and reduces the computational time required.

For the dynamic removal cases, the effect of the mass on the system is more significant. Firstly, the mass of the RC slab was calculated based on the assumed density and volume of the concrete and the steel. Then, at each level of loading replicated from the experimental programme, the additional mass to achieve the required weight was determined. This was then added to the concrete elements and uniformly distributed across the entire slab's volume. While during the experiments the applied load was loose, i.e. free to move independently of the slab, the video footage indicates that the slab and load move simultaneously in most cases. Therefore, the numerical efficiency gained by linking the two outweighs any slight improvement in the accuracy that might arise from modelling an independent load system.

During the pre-load period of the dynamic test, as the loading was increased before the support was removed, an acceleration of 9.81m/s^2 was applied to all parts of the model, including the non-structural masses, to replicate gravity loading. This was ramped linearly at a suitable rate to prevent any inertial effects affecting the simulation at this stage. Once the full load was reached, the loading was held constant to further ensure a static state. From this condition, the vertical reaction force from the temporary support was obtained. The fixed boundary condition was then replaced by this equivalent force and the model was ready for the removal phase.

While the model was under gravity loading condition, the equivalent temporary force was reduced from its full value to zero linearly, within the removal time period, typically 50ms. The support plate at the removal location, and the loaded slab, could then fall and separate under the influence of gravity. A schematic representation of the total load and the temporary support load against time is given in Figure 4.2, showing the linear increase in load under quasi-static conditions upto T_1 , and the sudden removal of the support by linearly reducing the support load between T_2 and T_3 .

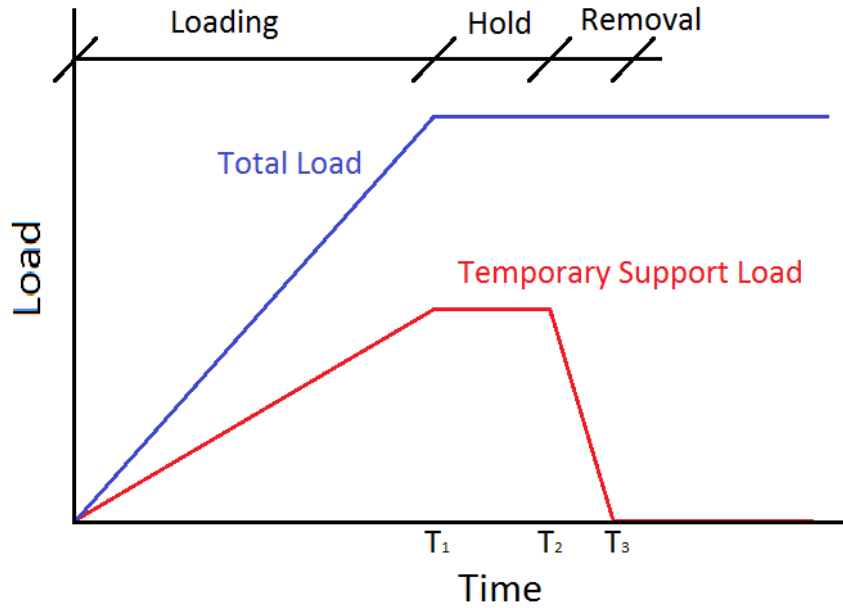


Figure 4.2: A schematic representation of the increase in total load and the removal of a support during dynamic tests

4.2.7 Modelling the nonlinear effects

Three causes for nonlinear behaviour are considered for this analysis. These are due to the material constitutive laws, geometric changes as a result of deformations, and changes in contact and boundary conditions. Material nonlinearity is a complicated issue and will be addressed fully in the following section.

As the RC deck was not vertically restrained or attached to the supports, uplift is possible. The contact definition described above accounts for this condition. During the experimental programme no other contact changes were observed and therefore are not included for these models.

Finally, account has been made of the nonlinearity caused by deformations changing the geometry of the structure. At every time increment the local system of axes for each element is updated and the change in load arrangement determined. This allows the effect of membrane action to be included.

4.3 Material models

4.3.1 Nonlinear material model for concrete

The behaviour of concrete is an important aspect in considering the damage in RC structures. Concrete's stress-strain relationship becomes highly nonlinear beyond its elastic limit with different behaviours in compression and tension. A FE model must include some approach for considering these changes in stiffness. Furthermore, slab elements experience biaxial stresses during high deflections, leading to a different response from the uniaxial.

As the tensile behaviour, and critically the effects on cracking, are usually the most significant for RC elements, Abaqus/Explicit includes two models for modelling the tensile nonlinear response. These are a brittle cracking model, and the Concrete Damaged Plasticity (CDP) model (Simulia, 2010).

The brittle cracking model uses a smeared crack approach to represent the sudden change in stiffness caused by a crack. A crack is said to have formed when the maximum principal tensile stress exceeds the specified tensile strength. After this point the crack, and any subsequent cracks, are treated as fixed and orthogonal. This model also includes a brittle failure criterion which removes elements from the analysis after material failure. This improves the stability of some simulations, where excessive distortions may occur when an element cannot carry further stress, however, it therefore is not suitable for situations where cyclic loading may occur as the element will not add to the compressive stiffness. Although the oscillations of the concrete in the dynamic experimental tests were not as severe as some dynamic applications, this limitation in the model may cause issues. Furthermore, as the model assumes all cracks are orthogonal and fixed, it is less suitable for the cracking patterns seen across the concrete slab surfaces during the experimental work. Finally, the model assumes a linear elastic compressive behaviour. While no signs of compressive damage due to crushing were observed experimentally, under extreme loading events a more robust material model may be required.

The alternative, and the one used in this study, is a plastic-damage model, referred to as CDP. This describes the behaviour of concrete beyond its elastic range under biaxial stresses with two aspects; plasticity and a reduction in the elastic stiffness. The CDP model is based on the Drucker-Prager hyperbolic function, given in Equation 4.3.1, to give the flow potential G .

$$G = \sqrt{(f_c - m \cdot f_t \tan \psi)^2 + \bar{p}^2} - \bar{q} \tan \psi - \sigma \quad (4.3.1)$$

Where ψ is the dilation angle to define the plastic flow, f_c and f_t are the uniaxial compressive and tensile stresses at failure. The eccentricity factor, m , controls the rate the function tends towards the asymptote, small values may therefore lead to convergence problems. Additionally, \bar{p} and \bar{q} are the effective hydrostatic pressure and Mises equivalent stresses respectively, defined by Equations 4.3.2 and 4.3.3.

$$\bar{p} = -\frac{\bar{\sigma} I}{3} \quad (4.3.2)$$

$$\bar{q} = \sqrt{\frac{3}{2} \bar{S} \cdot \bar{S}} \quad (4.3.3)$$

where \bar{S} is the deviatoric part of the effective stress tensor, $\bar{\sigma}$ (Jankowiak and Lodygowski, 2005).

The yield function, in terms of the effective stresses, \bar{p} and \bar{q} , is given in Equation 4.3.4, as proposed by Lubliner et al. (1989) and modified by Lee and Fenves (1998). This can be shown as the plane stress yield surface, as presented in Figure 4.3.

$$F = \frac{1}{1 - \alpha} \left(\bar{q} - 3\alpha\bar{p} + \beta(\bar{\epsilon}^{pl}) \langle \hat{\sigma}_{max} \rangle - \gamma \langle \hat{\sigma}_{max} \rangle \right) - \bar{\sigma}_c(\bar{\epsilon}_c^{pl}) = 0 \quad (4.3.4)$$

where:

$$\alpha = \frac{(\sigma_{b0}/\sigma_{c0}) - 1}{2(\sigma_{b0}/\sigma_{c0}) - 1} : 0 \leq \alpha \leq 0.5 \quad (4.3.5a)$$

$$\beta = \frac{\bar{\sigma}_c(\bar{\epsilon}_c^{pl})}{\bar{\sigma}_t(\bar{\epsilon}_t^{pl})} (1 - \alpha) - (1 + \alpha) \quad (4.3.5b)$$

$$\gamma = \frac{3(1 - K_c)}{2K_c - 1} \quad (4.3.5c)$$

As can be noted in Equations 4.3.5a, 4.3.5b and 4.3.5c, two terms are required to define the shape of function. The K_c factor is the ratio of the second stress invariant on the tensile meridian to the compressive meridian, as seen in Equation 4.3.6.

$$K_c = \frac{(\sqrt{J_2})_{TM}}{(\sqrt{J_2})_{CM}} \quad (4.3.6)$$

While σ_{b0}/σ_{c0} is the ratio of initial equibiaxial compressive yield stress to initial uniaxial compressive yield stress. The required plasticity inputs for Abaqus are given in Table

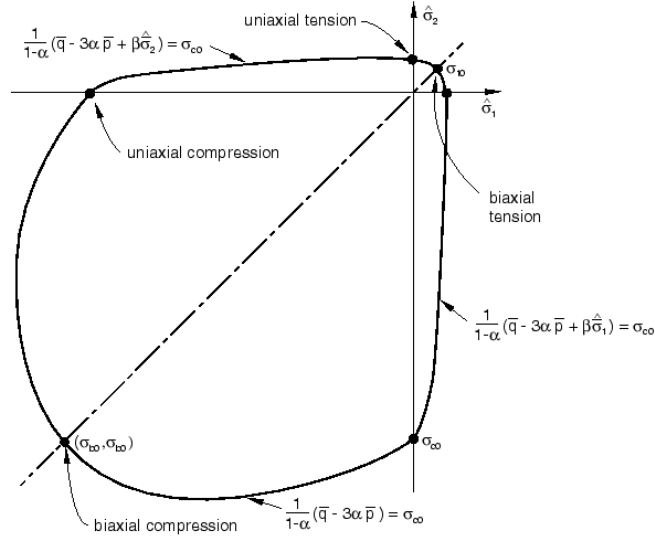


Figure 4.3: Yield surface in plane stress for the CDP model. Reproduced from the Abaqus user manual (Simulia, 2010)

Table 4.1: Concrete Damage Plasticity inputs

Dilation angle (ψ)	Eccentricity (m)	K_c	σ_{b0}/σ_{c0}
35°	0.1	2/3	1.16

4.1; these definitions and the values used come from the Abaqus user manual (Simulia, 2010). These are all default values, and convert the uniaxial stress strain relationship for compression and tension into the two dimensional yield surface (Jankowiak and Lodygowski, 2005).

The uniaxial stress-strain behaviour of concrete in compression, after the linear elastic phase, is modelled with Equation 4.3.7 from CEB-fip (2012). The normalised stress (σ_c/f_{cm}) against compressive strain is plotted in Figure 4.4, with the key aspects annotated.

$$\sigma_c = -f_{cm} \left(\frac{k \cdot \eta - \eta^2}{1 + (k - 2) \cdot \eta} \right) \quad (4.3.7)$$

Where $\eta = \epsilon_c/\epsilon_{c1}$ i.e. the ratio of compression strain to crushing strain, and k is the plasticity number taken as 2.15 for C25/30 concrete. This gives a parabola shape beyond the elastic limit, with a softening effect until the ultimate limit, f_{cm} , due to compressive micro-cracks. After this point, there is a reduction in capacity as the concrete crushes, however beyond a compressive strain of 0.035, the stress is considered as constant. While this full range is defined for completeness, the experimental programme

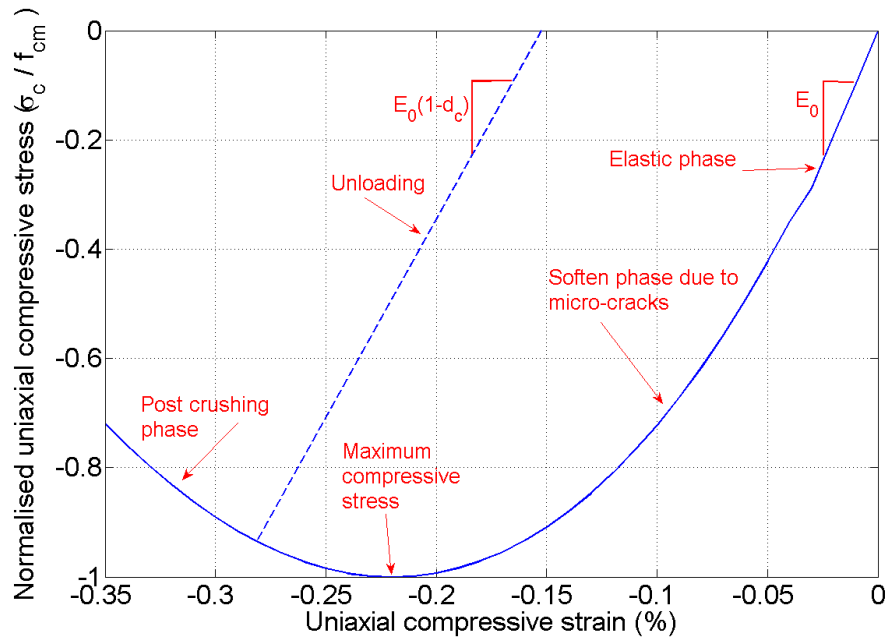


Figure 4.4: Uniaxial compressive model for concrete

did not indicate the crushing was a critical issue for these types of tests.

As a composite material, reinforced concrete experiences a complicated behaviour under tensile loading. Plain concrete cracks at relatively low levels of stress (8-13% of peak compressive stress), this will start with the formation of micro-cracks, which reduce the stiffness in a small failure zone. These will then develop into discrete cracks, resulting in a sudden drop in uniaxial capacity, although depending on the size of the crack, shear stresses may still be transmittable due to aggregate interlock. Furthermore, if loading is reversed, the crack can close again and carry compressive stresses. However, the presence of steel reinforcement changes the response. Not only will the steel, if adequately anchored into the surrounding concrete, carry tensile forces despite concrete cracks, but also concrete can remain bonded to the steel bars between discrete cracks and contribute to the uniaxial capacity. This results in a non-linear stress-strain graph, with some authors suggesting a power-form equation (Maekawa et al., 2003).

Alternatively, the Model Code (CEB-fip, 2012) recommends an elastic model up to 90% of the cracking stress, with a reduction in stiffness afterwards to account for micro-cracks. After cracks have formed, i.e. the stress exceeds the mean tensile strength f_{ctm} , a bilinear model between the stress and a fictitious crack opening is suggested, based on the fracture energy.

For this study, a strain based plasticity model is used to represent concrete cracks. This

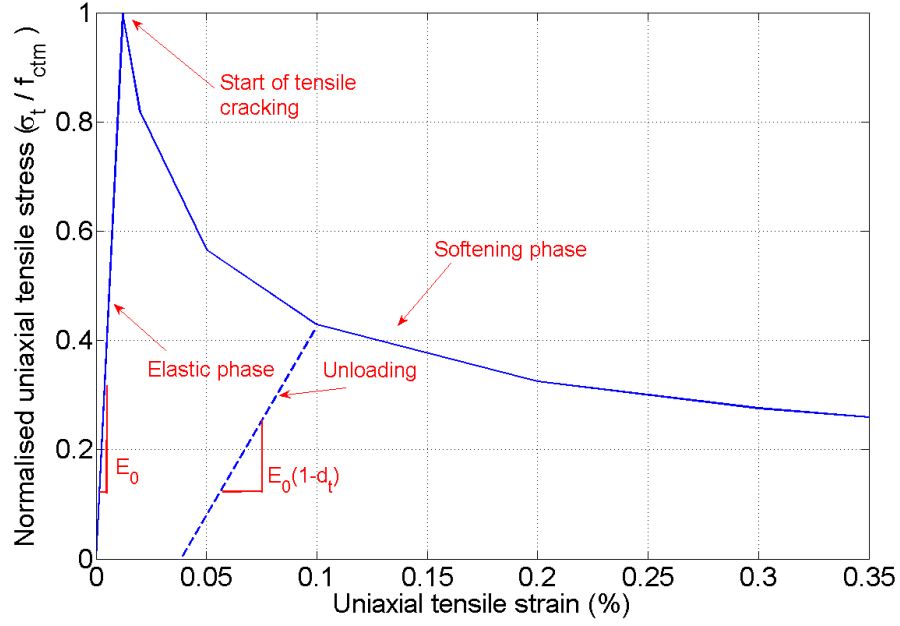


Figure 4.5: Uniaxial tensile model for concrete

means that rather than modelling discrete crack openings once the tensile stress is exceeded, the region is considered with plastic deformations which actually correspond to a continuum of micro-cracks. Therefore, accurate indication of the exact size and location of an individual crack is not possible, although the orientation of the cracks can be determined by viewing principle axes of the plastic strain regions. Concrete is taken to be linear elastic upto its cracking stress, afterwards a nonlinear tension softening model is used to account for the reduction in capacity of reinforced concrete. This is described by Equation 4.3.8 from Okamura and Maekawa (1990), where subscript t indicates tension, and ck is the cracking point, this relation is also shown in Figure 4.5.

$$\sigma_t = \begin{cases} E_0 \cdot \epsilon_t & \text{for } \sigma_t \leq f_{ctm} \\ f_{ctm} \cdot \left(\frac{\epsilon_{t,ck}}{\epsilon_t} \right)^{0.4} & \text{for } \sigma_t > f_{ctm} \end{cases} \quad (4.3.8)$$

The tensile plastic strain, ϵ_t^{pl} representing a crack, is determined with Equation 4.3.9 based on the cracking strain, ϵ_t^{ck} , tensile stress, σ_t and the current recoverable elastic stiffness.

$$\epsilon_t^{pl} = \epsilon_t^{ck} - \frac{d_t}{(1 - d_t)} \frac{\sigma_t}{E_0} \quad (4.3.9)$$

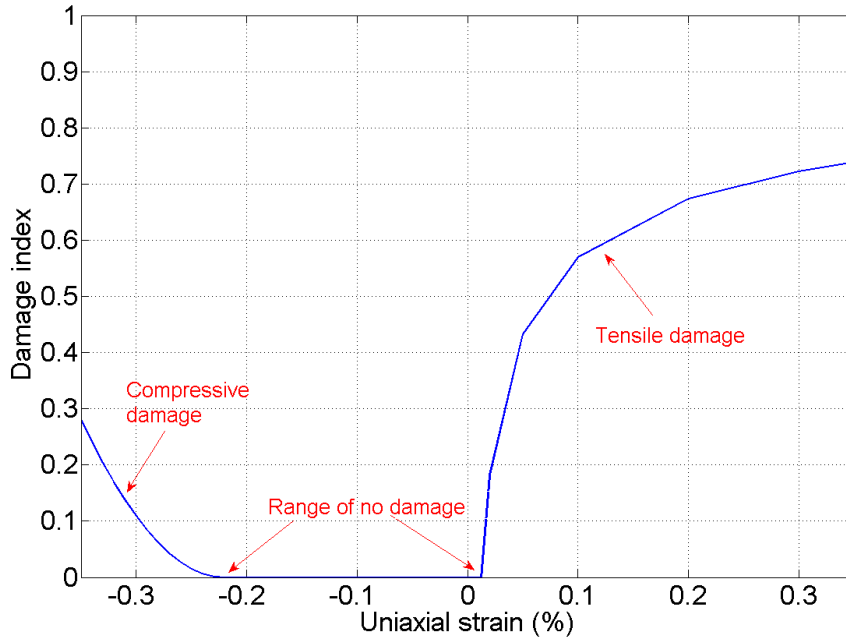


Figure 4.6: Compressive and tensile damage indices for concrete

The CDP model also accounts for the reduction in stiffness caused by cracking or crushing during the unloading or reloading phases. The initial stiffness, E_0 is reduced to the damaged elasticity, E_d by the damage index, d , according to Equation 4.3.10. The damage indices are defined for tension and compression conditions in Equations 4.3.11a and 4.3.11b respectively; a value of 0 indicates an undamaged state with its initial elastic stiffness while 1 represents a complete loss of stiffness. The damage index, for both compression and tension, is also presented graphically in Figure 4.6. The unloading behaviour is shown on Figures 4.4 and 4.5.

$$E_d = E_0(1 - d) \quad (4.3.10)$$

$$d_t = \begin{cases} 0 & \text{for } \sigma_t \leq f_{ctm} \\ 1 - \frac{\sigma_t}{f_{ctm}} & \text{for } \sigma_t > f_{ctm} \end{cases} \quad (4.3.11a)$$

$$d_c = \begin{cases} 0 & \text{for } \sigma_c \leq f_{cm} \\ 1 - \frac{\sigma_c}{f_{cm}} & \text{for } \sigma_c > f_{cm} \end{cases} \quad (4.3.11b)$$

Additionally, the CDP model accounts for dissipation of energy that occurs as the concrete is damaged. This energy level is related to the plastic deformations, either due to crushing or cracking, and the reduction in stiffness from the damage index. Therefore, during dynamic column removal analysis, the damping ratio of the displacement time response provides an indication in the extent of damage that has occurred.

The values of the maximum compressive and tensile stresses, f_c and f_t , are determined for each test based on the results of the concrete samples for each batch of concrete. The compressive strength was obtained from the averaged cube strengths on the test day, which are converted to an equivalent cylinder strength for use in Equation 4.3.7.

Determining concrete's tensile strength is more complicated. Direct tensions tests are rarely used, and were not conducted in the experimental programme. Estimations from the compressive strength are possible, however large scatterings in the results are common. Flexural tests on concrete prisms can be used to gain the ultimate uniaxial tensile stress, although this overestimates the true strength. The most common method, and the one used for this chapter, is to conduct indirect tension tests by splitting cylinders, however the Model Code notes that many studies have provided different conversion factors for this, increasing the uncertainty of its use (CEB-fip, 2012).

Strain rate effects

As described in Section 2.4.5, there is a well documented increase in the tensile strength of materials due to high strain rates. For concrete, Malvar and Ross (1998) compared published experimental data and determined there was a bilinear relationship between the tensile Dynamic Increase Factor (DIF) with strain rate, when plotted on a log-log graph. From this, a recommended equation was presented as shown below in Equation 4.3.12 (CEB-fip, 2012).

$$(f_t/f_{ts}) = \begin{cases} \left(\frac{\dot{\epsilon}_{ct}}{\dot{\epsilon}_{ct0}}\right)^{0.018} & \text{for } \dot{\epsilon}_{ct} \leq 10s^{-1} \\ 0.0062 \left(\frac{\dot{\epsilon}_{ct}}{\dot{\epsilon}_{ct0}}\right)^{1/3} & \text{for } \dot{\epsilon}_{ct} > 10s^{-1} \end{cases} \quad (4.3.12)$$

where

f_t/f_{ts} = the tensile DIF at $\dot{\epsilon}$

$\dot{\epsilon}_{ct0} = 10^{-6}s^{-1}$ (static strain rate)

For these models a constant increase in tensile capacity, of all the concrete, is applied at

the start of the dynamic removal step, this simplification is justified for the following reasons.

- Obtaining accurate estimations for the increased tensile capacity of concrete, and its post cracking behaviour, as a result of rate of straining is uncertain. Other authors have indicated that DIFs are often sensitive to the type of test being conducted (Wu et al., 2012; Chen et al., 2013).
- There is already uncertainty in the static uniaxial tensile capacity of the concrete as only indirect test methods were used.
- From the available experimental data of the steel strain gauges, and preliminary simulations, the maximum strain rate in the concrete is less than 0.35s^{-1} , corresponding to a DIF of 1.26 according to Equation 4.3.12.
- During a dynamic column removal, if the structure does not fail completely, then the maximum strain rate does not occur at the time of peak stress. Therefore, the increase in capacity is most relevant for tests where the concrete exceeds its static cracking stress, whilst straining at a high rate. Under such situations, the inertial effects involved suggest that the final stress, when the strain rate drops, would still exceed the amplified cracking stress value.
- Inclusion of a strain-rate dependant material law increases the computational time considerably.

For these reasons, rather than attempt to estimate a true DIF as a function of strain rate, a constant increase factor of 1.2 is applied to the tensile capacity.

4.3.2 Nonlinear material model for steel

The steel for the reinforcement was modelled with a tri-linear stress-strain relationship. Based on the tensile tests conducted on the used reinforcement, presented in Table 3.4 in Chapter 3, a value of 200GPa was used for Young's Modulus and the yield stress was taken as 650MPa. Poisson's ratio was specified as 0.2, as is usual for reinforcement steel. An isotropic hardening law was used for the strain hardening, after yielding, upto 685MPa and 1.5% strain. Beyond this point the material was considered to be perfectly plastic. Similar to the concrete model, as plasticity occurs in the steel elements, the related energy dissipation is applied. The material unloads with its initial elastic stiffness, E_0 . The stress-strain relationship used is plotted in Figure 4.7, including the unloading behaviour.

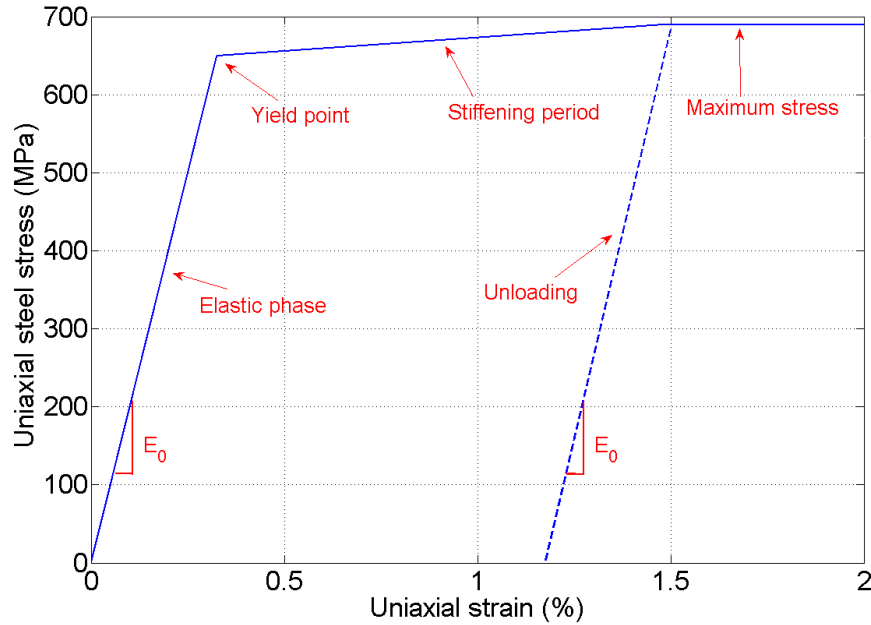


Figure 4.7: Uniaxial stress-strain relationship for reinforcement steel for compression and tension

No ultimate capacity was specified for this model and therefore it does not account for the potential for rupturing of the reinforcement at high strains.

4.4 Model checks

In order to ensure the FEA models do not provide spurious results due to numerical issues, a number of checks were conducted on the model and the results. These are summarised in this section.

4.4.1 Mesh sensitivity

The solutions from nonlinear FEA are usually influenced by the mesh refinement. In addition to the issues mentioned in Section 4.2.1, a coarse mesh will not replicate the true stress gradients across a section and therefore may not display the local reduction in stiffness, due to yielding or cracking, and result in the model, or a section of it, being too stiff and undamaged.

Alternatively, the post cracking or crushing behaviour of the CDP model can be sensitive to the refinement of the mesh. In situations where there are localised areas of high tensile stress, decreasing the mesh size results in narrower crack bands and does

not represent true distribution of stresses and strains. This effect is reduced by the presence of reinforcement which assists in the distribution of the stresses and prevents local stress concentrations. However, a very fine mesh may have many concrete elements that are not near a section of rebar and these sections may behave as plain concrete (Simulia, 2010).

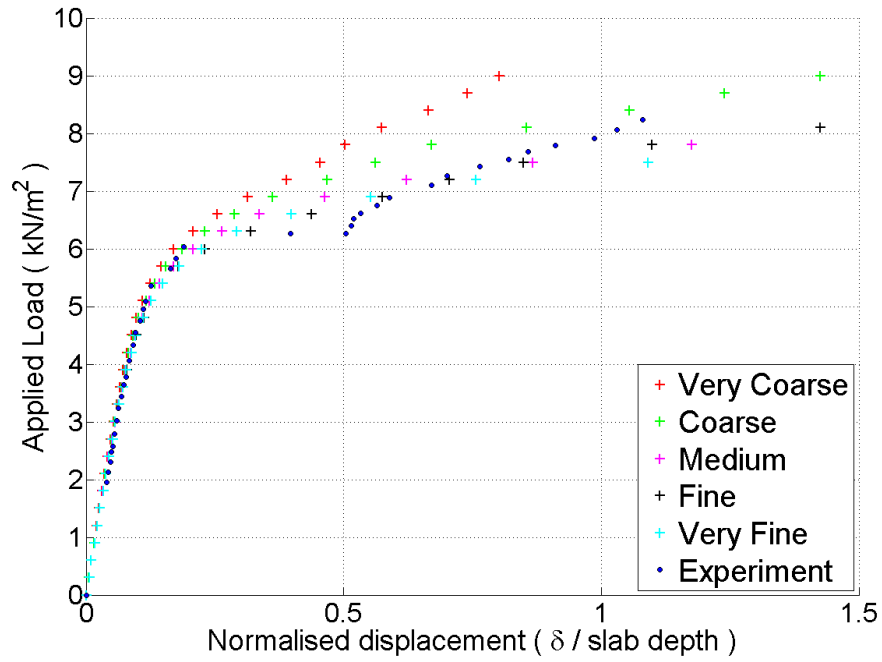
To determine a suitable mesh density a parameter study was conducted on the model for the corner removal with static loading condition (test C-S). The peak deflection against applied load for each of the different mesh densities, and the experimental results from Chapter 3, is given in Figure 4.8(a) and also presented in Table 4.2.

This information can be seen further in Figure 4.8(b), where the peak displacement at different loads for each model is plotted against the number of concrete elements used. Additionally, the results from the experimental slab are also plotted with the solid line for each loading level. Up to 7.0 kN/m^2 all the models converge well towards the experimental case. However, for higher loads the fine meshes provide results significantly higher due to the narrow crack bands reducing the local stiffness too much. Alternatively, the coarser meshes are too stiff as cracking occurs, as their larger element size does not capture the localised stress effects caused by the formation of cracks. This therefore means that these models are less useful for assessing the state of the structure and damage that has occurred.

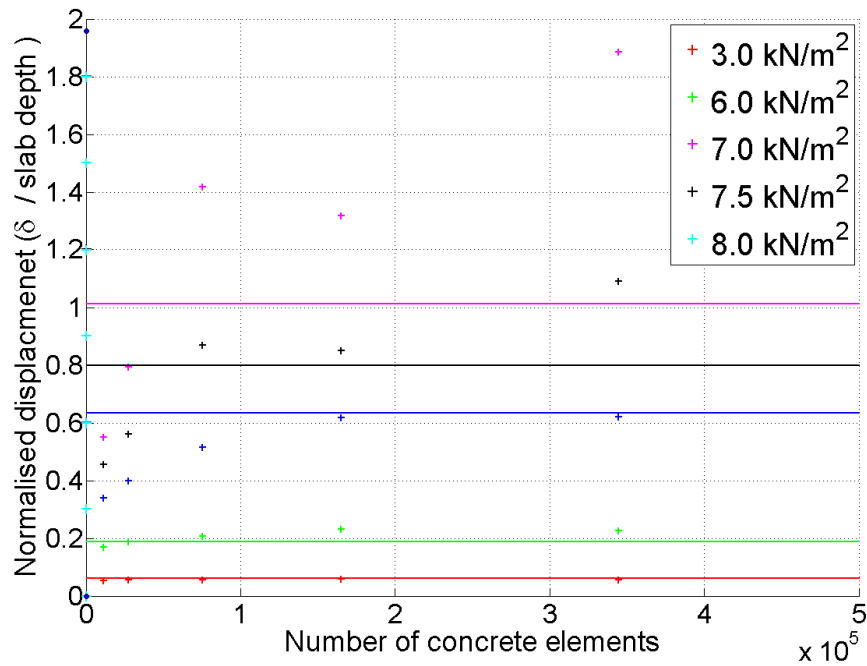
Based on this study, the Fine mesh density was used, i.e. concrete elements were $25 \times 25 \times 6.67 \text{ mm}$ according to Table 4.2. Both the Fine and Very Fine cases gave close predictions to the experimental results, and to each other, however the latter required considerably more computational time. While the selected refinement does over predict the deflections at the highest loadings levels, it shows a good agreement within the elastic range and into the early cracking phase.

4.4.2 Quasi-static loading

Explicit analysis solves for dynamic equilibrium at every time increment. For the static loading condition, and the pre-load for the dynamic removal cases, if the load is applied too quickly then parts of the model may have large velocities, as a result of the applied loading. This condition, combined with the inertial effects, may change the response of a structure if it is in the nonlinear range. To overcome this, a quasi-static loading method is used, where the rate of loading is kept low. This is checked by comparing the kinetic energy of a section to its internal energy. The internal energy of the system is taken as the sum of recoverable strain energy and the artificial strain included



(a) Force against displacement for different mesh refinements



(b) Influential of the number concrete elements used at different loadings

Figure 4.8: Effect of mesh refinement on FEA predictions for test C-S. Experimental results are also shown with solid lines.

Table 4.2: Results from mesh sensitivity parameter study - Test C-S

	Very Coarse	Coarse	Medium	Fine	Very Fine	Experimental
Number of concrete elements	1138	27552	75588	165312	344400	
Concrete Element Width (mm)	67.5	50	33.75	25	20	N/A
Concrete Element Depth (mm)	13.33	10	8	6.67	5	
Rebar Element Length (mm)	400	200	150	100	50	
Peak displacement at: (mm)	3.0kN/m ²	4.25	4.40	4.49	4.57	4.8
	6.0kN/m ²	13.62	15.00	16.61	18.44	15.1
	7.5kN/m ²	36.38	44.95	67.91	87.24	63.8
Computational Time (Hr)	16	28	79	264	431	N/A

to control distortions, combined with the energy lost due to plasticity and damage dissipation. For a reasonable quasi-static condition this ratio should not exceed 5–10% according to Simulia (2010).

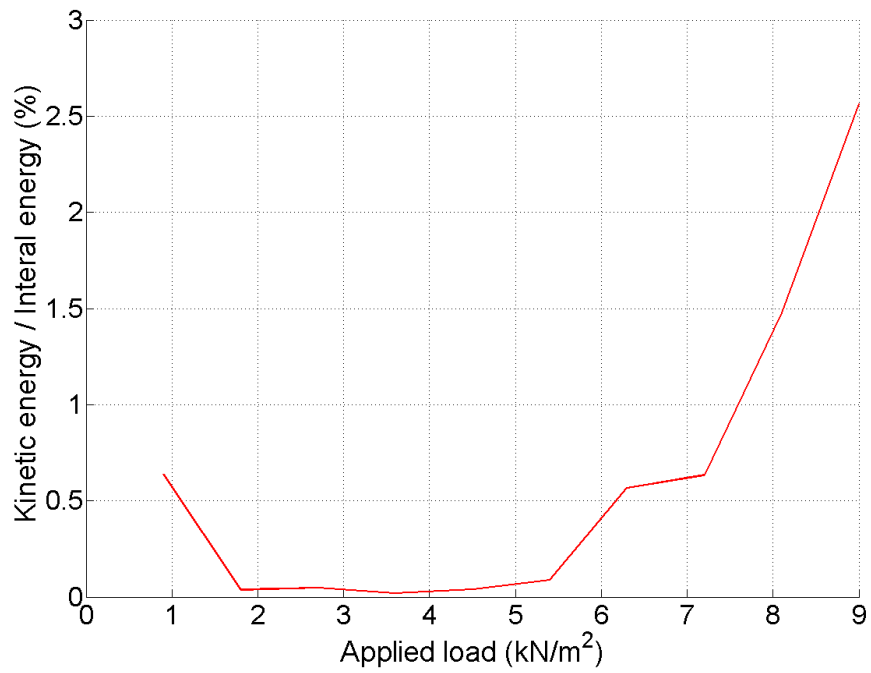
However, to consider a large structure, in a long enough time period to create a quasi-static condition, is usually very numerically demanding, requiring millions of time increments. This process can be made more efficient by increasing the mass matrix. As the stable time increment is inversely proportional to the square root of the mass terms, increasing the density by a factor of f^2 reduces the analysis time by a factor of f . As this makes inertial effects more significant, it is most suitable when applied to the small elements which limit the stable time increment and that do not move much, for example the bearing elements.

Examples of the energy balance are given in Figure 4.9, showing the total internal energy compared to the kinetic component. During the static test, Figure 4.9(a), for almost the entire testing range the kinetic energy is less than 0.6% of the total, with the early high value due to the sudden application of the initial load. The percentage rises to 2.6% towards the end, as plastic deformations cause additional movement. The dynamic case is even less significant with a peak kinetic energy at 0.9% of the total internal at the beginning. The ratio then drops, to less than 0.2%, for the remainder of the loading (see Figure 4.9(b)). These values demonstrate that the loading rate is suitable to achieve a quasi-static loading condition.

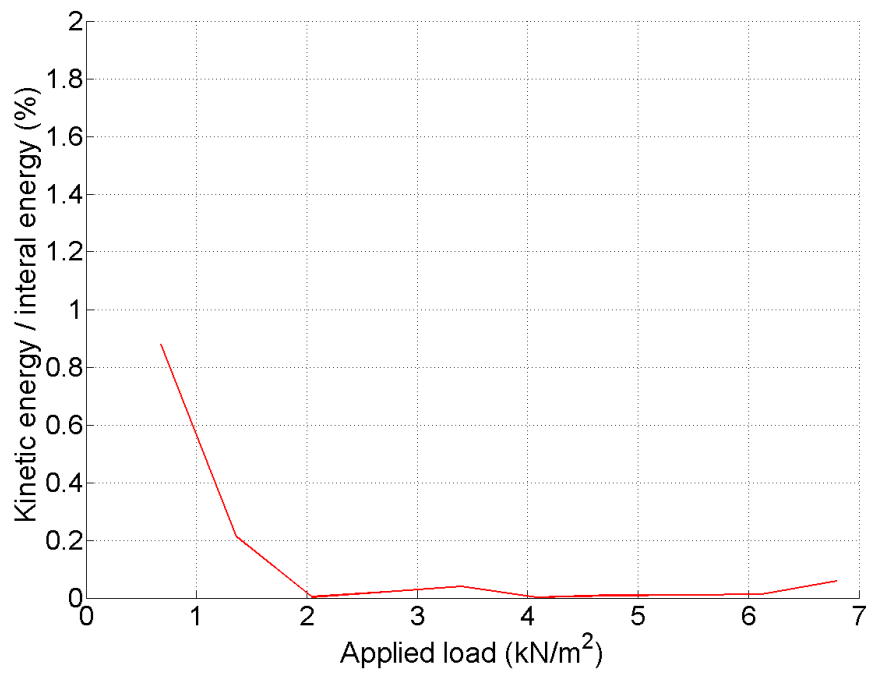
4.4.3 Artificial strain energy in the concrete elements

Elements with reduced integration points, such as the 8-node elements used for the concrete slabs, can exhibit an hour-glassing effect, also known as key-stoning, under bending conditions, as shown in Figure 4.10(a), resulting in deformations without any straining. To prevent numerical difficulties with such an event, Abaqus applies an artificial strain energy to such points to overcome the spurious zero-energy mode, however excessive use of non-real energies is not recommended outside of elastic analysis. Increasing the number of elements through the depth of the section gives a better bending profile, see Figure 4.10(b), and less required artificial strain. Hour-glassing can also occur if the mesh becomes too distorted, commonly caused by a concentration of force on one node.

Therefore, these models aim to keep the artificial strain energy below 1% of the internal energy of the section. An example is shown in Figure 4.11 for the static loading during test C-S. For the majority of the loading, the ratio of artificial strain energy in

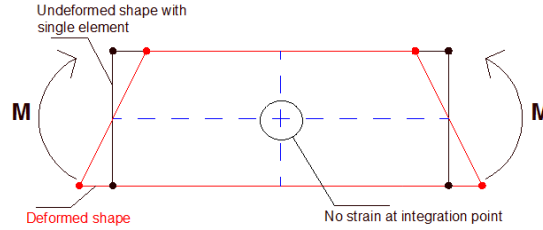


(a) Loading for static condition - Test C-S

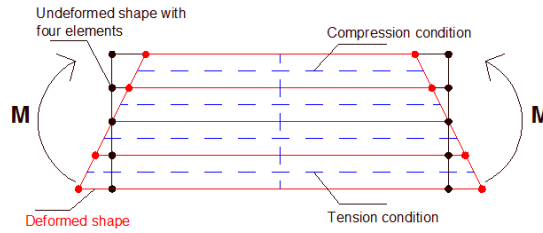


(b) Pre-loading to 6.8 kN/m² - Test C-D

Figure 4.9: Ratio of kinetic and internal energies during quasi-static loading for corner removal tests



(a) Bending of a section with a single element



(b) Bending of a section with four elements

Figure 4.10: Diagram demonstrating the hour glassing issue leading to bending deformation without straining

the concrete to the total internal energy is less than 5%, typically under 1%. This value does increase towards the end of the loading period, this is partially due to the much larger deformations that occur, as mentioned in the mesh sensitivity study in Section 4.4.1, and partially due to the concentration of stress at the edges of the supports causing localised deformation to the elements. However, in general, hour-glassing and the induced artificial strain energy to control it, is not an issue for these models.

4.4.4 Over-closures on the spherical bearings

As the curved surfaces for the spherical bearings are modelled with linear elements, over-closures between the two surfaces are possible. This occurs when the mesh is too coarse resulting in nodes from one surface penetrating the surface of the other whilst a 'hard' contact is specified. This effect is reduced with a finer mesh definition, additionally, tetrahedral elements were used for the bearings to give a smoother curved surface.

Before the first analysis step, Abaqus attempts to remove over-closures by moving the offending nodes. This adjustment is conducted before the first analysis step, or time increment, and does not cause any strain deformation to the elements. Any unresolved over-closures may result in local initial accelerations at the nodes once the

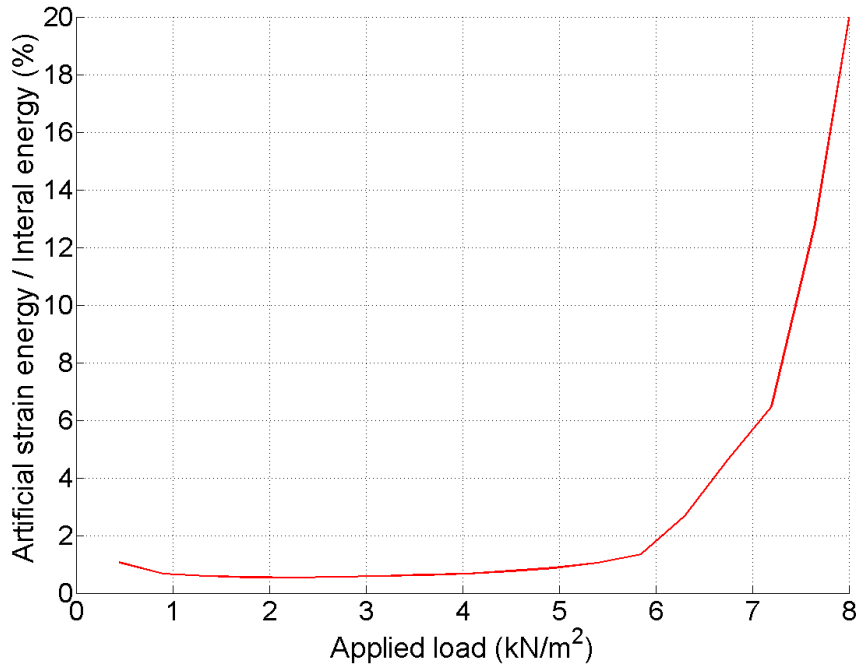


Figure 4.11: Internal and artificial strain energy for concrete elements during test C-S

analysis starts as the model attempts to enforce the hard contact rules. A second mesh study, separate to the concrete element refinement in Section 4.4.1, was conducted on the bearing elements. A summary of the maximum node movements and remaining over-closures is given in Table 4.3 for three different mesh refinements. As the same modelling approach was used for all tests, the data from only one model is presented. As can be seen, slight adjustment is required in each case however the maximum absolute movement is always small. Furthermore, the simulation removes practically all the over-closures before the analysis begins, indicating the definition of the bearing surfaces is adequate. As the coarse case would not give a smooth stress gradient as the bearing elements rotate, and the fine case is considerably more computationally demanding as the small element size decreases the stable time increment, the mid level of mesh refinement was used for further simulations. Although this had the highest amount of node adjustment, the over-closure is still completely removed before the analysis begins.

Table 4.3: Summary of adjustments made due to node over-closures between surfaces

Model	Bearing surface	Maximum node over-closure adjustments (mm)	
	mesh refinement (mm)	Strain-free node adjustment	Remaining over-closure
C-S	Coarse (25)	1.427	4.000×10^{-17}
	Medium (20)	1.897	2.905×10^{-17}
	Fine (8)	0.317	7.967×10^{-18}

4.5 Summary

This chapter introduces the numerical approach used to simulate a column loss event for flat slab structures. The use of Finite Element Analysis (FEA) is introduced and justified and a description of the model is presented covering the details regarding the geometry and loading.

The material models are an important aspect for considering the behaviour of structures under extreme loading. The options for nonlinear models used are presented and the used model described.

Finally, a series of preliminary investigations were conducted on the model to ensure the simulations will provide reliable results. These included checks on the mesh density and the energy balances.

The presented model is based on recognised theory and good modelling practice, and the preliminary results suggest it is suitable for modelling such events. In the next chapter it will be further validated against the experimental results before being used for a parameter study in Chapter 6.

Validation of the Finite Element Model

This chapter takes the Finite Element (FE) model presented in the previous chapter and uses it to replicate the experimental programme discussed in Chapter 3. The two sets of results are compared to validate the modelling assumptions.

5.1 Introduction and overview

As was described in the project objectives in Section 1.3.3, the purpose of this chapter is to:

Validate the numerical model against the results from the experimental tests.

Therefore, this section does not seek to tune material and modelling parameters with the aim of improving the correlation between the numerical and experimental results. Instead, using the modelling approach given in Chapter 4, with measured material inputs and known geometries, the FE results are compared to their equivalents from the experimental tests. All the data collected, analysed and discussed in Chapter 3 can therefore be compared to the numerical results and comments made on the similarities and differences. Due to the uncertainties that exist during experimental investigations, and the modelling assumptions made, perfect agreement is not expected or required between the cases. However, there should be similar patterns of behaviour, especially for the important issues identified in Chapter 3, such as the redistribution of forces and the influence of dynamic effects. The model can be said to be validated, and suitable for further investigations, if it provides a close estimate to the response of a flat slab

Table 5.1: Summary of all FE models including the variables that were compared to the experimental results

Slab ID	C-S	C-D			PC-S	PR-S	M-D		
Loading level (kN/m ²)		3.0	6.8	7.7			3.1	6.9	8.5
Reactions	✓	✓	✓			✓	✓		
Displacements	✓	✓	✓			✓	✓		✓
Strains	✓				✓	✓			
Strain rates			✓				✓		✓
Flexural damage	✓								
Frequency analysis		✓	✓	✓			✓	✓	✓

after a sudden column loss, compared to the observed experimental results.

In order to validate the presented numerical model, the experimental programme was replicated. Models representing each of the seven slabs listed in Table 3.1 were created according to their geometric and material properties. For the dynamic removal tests, the loading levels from Table 3.2 were used. The results of all these models were initially considered to identify the most suitable data for comparisons. The results that are presented and compared to the experimental cases in this chapter are summarised in Table 5.1. Note that most reliance has been placed on the C-S, C-D and M-D tests. Although the Penultimate removal tests gave very useful results for adding to the understanding of the response of slab elements after a column loss, especially for changes in stress distributions, issues with the support conditions and uplifting effects limited their comparison to the FE model. As the Corner and Middle removal cases also give a better representation of real structural arrangements further consideration is given to them.

5.2 Validation of Finite Element model against experimental results

To compare the FE model and experimental tests the following results were considered: changes in reaction forces to supports, displacements at different locations, reinforcement strains and strain rates, flexural damage based on reinforcement strains and concrete cracking, and frequency analyses after a sudden column loss. The models that these results are taken from are summarised in Table 5.1. Each of these aspects are considered and discussed separately below.

5.2.1 Force redistribution

Static loading

Reaction forces at each support were monitored during the static loading simulations, and the relative load to each support after a corner column removal case is shown in Figure 5.1. The solid lines show the numerical values while the data points from the experimental test are also plotted to allow comparison. For all positions, for most of the loading, a very similar response is shown; the model matches the experimental results to within 1.3 percentage points. Around 6kN/m^2 there is a higher deviation, with a maximum difference of 3.6 percentage points. This is due to the effects of cracking in the concrete reducing the stiffness and causing sudden changes in the span lengths, as was discussed previously in Chapter 3. The proposed model does not capture this effect fully, partly because the plastic damage rule used leads to a gradual reduction in stiffness after cracking, see Section 4.3.1, whilst concrete often undergoes a sudden change. However, past the initial cracking phase there is again a strong agreement between the results and the overall response is viewed to be good enough to make predictions on the demand placed on surrounding supports after a column loss.

The Penultimate removal case with reduced reinforcement, test PR-S, shows a different response. As can be seen in Figure 5.2, the model gives very similar values within the elastic range with an agreement of ± 2.2 percent points. However, beyond 5kN/m^2 this changes. In the experimental case, the back two corners lifted up and the load they were carrying was redistributed to the middle support. In this model however, there is a slight dip in load on the back supports but rather than continuing in this manner, the slab experiences further damage, and the load resumes and even increases slightly. At the same time, the middle support initially followed the experimental pattern but then drops again. However, the front supports remain very similar to the experimental case. The fact that the FE model does not capture the corner uplifting effect, and the related changes, is not considered to be a significant issue. Firstly, the differences in values is not very large and a good estimate can still be gained from the model. Additionally, real structures are vertically restrained due to their columns and will not uplift in these cases anyway.

Of further interest is the change in demand placed on a support before and after a column loss event. A large increase in vertical reaction force may exceed the shear capacity of an area and lead to progressive failure. This relative change in support load is given in Figure 5.3, and is taken as the ratio of the support load during the elastic range after column removal and the fully supported condition. This figure shows the comparison

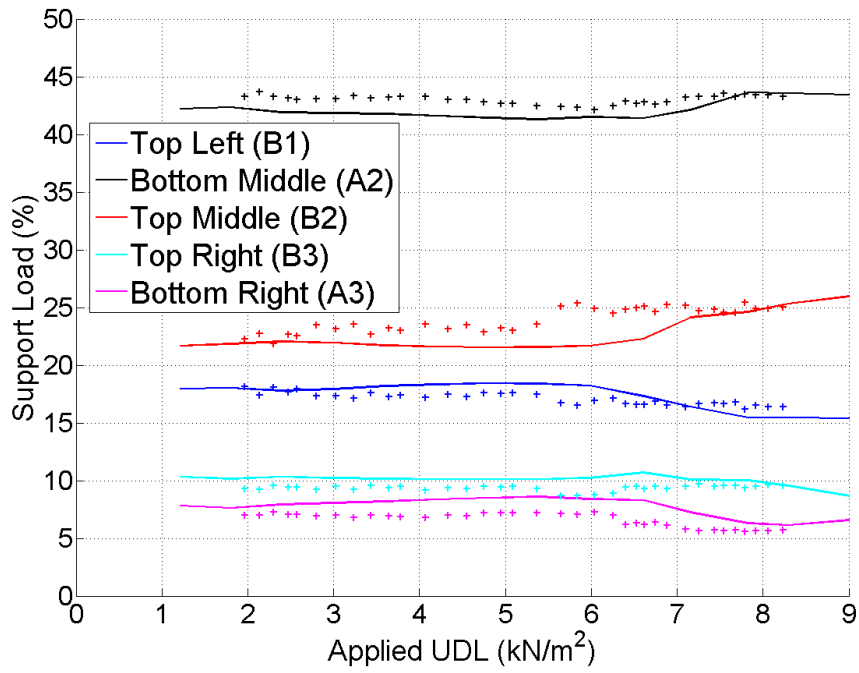


Figure 5.1: Distribution of forces to each support as loading increases - Test C-S. Solid line is numerical model, +'s the experimental results

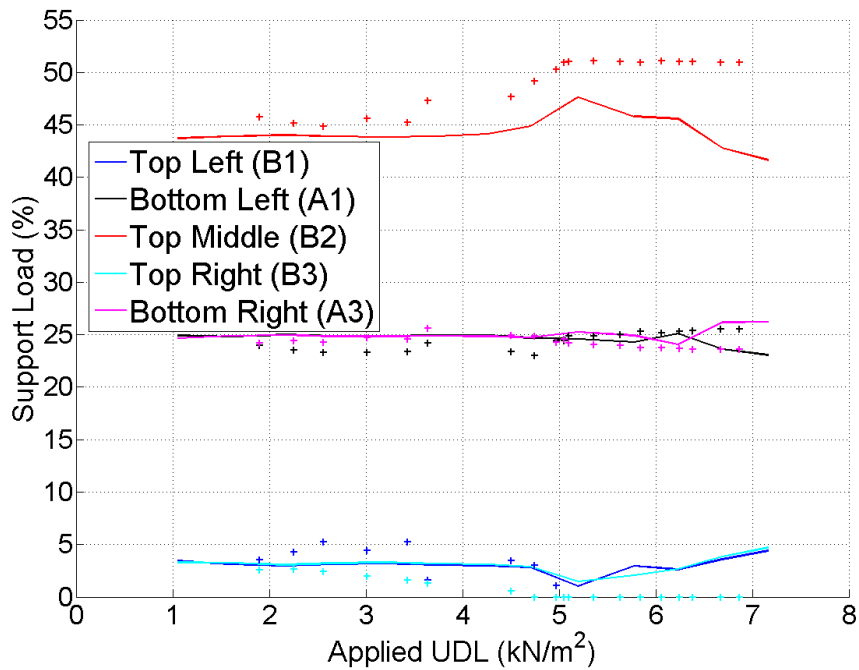
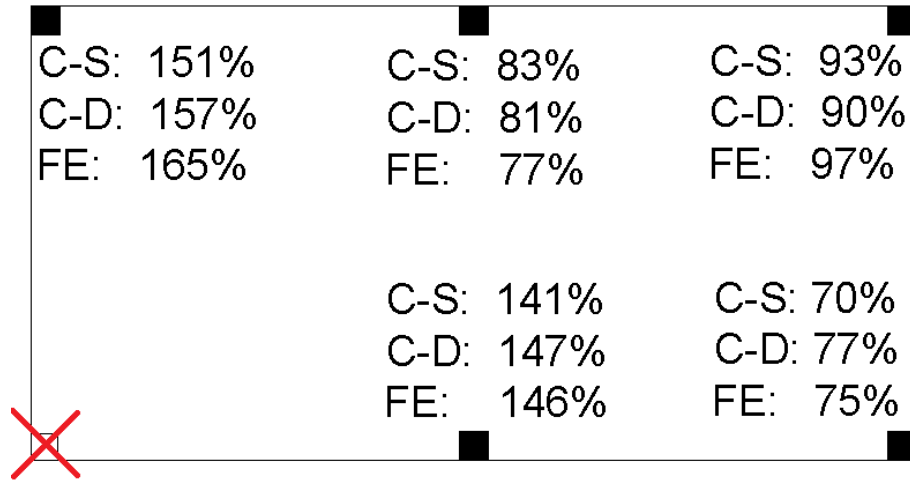


Figure 5.2: Distribution of forces to each support as loading increases - Test PR-S. Solid line is numerical model, +'s the experimental results



C-S: 151%	C-S: 83%	C-S: 93%
C-D: 157%	C-D: 81%	C-D: 90%
FE: 165%	FE: 77%	FE: 97%
	C-S: 141%	C-S: 70%
	C-D: 147%	C-D: 77%
	FE: 146%	FE: 75%

Figure 5.3: Mean change in distribution of forces to each support after column loss. Comparing experimental tests C-S and C-D for the FE model.

between numerical model under static loading, and the two experimental cases for the corner removal. As can be seen, there is the same pattern between the results with the closest supports showing a large increases in demand. However, the agreement to either of the experimental cases in actual values is not as strong, but in general falls close to the values expected. Therefore, while the model matches the distribution of forces seen in the lab for the general case, the uncertainties both from obtaining load cell values, and replicating the conditions with the model, result in different values for this test.

Dynamic removal

After a sudden column removal there is a dynamic change in the loading to each support. While the instrumentation used during the experimental programme was unable to monitor sudden changes in reaction forces after the column loss, the FE model does provide this information. Results from the corner column removal case is given in Figure 5.4. Here the reaction forces at the 5 remaining supports are plotted against time. Observing first the elastic test conducted at 3.0kN/m^2 of loading for test C-D, Figure 5.4(a), shows clearly that the closest two positions, Top Left (B1) and Bottom Middle (A2), have an increase in load. Additionally, there is also a much larger amplitude in oscillation for these locations compared to the further locations. For further comparisons the displacement against time at the column loss location is also plotted with a dashed line on the second vertical axis. Furthermore, as was suggested during experimental discussion, the maximum vertical loading occurs close to the moment the slab

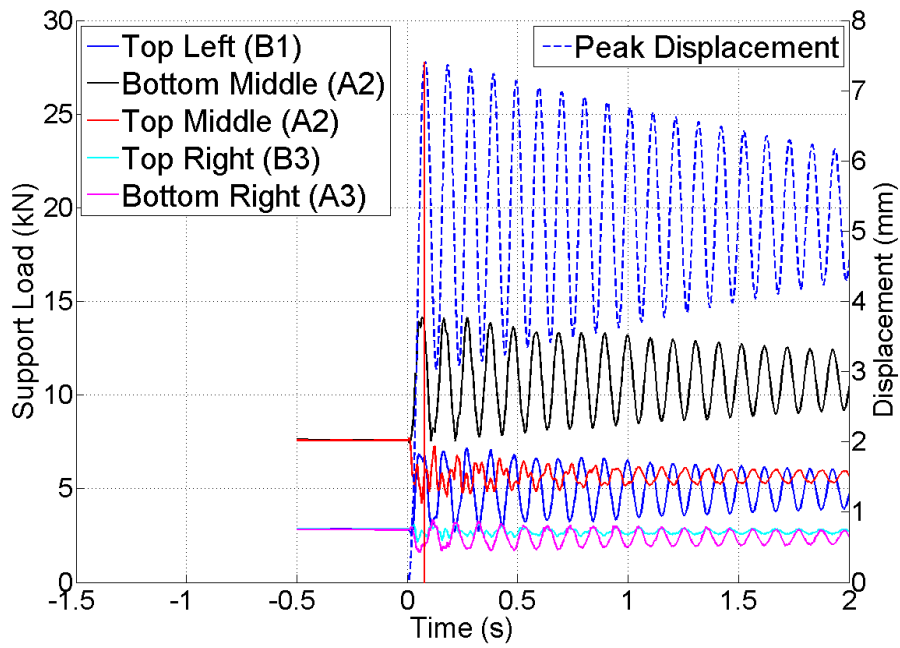
reaches its first peak and is at a temporary static condition, in this case 0.08s after removal. This can be seen by the annotated red vertical line. Figure 5.5 shows the Power Spectral Density (PSD), from a Fourier transform, of each of the support reactions and the peak displacement. Comparing the frequencies for the elastic case, Figure 5.5(a) demonstrates that the oscillation of the slab matches the changes in loading on the all the supports with a dominant frequency of 9.76Hz.

The 6.8kN/m² test shown in Figure 5.4(b) shows a similar response with the same changes in distribution of loading, with the time of maximum loading and peak displacement coinciding. These force plots are less smooth than the previous case, mainly due to the damage sustained before the first peak, leading to changes in the force distribution. These then settle down and give a smoother behaviour for the rest of the motion. Comparison between the displacement and force frequencies based on the response after the first peak, and plotted in Figure 5.5(b), also show a strong agreement with them all oscillating at 5.68Hz. However, the supports also show a higher frequency response which is not replicated in the displacement response. The damage near the supports leads to a change in behaviour and this creates the different response.

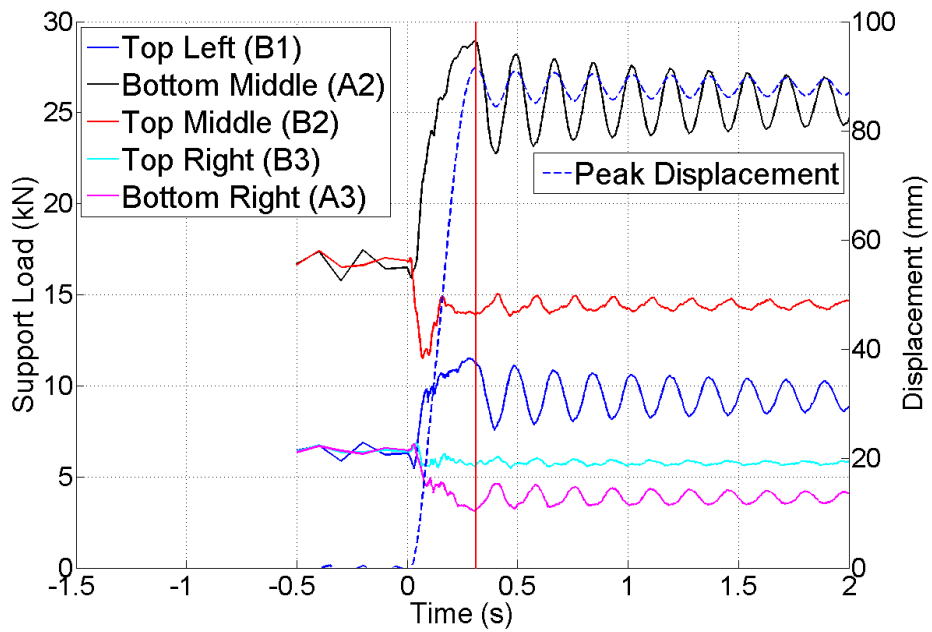
Figure 5.6 shows similar results for the larger slab with the middle edge support suddenly removed, with 3.1kN/m² of loading. These reaction forces have been presented as a percentage change from the fully supported condition before removal to highlight the change in demand experienced by each support. Additionally, the final reaction readings from the experimental results are plotted with dashed lines. Firstly, again the orthogonally adjacent supports, A2/A4 and B3, clearly take the load previously carried by the removed support, plus an additional amount due to the decrease in the other locations. The final readings match very well with the experimental results, especially for the nearest supports which are the most critical. Of further interest is the large peak and amplitude involved. The nearest supports peak reaction forces are 181% and 166% of their starting amount, Therefore, if these sections of slab were already near their design limit, such an action may cause sudden shear failures, similar to the observed situation in a different test, PR-D. This dynamic amplification also means that the maximum support load could be upto 29% higher than the value predicted from a static analysis.

5.2.2 Displacements from static tests

The force-displacement diagram after a column loss is one of the key indicators into the suitability of the numerical model. A good model should predict the elastic stiffness of a structure and identify the elastic limit. It can also provide an indication into

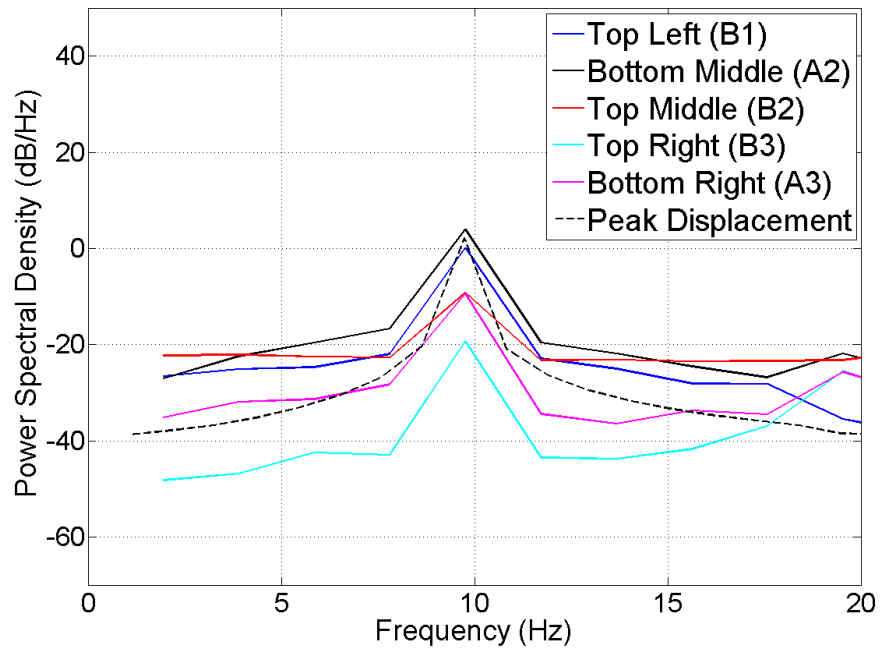


(a) Elastic test - 3.0 kN/m^2

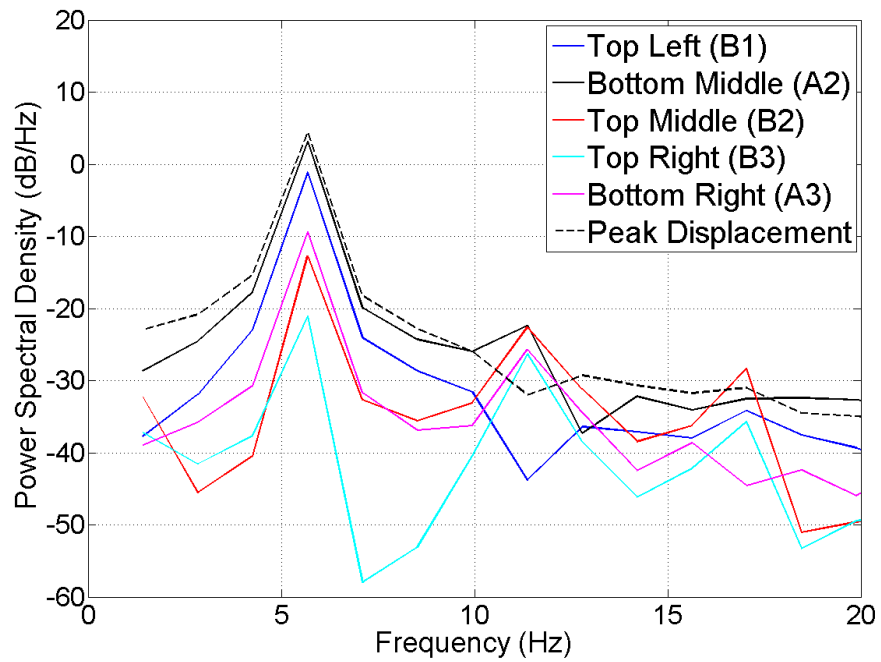


(b) Damage test - 6.8 kN/m^2

Figure 5.4: Reaction forces against time after column loss for each support.
Also showing the peak displacement against time - Test C-D



(a) Elastic test - 3.0kN/m^2



(b) Damage test - 6.8kN/m^2

Figure 5.5: PSD of support reactions following corner column loss. Also showing PSD for the peak displacement - Test C-D

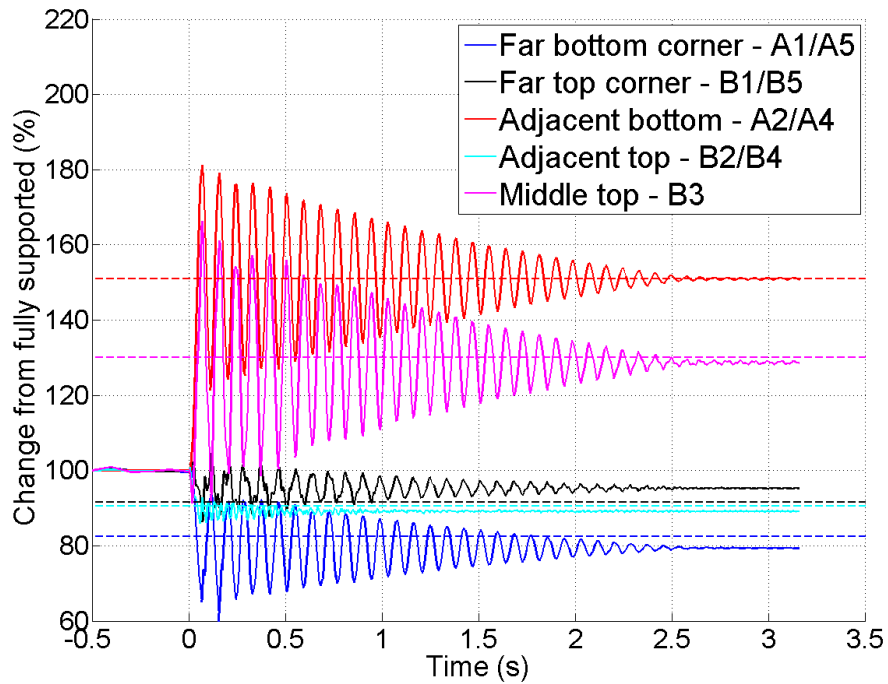


Figure 5.6: Percentage change in reaction forces to each support against time due to a dynamic column loss - Test M-D

ductility of the structure in the nonlinear range. As was observed in the experimental programme, there is an initial linear force-displacement response across the entire sample, however, once cracking starts to occur, there is a significant reduction in stiffness. Since levels of damage can often be compared to normalised deflection readings, an accurate representation of this response is important.

Considering the displacements against loading, shown in Figure 5.7, for the corner column loss condition shows a good agreement between the numerical model and the experimental results. The locations of the monitored points were given in Figure 3.6. Both the two positions presented, the removal location and the centre of the adjacent bay, match the initial stiffness of the experimental results at low levels of loading. After cracking occurs, there is a reduction in stiffness, however while there was a sudden increase in displacements observed in the experimental case, the FE model gives a more gradual response. This is due to the use of the gradual plastic reduction in capacity after cracking, described above in Section 4.3.1. Despite this effect, variation between the cases remains small for the load level tested.

The penultimate removal case with reduced reinforcement shows a poorer agreement. The normalised displacement against load at three positions are compared in Figure

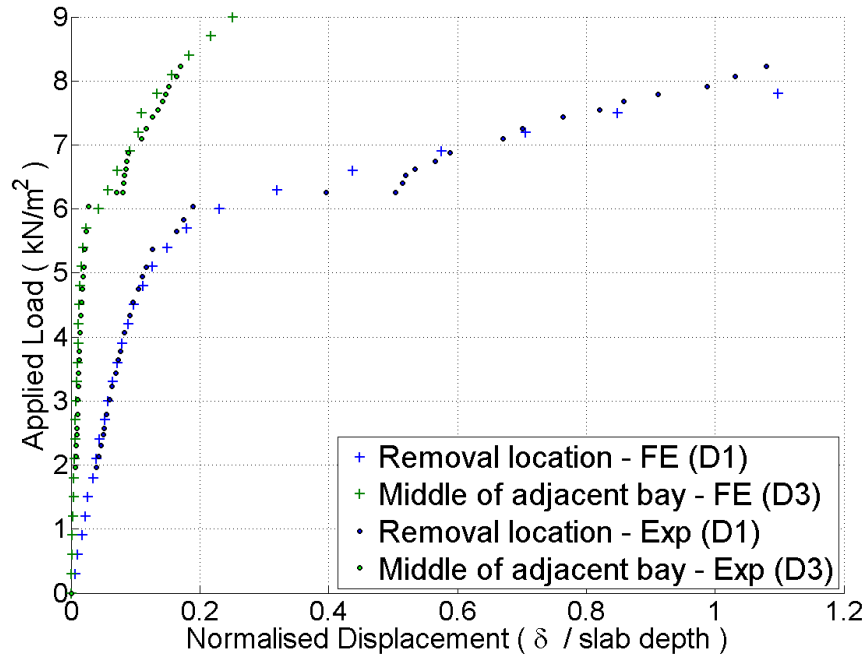


Figure 5.7: Normalised displacement against load for test comparing experimental results to the FE - Test C-S

5.8 with the locations shown previously in Figure 3.17. The cracking load predicted from the FE model is close the experimental value, however, the response then shows a gradual reduction in stiffness, see point D1, while the experimental case indicated a sudden change which then stays relatively constant. The main reason for this variation can be seen by considering the back support results. During the experiment there was uplift at this location allowing the slab to rotate towards the removed column, without causing as much flexural damage. However, the numerical model does not replicate this effect, hence the more significant cracking, and the reduction in stiffness that occurred. Overall however, this model still provides useful information into the response of the slab after the column loss. As mentioned previously while discussing Figure 5.2 in Section 5.2.1, the limitation of not including the uplift and rotational aspect is not a major issue as columns will usually restrain the slab vertically and prevent such effects.

5.2.3 Displacements from dynamic tests

Taking the displacements against time for the corner column loss test, C-D, a comparison can be made between the experimental results and the FE model. This is shown in Figure 5.9. For the elastic case at 3.0 kN/m^2 the model shows slightly higher deflections than the experimental. This is due to a lower level of stiffness, which also reduces

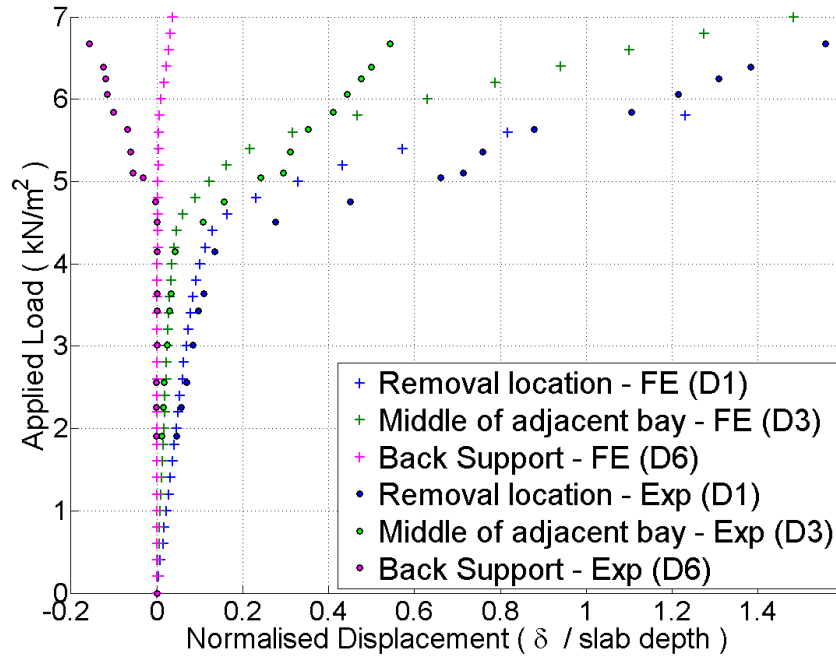


Figure 5.8: Normalised displacement against load comparing experimental results to the FE - Test PR-S

the oscillation frequency. The slab in the experimental case moved at 11.0Hz while this model predicts only 9.57Hz. The variation in the stiffness may be due to the uncertainties in the material properties, support conditions and accuracy of the measurements. However, the difference in deflections are less than 2mm, and the damping ratio for both cases is 0.01, indicating that responses are similar and that a suitable representation of the slab can be gained from the FE. At the higher loading, 6.8 kN/m^2 , the position in the middle of the adjacent bay shows a very similar relation to the experimental results, including a slight delay before moving. The peak displacements show a poorer agreement. Firstly, the numerical case shows that after the main effects have stopped, plastic drift continues to increase the deflections. While this was observed in some experimental tests it did not occur at this level. Additionally, a smaller peak is predicted from the numerical case, this could either be due to the simulated support removal time being too long, or the Dynamic Increase Factor (DIF) is too high for the strain rates.

Considering the strain rate further, the peak strain rate measured in the top steel over the adjacent support was 0.028s^{-1} , which, assuming the strain rate in the adjacent concrete is similar, corresponds to a DIF of 1.2 according Equation 4.3.12, the same value that was specified as a fixed increase factor. This occurred between 60 and 100ms after

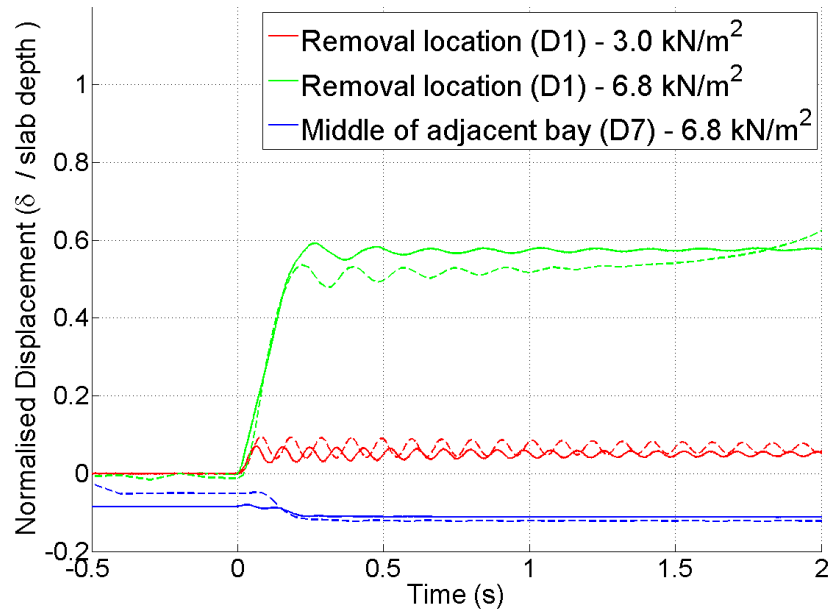


Figure 5.9: Normalised displacement against time for test at different locations and loadings. Experimental results (solid lines) and FE (dashed lines) are shown - Test C-D

removal, while the peak displacement did not occur until 0.22ms. At the moment of maximum displacement, the highest strain rate in the steel was a factor of 10 lower than the peak, which reduces the calculated concrete DIF to 1.15. This assessment indicates that the tensile concrete DIF is close to the correct value, although may still over estimate the additional capacity provided as the slab reaches its first peak, and therefore result in deflections that are too small. However, the difference in deflections between the numerical and experimental cases are small and are quickly damped out in both cases.

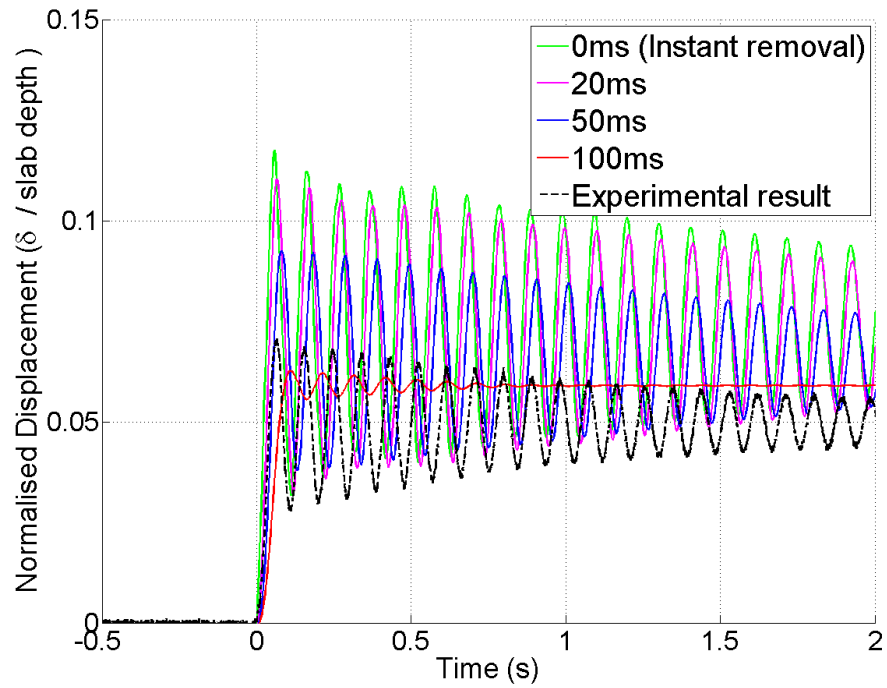
Figure 5.10 shows the displacements against time with different removal times. Four different time periods are used to reduce the reaction force provided by the temporary support, as described with Figure 4.2 on page 93. In the elastic test shown in Figure 5.10(a), all the cases overestimate the final deflections due to the reasons mentioned earlier. However, as the removal time changes there is significant difference in the response. The first two cases, 0ms and 20ms show very similar behaviour with close peaks and similar amplitudes. For the 50ms removal time the peak is noticeably reduced and is now 79% of the instantaneous peak. Additionally, it can be seen that the time of peak displacement is now later. With the 100ms case the peak is only 53% of the instantaneous removal and there is very little dynamic motion. Furthermore, the

ratio of peak to final displacements drops from 1.59 for the instantaneous case, to 1.42 and 1.06 for 50 and 100ms respectively. This demonstrates that the modelled removal time is an important factor. Based on the experimental results plotted, and assuming all other factors are accurate, the experimental removal time was between 50 and 100ms. However, as significant oscillations were seen in the experiment, it is likely to be closer to the 50ms value. Of final note, the experimental case reached its peak quicker than the 50ms case, despite the trend suggesting it should be longer. This may be due to the linear reduction in force at the support not truly representing the motion involved in suddenly pulling out the bar.

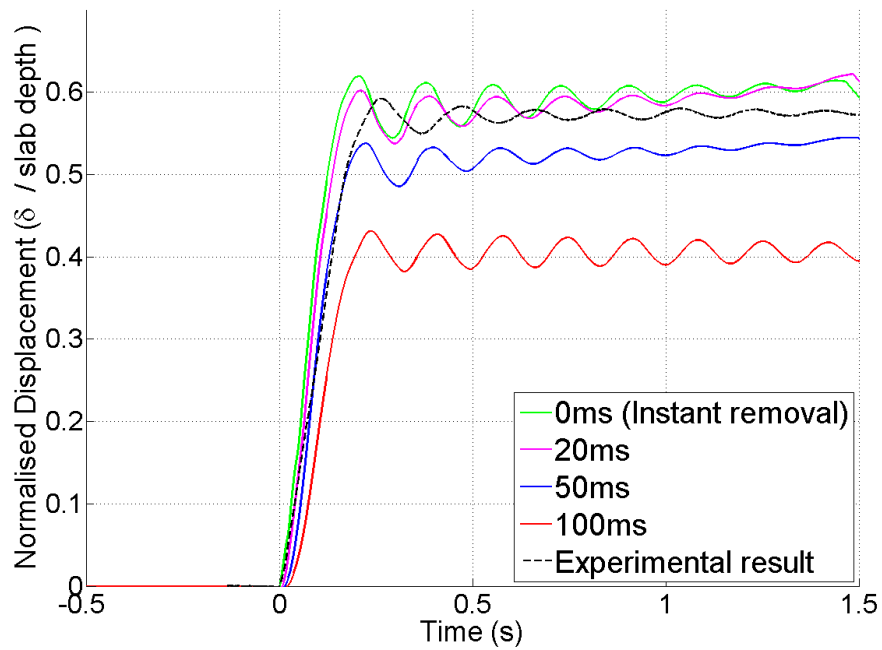
Considering also a higher loading case, presented in Figure 5.10(b), this again shows significant effect of removal time on the displacement response, with longer removal times creating smaller peaks. Since this test is also in the nonlinear range, a smaller peak results in less damage which in turn means that the final displacements are smaller. For this case, the peak experimental results appear to fit better with the 20ms case, although the speed of displacement matches the 50ms removal very well. Therefore, the 50ms case is a reasonable estimate of the removal time, however, towards the end of the motion, more damage occurred in the experiment than was predicted with the FE case resulting in the higher deflections.

The results of the dynamic removal on the 8.1m test with a continuous slab over the adjacent supports are presented in Figure 5.11. The locations of the monitored points were given in Figure 3.29 in Section 3.3.3. The first test was conducted with low levels of loading, within the elastic range, and is shown in Figure 5.11(a). It is clear that the FE model is less stiff than the experimental case with higher deflections observed. This can also be seen by the slightly lower frequency of oscillation in the numerical case, 11.1 Hz compared to 13.4 Hz taken from the experimental case. Such differences are likely when comparing results from a large specimen such as this due to the increased variations in the concrete properties and geometry that occurs from a large cast. However, the absolute values are still close ($<0.5\text{mm}$) and the same overall behaviour is observed. Furthermore, extracting the damping ratio from both signals shows that ζ is equal to 0.01 and 0.02 for the model and the experiment respectively, giving a good agreement for the dissipation of energy during the elastic test, primarily due to friction in the bearings.

At higher loading, 8.5 kN/m^2 in Figure 5.11(b), further differences can be observed. While the displacement values from the FE model tend towards similar values from the experimental case, in particular at the removal location, the motion is not as damped as the physical test. A clear oscillation motion can be seen from the numerical results



(a) 3.0kN/m² of loading



(b) 6.8kN/m² of loading

Figure 5.10: Displacements against time for different support removal times. Experimental results are shown as well - Test C-D

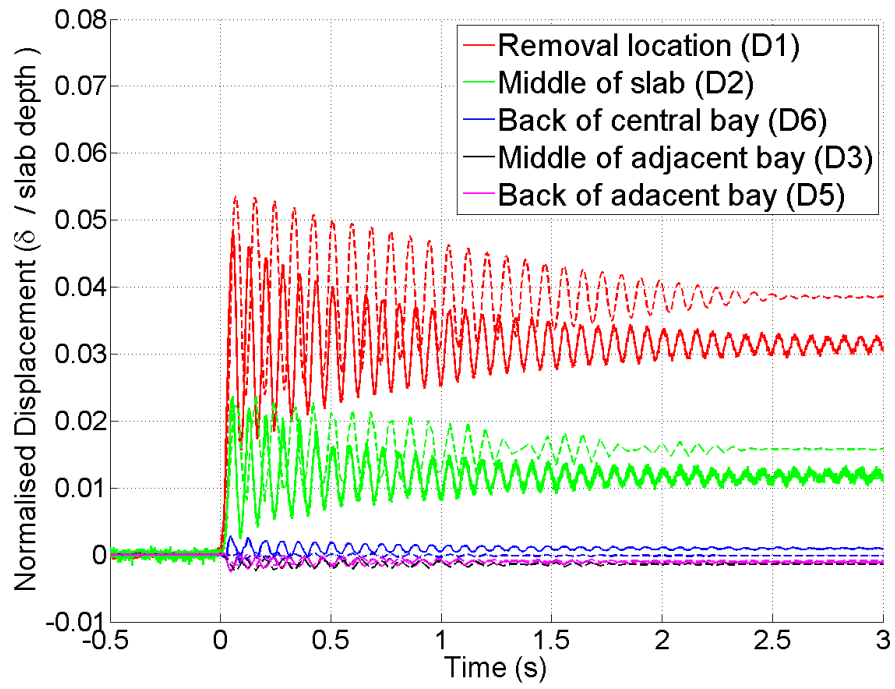
while the experiment reached its peak slower, and then remained there. Considering also the other monitored locations in the adjacent bay does show a better agreement, possibly as these locations experience smaller deflections and less dynamic influence. The experimental displacement-time response in the first 100ms after removal is not as smooth as other tests, this may be due to the support not being removed quickly and cleanly enough. Such an event would reduce the speed the slab fell, and cause closer to a static condition with little inertial effects.

The strain rate can be seen in Figure 5.12 for test M-D. Here the maximum tensile strain rate in the steel reinforcement is extracted from the FE model at every time step, as was done in with the experimental results according to Equation 3.3.2. This value is plotted separately for the top and bottom steel locations in order to compare the differences in hogging to sagging strain rates. Whilst these are taken from the steel, they will provide a close estimate into the tensile strain rate in the concrete which can be used to justify the DIF. The displacement against time at the removal location is also plotted on the second axis for further comparisons.

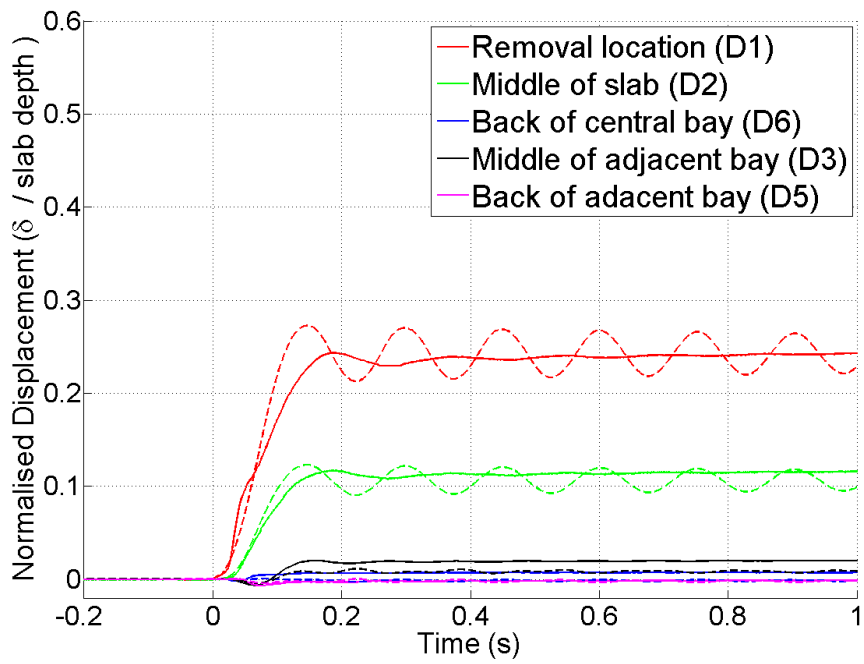
Considering the elastic test in Figure 5.12(a), the tension steel over the adjacent support experienced a maximum strain rate of 0.0055s^{-1} 60ms after removal. This is greater than the 0.0037s^{-1} for the sagging reinforcement. Within the first second after removal, faster motions were expected and so a higher sampling frequency was used, this explains, the change in response after 1s. At higher load, 8.5 kN/m^2 in Figure 5.12(b), it is again clear that the rate of strain of the top steel is greater than the bottom, with peaks of 0.0258 and 0.0155s^{-1} respectively. If these were concrete strain rates they would correspond to a DIF of 1.20 and 1.19 according to Equation 4.3.12, which was the value chosen. Of further interest is the times of the peaks. The top and bottom steels reached their maximum rates at 60 and 80ms after the support removal respectively, although note the sampling rate was only 10ms. This was much quicker than the time to maximum displacement, which was at 146ms after removal (recorded every 2ms). This emphasises the point made earlier that the maximum additional capacity, due to fast loading, does not occur at the point of maximum stress, and therefore the value of the DIF may not be critical.

5.2.4 Flexural damage

The damage profile is an important aspect for considering the effect of a column loss on a structure. This is monitored and compared to the experimental results in two ways; the cracking pattern and the reinforcement strains. Both these values provide information about the distribution of stresses and the areas that may experience damage or

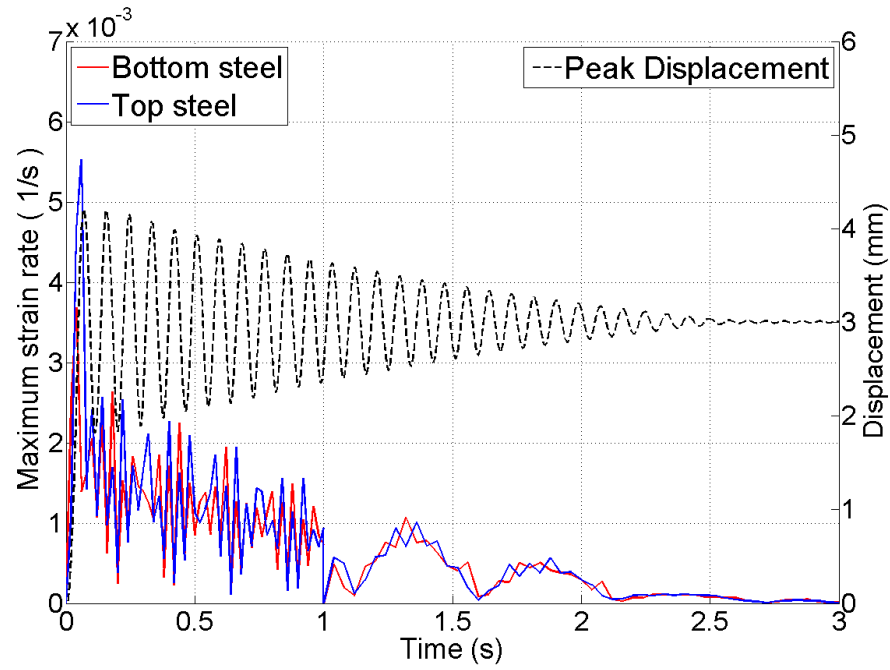


(a) 3.1 kN/m² loading

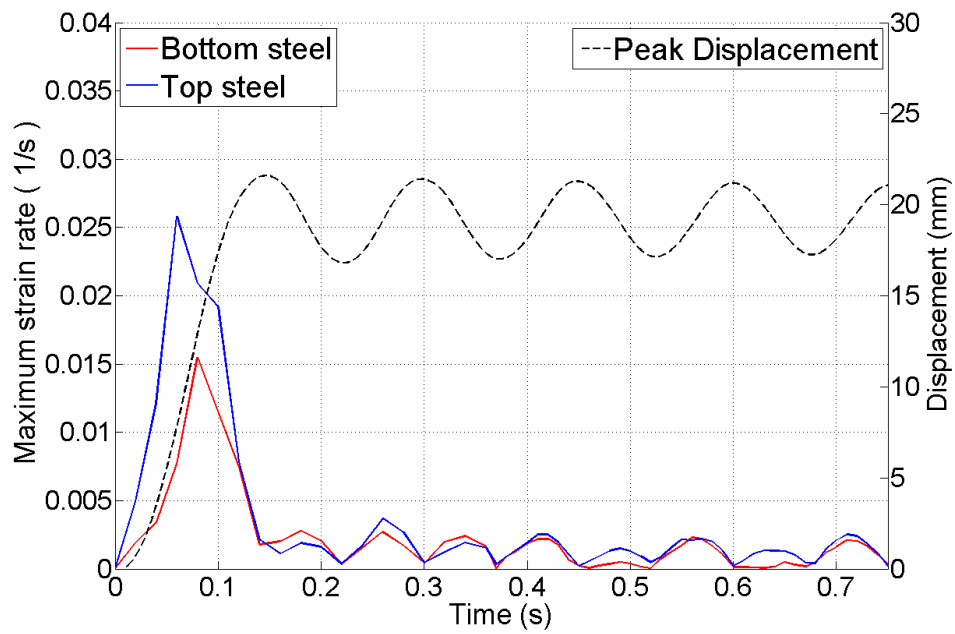


(b) 8.5 kN/m² loading

Figure 5.11: Displacements against time at different locations comparing comparing experimental results (solid lines) to the FE (dashed lines) - Test M-D



(a) 3.1 kN/m^2 loading



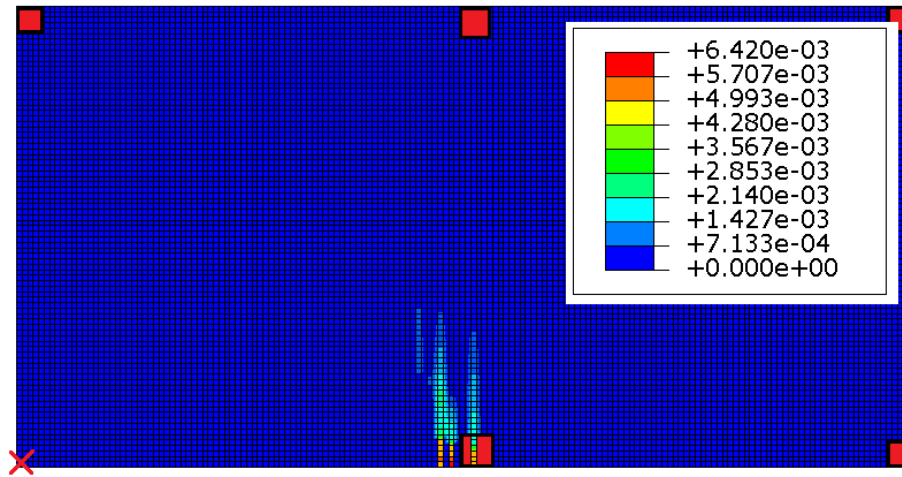
(b) 8.5 kN/m^2 loading

Figure 5.12: Maximum strain rate in the steel against time from FE model. Also showing the peak displacement against time - Test M-D

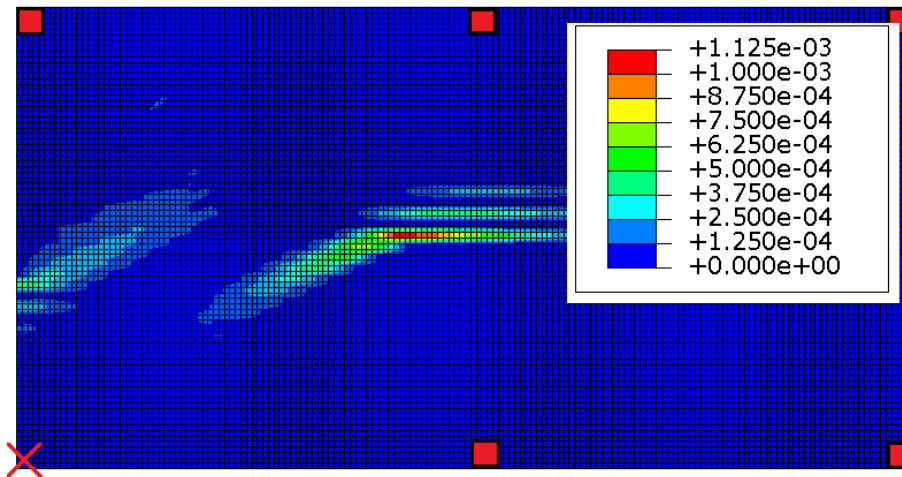
failure.

As has been mentioned previously, the Concrete Damaged Plasticity (CDP) model considers cracks to be a region of plastic deformation. Therefore, the location of the plastic strains should correspond to the location of cracks observed from the experimental case, while the orientation of the principal axes is perpendicular to the crack direction. Figures 5.13 and 5.14 show the location of plastic strains on the top and bottom surfaces of the concrete after a corner column loss, at two loading levels. At 5.4kN/m^2 of loading there is minimal cracking, with minor hogging cracks over the central support next to the removed support (Figure 5.13(a)). Cracking on the underside, is also minimal (Figure 5.13(b)), although the start of the diagonal cracks between the closest supports can be seen. This is much more noticeable at the higher loading level, 7.8kN/m^2 , in Figure 5.14(b). Here damage occurs across most of the slab. In the adjacent bay the cracks can be seen to follow the reinforcement locations, which are also annotated, as was seen from the experimental results. However, smaller cracks/plastic regions also occur between the steel bars. This is most likely due to the refinement of the element mesh resulting in many concrete elements being too far from a reinforcement element and therefore acting as plain concrete. This issue was discussed further in the Mesh Sensitivity discussion in Section 4.4.1. Considering the orientation of the maximum principal axes for the plastic strains shown in Figure 5.14(c) demonstrates again the direction of the cracks with the span between the two orthogonal remaining supports being critical. Finally, the cracks on the top surface, see Figure 5.14(a), suggest that while there is a large, damaging hogging moment over most of the width; most of the damage is concentrated near the support. All these patterns fit closely with the observed results presented in Chapter 3.

The deformations also cause damage to the reinforcement, once the yield strain is exceeded. Figure 5.15 compares the normalised strain readings between the FE model and the experimental results for test C-S. The positions are the same as those presented in the Chapter 3. At the lowest level plotted, 3.0kN/m^2 , there are only small strains, but the numerical model does over estimate the strain values. This is improved by 4.1kN/m^2 . However, once cracking starts to occur there is a large localised increase in the strain readings from the experimental case, just next to the support, on the side of the removed column. Yielding of the reinforcement occurred in the experimental case at this location, however, the FE model instead has a smoother strain profile over the central support. By the next presented load increment, 7.1kN/m^2 , the FE model has also yielded in this location and shows a similar response of a peak next to the support. The highest case demonstrates, again, the failure of the model to capture the correct

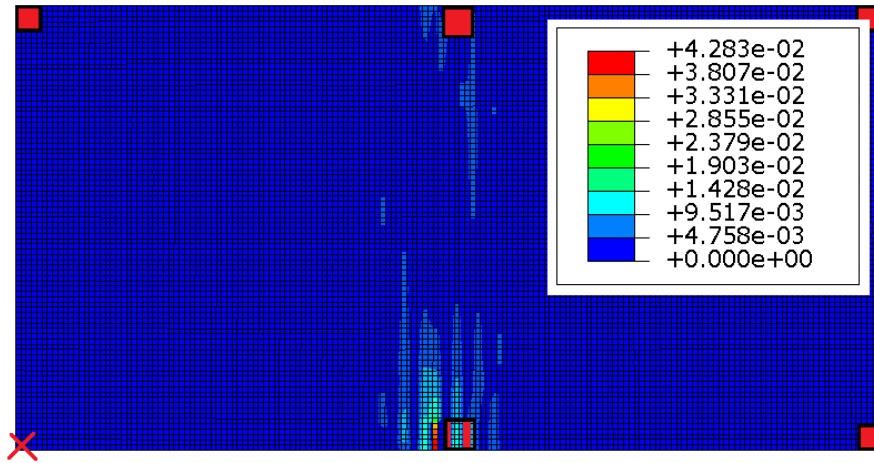


(a) Top Surface

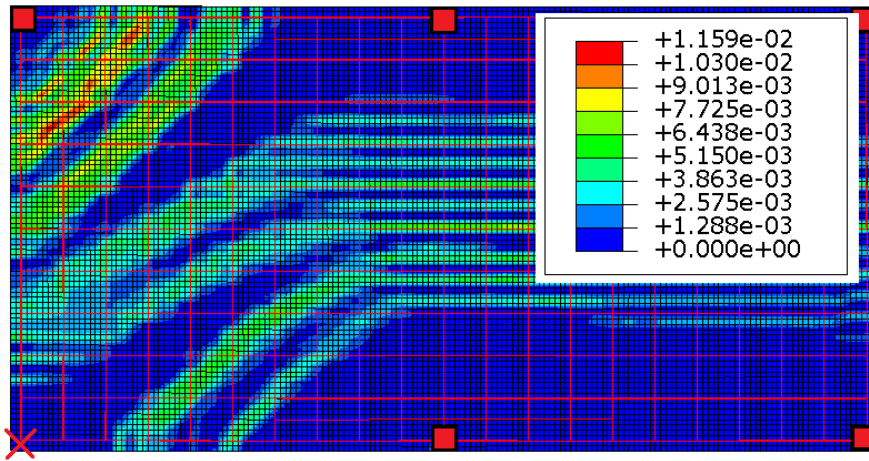


(b) Bottom Surface

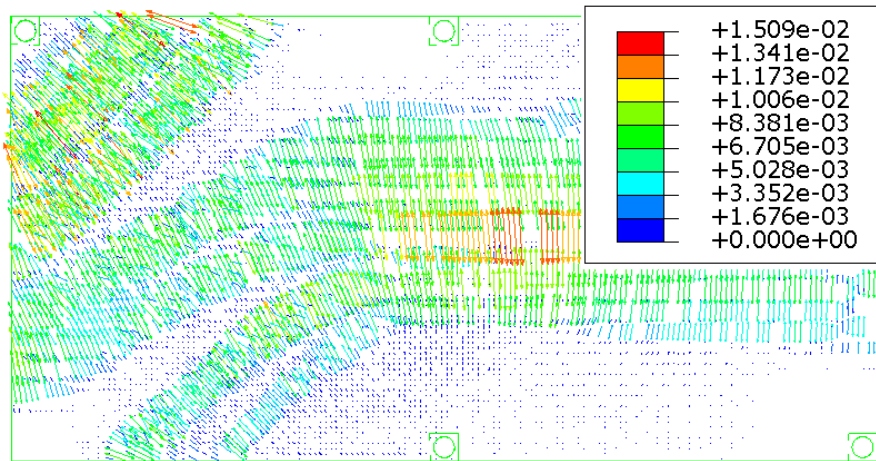
Figure 5.13: Location of tensile plastic strain regions in the concrete elements at 5.4kN/m² of loading for test C-S



(a) Top Surface



(b) Bottom Surface - Reinforcement is also annotated



(c) Bottom Surface - Orientation of the maximum principal axis for plastic strains

Figure 5.14: Location of tensile plastic strain regions in the concrete elements at 7.8kN/m^2 of loading for test C-S

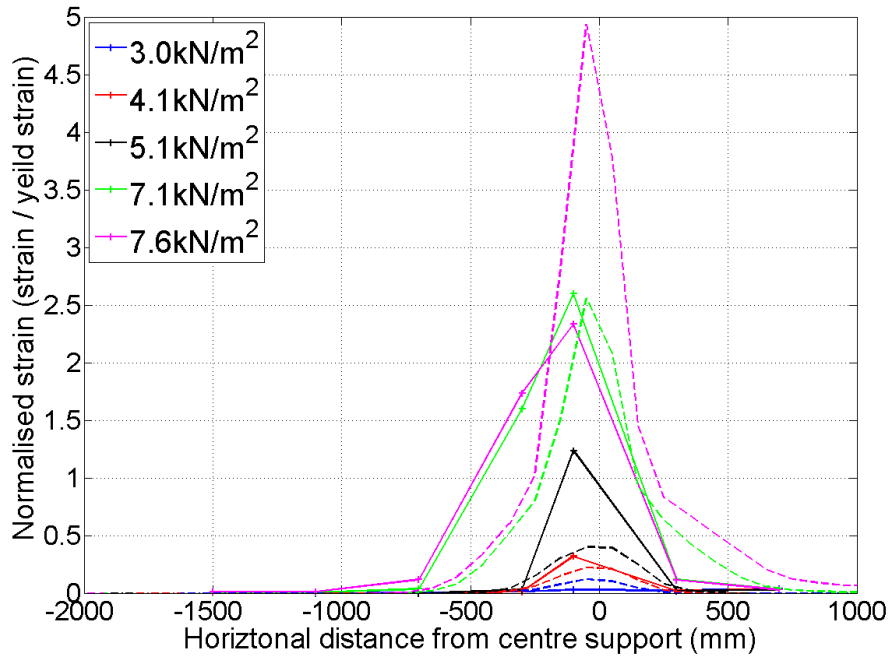


Figure 5.15: Normalised strain against position for the top steel. FE (dashed lines) and experiment results (solid lines) are shown for different loadings - Test C-S

level of damage at high loads. Whilst it can be seen that the plastic damage is focused around the support, the extent of the straining is far beyond the experimental readings; a situation also seen previously in the displacement results.

Figure 5.16 shows the progression of plastic deformation for the two penultimate removal tests. The continuous reinforcement case (Figures 5.16(a), 5.16(c) and 5.16(e)) is compared with the reduced case with the bottom steel removed through the central support (Figures 5.16(b), 5.16(d) and 5.16(f)). As was observed in the experimental tests and discussed in Section 3.3.2, the continuous case experiences yielding of its reinforcement at a lower load, and across most of the front bar. Once the reduced case starts to experience significant damage beyond 6.2 kN/m^2 , the plastic regions are localised in the original midspan and on the first bar that is continuous across the length of the specimen, that is, the third bar from the edge. At the highest load level there is extensive plastic yielding across the slab's bottom steel. However, the difference in stress distribution due to the different reinforcement layouts can be seen between Figures 5.16(e) and 5.16(f).

Comparing the flexural damage that occurs due to a column loss between the experimental data and the results of the FE model shows that a good representation can be

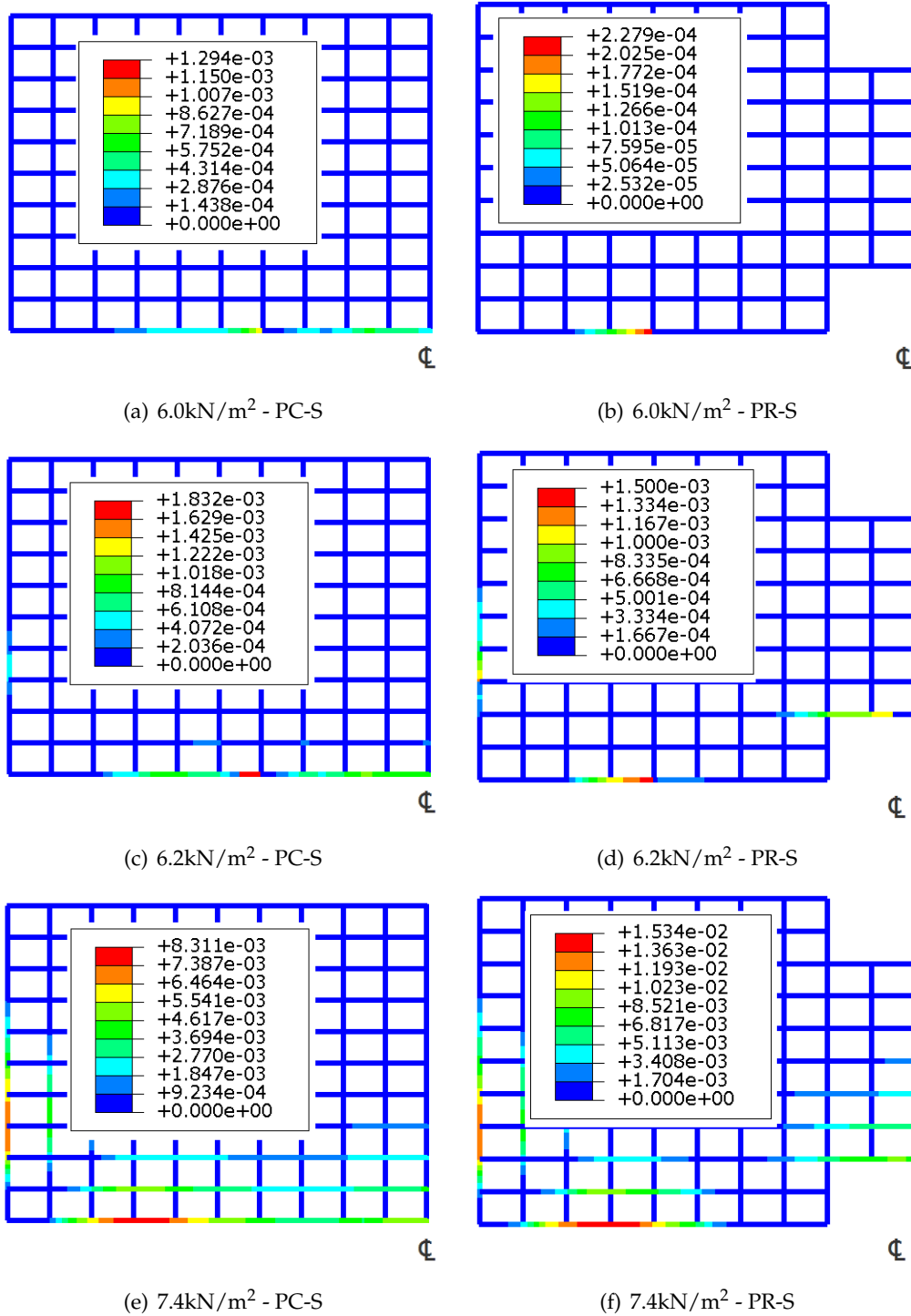


Figure 5.16: Plastic deformation for the bottom steel in tests PC-S and PR-S at different loadings

Table 5.2: Comparison of the frequencies from a modal analyses and the dominant frequency seen in the experimental and FE results - Test C-D

Loading (kN/m ²)	1st Mode (Hz)			2nd Mode (Hz)	
	Experiment	Finite Element		Finite Element	
	Displacements	Displacements	Modal	Modal	
3.0	11.0	9.76	13.6	30.5	
6.8	5.41	5.68	9.05	20.2	
7.7	3.54	N/A	8.53	19.1	

Table 5.3: Comparison of the frequencies from a modal analyses and the dominant frequency seen in the experimental and FE results - Test M-D

Loading (kN/m ²)	1st Mode (Hz)			2nd Mode (Hz)	
	Experiment	Finite Element		Finite Element	
	Displacements	Displacements	Modal	Modal	
3.1	13.4	11.1	15.1	30.1	
6.9	8.6	7.78	10.1	20.1	
8.5	6.0	6.64	9.1	17.9	

gained from using the numerical model. In general, concrete cracking and reinforcement yielding occurred at similar locations and loading levels observed in the experimental case. However, the extent of damage did not match as closely, particularly at high loading. Despite this, the presented nonlinear model can provide a very useful indication into the condition of a slab element after a column loss and can be used for further analysis.

5.2.5 Frequency analysis

Conducting a modal analysis of the models to obtain the mode shapes and associated natural frequencies will allowed further comparisons of the models. For dynamic tests, within the elastic range where damage has not occurred, the frequency of oscillation should correspond closely with the 1st modal frequency. At higher loading, the extensive damage will reduce the stiffness and therefore decrease the fundamental frequency leading to a different response from that predicted based on the initial state. The modal analysis is based on a linear perturbation, therefore nonlinear contact changes, such as uplift of supports, will not be captured. Additionally, the contact definitions, especially for the bearings, are not replicated and so will not rotate, or add to the flexibility of the

system. This will result in a stiffer response, and higher frequencies than obtained from the actual tests.

A summary of the results from the modal analysis is given in Tables 5.2 and 5.3 comparing them with the fundamental frequency of oscillation from the experimental programme and the dynamic FE tests. In both the corner and the middle removal cases presented, the first modal frequencies are higher than the experimental results at all loading levels. In the elastic range the overestimation is the smallest, and is because of the issues in considering the support conditions. At the higher loadings, there is a large decrease in the oscillation frequency in the experimental cases. This is due to both the increase in mass provided by the higher load and the reduced stiffness due to damage. However, the theoretical frequencies are based on elastic properties and so their reduction is purely due to the increased mass.

Observing the frequency of oscillation of the FE model at the higher loadings shows a much better agreement to the experimental case. This suggests that the full nonlinear model provides a good representation the reduced stiffness due to the damage and the distribution of the mass across the sample.

By comparing the modal frequencies to the oscillation, an indication into the extent of damage can be determined. As the natural frequency is a function of the stiffness and the mass, by conducting a modal analysis on the initial elastic state of a structure, with a known loading, the difference in dynamic oscillation after a sudden column loss is due to the reduction in stiffness as a result of damage. Such comparisons may provide a useful way to assess the state of a structure after a sudden column loss. This suggests, as expected, that only slight damage occurred in the middle load case, and extensive cracking and yielding occurred for the final test

The first three mode shapes are also given in Figures 5.17 and 5.18 for the corner and middle removal cases respectively. They demonstrate the expected result that the system is most flexible in the bay with the removed support, see Figures 5.17(a) and 5.18(a). The second mode in both cases, Figures 5.17(b) and 5.18(b) shows the vertical flexibility of the centre of the adjacent bay, or bays, with a frequency of approximately twice the first frequency (compare the results given in Tables 5.2 and 5.3 above). Finally, the 3rd mode, Figures 5.17(c) and 5.18(c), is again located in the damaged bay, primarily at the removal location, although it also demonstrates the uplift at the back of the bay.

Although the higher frequencies and mode shape do play a role in the response of the entire slab, the first mode is clearly the dominant case. Therefore, simplified approaches to analysing the dynamic motion of a slab after a column loss will give a

good approximation to the critical behaviour.

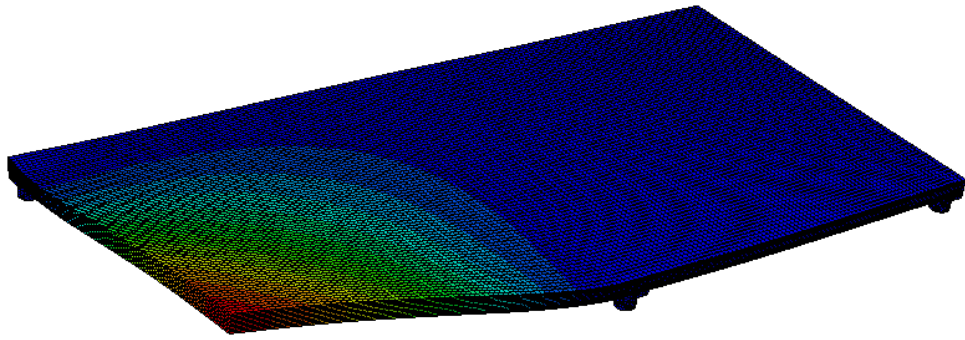
5.3 Summary

This chapter validates the Finite Element (FE) model that was previously introduced by comparing various results to the experimental programme.

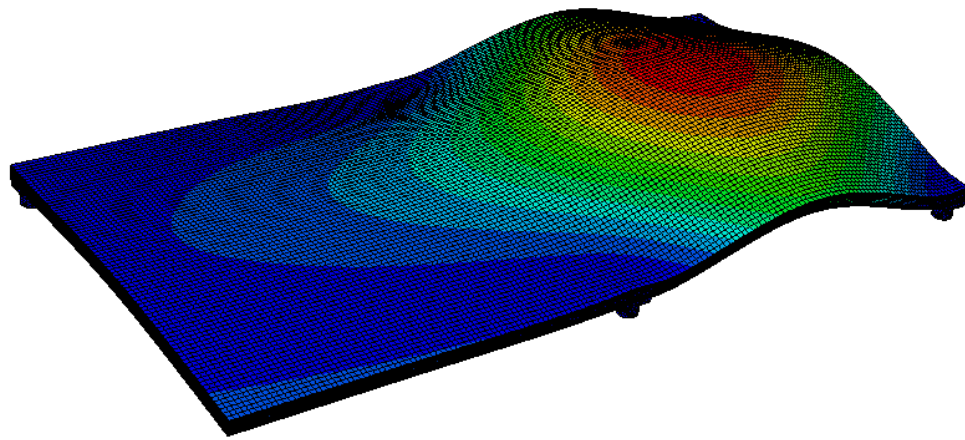
In general, the FE model correlates well to the results from the experimental slabs. In particular, the changes in reaction forces after a column loss show a close similarity, as does the location of concrete cracks and reinforcement yielding. This indicates that the stress distribution of numerical model matches the true behaviour. The static displacements against load also correspond well between the experimental and numerical cases, especially at the low loading. The higher loading conditions did show higher deviations due to the difficulty in describing accurate nonlinear conditions past the ultimate capacity. However, the results are still viewed to be suitable.

The dynamic cases showed a weaker agreement. The modal analysis over-estimates the first frequency, primarily as the support conditions were not correctly accounted for with a linear perturbation method. However, since further analysis will be conducted on a more realistic structural arrangement, i.e. with column elements included rather than pinned bearings, a better representation should be gained from later modal analyses. The displacements predicted from the dynamic analysis match reasonably well to the experimental cases, although the difficulty in modelling the removal time and the influence of the Dynamic Increase Factor (DIF) prevents complete replication of the experiment. Additionally, the accuracy of the softening region of the concrete tension model also affects the results, as it did for the static tests.

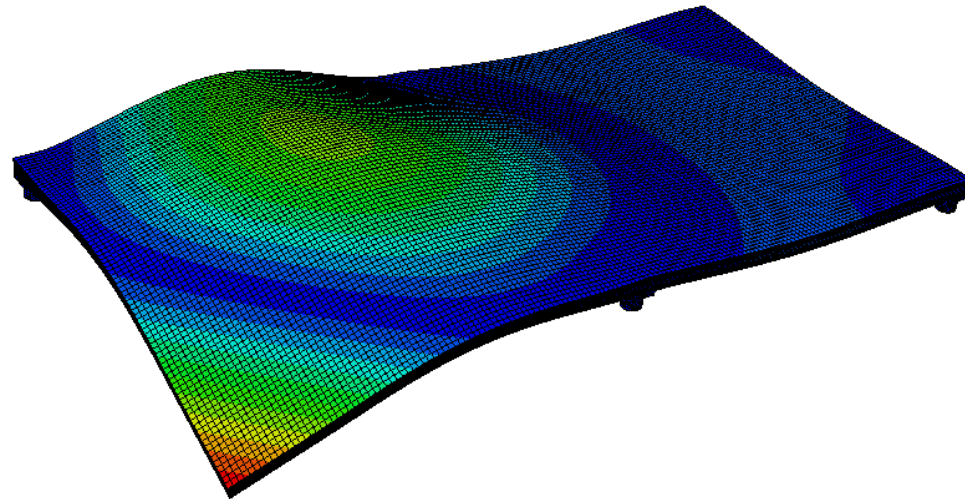
This model is considered to accurately represent the key aspects involved in the damage and change in response of a flat slab structure after a sudden column loss event. Therefore, this approach shall be used in the next chapter to consider the different factors that influence a larger structure's response to column loss and the potential for progressive failures.



(a) 1st mode shape

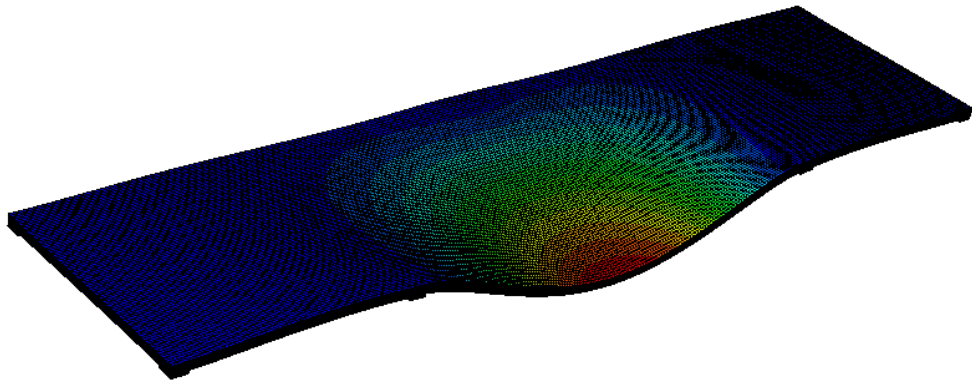


(b) 2nd mode shape

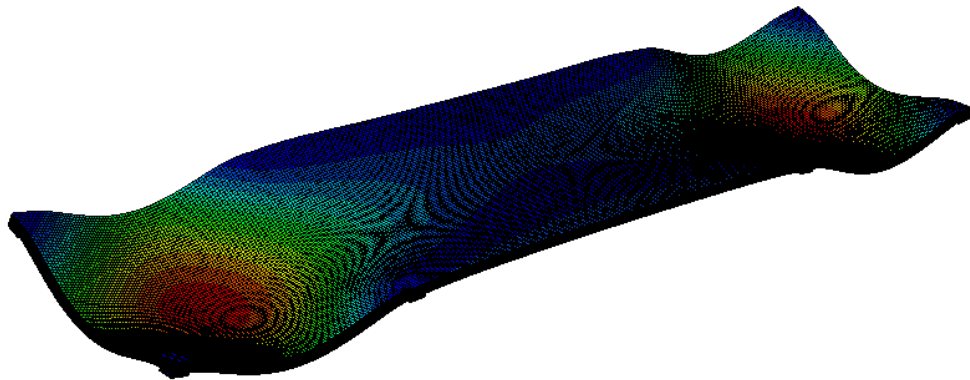


(c) 3rd mode shape

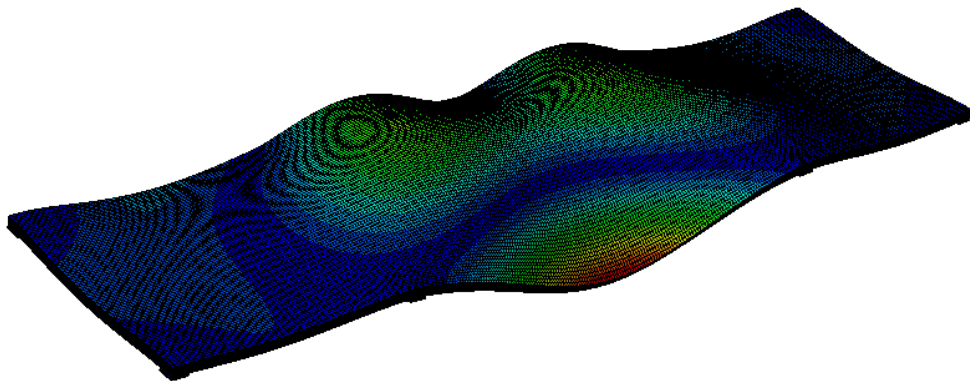
Figure 5.17: Predicted mode shapes for test C-D



(a) 1st mode shape



(b) 2nd mode shape



(c) 3rd mode shape

Figure 5.18: Predicted mode shapes for test M-D

Parameter Study on Different Floor Variables

In previous chapters a Finite Element (FE) model was developed and validated. In this chapter a larger model is considered representing an entire floor system of a flat slab structure under a column loss scenario, and a parameter study is conducted. Different aspects, including geometrical and material properties are varied within common ranges and their effect on the response of the structure, especially regarding the non-linear and dynamic aspects are discussed.

6.1 Introduction to parameter study

In Section 1.3.3, two project objectives were listed as:

Analyse a range of structural layouts and designs under a sudden column loss scenario considering different geometric, design and modelling variables.

and

Use the results of the parametric study to identify key factors influencing the potential for progressive collapse.

Therefore, a FE model of a full scale flat slab floor was developed. This used the validated numerical model presented in Chapters 4 and 5. The model represented one storey of a three bay floor; a graphical rendering of the structure considered with the FE model is shown in Figure 6.1.

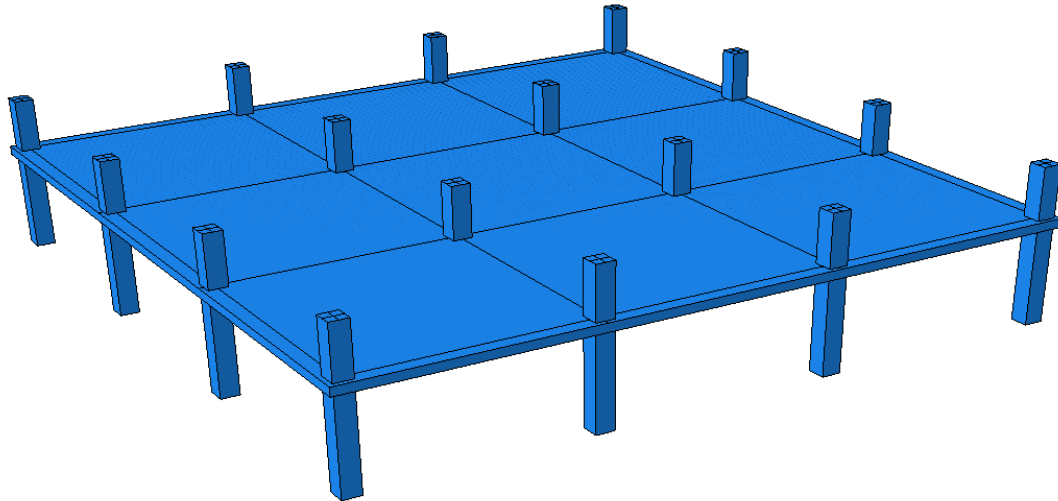


Figure 6.1: Graphical rendering of the multi-bay floor model

The span length, slab thickness and concrete strength were varied within common ranges and different column removal scenarios conducted. Key results to assess the response of the structure, including displacements, damage patterns and reaction forces were monitored. These outputs were then compared between the different models to determine the changes that occur. Furthermore, as both a static push down condition and a dynamic removal scenario were considered, comparisons between the results allow identification of the dynamic effects involved.

6.2 Description of multi-bay floor model

This section describes the method used to design and create the required models for the parameter study.

6.2.1 Design of the model

A plan and elevation of the floor model is shown in Figure 6.2. Due to the resources available, not all aspects could be varied. Therefore, this work focuses on the area viewed to be most critical during the design of a structure. Table 6.1 lists the geometric dimensions that were varied for the parameter study, that is the slab spans and depths. The values used were limited by common configurations and the requirement to meet design guidelines. Table 6.2 defines the values for the dimensions that were constant in all models. Although varying these aspects may lead to changes in the structural response, they are beyond the scope of this work.

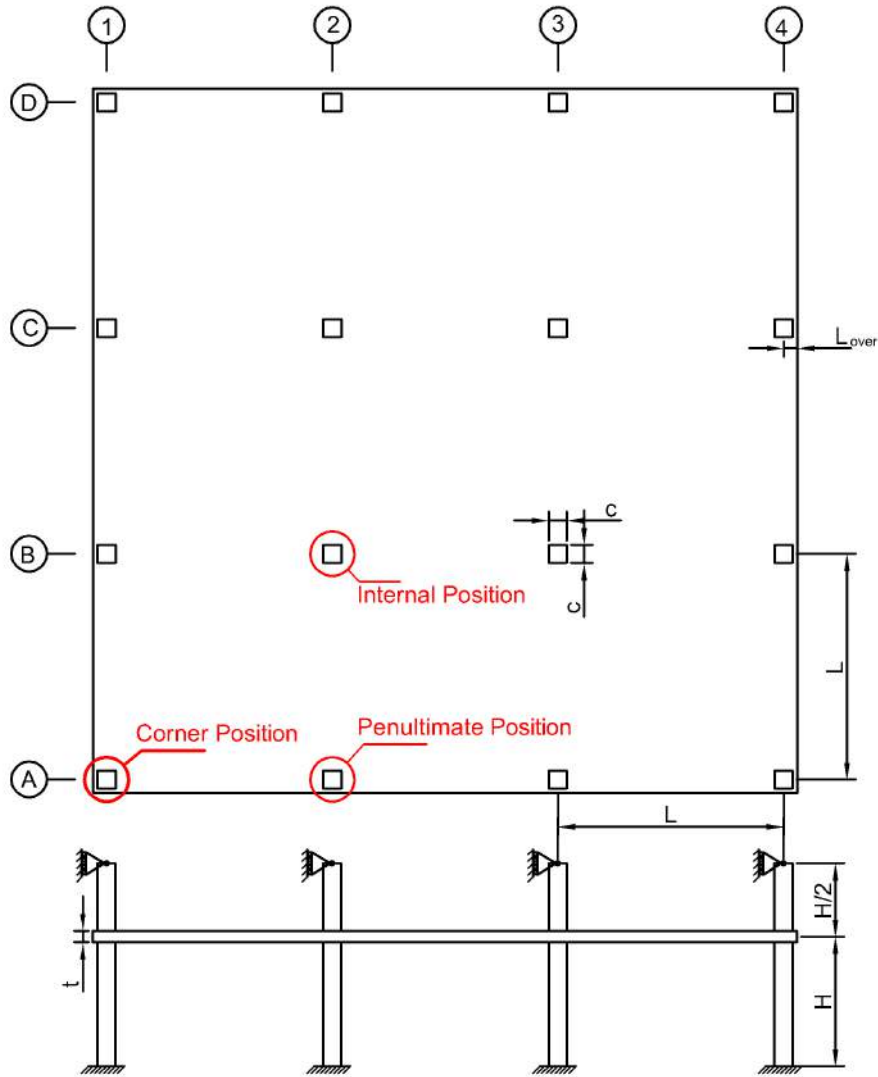


Figure 6.2: Plan and elevation of floor slab for parameter study showing dimension labels, key column locations and grid markings

Table 6.1: Values for the varied dimensions in Figure 6.2

Symbol	Label	Values (mm)
L	Span length	4000, 5000 and 6000
t	Slab thickness	180, 200, 250 and 300

Table 6.2: Values for the fixed dimensions in Figure 6.2

Symbol	Label	Value (mm)
L_{over}	Overhang	200
c	Column width	400
H	Storey height	3000

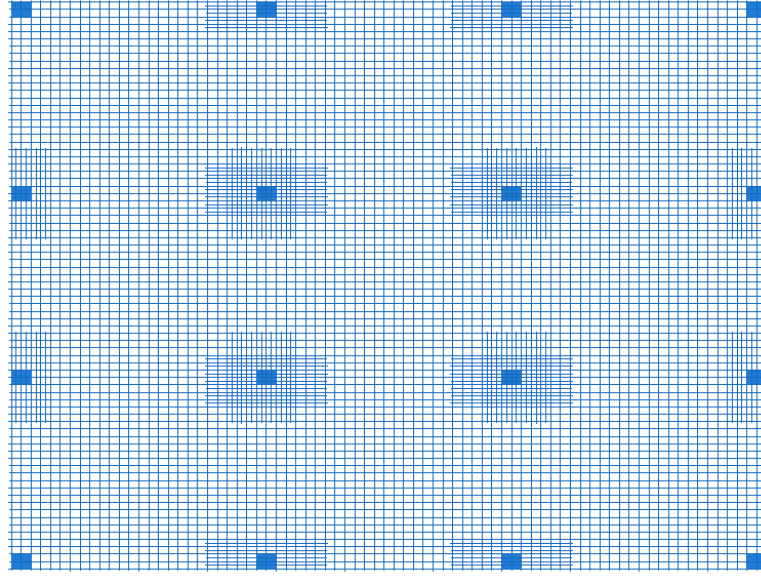


Figure 6.3: Example of the top flexural steel layout for the model with column positions marked

Each of the models was designed to meet current Eurocode requirements according to EN 1991-1-1 (2002) and EN 1992 (2004). The structure was analysed using the equivalent frame method to obtain the required bending moments and shear forces. Characteristic dead loading was based on the selfweight of the material, taken as 25kN/m^3 , plus an additional 1.0kN/m^2 to account for other finishes. Live loading for design was taken at 2.5kN/m^2 . For simplicity, no account was taken of cladding loading on the structure, either in design or in the FE model. Design was conducted at the Ultimate Limit State (ULS) load case. Based on the design forces, adequate flexural steel was provided, including the requirement to place 50% of the tensile steel for hogging moments within 0.125 times the span width. In all locations, for both top and bottom steel, at least a minimum area of steel was provided according to Equation 6.2.1. To meet durability specifications, 25mm of cover was provided to all steel.

$$A_{s,min} = \frac{0.26f_{ctm}A_c}{f_{yk}} \quad (6.2.1)$$

Figure 6.3 shows a typical layout of the top steel used for the models.

Each designed model configuration met the required shear stress capacity without the inclusion of extra reinforcement. Therefore, longer spans or thinner slabs, are possible if shear reinforcement is included. Although such arrangements are commonly used, they are beyond the scope of this study.

6.2.2 Details of the FE model

The FE model was created using the same approach introduced in Chapter 4. The same concrete and steel material models were used, as well as the same choice of solid and beam elements. Additionally, the same checks were conducted on the models, before the analyses, to ensure suitable results would be obtained. The aspects of this model which differ from the previous case, are briefly discussed in this section.

Concrete properties

As before, the Concrete Damaged Plasticity (CDP) model was used to account for non-linearity in the concrete, due to either crushing or cracking, as well as the reduction in elastic stiffness as a result of damage. The plasticity parameters and the stress-strain relation were the same as those used previously and are not repeated here. However, compressive and tensile strengths are required, as well as a value for Young's modulus. These are taken from the equations presented in EN 1992 (2004). The peak compressive strength was taken as the characteristic cylinder strength, f_{ck} , which was used to estimate the mean tensile strength, f_{ctm} , according to Equation 6.2.2.

$$f_{ctm} = 0.30(f_{ck})^{(2/3)} \quad (6.2.2)$$

Similarly, Young's modulus, E_{cm} , is based on Equation 6.2.3.

$$E_{cm} = 22 \left(\frac{f_{cm}}{10} \right)^{0.3} \quad (6.2.3)$$

The mean compressive strength, f_{cm} , is given in Equation 6.2.4.

$$f_{cm} = f_{ck} + 8 \quad (6.2.4)$$

Modelling the columns

As the model introduced and validated in Chapters 4 and 5 was based on the experimental programme from Chapter 3, it replicated the support conditions used there. That is, steel bearings that were allowed to rotate and separate from the slab. The model used for the parameter study more closely replicates a typical structure by including column sections. Each of the columns is modelled with solid, 8 node, brick elements, ID C3N8R, the same as used for the concrete slab. The columns were tied to the top and bottom surfaces of the slab. As shown in Figure 6.2, the lower columns represent

ground floor locations, and the nodes at the bases were restrained against translational movement. The upper columns were modelled at half height and pinned to allow rotations due to bending of the column as an estimation for the point of contra-flexure. Vertical movement was allowed at these positions, while horizontal deflections were prevented, providing an approximation to the restraint caused by the slab at higher levels. Finally, 4 steel reinforcement bars were included within the column over its entire height, passing through the slab. As the response of the column elements was not of interest for this study, this reinforcement primarily acted to prevent unreasonable damage at the slab-column interface, and to improve the behaviour of the CDP model used for the columns. Although increasing the level of reinforcement in this location may change the response of the structure, its effects are viewed to be very localised and do not influence the wider structure and behaviour. This aspect will be discussed further during the results.

Loading on the slab

As was described in Section 4.2.6, during the introduction of the FE model, two types of loading are considered. These are a static increase in the loading, after a column removal, and a dynamic column loss after the full load is applied.

During the static loading condition, a Uniformly Distributed Load (UDL) is applied to the entire slab area and is linearly increased up to the accidental load combination, w_{ac} , as given in Equation 6.2.5 from GSA (2013), where DL and LL are the Dead and Live Loads respectively. While other load factors could be used to account for suitable loading during an accidental event, this requirement is one of the highest commonly used.

$$w_{ac} = 1.2DL + 0.5LL \quad (6.2.5)$$

Once this level has been reached, a further UDL is applied only to the bays around the lost column. The loading in this area is increased linearly up to a value of $2w_{ac}$. This additional load replicates the dynamic influence affecting those bays. All loading is applied quasi-statically, as described in Section 4.4.2.

Dynamic removal simulations are conducted with a uniform load of w_{ac} applied to the whole slab. The Dynamic Amplification Factor (DAF), that is the required increase in applied force for a static analysis to represent the inertial effects from a dynamic case, can be determined by comparing the results from the two simulations. This can be achieved in two ways, comparing the displacement values and comparing reaction

force values. As the static displacement at the column loss location is a function of the loading, w , when the static displacement, δ_{static} , is equal to the peak dynamic displacement, $\delta_{dyn,peak}$, the DAF can be calculated. Equation 6.2.6 describes this method.

$$\delta_{dyn,peak} = \delta_{static}(DAF \times w_{ac}) \quad (6.2.6)$$

A similar approach is also applied to compare reaction forces. While Equation 6.2.6 is suitable for attempts to correlate flexural damage between static and dynamic analysis, which is related to the deflection response, the shear force increase is not directly related to deflections. Therefore a DAF based on the peak reaction force occurring at a column, compared to the static increase condition will also be considered.

6.3 Parameters varied for the study

To investigate the response of Reinforced Concrete (RC) flat slab structures to a column loss event, a number of models were created with different details. A description of the variables considered is given in this section.

6.3.1 Span to depth ratio

The span to depth ratio is a common method of characterising a slab structure. This ratio compares two geometrical aspects which influence both the demand and capacity of a section. A longer span length will have larger bending moments associated at both the midspan and the columns, as well as larger total loads which increases the shear forces. Increasing the depth of the slab on the other hand creates a stiffer section with a higher moment and shear capacity. By varying both the span and the depth, a range of design options can be considered. As each arrangement included enough flexural reinforcement and shear capacity to pass normal criteria, any influence that increasing the span to depth ratio has on the response of a structure after a column loss can be determined. Additionally, a modal analysis will also provide information into the relative stiffness of each model.

In total, seven different arrangements were considered as listed in Table 6.3. The span to depth ratios are based on the effective span length, L_{eff} , of an internal bay with a continuous slab over the supports according to Equation 6.3.1.

$$L_{eff} = L - 2\left(\frac{c}{2}\right) + 2\left(\frac{t}{2}\right) \quad (6.3.1)$$

Table 6.3: Span length and slab thickness for each model

Span, L (mm)	Thickness, t (mm)	Effective span, L_{eff}	Span to depth ratio, L_{eff}/t
4000	180	3780	21.0
4000	200	3800	19.0
4000	250	3850	15.4
5000	200	4800	24.0
5000	250	4850	19.4
5000	300	4900	16.3
6000	250	5850	23.4

The terms L , c and t are the span length, column width and slab thickness respectively, as identified in Figure 6.2 and Tables 6.2 and 6.3. All bays were square and had the same span lengths, i.e. the aspect ratio of both the bays and the entire floor was constant. Also note, that the terms thickness and depth are considered interchangeably. This is different, however, from the effective depth used during design.

6.3.2 Concrete strength

The compressive strength of concrete can influence the response of the structure after an extreme event in a number of ways. Most noticeably a lower compressive strength correlates to a lower tensile strength, which reduces the flexural and shear capacity of a section. For normal design this can be offset by deeper sections and more steel reinforcement in the required area, therefore a lower grade of concrete does not necessarily increase the likelihood of progressive collapse. However, the strength of concrete also affects other aspects. According to Equation 6.2.3 the elastic modulus is related to the concrete strength, therefore, the elastic behaviour of the structure will also change with different concrete strengths. Additionally, the minimum required flexural reinforcement area, $A_{s,min}$ in Equation 6.2.1, is also dependant on the concrete strength. Whilst for normal usage, the reduction in steel area due to lower strength concrete is not significant, during a column loss event the Alternative Load Paths (ALPs) that develop will stress these areas and their flexural capacity will influence the potential for progressive failure.

In this study, three different concrete compressive strengths grades are considered, 20, 30 and 40MPa, and their results compared.

6.3.3 Removal location

As identified in Figure 6.2, different column removal locations were considered. For all arrangements the loss of a corner or an internal column was simulated. Corner columns, as an external element, are often vulnerable to attack or accidental actions originating from outside the structure. An internal column loss is less common, however, its destruction influences a larger part of the structure. Additionally, two further scenarios were included; the loss of a penultimate edge column and the loss of two external columns. The two column loss scenario goes beyond the usual requirements when considering the robustness of the structure, however, it addresses the potential that a large explosion may damage or destroy more than one load bearing element. By comparing the results from each column removal scenario, the critical case can be identified. That is, the event that results in the most damage to the structure.

6.3.4 Removal time

Whilst the sudden column loss scenario typically assumes that the support from the element is removed instantaneously, the dynamic response of the structure is heavily dependent on the removal time. Naturally, if the column is removed slowly enough then the response tends towards the static case. A range of removal times, normalised against the fundamental period of the structure, are considered, and the changes to the maximum deflection and reaction forces, along with the time to the peak are determined.

6.3.5 Dynamic Increase Factor for concrete

As has been mentioned previously, the tensile capacity of concrete changes with higher strain rates. As a complete strain rate dependent material model is both too computationally demanding and adds additional uncertainties, such an approach is not taken. However, by first considering the maximum strain rates that occur for the structure experiencing a sudden column loss, an approximate Dynamic Increase Factor (DIF) can be calculated. The models can then be rerun with this increased concrete tensile capacity. This overestimates the influence of such effects, but allows a comparison to be made to determine how significant these effects are.

6.4 Outputs monitored during analysis

This section provides an overview of the different results taken from the models. Details of how each value was obtained and its uses are stated.

6.4.1 Displacement values

During every simulation, vertical displacements were monitored for the slab. In each case these were normalised against the slab thickness to allow comparison between different arrangements. For the static push down tests, the displacement values were recorded as the loading was increased, primarily at the column loss location, but also in the middle of nearby bays. This provides information into the extent of damage that is occurring due to the lost support, as well as considering how much of the structure is affected by the removal.

For the dynamic loss situation, the normalised displacement against time was recorded at the column loss location. This was sampled at 250Hz, as was used in previous simulations. This rate ensures that the sudden changes immediately after a column loss are captured. As well as comparing the maximum deflection between models, a Fourier Transform of the displacement-time response provides the frequency of oscillation for the model, which can be compared to the results from a modal analysis. As the modal analysis is based on the elastic response, the difference in oscillation frequency is due to a reduction in stiffness. Additionally, as the major energy dissipation method specified is based on the plasticity and damage of the concrete, included in the CDP model, and from yielding of the reinforcement, the damping ratio can be extracted from the response. Both these results provide an indication into the level of damage that the slab has undergone.

6.4.2 Reaction forces

All the nodes at the base of each column were restrained vertically, and the reaction forces for these locations were recorded throughout the analysis. For static analyses, that is the static push down condition and the pre-load for the dynamic, the sum of the reactions were taken at each load increment for each column. Similarly, after the column was removed dynamically, the sum of the reaction forces was recorded against time. This method provides the total vertical force transmitted via that column, but does not account for the moment effect. As only a single floor is considered, this force represents the shear force that is transferred around the slab-column connection. How-

ever, the shear stresses required for assessing punching shear failure are dependant also on the transfer of bending moments into the column. Due to the construction of the model, these values could not be accurately determined and therefore an exact description of the potential of failure cannot be specified. Despite this limitation, a strong indication into the areas that may be susceptible to such failures can be determined by considering the change in vertical force demand at that support. This is achieved by taking the vertical reaction while the model is fully supported and carrying load w_{ac} . The reaction forces after a column loss can then be expressed as a percentage of this value, less than 100% indicates that demand has reduced for that column. However, anything over 100% should be considered carefully for progressive shear failure as the column loss event has increased the shear force at that location and may now exceed the designed capacity.

6.4.3 Steel strain rates

In order to assess the influence of strain rate effects in changing the material properties of the concrete after a dynamic column loss, the strain rates in the steel reinforcement were recorded with time. While the strains in the concrete will be slightly different from the steel, the large number of concrete elements are more computationally demanding to monitor and will be of the same order of magnitude as the steel rates. At every sampled time step, the maximum strain rate in the steel is recorded, this provides an indication into the most critical values, and an upper bound for a DIF of the tensile strength of concrete.

6.4.4 Tensile damage to the concrete

The most common form of damage that RC structures experience is flexural cracking of the concrete, and therefore should be suitably considered. The CDP model used, described in Section 4.3.1, represents cracks as a region of plastic deformation and as a region with reduced elastic stiffness according to its damage index. During the static loading the regions of the concrete that undergo tensile failure, due to the increased hogging and sagging moment demand on surrounding supports and midspans respectively, can be visualised indicating the progression of cracks. This highlights how much of the structure is affected by the column loss and regions that may be susceptible to flexural failure.

6.4.5 Fundamental frequencies

A modal analysis of each model was conducted. This was based on the elastic properties of the structure after the relevant column has been removed, and includes the load, and associated mass, from the accidental load case, w_{ac} from Equation 6.2.5. The additional mass from imposed loading was applied as a uniformly distributed nonstructural mass to the concrete elements, in the same manner described in Section 4.2.6.

As the modal analysis provides the fundamental frequency of the linear elastic, undamaged structure, comparisons to the frequency of oscillation during the dynamic analysis gives an indication into the reduction in stiffness, due to concrete or steel damage.

6.5 Numerical results and discussion

In this section the results from all the models are presented and described. The results from static push down simulations and the sudden dynamic removal condition are treated separately and their significant factors highlighted. In particular, this allows a clearer identification of the nonlinear effects involved. Finally, the two cases are directly compared to consider the influence of dynamic effects and the associated DAF.

6.5.1 Static results

Displacement response at the removal location

The deflection response of different RC flat slab systems with a corner column removed is presented in Figure 6.4. The effect of varying the span to depth ratios is shown in Figure 6.4(a) for different loading levels. Of immediate note is the relatively low levels of vertical displacement, especially when the loading is below 100% of w_{ac} . Additionally, there is not a strong relationship between increasing the span to depth ratio and the normalised displacement. In particular, when $L_{eff}/t=23.4$ the values are much higher than at 24.0. From considering the details of these models in Table 6.3 reveals that this case has both a longer span and a deeper depth than the case with the higher span to depth ratio. As the self-weight of the structure plays a key role in the total loading, a deeper section has a much higher loading, resulting in higher normalised deflections despite the additional capacity that a thicker section can provide.

This can be seen further in Figure 6.4(b), which shows the entire displacement against load profile for each of the models. It can be seen that, with exception of the two highest L_{eff}/t cases, there is a strong linear trend up to w_{ac} . Furthermore, nonlinearity becomes

more significant after a displacement of 0.05 times the slab depth for all cases.

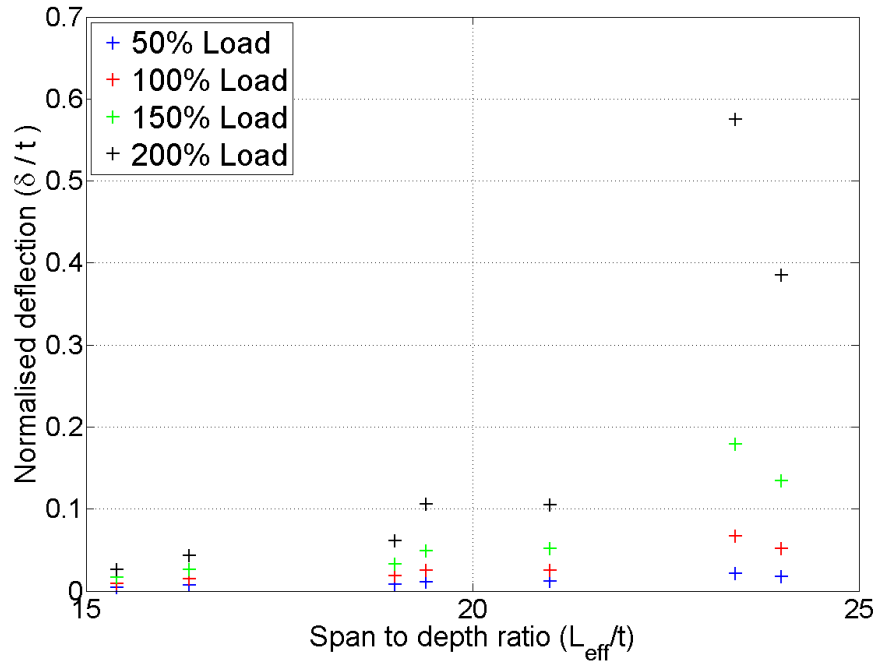
The non-constant relationship seen in Figure 6.4 indicates that normalising the response by the span and deflections over the thickness does not represent the complete behaviour. After a column loss event the load paths of the slab changes, and therefore the effective span lengths also change. Due to the two-dimensional bending behaviour of slabs, the new span is not simply twice the previous length, as would be the case for a beam element. As a result of this, increasing the span length of a structure, creates a nonlinear increase in the bending moment after a column loss. Additionally, increasing the section depth, increases the moment resistance, but also increases the selfweight and therefore the moment demand. As the span to depth ratio is a useful method of characterising typical structures, and a suitable normalisation based on the geometry and design of the slab is beyond this project, an alternative method of considering the displacement response is used. As the factor of interest is the nonlinear behaviour as a result of level of displacement, an approach from nonlinear push over analysis for seismic response is used. EN 1998-1 (2004) recommends creating a bilinear, perfectly plastic, force displacement behaviour. With this, the displacements, δ , can then be compared to the yield displacement δ_y to obtain a displacement ductility factor, μ_δ , as given in Equation 6.5.1.

$$\mu_\delta = \frac{\delta}{\delta_y} \quad (6.5.1)$$

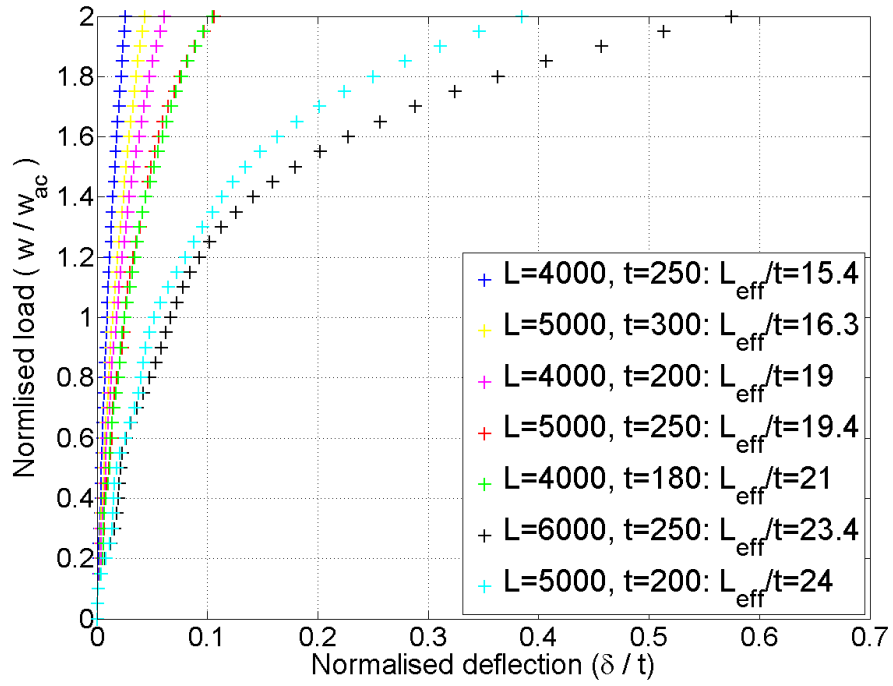
Therefore, the yield displacement is obtained for each analysis, based on a similar approach to EN 1998-1 (2004) where a bilinear relationship is fitted to the response with the requirement to ensure the area under the simplified model is equal to the area under the measured curve. As δ/t is still a useful relationship in considering the relative magnitude of the deflections on the structure, both this ratio and the ductility factor will be used to discuss the response.

Figure 6.5 plots the corner displacement results against span to depth ratio again, but normalised against the yield displacement. With this case there is a stronger relationship between increasing the span to depth ratio and increasing non-linearity.

The displacement results of the corner removal case are presented in Table 6.4. As the yield displacement varies between 0.013 and 0.067 times the slab depth, matching the response seen in Figure 6.4(b). Up to the accidental load case there are small displacements for all cases and usually a very strong linear trend, as displacements are usually less than δ_y . The weakest goodness of fit, based on the coefficient of determination of a linear fit, R^2 , is 0.958 indicating that there has only be a minor reduction in stiffness due



(a) Varying span to depth ratio



(b) Varying applied load

Figure 6.4: Normalised displacement after corner column removal

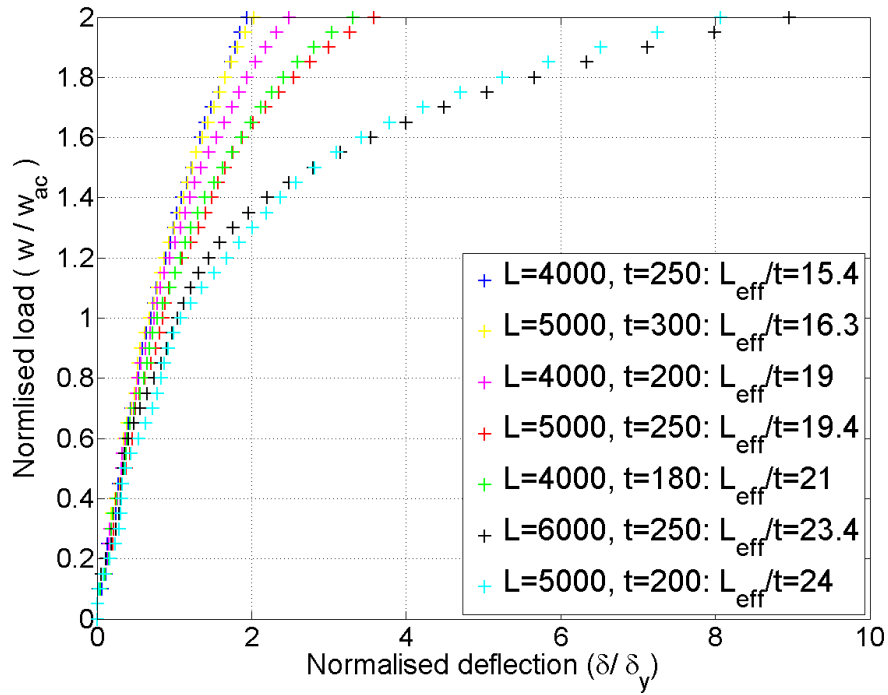


Figure 6.5: Displacement ductility factor, μ_δ , after corner column removal

to cracking. As the load is increased further, displacements in the lower span to depth ratios remain small, while beyond a L_{eff}/t of 19.4 larger relative displacements, and associated damage occur. However, as geometric nonlinearity, primarily the formation of a tensile membrane, typically only becomes significant beyond displacements of 0.5 times the slab depth, these results do not suggest this is a factor.

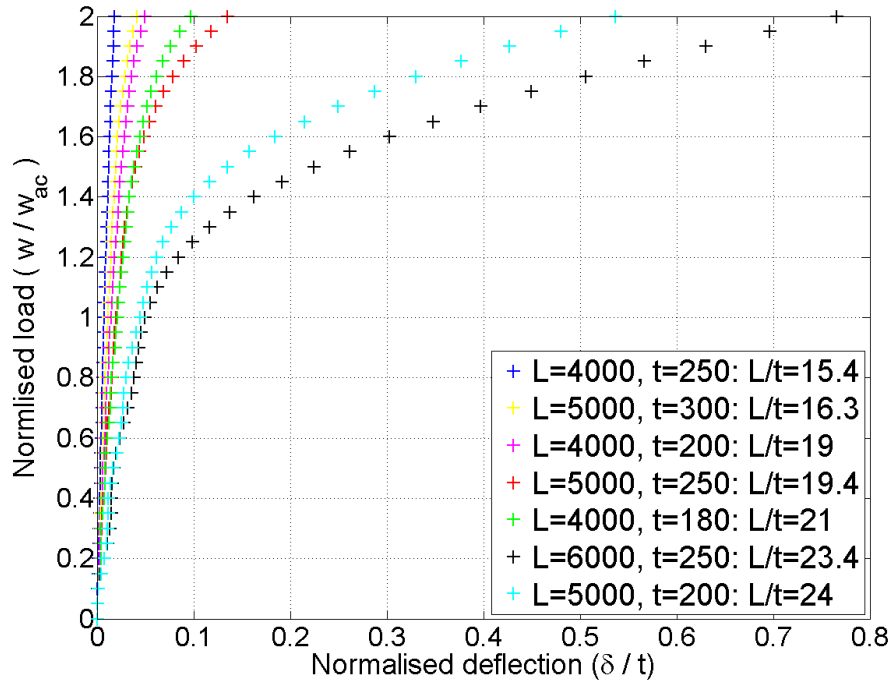
A similar response is observed from an internal column loss, shown in Figure 6.6. In general, with a larger L_{eff}/t , greater normalised displacements occur, for both δ/t and δ/δ_y in Figures 6.6(a) and 6.6(b) respectively. However, it can be seen that while 19.4 and 21 start off similar, by $2w_{ac}$ the theoretically stiffer model experiences high relative displacements. This effect is also seen again for the 23.4 and 24.0 cases. The 19.4 case has a thicker section depth, 250mm compared to 180mm, and therefore a higher loading, which becomes more significant once concrete damage starts to occur. The tabulated values in Table 6.5 demonstrate that upto a loading of w_{ac} the system remains in the elastic range, however, once cracking starts to occur significant nonlinearity can occur, as seen by the high ductility factors in Figure 6.6(b).

Table 6.4: Summary of static deflections - Corner removal

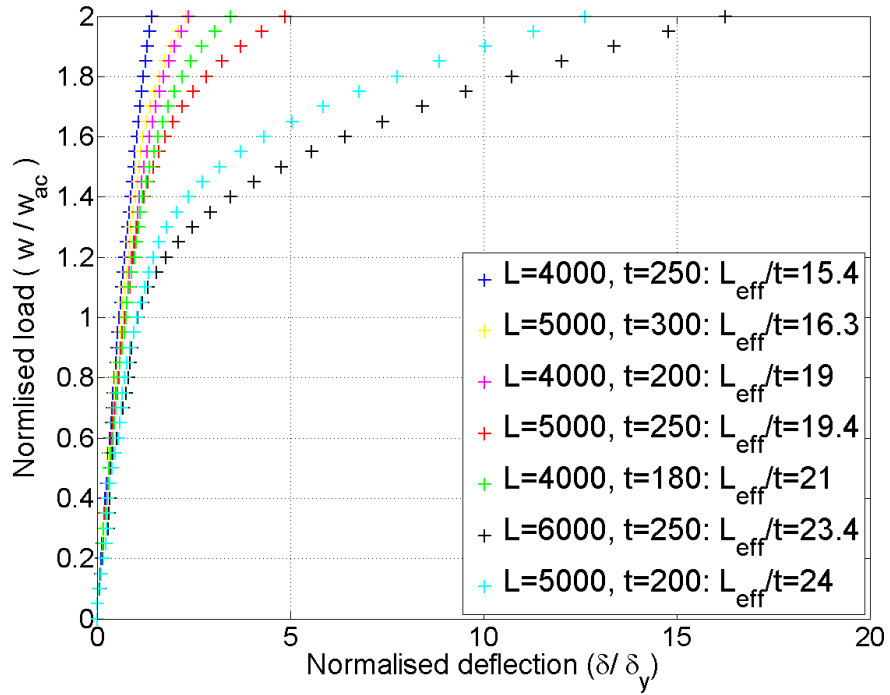
Span to depth ratio, L_{eff}/t	Normalised yield displacement, δ_y/t	δ/t at w_{ac}	R^2 up to w_{ac}	δ/t at $2w_{ac}$
15.4	0.013	0.009	0.995	0.026
16.3	0.021	0.015	0.991	0.043
19.0	0.025	0.018	0.989	0.061
19.4	0.030	0.025	0.984	0.106
21.0	0.032	0.025	0.988	0.105
23.4	0.064	0.067	0.958	0.575
24.0	0.048	0.052	0.980	0.385

Table 6.5: Summary of static deflections - Internal removal

Span to depth ratio, L_{eff}/t	Normalised yield displacement, δ_y/t	δ/t at w_{ac}	R^2 up to w_{ac}	δ/t at $2w_{ac}$
15.4	0.013	0.008	0.997	0.018
16.3	0.018	0.011	0.993	0.041
19.0	0.021	0.015	0.995	0.049
19.4	0.028	0.020	0.991	0.135
21.0	0.028	0.021	0.991	0.097
23.4	0.047	0.050	0.981	0.765
24.0	0.043	0.044	0.981	0.537



(a) Normalised with δ/t



(b) Normalised with δ/δ_y

Figure 6.6: Normalised displacement against static loading for different span to depth ratios. Internal column removal

Displacement response at the other locations

Of further interest is the response of other parts of the structure to a column loss. Figure 6.7 shows the normalised displacements against loading for different locations, after the corner column has been removed. From Figure 6.7(a) it is clear that the displacements in the bay adjacent to the one containing the removed column experience very small relative displacements. As expected, these are smallest for the stiffest structures. Considering this further, Figure 6.7(b) shows a closer view of other locations, further from the damaged area. All the positions, and all the models, show a linear relationship upto w_{ac} . Beyond this point, load is only applied to the bay around the lost column, due to this effect the adjacent bay and the middle bays do show a slight uplift, while the furthest bay on the other side of the structure appears to be unaffected. Of final note is the response of the adjacent bay for the model with $L_{eff}/t=21.0$. At the highest loading level the pattern changes from an uplift to a slight downward trend. This is related to the damage sustained spreading into the adjacent bay and reducing its stiffness.

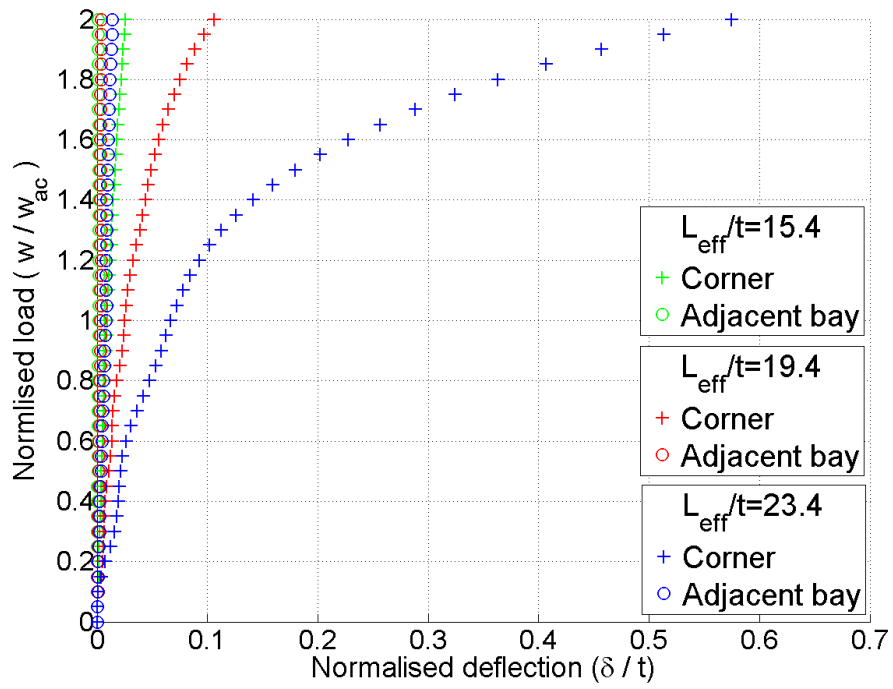
The response of structure after other column loss events is shown in Figure 6.8. After a penultimate edge column is removed, see Figure 6.2 for its location, there is a linear response of displacements at all locations up to w_{ac} (Figure 6.8(a)). After this, as further load is applied over the removed column, the damage to the slab causes the nonlinear relationship at the removal location. For the surrounding bay, displacements remain small and relatively unaffected by the lost support.

When two columns are removed, Figure 6.8(b), a similar response is observed, however, the structure is clearly less stiff in the elastic range, and enters the nonlinear range at a lower level of loading. Although the surrounding bays only undergo minimal relative deflections, they appear to be more affected by the column loss than other cases. This is, again, due to the slab experiencing large levels of damage which spreads into the surrounding bays therefore reducing their stiffnesses.

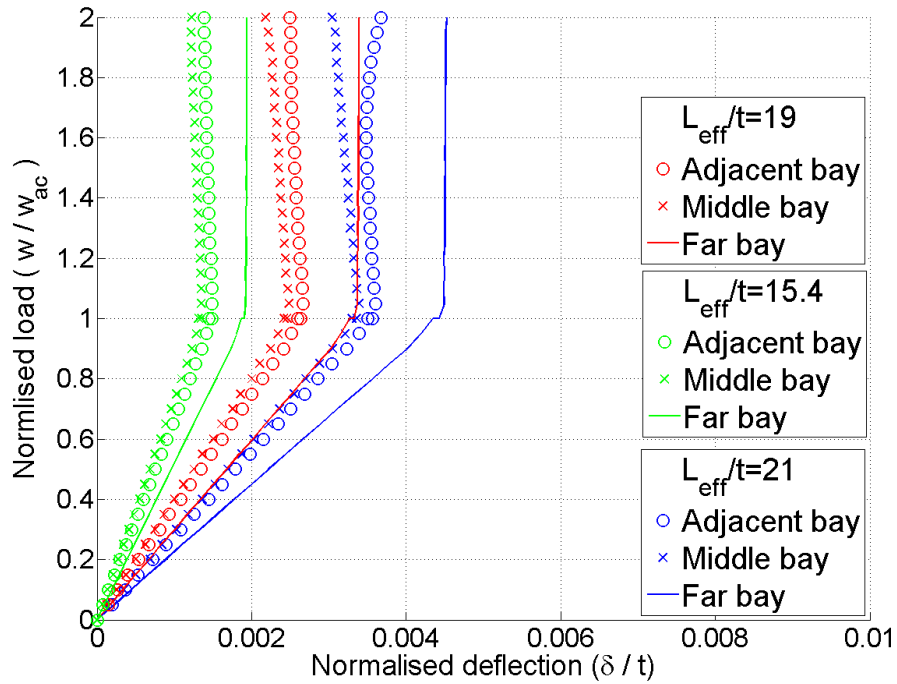
Comparison of removal location on the displacement response

By comparing the maximum displacement for each removal condition, an indication into which situation is most critical can be determined. Figure 6.9 shows the normalised displacement against load, for models with two different span to depth ratios and for the four removal locations.

With $L_{eff}/t=19.4$ all the single column loss scenarios show a very similar response, this is the case whether the results are normalised against thickness, Figure 6.9(a), or yield displacement, Figure 6.9(b). These values are also presented in Table 6.6, at a

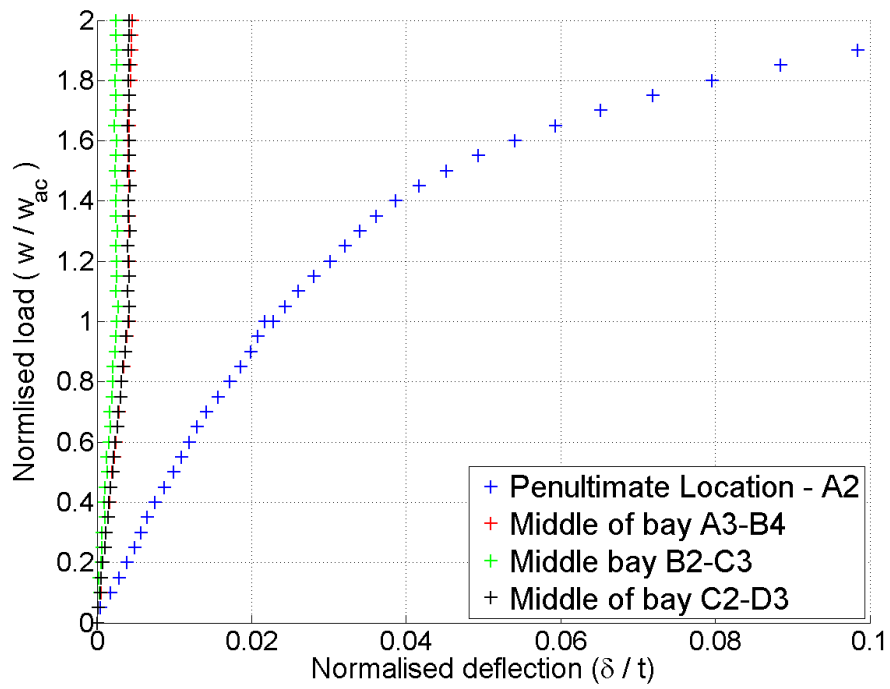


(a) Corner location and adjacent bay

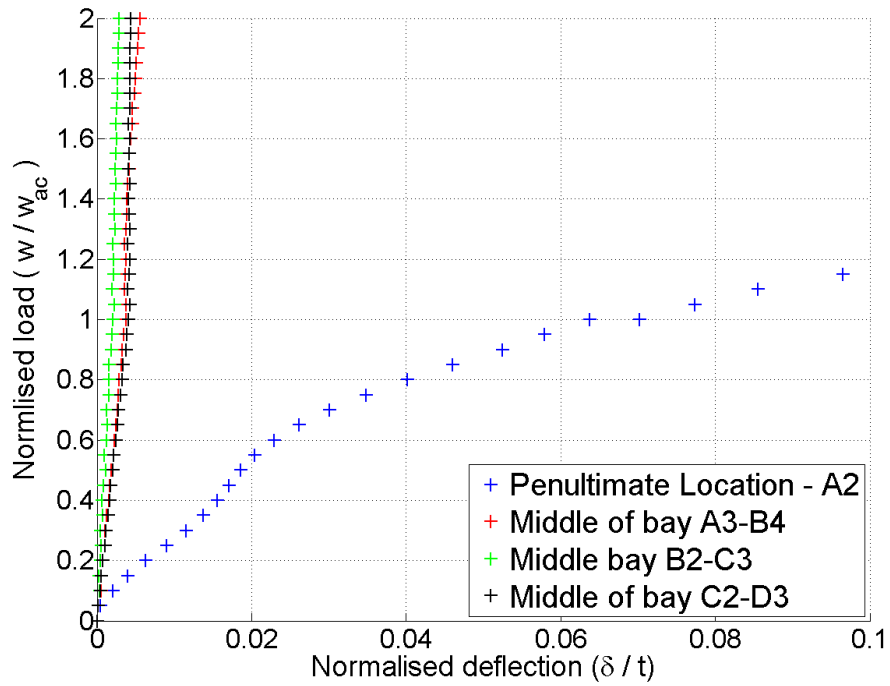


(b) Other areas

Figure 6.7: Normalised displacement at different locations against static loading. Corner column removed with different span to depth ratios



(a) Penultimate column removal



(b) Two column removal

Figure 6.8: Normalised displacement at different locations against static loading for different column loss scenarios

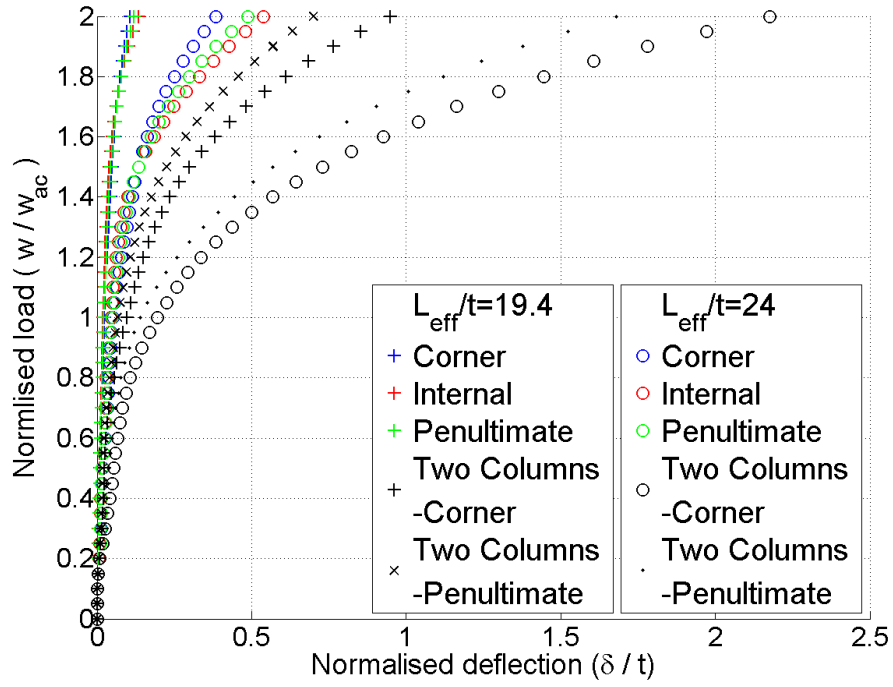
loading of w_{ac} the corner column loss shows the largest deformation by a small amount, however all three cases have very similar yield displacements, and remain within the elastic range. By $2w_{ac}$ the loss of an internal column is slightly worse. In this case, these differences are not very significant, with a maximum deviation of 7.25mm in a 250mm slab. Considering the case with $L_{eff}/t=24$, again shows that the three cases show a very similar response at low loading, although by w_{ac} they have reached the yield displacement. Additionally, there is the same change in critical scenario which becomes apparent after $1.5w_{ac}$ as the internal loss shows the highest deflections.

Table 6.7 provides the ductility factor for the models, at different levels of loadings, and for the different column removal scenarios. This highlights that for a single column loss, material nonlinearity is not a factor, up to the accidental load case. However, by a 50% increase in loading on the damaged bay there are displacements of upto 1.65 times the yield displacement, for span to depth ratios below 19.4. An even larger non-linear response was measured for the highest case. With a load factor of two, currently recommended for a static analysis, the displacements may exceed 10 times the yield displacement, indicating a very strong nonlinear behaviour.

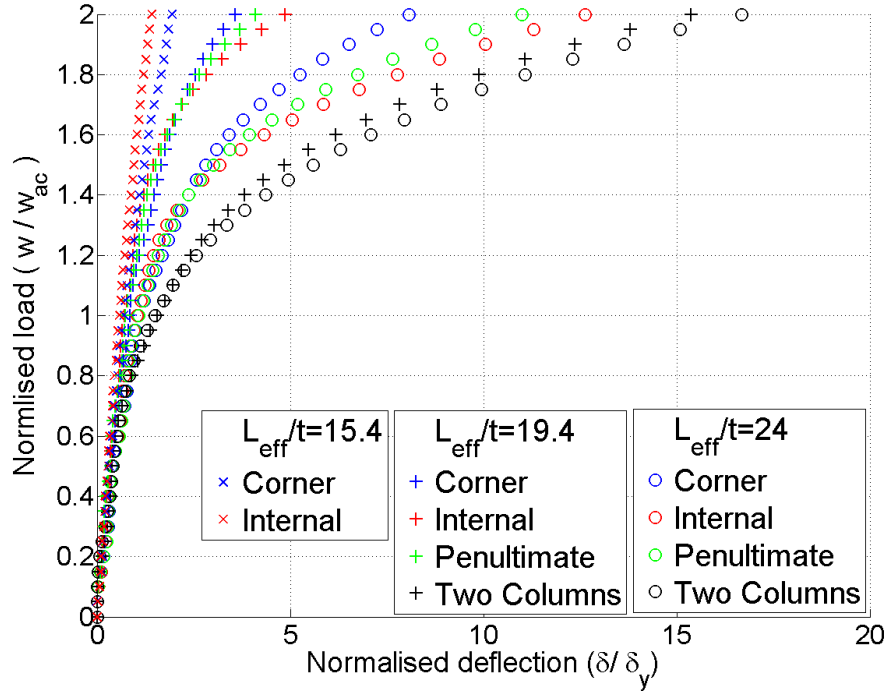
The loss of two columns, a corner and a penultimate edge, naturally creates a worse scenario with deflections that are higher than any of the other cases, with peak deflections more than four times the next largest value, see Tables 6.6 and 6.7. These much larger values indicate that a structure that is considered safe against a single column loss may remain vulnerable to progressive failures should a second support fail, and the structure does not have enough ductility to maintain integrity. The extent of this larger damage can be seen by the deflection data plotted from the two column removal case at location A2 in Figure 6.9(a). The normalised displacement is still higher than caused by removing any single column, demonstrating that the high deflections are not localised to the worst area.

Displacement response for different concrete strengths

A final comparison is made between three different compressive concrete strengths, based on their displacements against loading. This is plotted in Figure 6.10. Two removal scenarios are presented for a model with $L_{eff}/t=19.4$. Up to w_{ac} there is no significant difference in the response of the structures with different concrete strengths, this can be also seen from the values in Table 6.8 as displacements remain below, or close to the yield displacement. Total variation is less than 3mm for a slab with a depth of 250mm. However, as the loading is increased further, the lower strength concrete structure shows a much bigger difference with final differences of 88.2 and 58.4mm for



(a) Normalised with δ/t



(b) Normalised with δ/δ_y

Figure 6.9: Normalised displacement against static loading for different column loss scenarios

Table 6.6: Summary of static deflections - All column removal locations

Span to depth ratio, L_{eff}/t	Column location	Normalised yield displacement, δ_y/t	δ/t at w_{ac}	R ² up to w_{ac}	δ/t at $2w_{ac}$
19.4	Corner	0.029	0.025	0.984	0.106
	Internal	0.028	0.020	0.991	0.135
	Penultimate	0.029	0.022	0.988	0.121
	Two Columns	0.062	0.097	0.908	0.949
24.0	Corner	0.048	0.052	0.980	0.385
	Internal	0.043	0.044	0.981	0.537
	Penultimate	0.044	0.048	0.983	0.487
	Two Columns	0.131	0.195	0.926	2.177

Table 6.7: Displacement ductility factor, μ_δ , at different loadings for all column removal locations

Span to depth ratio, L_{eff}/t	Column location	$w = w_{ac}$	$w = 1.5w_{ac}$	$w = 2w_{ac}$
15.4	Corner	0.70	1.23	1.94
	Internal	0.58	0.94	1.41
19.4	Corner	0.86	1.65	3.59
	Internal	0.71	1.46	4.87
	Penultimate	0.75	1.52	4.11
	Two Columns	1.57	4.86	15.37
24.0	Corner	1.08	2.82	8.07
	Internal	1.02	3.18	12.64
	Penultimate	1.08	3.01	10.99
	Two Columns	1.50	5.59	16.68

the internal and corner losses respectively. This large increase is despite the fact that the structure was designed with lower strength concrete specified. Of further note is the change in critical column loss scenario between corner and internal column removal cases. At all strengths the corner loss causes a higher displacement at low loading. However, damage starts to occur at a lower load for the internal case which reduces its stiffness and causes higher final deflections. As the changeover point is dependent on flexural damage, a higher concrete strength delays this effect.

Concrete cracking under static loading

During the static analysis, cracking in the concrete elements was monitored to understand which areas of the structure were susceptible to flexural damage. The following results are based on the response of the model with a span to depth ratio of 19.4. However, as was seen in the displacement results, increasing the span to depth ratio primarily causes nonlinear behaviour due to cracking to occur earlier, but does not change the progression of damage patterns. Figures 6.11 shows the location and extent of plastic strains, representing cracks, that occurred after a corner column loss. The progression of damage across the bottom surface is given in Figures 6.11(a), 6.11(c) and 6.11(e) as the load is increased. Similarly, Figures 6.11(b), 6.11(d) and 6.11(f), show the equivalent state of the top surface and the cracks due to the hogging moments. When the loading is equal to the accidental load case, w_{ac} , there is very little cracking, with just

Table 6.8: Summary of static deflections for different concrete strengths, $L_{eff}/t=19.4$

Column location	Concrete strength, f_{ck} (MPa)	Normalised yield displacement, δ_y/t	δ/t at w_{ac}	R^2 up to w_{ac}	δ/t at $2w_{ac}$
Corner	20	0.029	0.033	0.973	0.304
	30	0.030	0.025	0.983	0.106
	40	0.031	0.021	0.988	0.070
Internal	20	0.026	0.024	0.986	0.417
	30	0.028	0.020	0.991	0.135
	40	0.031	0.018	0.992	0.064

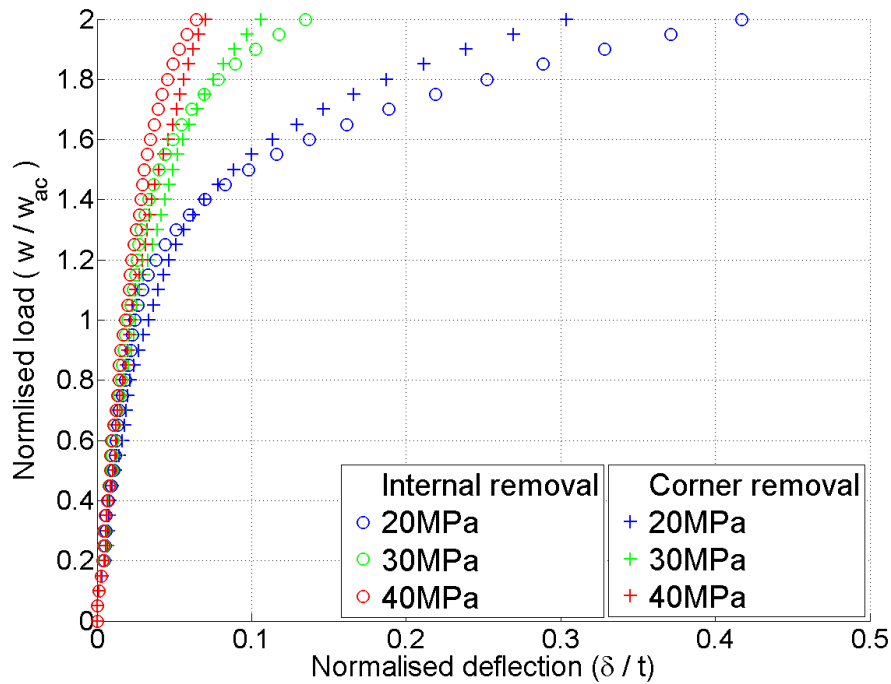


Figure 6.10: Normalised displacement against static loading for concrete strengths. Corner and internal column removal. $L_{eff}/t=19.4$

minor cracks over the the two adjacent supports. As the load increases, these cracks develop further. Additionally, as the column above the removal location is partly restrained, this creates a stress at its base as the slab deforms, resulting in the localised cracks in this region, as seen in Figure 6.11(c). Consideration of the entire multi-storey structure, and the deformation of the columns would be required to assess this effect further. Finally, as the loading increases towards its maximum, $2w_{ac}$, cracking becomes much more extensive. On the bottom surface diagonal cracks between the two orthogonally adjacent supports develop, as was observed during the experimental programme. However, these are limited to the bay directly around the removed column. On the top surface, Figure 6.11(f), the cracks span between the surrounding supports, although the locations directly adjacent to the columns is still the most critical area. Additionally, the start of a diagonal crack between columns A2 and B1 can be seen.

After an internal column removal, Figure 6.12, a similar response is observed with cracks focused directly next to the adjacent supports at relatively low loading. As the load increases, a large area of the structure is affected with excessive cracking on both the bottom surface, Figure 6.12(e), and the top, Figure 6.12(f). As these plastic strains are larger, and cover more of the structure, than the corner condition, this explains why the internal case has higher displacements, as seen in Figure 6.9. Whilst the hogging

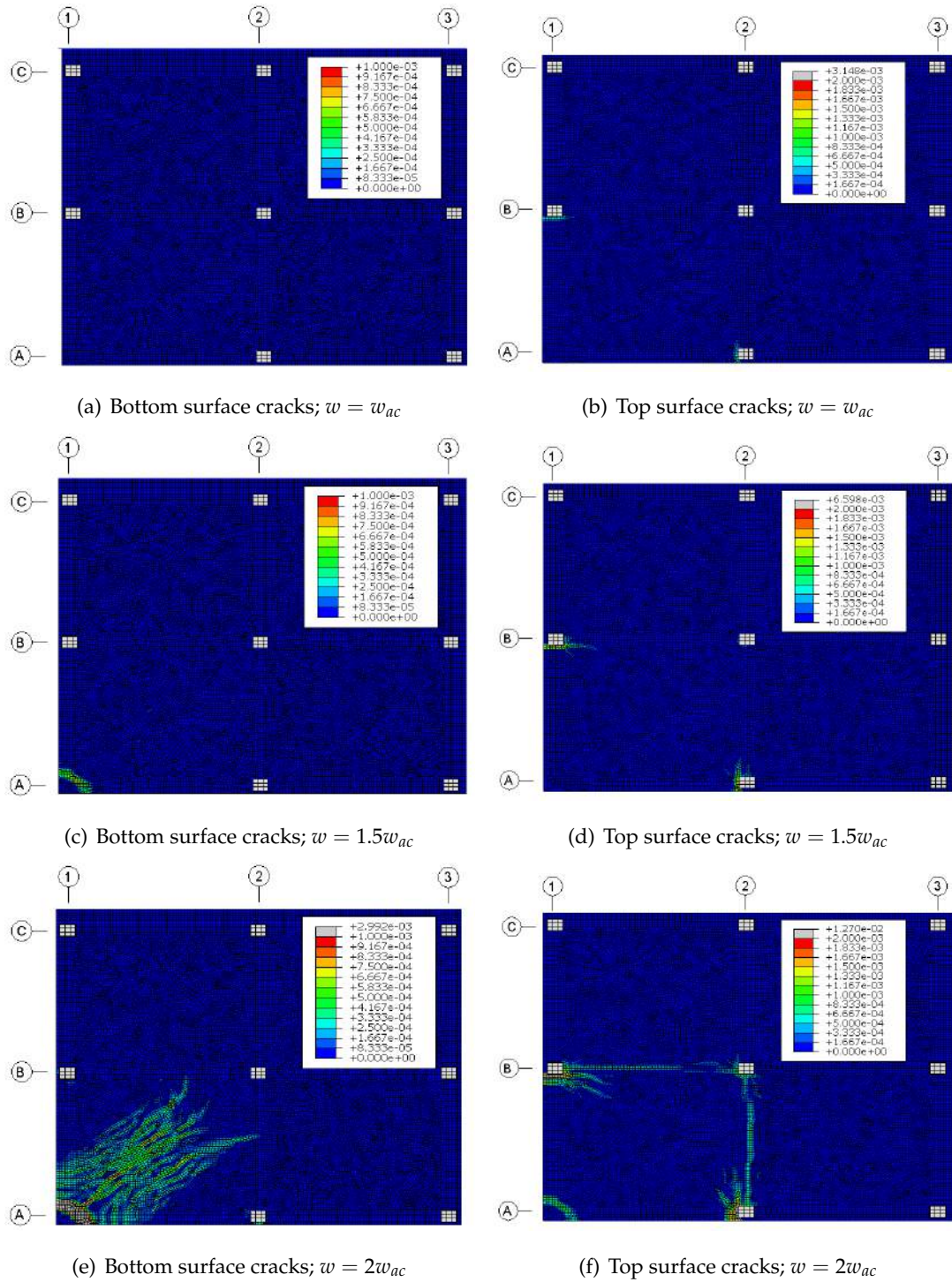


Figure 6.11: Location of tensile plastic strain regions in the concrete elements after corner column (A1) removal

moments create cracks that surround the damaged bay and the sagging condition results in many cracks in the middle of the bay, the rest of the structure remains largely unaffected.

Removing column A2, a penultimate edge column, created the damage response seen in Figure 6.13. Of note in this case are the regions of plastic deformation on the bottom side of the concrete at the higher loadings, i.e. Figures 6.13(c) and 6.13(e). Firstly, the damage is uneven, with more damage occurring in bay 1-2 than 2-3. This is due to the influence of the rest of the structure beyond grid line 3, which counterbalances the deformation and reduces the stresses. Additionally, while cracks do occur at the column loss location, this is not the most critical area. The largest plastic strains, and therefore cracks, occurred close to the middle of bay A1 to B2 and spanned diagonally. This, therefore, is the area that should be investigated further. Furthermore, as the curvature of the slab is approximately zero at the column removal location for this, and the previous internal case, there is not a bending moment transferred into the higher column. Therefore the cracks seen in this region for the corner case do not occur in Figures 6.12(d) and 6.13(d).

When the worst case scenario is considered, removing two edge columns, this naturally results in the most flexural damage, as seen in Figure 6.14. When loading is at $1.5w_{ac}$, as shown in Figures 6.14(c) and 6.14(d), there are extensive sagging cracks between supports A3 and B2 as well as the start of perpendicular hogging cracks on the top surface in the same region. By the time the maximum load is applied, the entire span B1 to B2 is considered as a plastic region, indicating a number of very wide cracks resulting in a plastic hinge forming. Additionally, this is the only case where flexural cracks on the bottom surface extend beyond the immediate bays, and continue into the surrounding area. However, as before, the most critical area is still the hogging cracks directly next to the surrounding columns, i.e. B1, B2 and A3. These are the most likely areas for complete flexural failure.

Considering the flexural damage to the concrete, from all these scenarios, suggests that up to $w = 1.5w_{ac}$, damage is fairly minimal, as previously discussed with the force displacement response. As the DAF is increased to 2.0, then further damage occurs. For the hogging case this was focused at the orthogonally adjacent columns, although may progress further. Sagging cracks developed later and demonstrate the change in load spans as a result of the column loss, with the largest plastic strains not necessary at the removed column location but rather diagonally between adjacent support, where only minimum reinforcement was provided. However, all cases demonstrated that damage remains limited to the immediate bay around the removed column and does

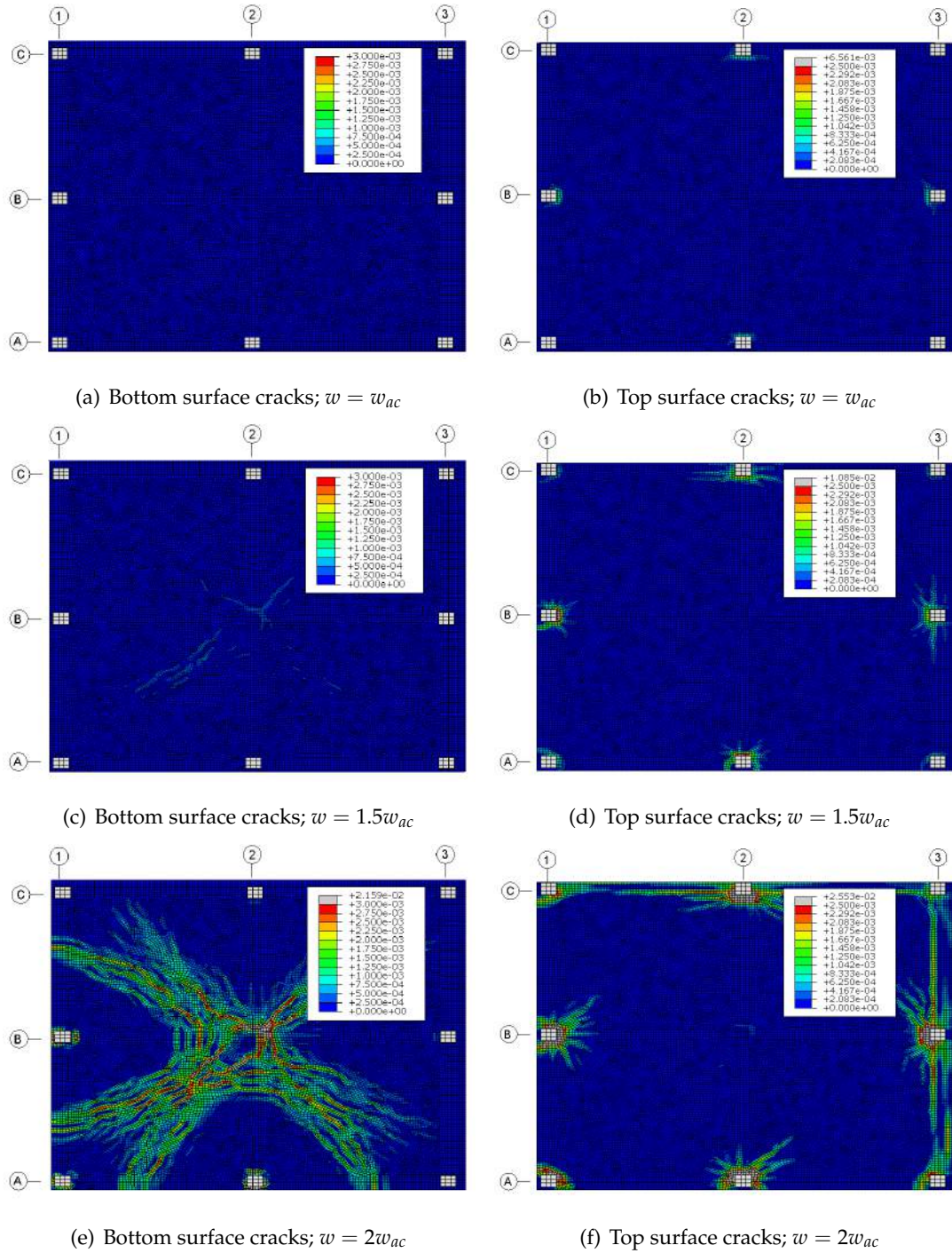


Figure 6.12: Location of tensile plastic strain regions in the concrete elements after internal column (B2) removal

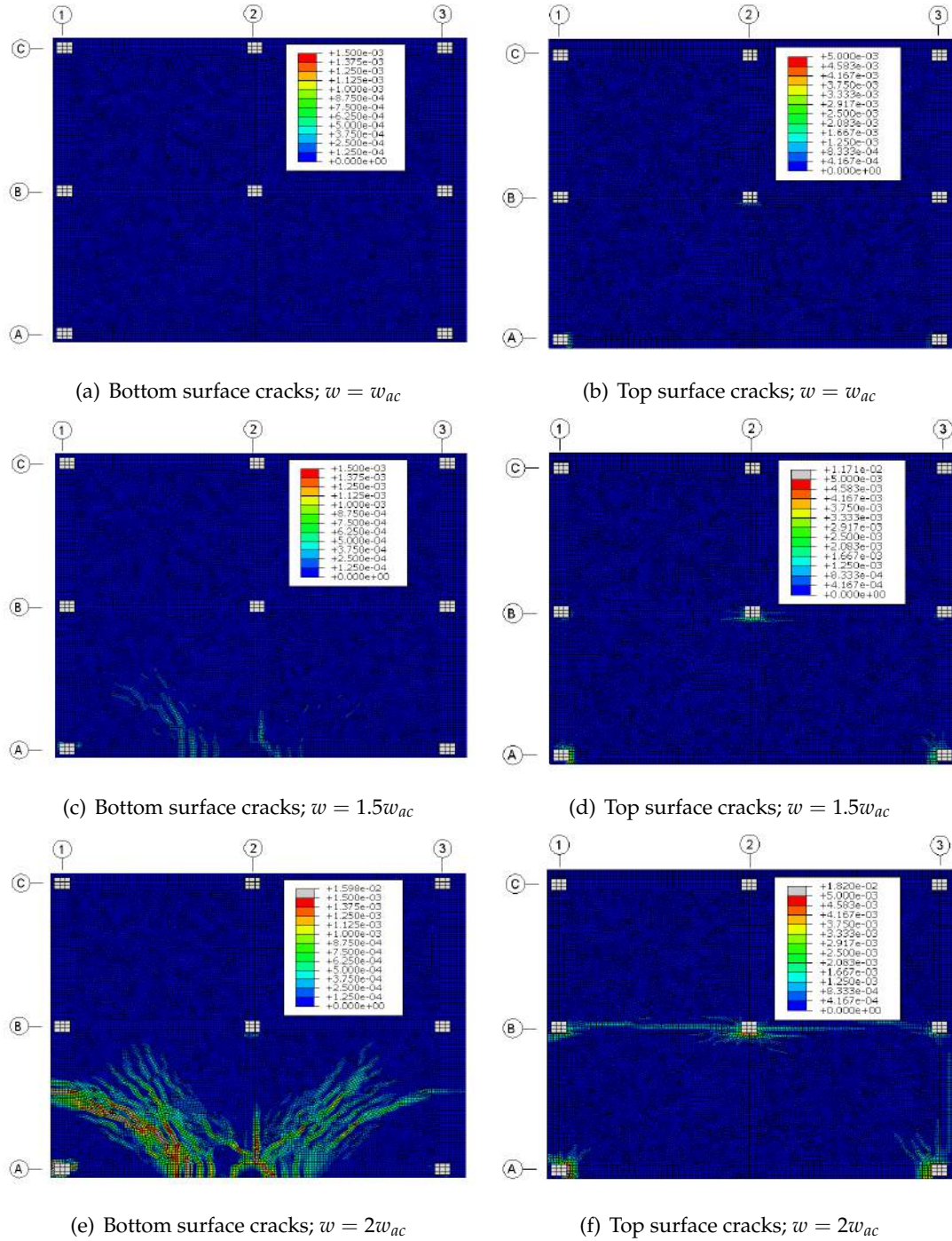


Figure 6.13: Location of tensile plastic strain regions in the concrete elements after penultimate column (A2) removal

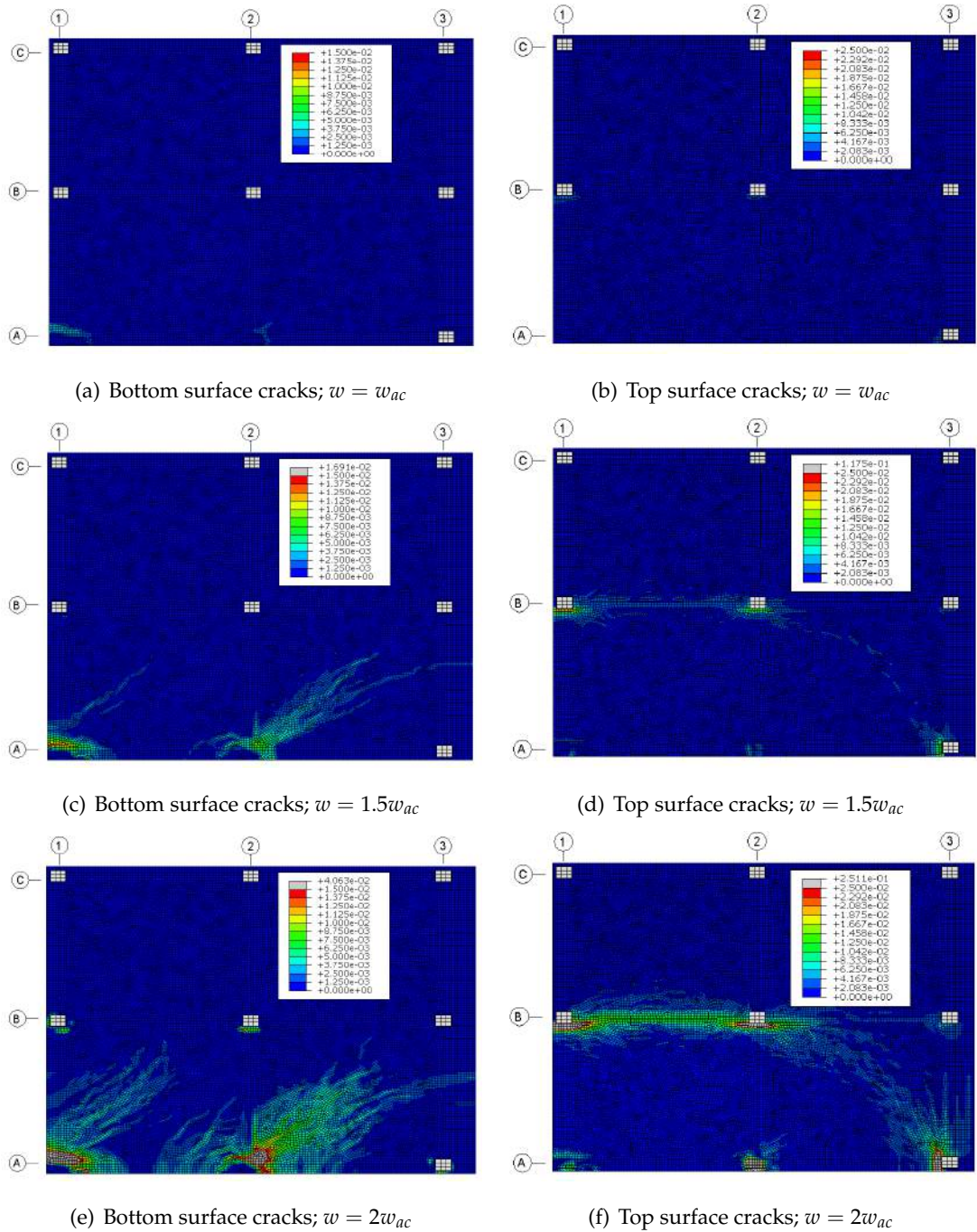


Figure 6.14: Location of tensile plastic strain regions in the concrete elements after two column (A1/A2) removal

not progress into the wider structure.

Reaction forces in the remaining columns

As has been mentioned, the change in vertical reaction forces at a column's support, as a result of a column loss, is an important consideration for progressive failure. Figure 6.15 shows the sum of reaction forces at two column bases as static load is increased after a corner column loss. Column A2 is an orthogonally adjacent column to the removed location, see Figure 6.2, and experiences the highest increase in reaction force. For further comparison, column B2 is across the diagonal from the removed column. The experimental programme indicated that this location may experience a reduction in relative loading as a result of the column loss. The seven models with different span to depth ratios are plotted and the reaction forces normalised against the fully supported condition with a load of w_{ac} . The main observation is there is no significant difference in relative demand for structures with different span to depth ratios. As a result, unless otherwise stated, all other comparisons will be made with just one configuration, $L_{eff}/t=19.4$. Furthermore, at a loading of $w = w_{ac}$ applied to the entire structure, column B2 does have a relative load of slightly less than 100%, demonstrating the demand is reduced. However, as loading is increased in just the critical bay, this results in a slight increase in loading at this location.

After a column loss, some of the the remaining columns can experience a much higher load than they were previously carrying. This can be seen further in Figures 6.16, 6.17, 6.18 and 6.19, showing the changes in reaction forces for all the columns, after each of the column loss scenarios. Due to the symmetry of the structure only half the columns are plotted for the corner and internal cases, see Figure 6.2. Additionally, the horizontal dotted lines indicate the upper and lower bounds for the reaction forces at the ULS for the structures. Therefore, if values are above this line, the shear force demand may exceed the designed capacity.

Considering all these scenarios it can be seen that the two orthogonally adjacent columns have the largest increase in vertical loading. From the summary given in Table 6.9, even without a DAF applied, these locations may be overloaded by at least 35%.

As was observed during the experimental programme, there is a linear increase in loading to each support, as total load is increased. However, while this relationship is good at lower levels of loading, it can be seen that at the higher loadings the effect of damage around the column changes this response. This is due to the changes in span lengths, as a result for local reductions in stiffness, as discussed previously in Chapter 3.

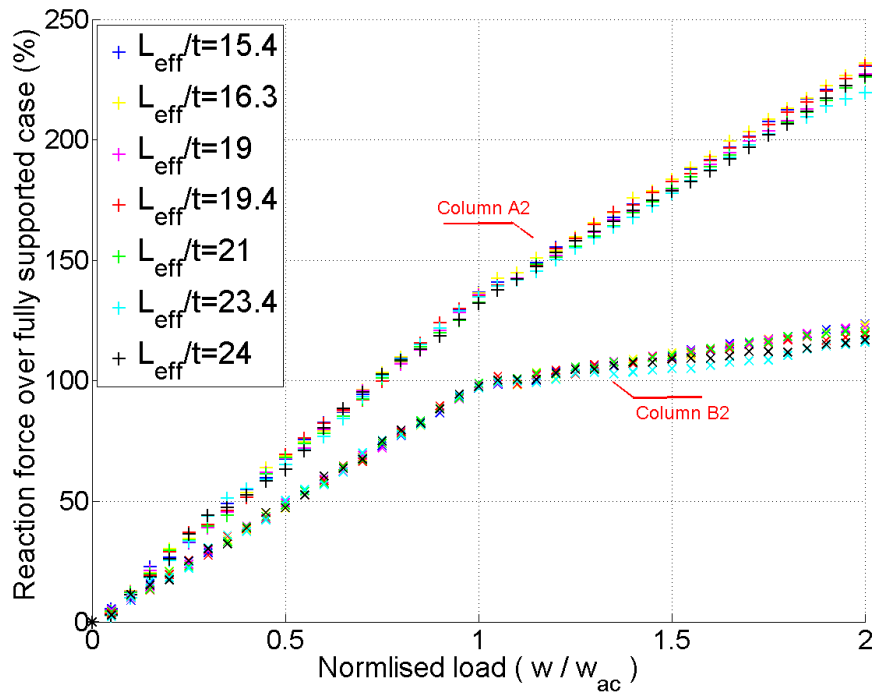


Figure 6.15: Change in column reaction forces due to static load increases for different span to depth ratios. Corner column removal

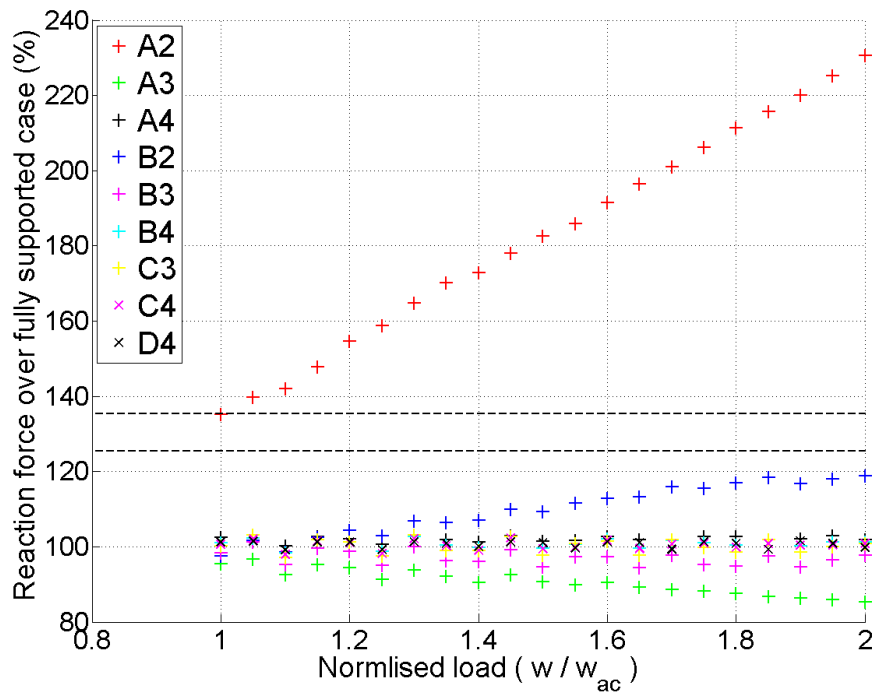


Figure 6.16: Change in column reaction forces due to static load increases. Corner column removal. $L_{eff}/t=19.4$

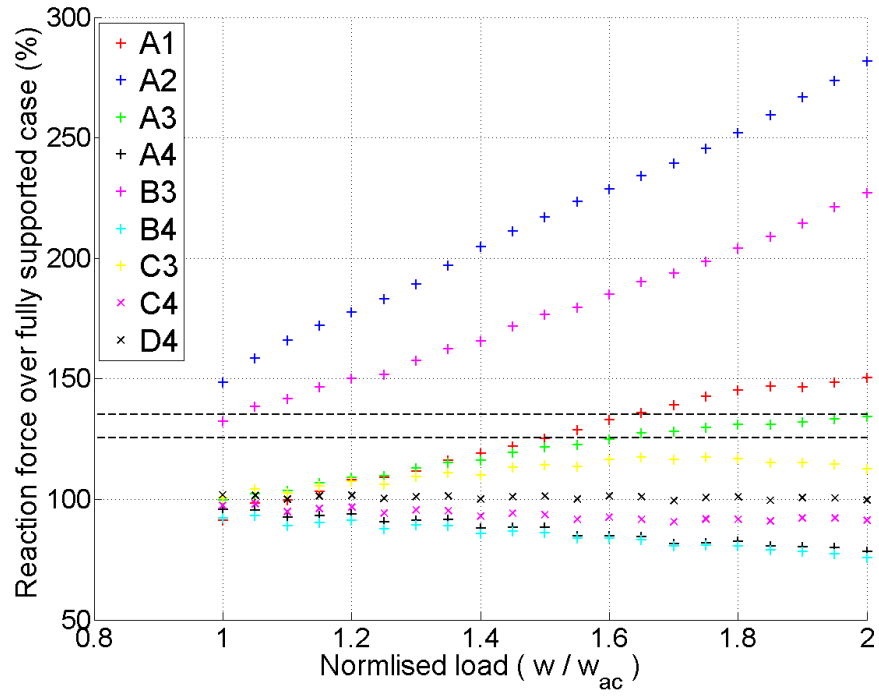


Figure 6.17: Change in column reaction forces due to static load increases. Internal column removal. $L_{eff}/t=19.4$

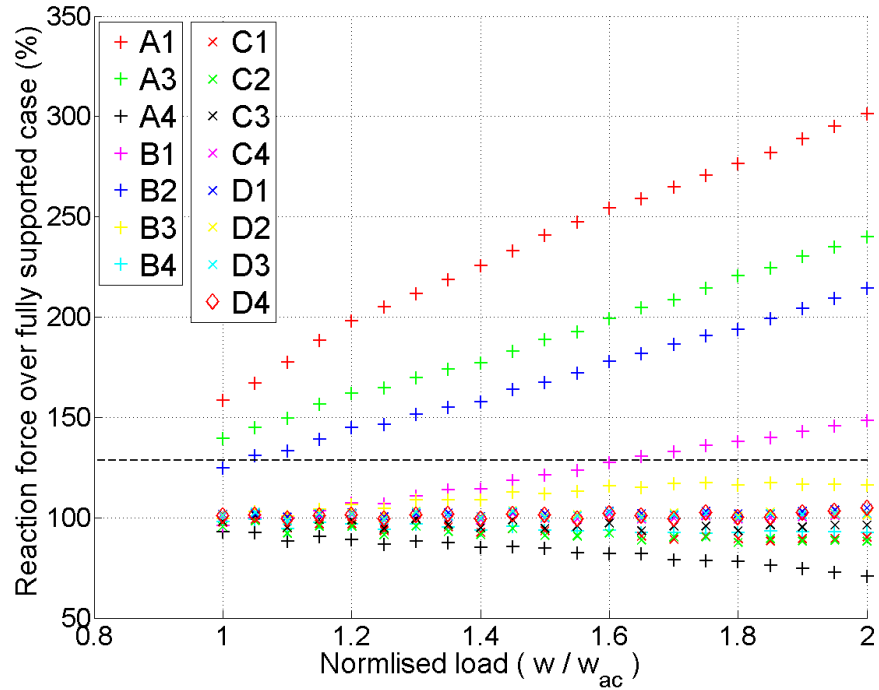


Figure 6.18: Change in column reaction forces due to static load increases. Penultimate column removal. $L_{eff}/t=19.4$

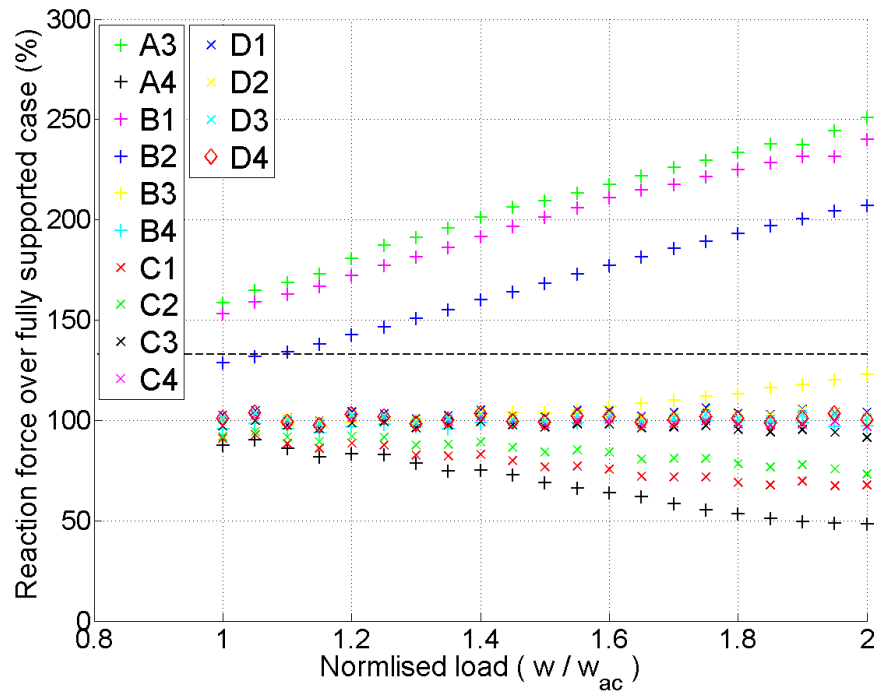


Figure 6.19: Change in column reaction forces due to static load increases. Two column removal. $L_{eff}/t=19.4$

These results can also be used to identify the area the column loss event affects. For example, in Figure 6.16, after column A1 is removed, its immediate neighbours A2 and B1 carry the majority of the loading. This is even more significant as columns further away, such as A3, show a decrease in relative loading. Beyond these locations, the further supports appear unaffected by the column loss, with a relative loading of around 100%. This ratio remains constant even as one bay is overloaded by a factor of 2.

Finally, from Table 6.9, as the DAF was increased to 2.0, critical columns are overloaded by upto 3 times their fully supported condition. Of further note is the critical removal scenario, that is, the event that results in the highest increases in shear forces. Although removing two columns may appear to be the worst case, as such an event influences a larger portion of the structure, the load can be redistributed to more columns and reduce the demand on a single location.

6.5.2 Dynamic results

The scenarios considered with the static analysis above were repeated with a sudden, dynamic column loss. The displacements, reactions and strain rates with time are pre-

Table 6.9: Summary of static reaction forces at remaining columns

Removed column(s)	Critical column(s)	Increase in reaction at:	
		w_{ac}	$2w_{ac}$
Corner (A1)	A2/B1	135%	231%
Internal (B2)	A2/B1	148%	282%
Penultimate (A2)	A1	158%	301%
Two Column (A1 and A2)	A3	159%	251%

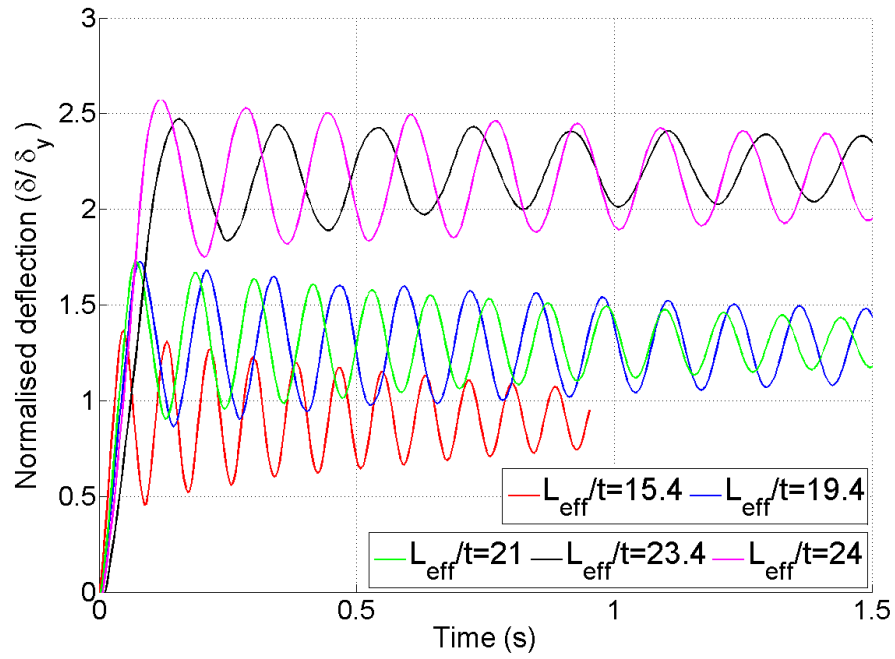
sented in this section.

Displacement response for different span to depth ratios

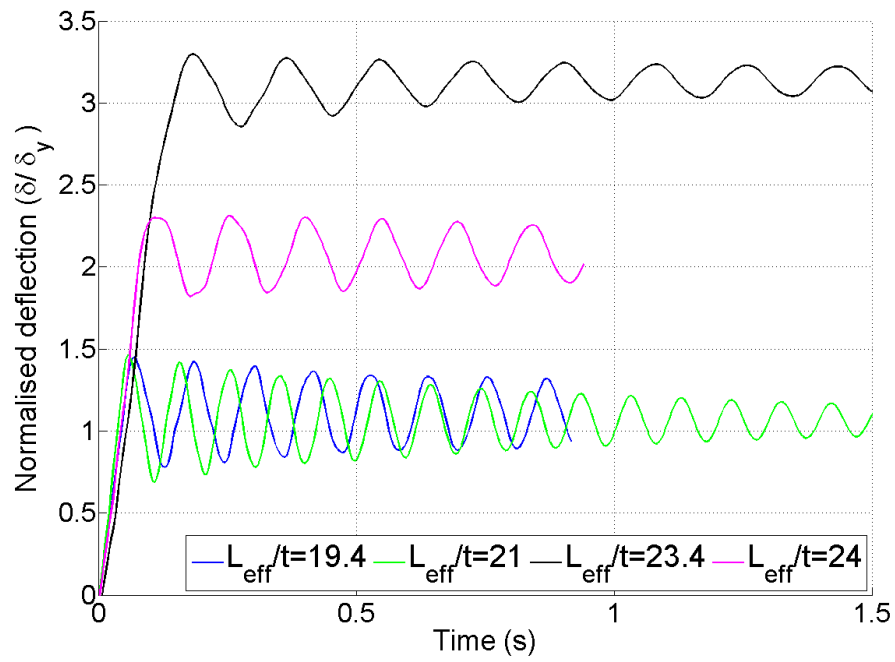
Figure 6.20 shows the normalised displacements against time for models with different span to depth ratios, additionally, the key displacement results are presented in Table 6.10 from all the models. As was seen from the static condition, increasing L_{eff}/t , in general, results in larger normalised deflections. The exception to this can be observed again with $L_{eff}/t = 23.4$ and 24 based on the δ_{max}/t normalisation. However, when the ductility factor, μ_δ , is used, a stronger relationship to the span to depth ratio occurs. In all the cases, while the deflections as a function of the depth remained low, less than 0.159 times the thickness for a single column loss, the level of nonlinearity demonstrated that the structure may be stressed beyond its elastic limit, by up to 3.31 times δ_y in the highest case. Additionally, removing two columns naturally creates a larger displacement response, with a higher δ_{max}/δ_y ratio, although δ_{max}/t is still only 0.283. This suggests that although material nonlinearity may occur, the slab has not deformed enough for geometric effects to be dominant.

A further comparison is given in Table 6.11 which shows the frequency and damping values for the models. In each case, the frequency of oscillation is slightly lower than the value obtained from the modal analysis. This is due to the reduction in stiffness to the concrete elements as a result of damage. However, this change is not typically very large, indicating that the system is close to being elastic. Similarly, the damping ratio, due to energy dissipated by concrete cracking, is typically under 2%, suggesting the damage sustained has not affected the response of the structure significantly.

A comparison of the displacements against time for the four removal scenarios is given in Figure 6.21. From these results all the single column loss events show a similar level of normalised displacement, with the corner case slightly higher than the others at this span to depth ratio. When two columns are removed, significantly higher deflections



(a) Corner column removal



(b) Internal column removal

Figure 6.20: Normalised displacement against time for different span to depth ratios

Table 6.10: Summary of dynamic displacements

Removal location	Span to depth ratio, L_{eff}/t	Max displacement	
		δ_{max}/t	δ_{max}/δ_y
Corner	15.4	0.018	1.37
	19.4	0.051	1.73
	21.0	0.055	1.73
	23.4	0.159	2.47
	24.0	0.123	2.58
Internal	19.4	0.040	1.45
	21.0	0.041	1.46
	23.4	0.156	3.31
	24.0	0.098	2.31
Penultimate	19.4	0.046	1.55
Two Edge	19.4	0.283	4.58

Table 6.11: Summary of dynamic values from the displacement response

Removal location	Span to depth ratio, L_{eff}/t	Modal frequency (Hz)	Displacement frequency (Hz)	Damping ratio
Corner	15.4	11.96	11.85	0.014
	19.4	7.96	7.78	0.012
	21.0	8.94	8.71	0.016
	23.4	5.64	5.23	0.011
	24.0	6.51	6.19	0.011
Internal	19.4	9.01	8.75	0.012
	21.0	10.46	10.0	0.020
	23.4	7.45	5.63	0.010
Penultimate	19.4	8.74	7.62	0.016
Two Edge	19.4	5.44	4.90	0.026

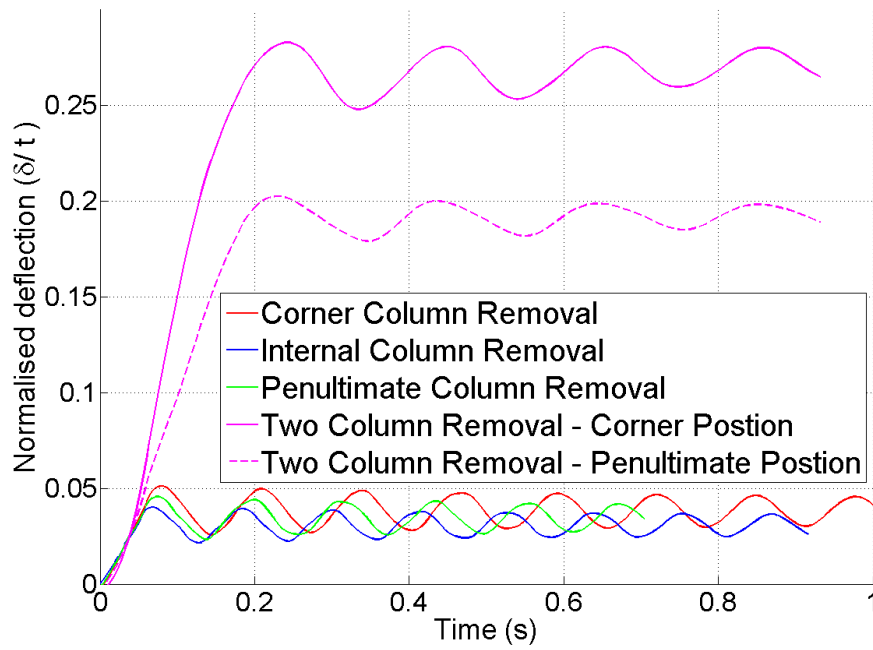
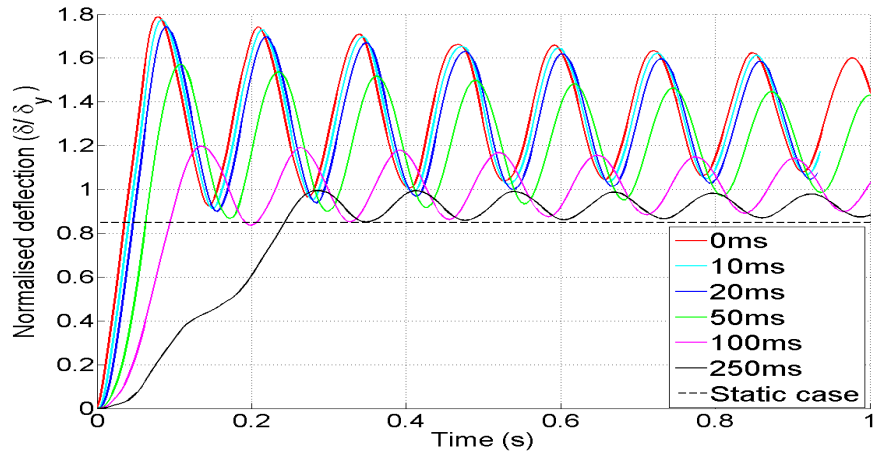


Figure 6.21: Normalised displacement against time for different column loss scenarios. $L_{eff}/t = 19.4$

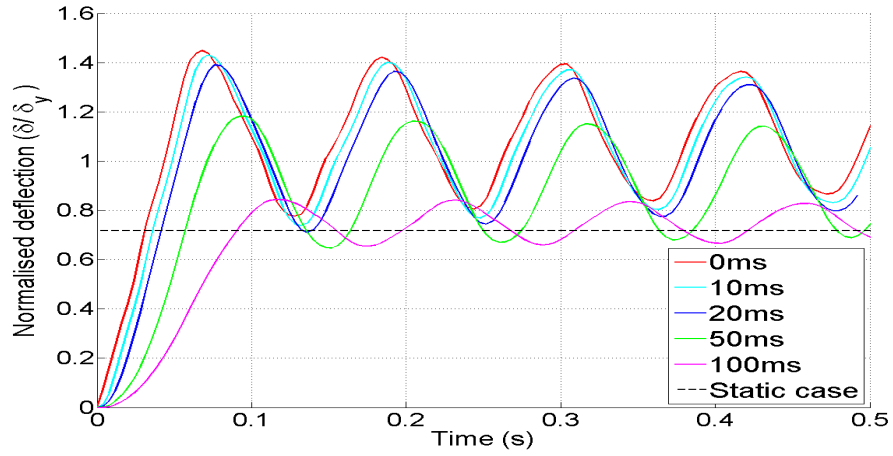
occur, although the frequency of oscillation is smaller, as also shown in Table 6.11.

Displacement response for different removal times

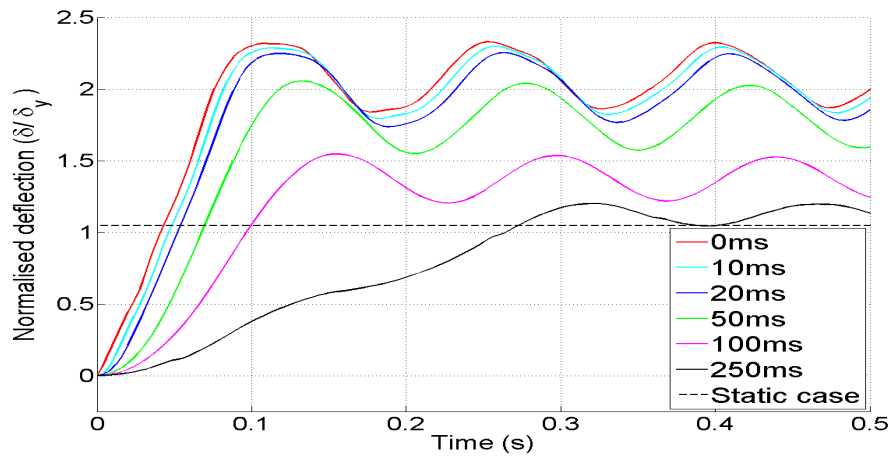
The previous results were all based on an instantaneous column removal. In reality, depending on the cause, it may take longer for the support to be completely removed. Changing this removal time changes the dynamic response of the structure, as can be seen in Figure 6.22. For the corner column removal, Figure 6.22(a), a longer removal time results in a smaller and later peak displacement for all cases. However, upto 20ms, all the results are very similar indicating the removal time does not play a significant role in this range. However, the response is noticeably different with longer removal times. Furthermore, for the 250ms case it can be seen the removal is so slow that it interrupts the motion of the slab. Additionally, the internal column removal, Figures 6.22(b) and 6.22(c), show a similar behaviour. The displacement from the static analysis, with w_{ac} of loading, is also plotted with the dashed line, demonstrating that as the removal time is increased, the response tends towards the quasi-static. However, even at the longest times considered, the dynamic effects are still evident. Additionally, the nonlinearity in the dynamic response can be seen with nearly all cases exceeding the yield displacement.



(a) Corner column removal: $L_{eff}/t=19.4$



(b) Internal column removal: $L_{eff}/t=19.4$



(c) Internal column removal: $L_{eff}/t=24$

Figure 6.22: Normalised displacement against time for different removal times

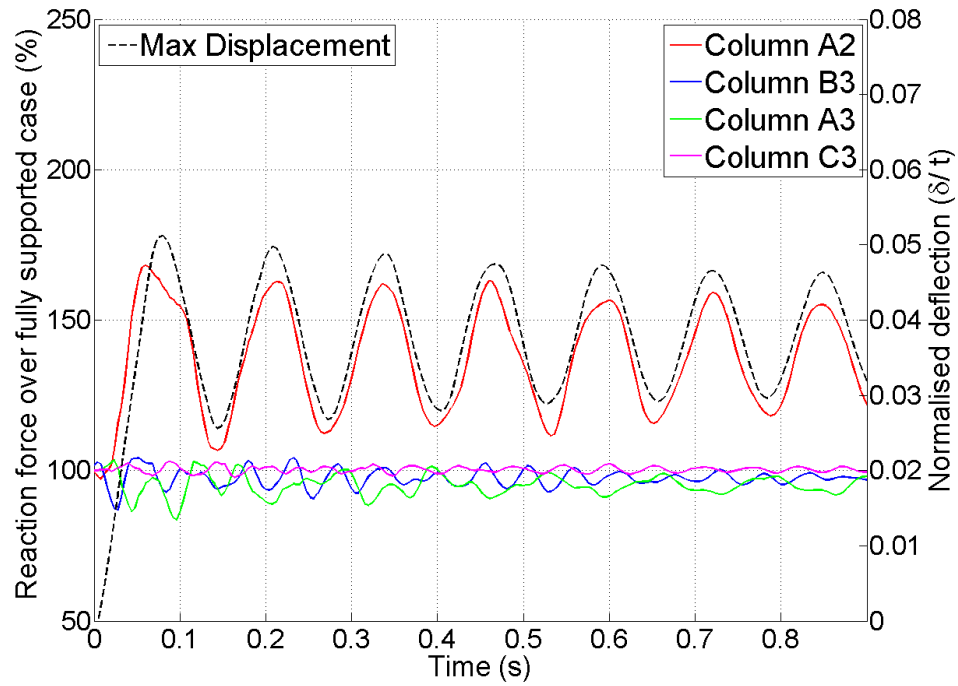


Figure 6.23: Change in column reaction forces against time. Corner column removal. $L_{eff}/t=19.4$

These effects will be considered further in Section 6.5.3.

Reaction forces against time in the remaining columns

Similar to the static case, reaction forces at the bases of all columns were monitored after the column loss event to provide an indication into the increase in shear force demand at those locations.

Figure 6.23 shows the change in reaction forces at 4 remaining columns after a corner column is lost. Also plotted is the maximum displacement with time to allow comparison between the responses. As with the static case, the immediately adjacent column, A2, shows the largest increase in loading, with other locations, such as A3, experiencing a decrease. It can also be seen that the force-time response for the critical column matches the displacement response. That is, the highest shear forces are transmitted through the column at the moment the slab reaches its temporary static condition. However, the force response is not as smooth as the displacement readings, especially during the first oscillation. This is to be expected as reaction forces are related to the acceleration of the slab and therefore emphasises higher frequency components of the motion.

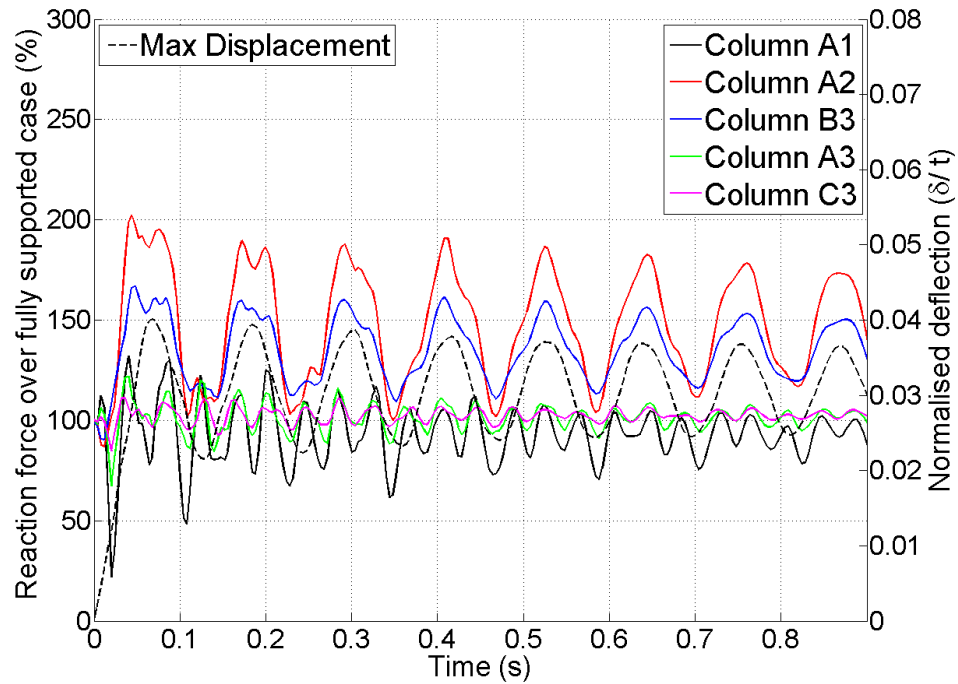


Figure 6.24: Change in column reaction forces against time. Internal column removal. $L_{eff}/t=19.4$

Considering the dynamic removal of an internal column, Figure 6.24, shows a similar response. After column B2 is removed, A2 and B3 have the highest increase. In this case, the higher frequencies can be seen even more clearly, although the dominant frequency still follows the displacement response. Additionally, as the motion continues, and the accelerations become smaller, the peak force profile matches the displacement response more closely.

Considering the penultimate column loss in Figure 6.25 it can be seen that the 3 orthogonally adjacent columns show very similar responses. In this case the corner column, A1, undergoes the largest change from the fully supported condition. This plot also shows the response of Column B3, a support diagonally across the bay from the removal location. The relative load here oscillates around a value close to 100%, indicating that the dynamic motion of the slab influences this location, and still creates an increase in demand, even though the static analysis predicted it would reduce.

Finally, Figure 6.26, provides the reaction response after two column are removed suddenly. This case shows the most complicated response. Although the dominant frequency and behaviour follows the peak displacement of the slab, other frequencies can be seen within the signal. This is partly due to the acceleration effects mentioned ear-

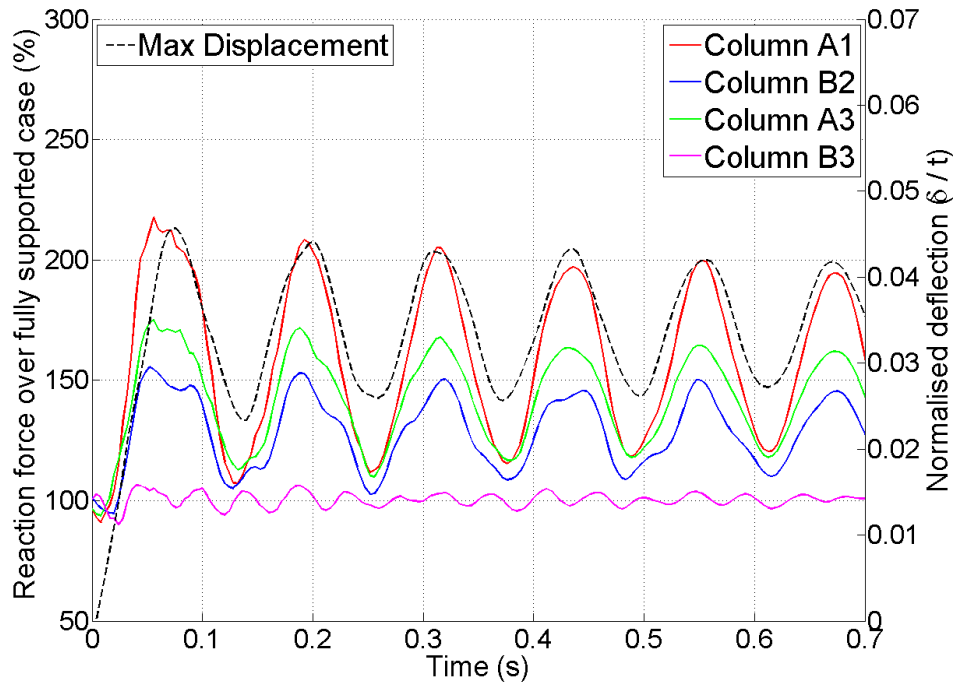


Figure 6.25: Change in column reaction forces against time. Penultimate column removal. $L_{eff}/t=19.4$

lier as well as a consequence of a larger portion of the structure being involved in the motion.

The influence of the removal time on the reaction forces is shown in Figures 6.27 and 6.28. As with the displacement results shown previously, increasing the removal time results in a lower and later peak.

Peak reaction forces in the remaining columns

When a column is removed suddenly, the oscillation effect as forces are distributed to the surrounding supports, can create unexpected increases in the shear forces at locations away from the removal location. Figures 6.29, 6.30, 6.31 and 6.32 show the maximum relative increase in reaction forces at each column, compared to its fully loaded condition for each removal scenario considered. The critical, or highest, value is shown in bold font and, where applicable due to symmetry, only half the values are given. From all the cases, all the supports have values greater than 100%. This indicates that, at least for a moment during the slabs motion, a higher shear force is transferred through each column than was previously the case. This is significant, as a static analysis, even with a DAF does not replicate this effect. However, all these values

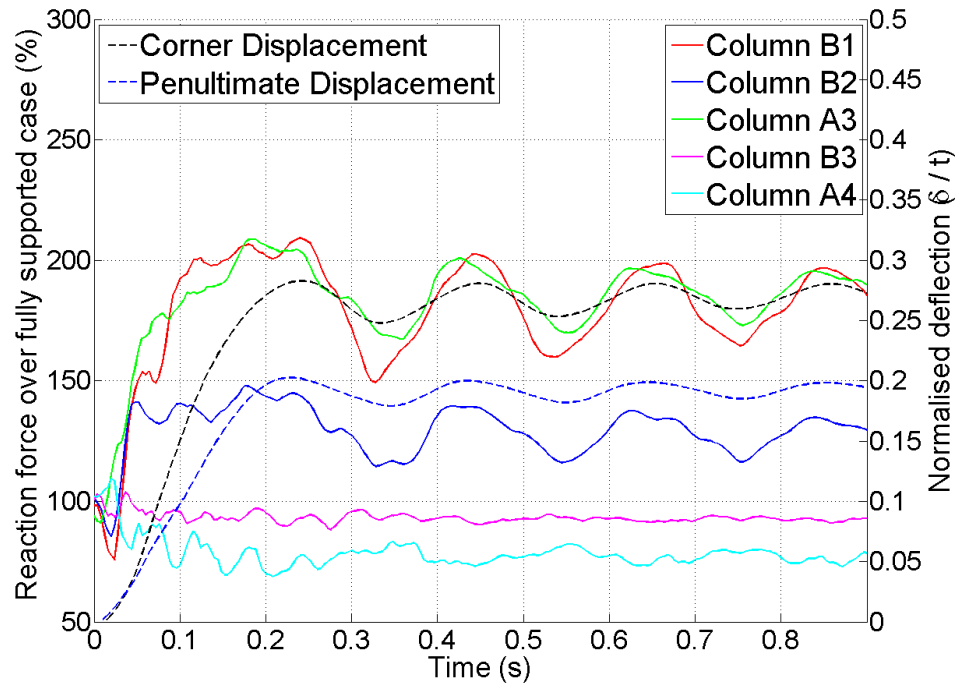


Figure 6.26: Change in column reaction forces against time. Two column removal. $L_{eff}/t=19.4$

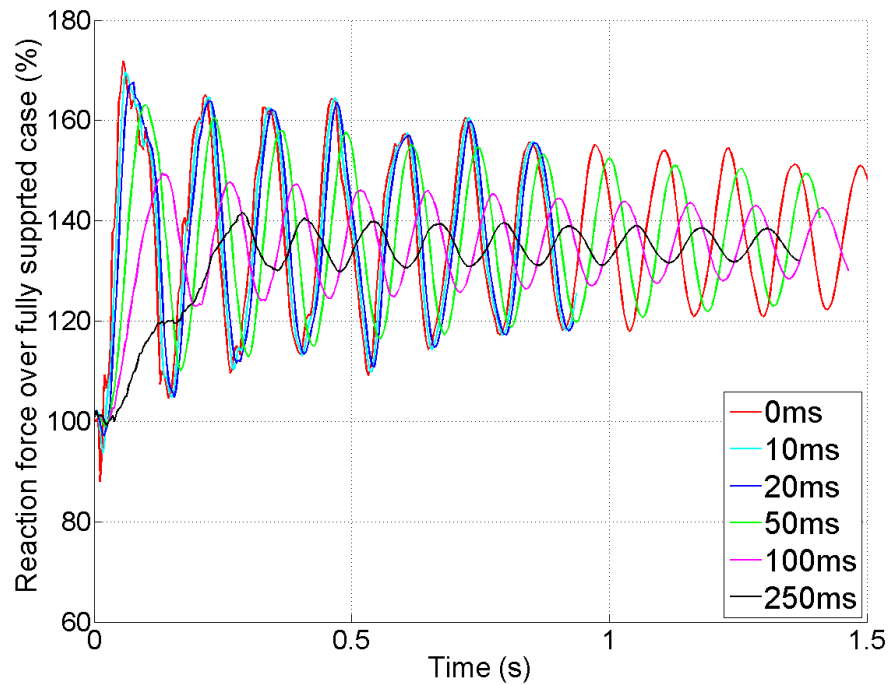
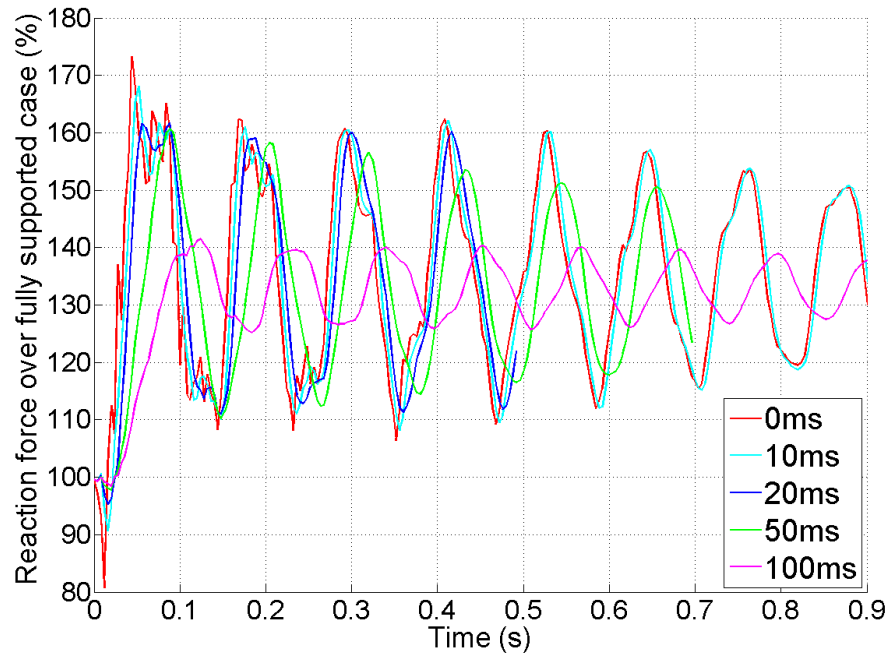
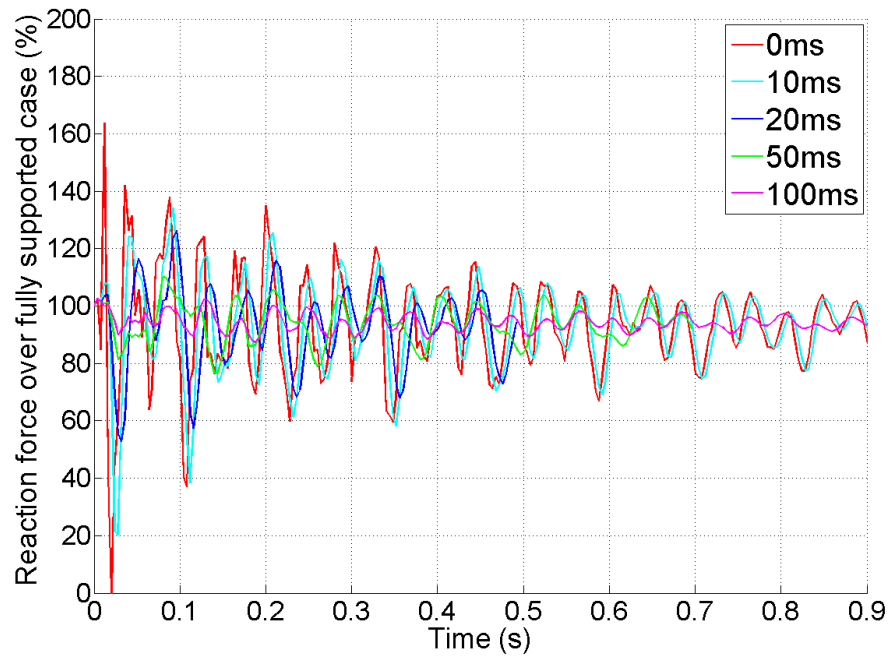


Figure 6.27: Change in column reaction forces against time for different removal times. Corner column removal. $L_{eff}/t=19.4$



(a) Reactions at Column B3



(b) Reactions at Column A1

Figure 6.28: Change in column reaction forces against time for different removal times. Internal column removal. $L_{eff}/t=19.4$

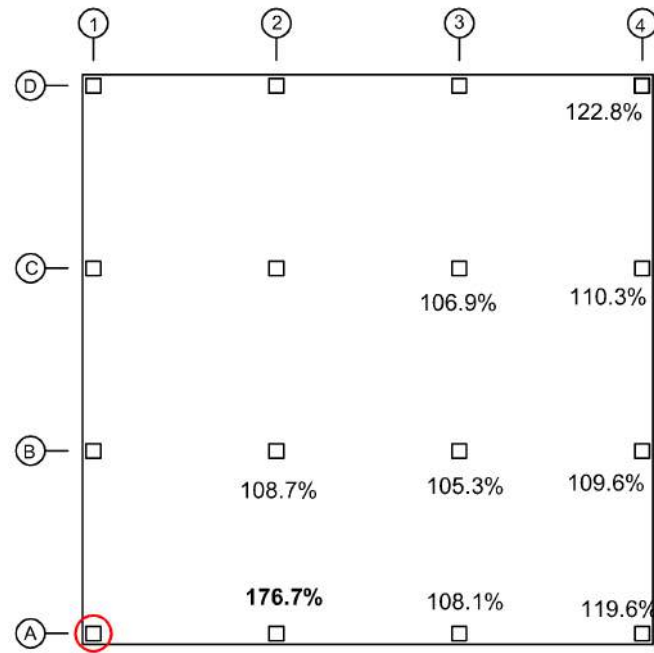


Figure 6.29: Maximum increase in column reaction forces compared to the fully supported condition. Corner column removal.

are far less than the orthogonally adjacent location, and therefore, progressive failure will initiate there if at all.

The most critical removal scenario, in terms of increased shear forces, can be seen in Figure 6.33 which compares the four cases. The remaining column with the largest increase in each case is plotted. From this it can be seen that the corner column is the most critical situation, after its adjacent support is removed. The two column removal causes a maximum which is close to this value, although it takes longer to reach its maximum, corresponding to the slower deflection response.

6.5.3 Static to dynamic comparison

As both static push down tests with an additional force factor and dynamic removal simulations have been conducted on the same models, comparisons can be made to determine the influence of dynamic effects, especially the Dynamic Amplification Factor (DAF). Figure 6.34 compares the displacement at the column removal location for the two conditions. The DAF is taken as the load factor applied to the bays around the removed column, which results in the same displacement as the peak dynamic result, as described by Equation 6.2.6 in Section 6.2.2.

Considering just the corner column loss scenario in Figure 6.34(a) for different span

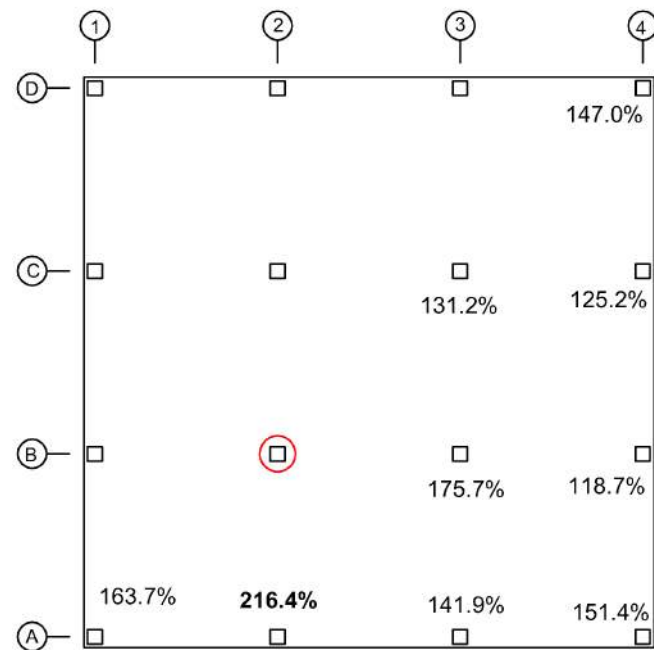


Figure 6.30: Maximum increase in column reaction forces compared to the fully supported condition. Internal column removal.

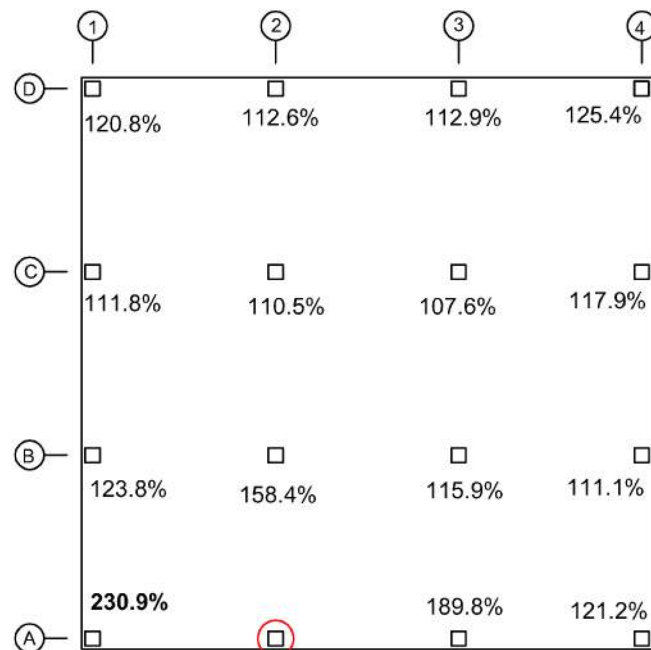


Figure 6.31: Maximum increase in column reaction forces compared to the fully supported condition. Penultimate column removal.

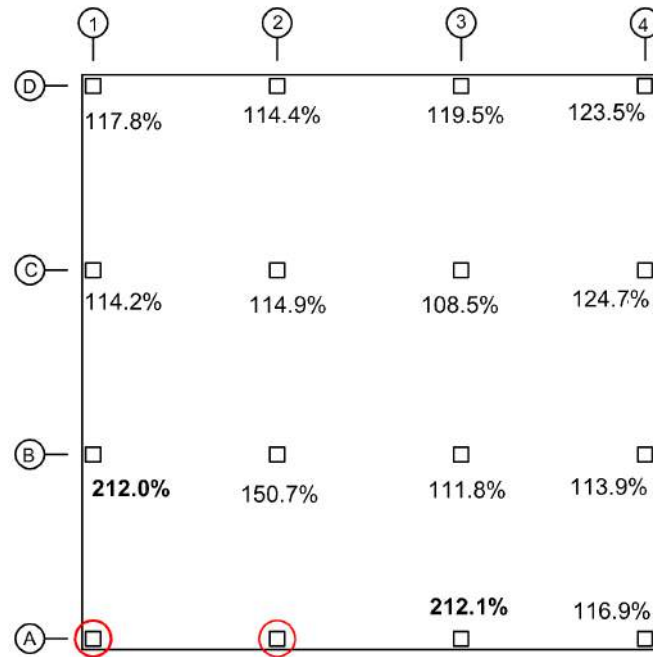


Figure 6.32: Maximum increase in column reaction forces compared to the fully supported condition. Two column removal.

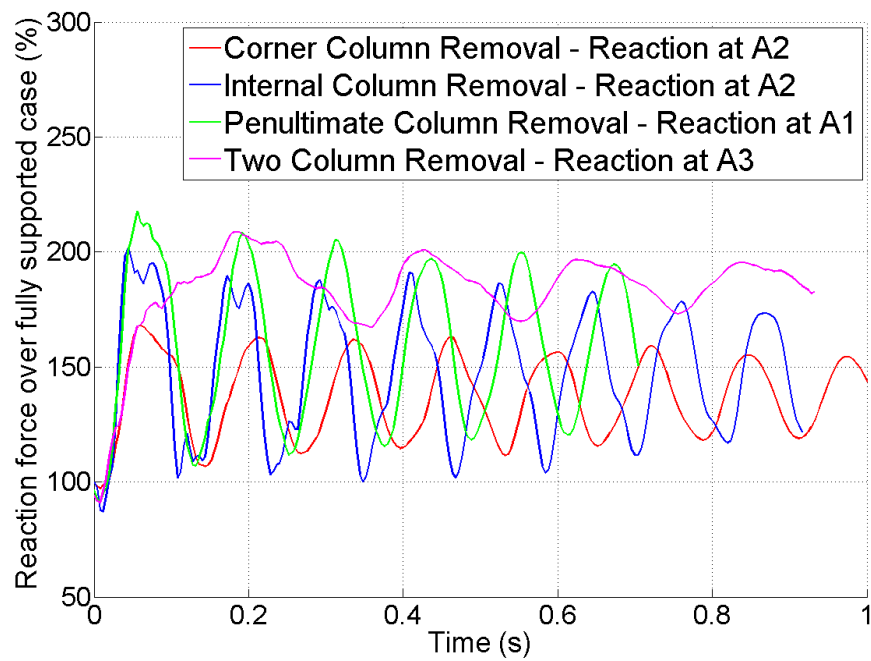
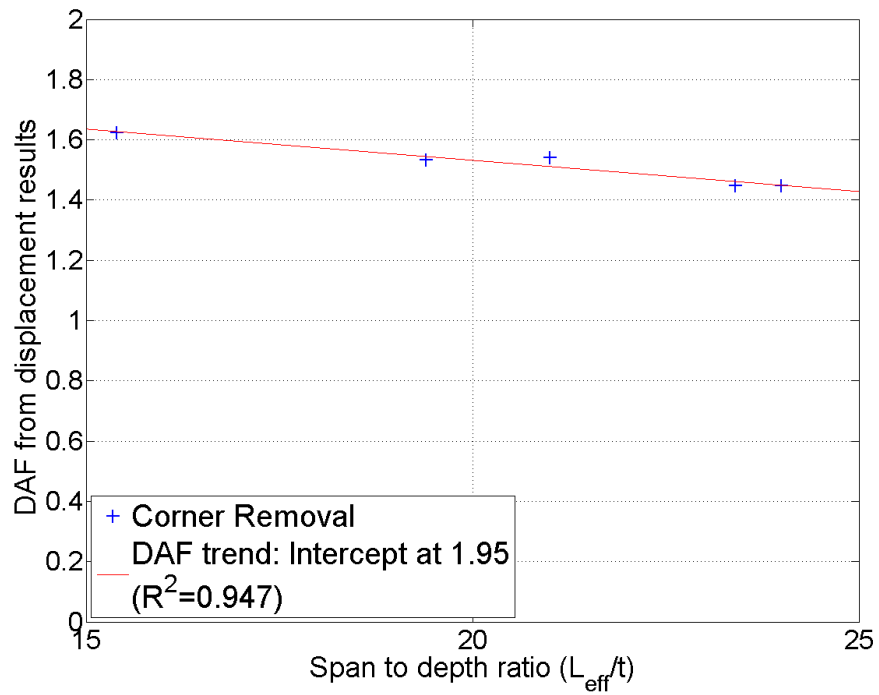
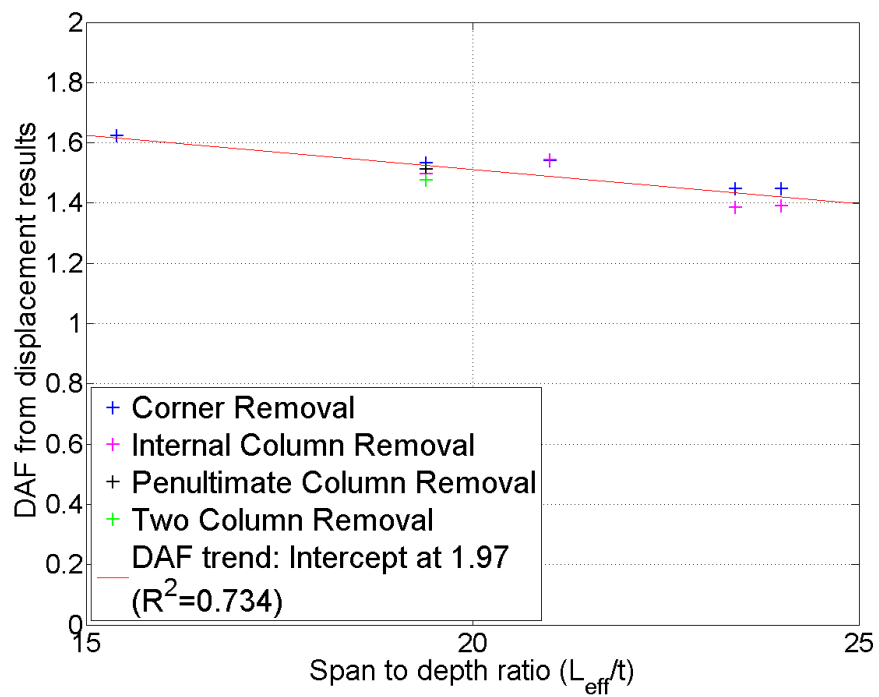


Figure 6.33: Maximum change in column reaction forces against time for different column loss scenarios. $L_{eff}/t=19.4$



(a) Corner column removal scenario



(b) All column removal scenarios

Figure 6.34: DAF from displacement values for different span to depth ratios

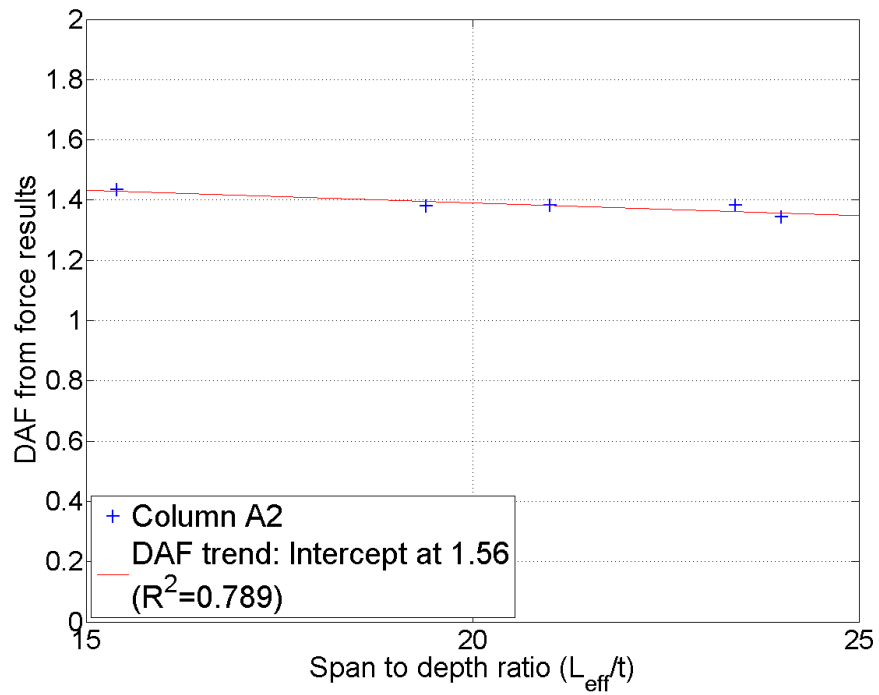
to depth ratios. There is a strong linear relationship between the DAF and the span to depth ratio of the structure, with the factor becoming smaller as this increases. For the range of structures modelled, the DAF varies between 1.45 and 1.62. Additionally, by extrapolating beyond the data it can be seen that as the structure becomes stiffer the DAF tends towards 1.95. This suggests that the influence of inertia is not directly related to the span to depth ratio of the structure, but rather the extent of damage, and therefore nonlinearity in the force displacement response. For a purely elastic, single degree of freedom system, with no damping, a factor of 2 is expected. However, as structures within the normal design range undergo nonlinear behaviour in such conditions, the DAF can be reduced accordingly.

This can be seen further with the results from all the removal scenarios available, shown in Figure 6.34(b). There is a weaker linear trend for this data, although the y intercept is at a similar value. The DAF ranges between 1.39 and 1.62 for these cases.

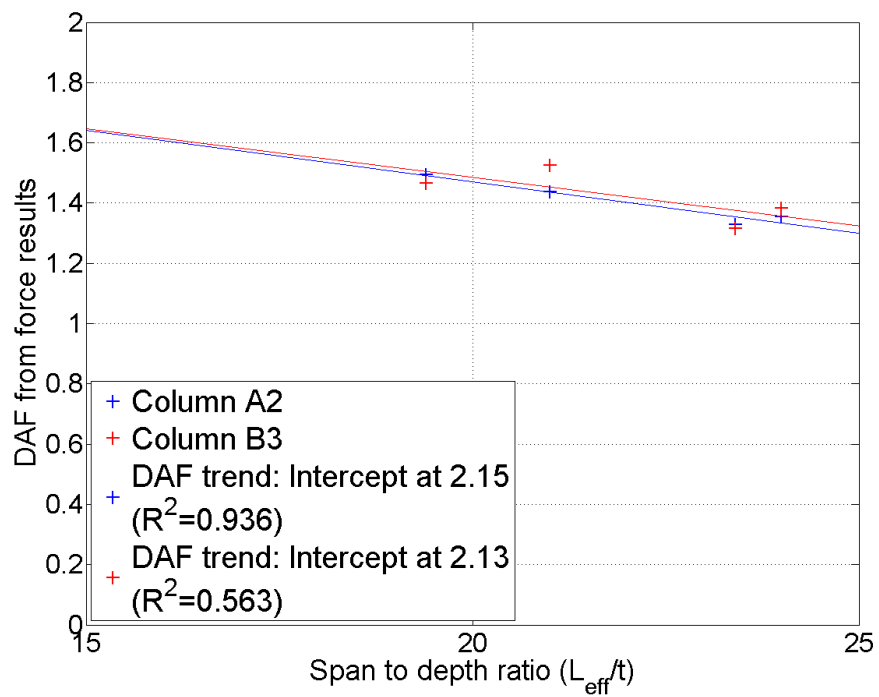
A similar comparison can be made based on the maximum column reaction forces. Standard approaches for the DAF assume that the loading on the surrounding supports is increased by the same factor as displacement conditions. However, as reaction forces are less influenced by nonlinear effects, such approaches may not be appropriate. Figure 6.35 shows the required DAF to create the same static forces in the critical surrounding columns, as caused by the peak dynamic case. As with the displacement values, the amplification factor is compared to the span to depth ratios.

For the corner loss condition, with column A1 removed, the reaction based DAF is given in Figure 6.35(a). There is a weak linear relationship against the span to depth ratio, and the DAF ranges between 1.38 and 1.43 for usual structural arrangements. Considering the internal column removal, B2, in Figure 6.35(b), shows that the two most critical remaining columns have very similar trend lines, although column B3 has a much weaker agreement based on its R^2 value. With this case the DAF varies between 1.31 and 1.53. However, when these trends are extrapolated for stiffer structures, they reach maximum values of 2.13 and 2.15. This response may indicate that for structures with very short spans, the distribution of loads to surrounding columns changes from the typical bending profile.

As was noted when discussing the dynamic results, increasing the removal time for the column decreases the influence of the dynamic effects. Based on this, a modification to the DAF can be applied, this is defined as the ratio of the DAF from instantaneous removal, to the DAF calculated from the slower period. Figure 6.36 plots this factor against a normalised removal time, based on the fundamental period of floor section with elastic properties. The nature of this reduction factor means that as the



(a) Corner column removal scenario



(b) Internal column removal scenario

Figure 6.35: DAF from reaction forces for different span to depth ratios

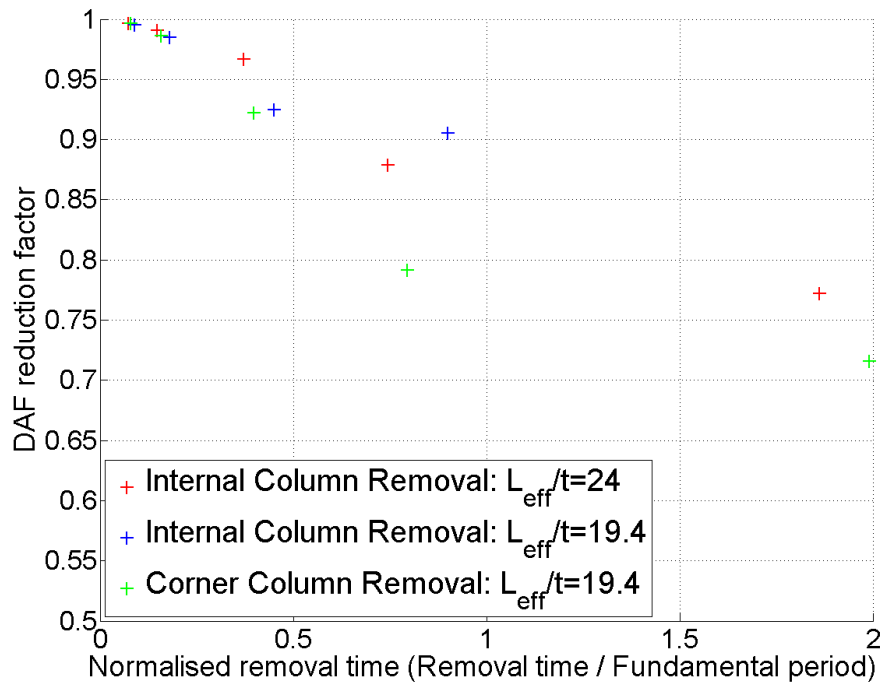


Figure 6.36: Reduction in DAF from displacement values due to column removal time

value reaches 1, the response matches that of an instantaneous removal. Additionally, the lowest value would be 0.5, occurring during an elastic analysis, with no damping and removed slowly enough to remove all inertial effects. For the range of conditions presented, if the support is removed within 10% of the fundamental period the the reduction factor is above 0.995. Similarly, even at 20%, the factor exceeds 0.975. Beyond this range, there is much more scatter within the results, however, if we take the corner case, with removal time of 80% of the fundamental period, the DAF is reduced to 1.21, demonstrating inertial effects may still be significant. At the longest case considered, twice the fundamental period, which, as seen in Figure 6.22, was slow enough to change the motion of the slab, results in a reduced DAF of 1.10 and therefore does not remove the entire dynamic effect.

6.5.4 Influence of strain rate effects

A final consideration was given to the strain rates in the steel reinforcement after a column loss. By measuring the maximum rate of straining that occurs, an upper bound can be determined for its influence on the material properties.

Figure 6.37 shows the maximum strain rate against time from all the top flexural rein-

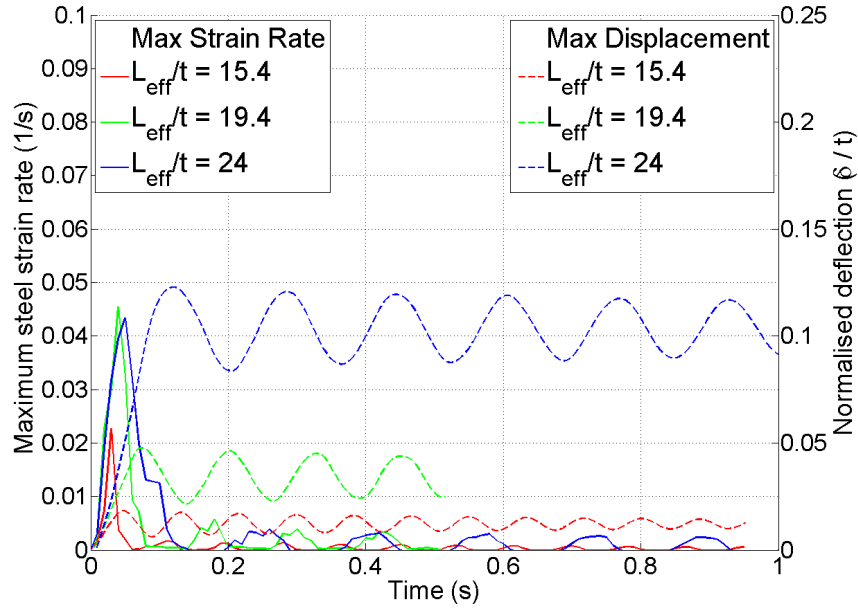


Figure 6.37: Maximum steel strain rate against time after corner column loss for different models. Also showing peak displacements against time.

forcement after a corner column is removed, for models with different span to depth ratios. Also plotted is the displacement against time for the simulation to allow comparisons. It can be seen that the maximum strain rate does not occur at the time of highest displacement, and therefore stress. Instead it naturally reaches its peak whilst the slab is moving towards its first peak. After this, the rate of straining in the steel during the subsequent oscillations are far smaller than the initial peak. Additionally, structures with larger span to depth ratios can result in higher strain rates occurring, primarily because higher deflections occur within the short time period. However, the case with the highest span to depth ratio, $L_{eff}/t = 24.0$, shows very similar peak values to the previous, despite higher deflections. This suggests that even if more of the structure is damaged, an individual section of steel reinforcement will not always strain at a faster rate. This is further indicated by the wider peak for this condition, suggesting more of the steel reinforcement is involved for a longer period.

The peak strain rate values from are 0.023 and 0.043s^{-1} for $L_{eff}/t = 15.4$ and 24.0 respectively. Based on Equation 4.3.12 this corresponds to a DIF for the concrete of 1.20 and 1.21 for the two cases. This small variation suggests that, for the range and conditions for normal structures, the DIF for concrete is around 1.20 at its most critical, and much lower past the initial peak.

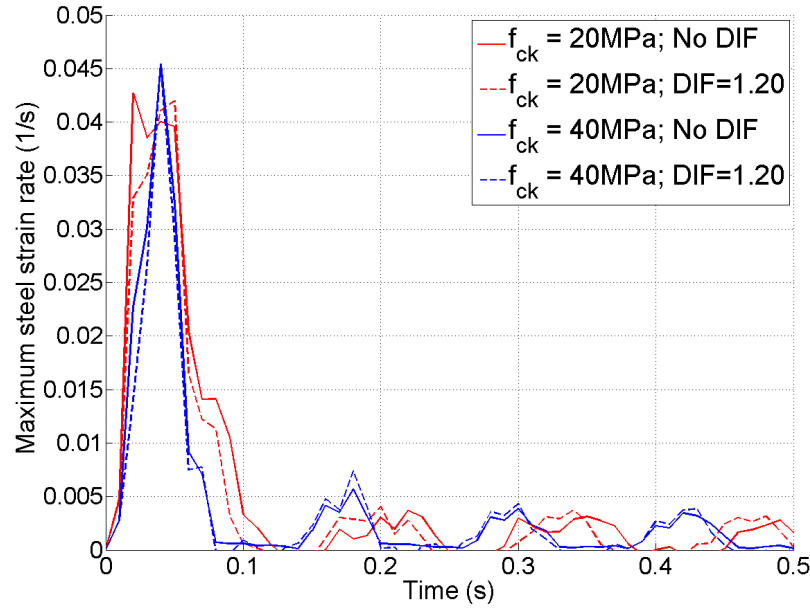


Figure 6.38: Maximum steel strain rate against time after corner column loss for different concrete strengths for model with L_{eff}/t of 19.4

With this value for the increase in tensile strength for concrete, comparisons were made to determine its significance. Figure 6.38 plots the maximum strain rates for models with different concrete strengths. For the higher grade concrete, increasing the tensile strength, further due to dynamic effects, does not change the maximum strain rate with both cases peaking at 0.045s^{-1} . For the 20MPa, applying a DIF does change the strain rate response. Although the peaks are almost identical, 0.042 and 0.043s^{-1} respectively for with and without the DIF applied, the case with the higher tensile strength shows a later, and narrower, peak as a result of less damage occurring. Figure 6.39 compares the influence of the concrete DIF on the strain rate for a model with a lower span to depth ratio. As would be expected, these values are smaller than the previous, with peaks of 0.023 and 0.019s^{-1} . In this case, applying the DIF has slightly changed the strain rate response, however the difference in tensile strength increase only changes by 0.01 as a result, indicating these variations are not significant.

The effect of applying a DIF to the model can be seen in Figure 6.40, which compares the normalised displacement against time. As the span to depth ratio is increased, Figure 6.40(a), the effect of the higher tensile capacity, due to strain rates, becomes more noticeable. This is logical as these cases have already been shown to experience more flexural damage and therefore increasing the capacity will improve this response. However, the maximum difference observed here is still less than 8mm , or 3% of the slab depth.

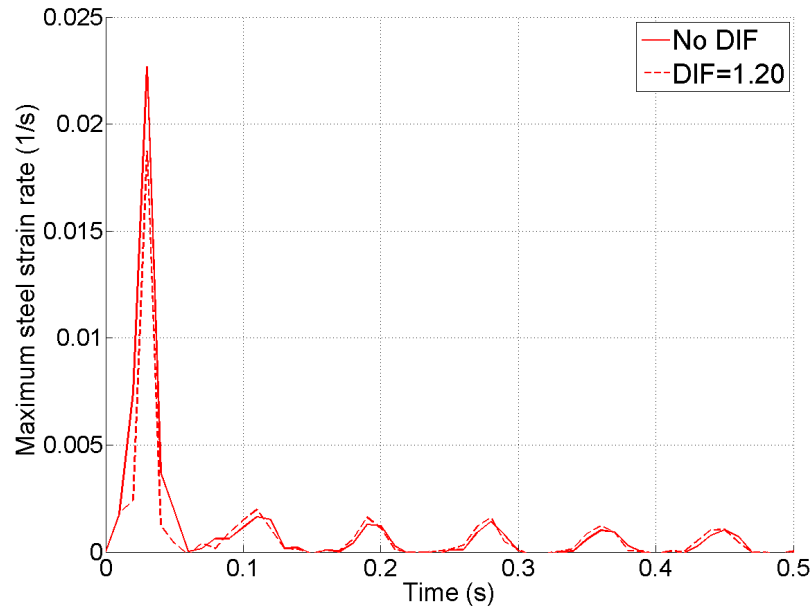
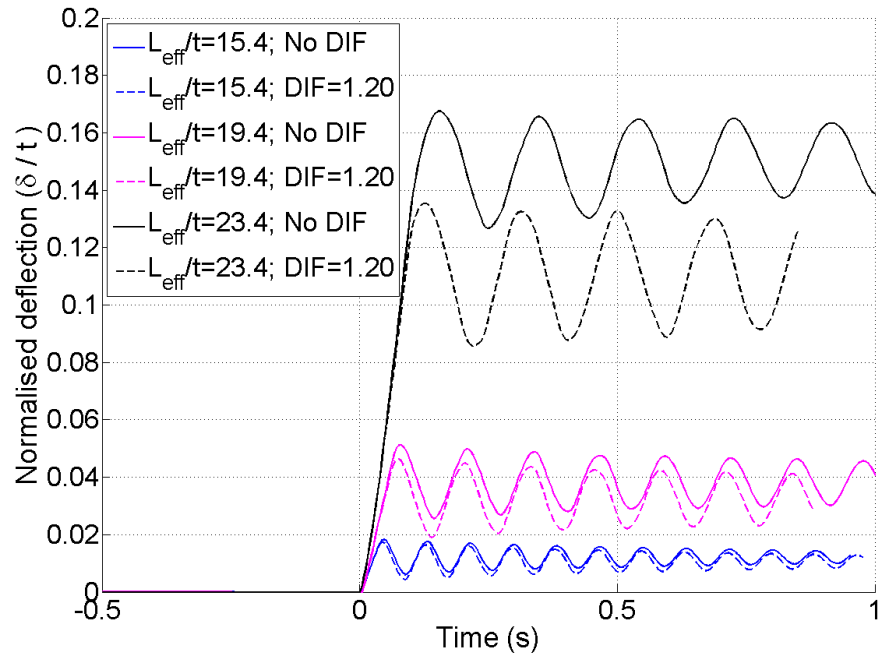


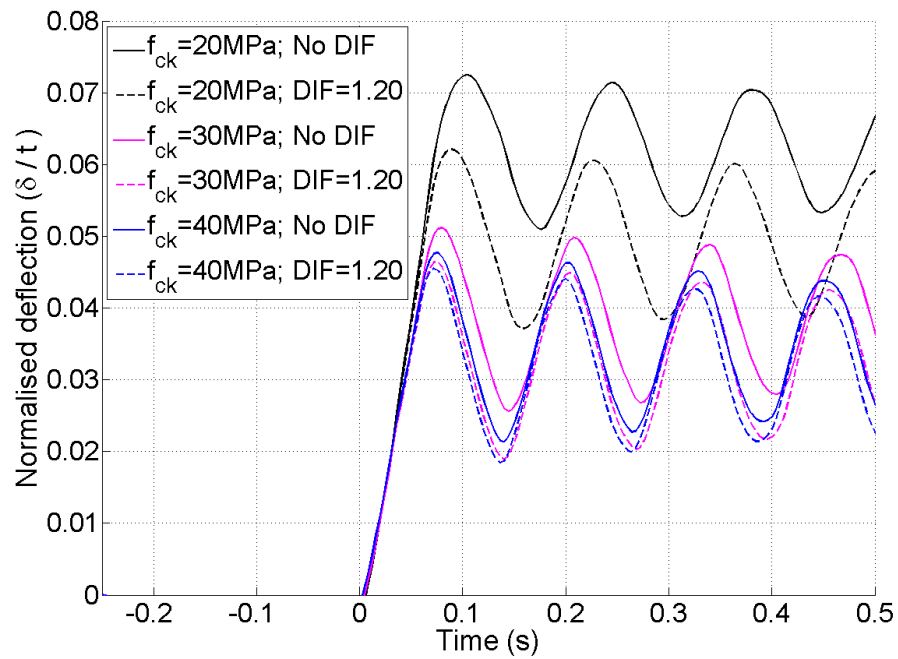
Figure 6.39: Maximum steel strain rate against time after corner column loss for model with L_{eff}/t of 15.4

Furthermore, considering the effect on structures with different concrete grades, Figure 6.40(b), shows the same pattern. Structures that experience higher deflections due to their material or geometric properties benefit more from the additional capacity. However, in this case the maximum decrease in deflections was only 1% of the slab depth. Also note that, as the increase in concrete strength was applied to the entire model for the whole analysis, these plots represent the maximum possible change due to the DIF. In reality the response will be closer to the normal condition.

The previous discussion was based on the results from the top steel after a corner column loss. Figure 6.41 presents the maximum strain rates from an internal removal. This case affects more of the structure and includes the response of the bottom steel under sagging conditions. The first case shown in Figure 6.41(a) demonstrates again that the peak strain rates occurs before the first displacement peak, and after this point are an order of magnitude smaller. Comparing the response of the top and bottom steel shows the peaks are 0.055 and 0.071s^{-1} respectively. This corresponds to a concrete DIF of 1.22 for both cases. The bottom steel peaks occur after the top steel. This is due to the slab changing from a hogging to a sagging condition after the column is removed, therefore cracking does not occur in this area until later. Of final note is the location of the maximum strain rates in the top steel. The most critical area is over supports that are at the edge of the structure, i.e. B1 and A2. However, when these areas are



(a) Varying span to depth ratio



(b) Varying concrete strength

Figure 6.40: Normalised displacement against time after corner column loss comparing effect of applying a DIF

excluded, the internal columns still undergo strains at a rate of upto 0.043s^{-1} .

A different response is observed in Figure 6.41(b). As has been previously mentioned, this model results in the highest deflections due to its higher self weight. In this case first peak strain rates for the top and bottom steel are 0.041 and 0.081s^{-1} respectively, i.e. within the same range as previous cases. However, while the hogging rate reduces to a minimum value after this point, the bottom steel does not follow this behaviour. During each subsequent oscillation, very large increases in the strain rate were observed, peaking at 0.162s^{-1} . As the model was based on the assumption that full bond remains between the steel and the concrete, and concrete cracks are treated as a region of plastic deformation, such results may occur. If large cracks are caused by the deformation, which then open and close as the slab oscillates, the steel reinforcement in this area will strain at the same rate as the concrete. Since after a crack occurred on the first peak, the stiffness of the concrete is significantly reduced in these areas, such effects are likely. However, even with this excessive strain rate, the corresponding DIF is still only 1.24, demonstrating that the range of likely values for a DIF does not vary significantly.

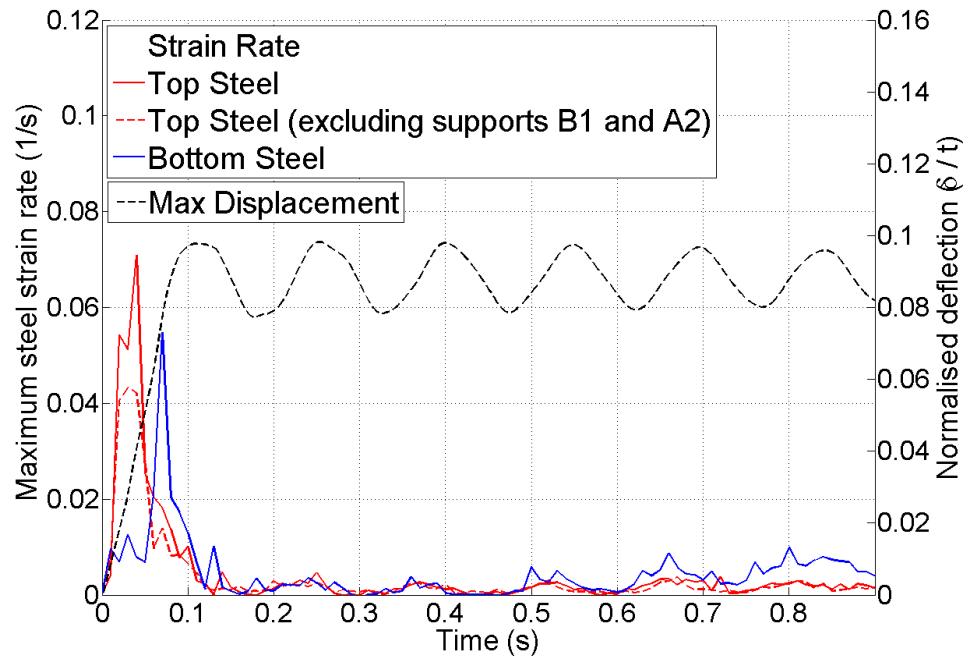
6.6 Summary

This chapter sought to consider the response of typical structural arrangements to a sudden column loss event. Finite Element Analysis (FEA) is used to analyse a range of parameters and monitor the extent of damage that occurred.

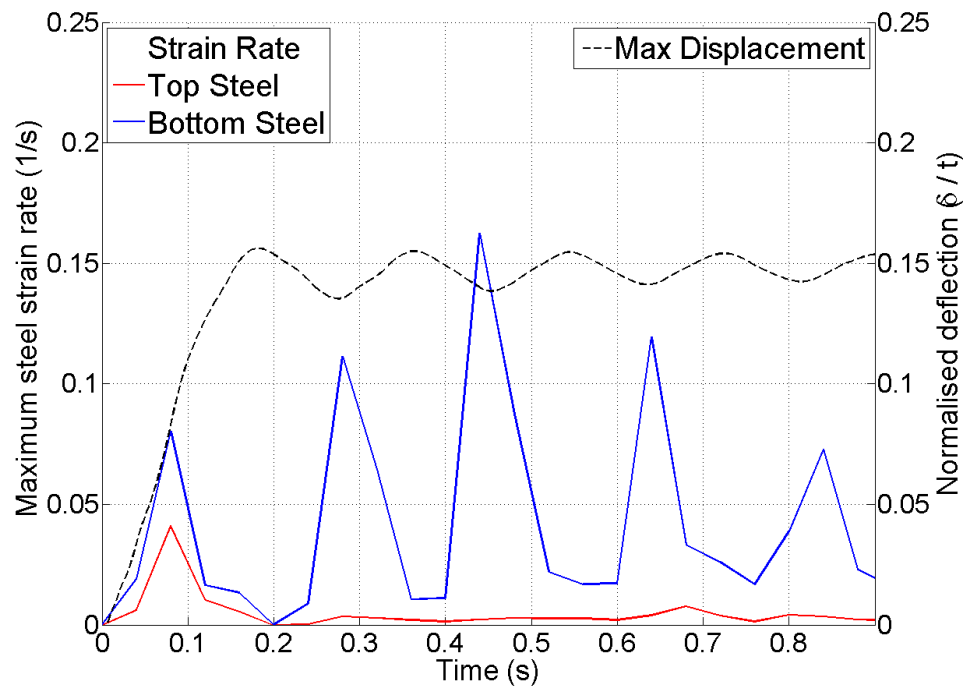
The main observation was that flat slab structures can be considered to be very robust. They effectively utilise ALPs after a local damaging event, such as a column loss. Due to their nature, they can span in two directions and redistribute the loading. While this does stress parts of the structure that were not explicitly designed for such conditions, minimum reinforcement ensures that the structure has sufficient resistance to these flexural demands with only small amounts of damage occurring.

Once the slab exceeded its elastic limits, damage and a permanent reduction in its stiffness occurred, mainly due to cracking of the concrete. However, the nonlinear response was not very severe in most cases and the additional capacity that RC structures can provide was not fully required within the ranges of tests considered. This further suggests that slab structures will not fail progressively due to a column loss.

However, this statement is based on the flexural capacity of the elements. Brittle failure modes, such as punching shear, have previously demonstrated that damage can progress through a slab element, see Section 2.2.4 for examples. These simulations



(a) $L_{eff}/t = 24$



(b) $L_{eff}/t = 23.4$

Figure 6.41: Maximum steel strain rate against time after an internal column loss for model

demonstrate that under static conditions, and without a Dynamic Amplification Factor (DAF) applied, shear forces through a slab-column connection can be increased to 159% of their fully supported condition. This may exceed the shear resistance provided, especially if the effect of an increased hogging moment, creating a non-uniform stress distribution, is included.

Considering the influence of dynamic effects on the structure demonstrates that a sudden removal increases the peak displacements and the shear forces from the static condition. The DAF for displacement values is related to the extent of damage and nonlinearity within the force displacement response. While all cases were lower than a factor of 2.0, the highest ratio was still only 1.62. Similar amplification factors were measured for the reaction forces, with peak shear forces exceeding 200% of the fully supported condition.

Additionally, the results demonstrated the expected behaviour that removing a column slower results in smaller peak deflections. This can be compared to the natural period of the elastic floor section. If the support is lost within 10% of the period, the response is almost identical to the instantaneous condition. As this time increases, the equivalent DAF also decreases, however, even at a time length of twice the natural period, dynamic effects still play a role, indicating that to achieve the static removal scenario requires a much slower case.

Finally, although the sudden removal, and the related strain rates, do change the material properties, their influence is limited. Based on the measured strain rates in the steel reinforcement, the peak concrete Dynamic Increase Factor (DIF) was around 1.20, according to Equation 4.3.12. However, this value is only relevant in limited areas and for a short period of time. Furthermore, comparing the effect of increasing the tensile capacity of the concrete, demonstrates that such an increase does not significantly change the response of the structure. This is partly due to the previously discussed fact that, for the range of slabs considered, the concrete was not stressed far beyond its elastic limits in most cases. Exceptions for this may occur with low strength concrete, or very severe damaging events such as multiple column loss.

Conclusions and Further Work

This chapter provides an overview of the project, including its stated aim, and presents the main conclusions from the investigations. It also highlights areas of further work that arise from this project.

7.1 Overview of the thesis

Previous case studies have demonstrated that structures may fail progressively as a result of damage to a small part of the structure. In particular, flat slab construction has been highlighted as potentially vulnerable to such events due to punching shear failures at multiple column locations. However, there is a lack of experimental and numerical data regarding the behaviour of such structures to an extreme event, such as a sudden column loss. This project sought to investigate this issue and identify the key aspects involved.

Section 1.3 stated the following hypothesis:

It is postulated that Reinforced Concrete (RC) flat slab structures may undergo progressive failure after a sudden column loss, and that nonlinear and dynamic effects are important in assessing this potential.

In order to assess this statement and draw conclusions on its validity, the project's aim was specified as:

The aim of this project is to investigate the behaviour of flat slab structures after a sudden column loss event. The extent of damage and the influence of dynamic effects and nonlinear capacity will be examined to con-

sider their roles in assessing the potential for progressive failures. Different structural configurations will also be investigated.

To achieve this aim, Finite Element Analysis (FEA) was used to simulate a sudden column loss scenario. This model was validated against an experimental programme that replicated a sudden column loss event on scaled slab elements.

The experimental programme presented in Chapter 3 demonstrated that sudden column loss can be considered within a lab environment. Whilst boundary and support conditions are important in assessing the behaviour of real structures, the use of a sub-structure can still provide valuable information into the response of slab elements. Additionally, the dynamic response of a structure can be monitored suitably using a High Speed Camera (HSC) and Digital Image Correlation (DIC), along with Linear Variable Differential Transformers (LVDTs). This provides information into the maximum deflections that occur, as well as allowing further analysis to be conducted on the displacement-time results, such as determining the frequency of oscillation or damping ratio. In cases where progressive failures occurs, typically by punching shear, images from the HSC can be used to identify the moment, location and progression of such failures.

The experimental results showed that flat slab structures can have significant additional capacity beyond their elastic limits, due to the nonlinear material properties, which allows the structure to maintain integrity after undergoing damage, either due to concrete cracking or steel yielding. Additionally, such structural forms are able to resist progressive collapse due to their ability to span in two directions and therefore develop Alternative Load Paths (ALPs).

The tests were then replicated using a Finite Element (FE) model, as described in Chapter 4. This model sought to include the nonlinear and dynamic aspects observed during the physical testing. Results from the numerical model were then compared to the experimental results in Chapter 5 to validate the material laws and modelling approach. While good agreement was achieved for the redistribution of forces after a sudden column loss, and the response of the structure within the elastic range, the Concrete Damaged Plasticity (CDP) model used for the nonlinear behaviour of concrete elements overestimated the extent of damage at high deflections. Despite this, the model was viewed to be suitable to assess other structural configurations.

From the parameter study conducted on a number of variables in Chapter 6, further conclusions related to the initial hypothesis of the project can be made. The results demonstrated that at high levels of loading and deflection, nonlinear material proper-

ties change the response the structure. For some arrangements, typically for structures with smaller span to depth ratios, the material is not commonly stressed far beyond its elastic limits, making such effects less significant. However, with larger span to depth ratios, the loss of a column resulted in much larger observed nonlinearity.

Three claims were presented in the hypothesis, the first is that progressive failures may occur as a result of a sudden column loss. From the available data it is concluded that in most cases the removal of a single column, does not result in progressive failures due to the increased moment demand throughout the slab. Furthermore, it was noted during the experimental investigations and the numerical simulations that flexural damage is limited to the bay directly around the removed column, and does not influence the wider structure. However, there is strong potential for punching shear failures to occur. This was especially noted to be an issue for corner column connections after an adjacent column is lost, with increases in shear forces during a dynamic case of upto 2.31 times their previous fully supported condition. Due to the small shear perimeter around a corner column, combined with the large moment transfer into the column, large shear stresses are created that may exceed the provided capacity.

Secondly, it was suggested that nonlinear effects are important in assessing the response of flat slab structures. It is clear that if the structure is stressed beyond its design, or elastic, limits, the nonlinear material behaviour provides additional capacity. If the structure is then deformed even further, geometric non-linearity in the form of a tensile membrane can further increase this effect. However, based on the results, the extent of non-linearity, given by the ductile displacement factor, μ_δ , depends on the span to depth ratio, with peak values of between 1.37 to 3.31 from the dynamic analysis of a single column loss. As the increase in moment demand after a column loss is related to the span length, such an effect is to be expected. Additionally, if a Dynamic Amplification Factor (DAF) of 2.0 is applied to the structure during a static analysis, much higher μ_δ were measured, indicating that applying such a factor may result in over conservative designs. Furthermore, while material nonlinearity was observed, for the range of typical structures considered, deformations were not large enough to cause geometric effects to be significant as the peak displacement was only 0.159 times the slab depth.

Finally, the influence of dynamic effects was considered. The most significant dynamic effect is the increase in deflections and reactions forces, from an equivalent static case, due to inertial effects. A comparison between static and dynamic conditions is typically achieved by use of a DAF. Based on the range of parameters considered, this factor was always under 1.62. Additionally, it was identified that as damage becomes more significant then this ratio reduces further. This is due to the nonlinear relation-

ship between force and displacement beyond the elastic range, as well as increases in the damping ratio of the system as energy is dissipated due to concrete cracking and reinforcement yielding.

An additional dynamic effect considered was the influence of high strain rates on the response of the structure. Based on the measured steel strain rates during the experimental programme, as well as the values from the numerical models, the peak strain rates were typically between 0.01 and 0.1s^{-1} , with no case exceeding 0.35s^{-1} . According to the Model Code's equation for the Dynamic Increase Factor (DIF) of the tensile strength of concrete (fib, 2012), this corresponds to a typical maximum factor of between 1.18 and 1.23, with an upper bound of 1.26. However, as was noted, such an increase in strength is only relevant during the initial period that the slab is in motion, and before it reaches its maximum displacement condition. Additionally, only very limited areas of the slab are stressed at this rate. Therefore, the additional capacity that the concrete gains from the fast loading after a column loss is not significant in most cases. This was further backed up by simulations that included a higher tensile strength, which led to only small decreases in vertical deflections.

7.2 Conclusions

Based on all these findings it can be concluded that, in general, a flat slab structure may undergo progressive failures as a result of a sudden column loss. However, this is only likely to occur if the punching shear stress around the adjacent columns exceeds the capacity, as a result of the redistribution of loading and the dynamic effects. Provided that the slab contains continuous flexural reinforcement throughout the span, then complete flexural failures are unlikely to occur. Related to this, the extent of damage sustained in most cases remains fairly small and does not pose an immediate risk to the structure. As a result of this, inclusion of the full nonlinear behaviour of the slab elements may not be required in assessing its potential for progressive failure or collapse. However, dynamic effects caused by the inertia of the moving slab after a sudden removal can play a significant role. Although the value of the DAF depends on the layout and design of the structure, with particular focus on the extent of damage that occurs as a result of a column loss, the factor was always below 1.62. As GSA (2013) recommends a value of 2.0, this indicates that following such guidelines may result in over conservative designs, especially for punching shear capacity.

In summary the main conclusions of this work are expressed below.

- Reinforced Concrete (RC) flat slab structures are robust and can resist progressive

collapse provided brittle failures, such as by punching shear, are prevented.

- For common structural designs, the extent of material nonlinearity depends on the design of the slab, with displacements up to 3.31 times the yield displacement measured during dynamic analysis. However, geometric nonlinearity was not significant in assessing the response of the structure.
- Dynamic factors, primarily the increase in deflections and shear forces due to inertial effects, can be significant, with a Dynamic Amplification Factor (DAF) up to 1.62 calculated. This factor decreases with higher nonlinearity in the structural response.

7.3 Further Work

Although this work is viewed to address the main factors involved for progressive collapse of flat slab structures, further work is required to provide a more detailed understanding. Firstly, more experimental tests are required to increase the confidence of theoretical models. Ideally, this should be conducted on full size structural elements which represent typical designs. This work should be focused on assessing the dynamic response of slab elements after a column loss and consider the potential for sudden punching shear failures.

Similarly, further numerical work should be conducted considering more structural layouts, as well as assessing the influence of changing other geometric or material properties, such as column sizes or reinforcement arrangement. Additionally, consideration should be given to flat slab construction containing shear reinforcement. The work would address whether shear reinforcement will always preclude progressive punching shear failures after a column loss, and if the increased span to depth ratios that are possible increase the potential for flexural failures.

Finally, further results are required to allow broad guidelines to be suggested to aid designers in preventing a progressive collapse from occurring. This requires detailed information into the nonlinear capacity of the structure, as well as a good understanding of the demand placed on various parts of the structure as a result of dynamic inertial effects.

References

- EN 1990. BS EN 1990: Eurocode 0 - Basis of structural design, 2002.
- EN 1991-1-1. BS EN 1991-1-1: Eurocode 1. Actions on structures. General actions, 2002.
- EN 1991-1-7. BS EN 1991-1-7: Eurocode 1 - Actions on structures - Part 1-7: General actions - accidental actions, 2006.
- EN 1992. BS EN 1992: Eurocode 2 - Design of concrete structures - Part 1-1: General rules and rules for buildings, 2004.
- EN 1998-1. BS EN 1998-1: Eurocode 8. Design of structures for earthquake resistance. General rules, seismic actions and rules for buildings, 2004.
- M. S. A. Abbasi, M. H. Baluch, A. K. Azad, and H. H. A. Rahman. Nonlinear Finite-Element Modeling of Failure Modes in RC Slabs. *Computers & Structures*, 42(5):815–823, 1992.
- J. Abruzzo, A. Matta, and G. Panariello. Study of mitigation strategies for progressive collapse of a reinforced concrete commercial building. *Journal of Performance of Constructed Facilities*, 20(4):384–390, 2006.
- A. Agbossou and J. P. Mougín. A layered approach to the non-linear static and dynamic analysis of rectangular reinforced concrete slabs. *International Journal of Mechanical Sciences*, 48(3):294–306, 2006.
- K. Ali, G. Mohsen, and M. Farshad. Assessment of the dynamic effect of steel frame due to sudden middle column loss. *Structural Design of Tall and Special Buildings*, 23(5):390–402, 2014.
- ASCE. Minimum design loads for buildings and other structures, 2006.
- C. G. Bailey. Membrane action of unrestrained lightly reinforced concrete slabs at large displacements. *Engineering Structures*, 23(5):470–483, 2001.

REFERENCES

- J. W. Baker, M. Schubert, and M. H. Faber. On the assessment of robustness. *Structural Safety*, 30(3):253–267, 2008.
- X. L. Bao and B. Li. Residual strength of blast damaged reinforced concrete columns. *International Journal of Impact Engineering*, 37(3):295–308, 2010.
- Y. Bao, H. S. Lew, F. Sadek, and J. Main. A Simple Means for Reducing the Risk of Progressive Collapse. *Concrete International*, 35(12):33–38, 2013.
- Z. P. Bazant and M. Verdure. Mechanics of progressive collapse: Learning from world trade center and building demolitions. *Journal of Engineering Mechanics-ASCE*, 133(3):308–319, 2007.
- Z. P. Bazant, J. L. Le, F. R. Greening, and D. B. Benson. What did and did not cause collapse of world trade center twin towers in New York? *Journal of Engineering Mechanics-ASCE*, 134(10):892–906, 2008.
- A. W. Beeby. Safety of structures, and a new approach to robustness. *The Structural Engineer*, 77(4):6, 1999.
- R. M. Bennett. Formulations for Probability of Progressive Collapse. *Structural Safety*, 5(1):67–77, 1988.
- R. D. Bertero and V. V. Bertero. Redundancy in earthquake-resistant design. *Journal of Structural Engineering-ASCE*, 125(1):81–88, 1999.
- C. E. Broms. Ductility of flat plates: Comparison of shear reinforcement systems. *ACI Structural Journal*, 104(6):703–711, 2007.
- M. N. Bussell and A. E. K. Jones. Robustness and the relevance of Ronan Point today. *The Structural Engineer*, 88(23):20–25, 2010.
- M. Byfield and S. Paramasivam. Catenary action in steel-framed buildings. *Proceedings of the Institution of Civil Engineers-Structures and Buildings*, 160(5):247–257, 2007.
- M. Byfield and S. Paramasivam. Murrah Building Collapse: Reassessment of the Transfer Girder. *Journal of Performance of Constructed Facilities*, 26(4):371–376, 2012.
- J. L. Chen, X. Huang, R. L. Ma, and M. J. He. Experimental Study on the Progressive Collapse Resistance of a Two-Story Steel Moment Frame. *Journal of Performance of Constructed Facilities*, 26(5):567–575, 2012.
- X. D. Chen, S. X. Wu, J. K. Zhou, Y. Z. Chen, and A. P. Qin. Effect of Testing Method and Strain Rate on Stress-Strain Behavior of Concrete. *Journal of Materials in Civil Engineering*, 25(11):1752–1761, 2013.

REFERENCES

- H. Choi and J. Kim. Progressive collapse-resisting capacity of RC beam-column sub-assembly. *Magazine of Concrete Research*, 63(4):297–310, 2011.
- J. W. Choi and J. H. J. Kim. Experimental Investigations on Moment Redistribution and Punching Shear of Flat Plates. *ACI Structural Journal*, 109(3):329–337, 2012.
- W. G. Corley. Lessons learned on improving resistance of buildings to terrorist attacks. *Journal of Performance of Constructed Facilities*, 18(2):68–78, 2004.
- David Cormie, Geoffrey Mays, and P. D. Smith. *Blast effects on buildings / edited by David Cormie, Geoff Mays and Peter Smith*. Thomas Telford, 2009. Includes bibliographical references and index.
- S. K. Das and C. T. Morley. Compressive membrane action in circular reinforced slabs. *International Journal of Mechanical Sciences*, 47(10):1629–1647, 2005.
- P. X. Dat and T. K. Hai. Membrane actions of RC slabs in mitigating progressive collapse of building structures. *Engineering Structures*, 55:107–115, 2013.
- Y. L. Dong and C. J. Zhu. Limit Load Carrying Capacity of Two-Way Slabs with Two Edges Clamped and Two Edges Simply Supported in Fire. *Journal of Structural Engineering-ASCE*, 137(10):1182–1192, 2011.
- Fédération Internationale du Béton. *Model code 2010 : final draft*. Bulletin / Federation Internationale du Beton ; 65-66. International Federation for Structural Concrete (fib), 2012. Prepared by fib Special Activity Group 5, New Model Code.
- A. Y. Elghazouli and B. A. Izzuddin. Failure of lightly reinforced concrete members under fire. II: Parametric studies and design considerations. *Journal of Structural Engineering-ASCE*, 130(1):18–31, 2004.
- C. Fang, B. A. Izzuddin, A. Y. Elghazouli, and D. A. Nethercot. Robustness of steel-composite building structures subject to localised fire. *Fire Safety Journal*, 46(6):348–363, 2011.
- C. Fang, B. A. Izzuddin, R. Obiala, A. Y. Elghazouli, and D. A. Nethercot. Robustness of multi-storey car parks under vehicle fire. *Journal of Constructional Steel Research*, 75:72–84, 2012.
- C. Fang, B. A. Izzuddin, A. Y. Elghazouli, and D. A. Nethercot. Simplified energy-based robustness assessment for steel-composite car parks under vehicle fire. *Engineering Structures*, 49:719–732, 2013.

REFERENCES

- S. Farazman, B. A. Izzuddin, and D. Cormie. Influence of Unreinforced Masonry In-fill Panels on the Robustness of Multistory Buildings. *Journal of Performance of Constructed Facilities*, 27(6):673–682, 2013.
- D. M. V. Faria, V. J. G. Lucio, and A. P. Ramos. Post-punching behaviour of flat slabs strengthened with a new technique using post-tensioning. *Engineering Structures*, 40: 383–397, 2012.
- Jacob Feld and Kenneth L. Carper. *Construction failure*. Wiley-Interscience publication. John Wiley, 1997. Includes bibliographical references and index.
- G. Flint, A. Usmani, S. Lamont, B. Lane, and J. Torero. Structural response of tall buildings to multiple floor fires. *Journal of Structural Engineering-ASCE*, 133(12):1719–1732, 2007.
- S. J. Foster and P. Marti. Cracked membrane model: Finite element implementation. *Journal of Structural Engineering-ASCE*, 129(9):1155–1163, 2003.
- S. J. Foster, C. G. Bailey, I. W. Burgess, and R. J. Plank. Experimental behaviour of concrete floor slabs at large displacements. *Engineering Structures*, 26(9):1231–1247, 2004.
- N. J. Gardner, J. Huh, and L. Chung. Lessons from the Sampoong department store collapse. *Cement & Concrete Composites*, 24(6):523–529, 2002.
- G. V. Gudmundsson and B. A. Izzuddin. The ‘sudden column loss’ idealisation for disproportionate collapse assessment. *The Structural Engineer*, 88(6):5, 2012.
- N. M. Hawkins and D. Mitchell. Progressive Collapse of Flat-Plate Structures. *Journal of the American Concrete Institute*, 76(7):775–808, 1979.
- J. R. Hayes, S. C. Woodson, R. G. Pekelnicky, C. D. Poland, W. G. Corley, and M. Sozen. Can strengthening for earthquake improve blast and progressive collapse resistance? *Journal of Structural Engineering-ASCE*, 131(8):1157–1177, 2005.
- M. Husain and P. Tsopelas. Measures of structural redundancy in reinforced concrete buildings. I: Redundancy indices. *Journal of Structural Engineering-ASCE*, 130(11): 1651–1658, 2004.
- Engineers Institution of Structural. *Practical guide to structural robustness and disproportionate collapse in buildings*. Institution of Structural Engineers, 2010. (Great Britain) "This guide has been prepared by an Institution of Structural Engineers’ Task Group"—Foreword. Includes bibliographical references (p. 69-70).

REFERENCES

- B. S. Iribarren, P. Berke, P. Bouillard, J. Vantomme, and T. J. Massart. Investigation of the influence of design and material parameters in the progressive collapse analysis of RC structures. *Engineering Structures*, 33(10):2805–2820, 2011.
- B. A. Izzuddin and A. Y. Elghazouli. Failure of lightly reinforced concrete members under fire. I: Analytical modeling. *Journal of Structural Engineering-ASCE*, 130(1):3–17, 2004.
- B. A. Izzuddin, A. G. Vlassis, A. Y. Elghazouli, and D. A. Nethercot. Assessment of progressive collapse in multi-storey buildings. *Proceedings of the Institution of Civil Engineers-Structures and Buildings*, 160(4):197–205, 2007.
- B. A. Izzuddin, A. G. Vlassis, A. Y. Elghazouli, and D. A. Nethercot. Progressive collapse of multi-storey buildings due to sudden column loss - Part I: Simplified assessment framework. *Engineering Structures*, 30(5):1308–1318, 2008.
- B. A. Izzuddin, M. F. Pereira, U. Kuhlmann, L. Rolle, T. Vrouwenvelder, and B. J. Leira. Application of Probabilistic Robustness Framework: Risk Assessment of Multi-Storey Buildings under Extreme Loading. *Structural Engineering International*, 22(1):79–85, 2012.
- T. Jankowiak and T. Lodygowski. Identification of parameters of concrete damage plasticity constitutive model. *Foundations of Civil and Environmental Engineering*, (6):53–69, 2005.
- R. Jayasooriya, D. P. Thambiratnam, N. J. Perera, and V. Kosse. Blast and residual capacity analysis of reinforced concrete framed buildings. *Engineering Structures*, 33(12):3483–3495, 2011.
- Q. Kai and B. Li. Dynamic performance of RC beam-column substructures under the scenario of the loss of a corner column-Experimental results. *Engineering Structures*, 42:154–167, 2012.
- M. R. Karim and M. S. H. Fatt. Impact of the Boeing 767 aircraft into the World Trade Center. *Journal of Engineering Mechanics-ASCE*, 131(10):1066–1072, 2005.
- L. Keyvani, M. Sasani, and Y. Mirzaei. Compressive membrane action in progressive collapse resistance of RC flat plates. *Engineering Structures*, 59:554–564, 2014.
- J. Kim and S. Hong. Progressive collapse performance of irregular buildings. *Structural Design of Tall and Special Buildings*, 20(6):721–734, 2011.

REFERENCES

- J. Kim and M. K. Jung. Progressive collapse resisting capacity of tilted building structures. *Structural Design of Tall and Special Buildings*, 22(18):1359–1375, 2013.
- J. Kim and Y. H. Lee. Progressive Collapse Resisting Capacity of Tube-Type Structures. *Structural Design of Tall and Special Buildings*, 19(7):761–777, 2010.
- J. Kim and J. Yu. Analysis of reinforced concrete frames subjected to column loss. *Magazine of Concrete Research*, 64(1):21–33, 2012.
- Jinkoo Kim and Jieun Kong. Progressive collapse behavior of rotor-type diagrid buildings. *Structural Design of Tall and Special Buildings*, 22(16):1199–1214, 2013.
- S. King and N. J. Delatte. Collapse of 2000 commonwealth avenue: Punching shear case study. *Journal of Performance of Constructed Facilities*, 18(1):54–61, 2004.
- S. Kokot, A. Anthoine, P. Negro, and G. Solomos. Static and dynamic analysis of a reinforced concrete flat slab frame building for progressive collapse. *Engineering Structures*, 40:205–217, 2012.
- R. Koppitz, A. Kenel, and T. Keller. Punching shear of RC flat slabs - Review of analytical models for new and strengthening of existing slabs. *Engineering Structures*, 52:123–130, 2013.
- K. J. LaMalva, J. R. Barnett, and D. O. Dusenberry. Failure Analysis of the World Trade Center 5 Building. *Journal of Fire Protection Engineering*, 19(4):261–274, 2009.
- A. Laskar, H. C. Gu, Y. L. Mo, and G. B. Song. Progressive collapse of a two-story reinforced concrete frame with embedded smart aggregates. *Smart Materials & Structures*, 18(7):–, 2009.
- Jia-Liang Le and Bing Xue. Probabilistic analysis of reinforced concrete frame structures against progressive collapse. *Engineering Structures*, 76(0):313–323, 2014.
- J. H. Lee and G. L. Fenves. Plastic-damage model for cyclic loading of concrete structures. *Journal of Engineering Mechanics-ASCE*, 124(8):892–900, 1998.
- J. Li and H. Hao. Numerical study of structural progressive collapse using substructure technique. *Engineering Structures*, 52:101–113, 2013.
- Y. C. Loo and H. Guan. Cracking and punching shear failure analysis of RC flat plates. *Journal of Structural Engineering-ASCE*, 123(10):1321–1330, 1997.
- Imetrum Ltd, September 2014. URL <http://www.imetrum.com>.

REFERENCES

- J. Lubliner, J. Oliver, S. Oller, and E. Onate. A Plastic-Damage Model for Concrete. *International Journal of Solids and Structures*, 25(3):299–326, 1989.
- Koichi Maekawa, A. Pimanmas, and Hajime Okamura. *Nonlinear mechanics of reinforced concrete / K. Maekawa, A. Pimanmas, and H. Okamura*. Spon Press, 2003. Includes bibliographical references and index.
- L. J. Malvar and C. A. Ross. Review of strain rate effects for concrete in tension. *ACI Materials Journal*, 95(6):735–739, 1998.
- N. F. S. Mamede, A. P. Ramos, and D. M. V. Faria. Experimental and parametric 3D nonlinear finite element analysis on punching of flat slabs with orthogonal reinforcement. *Engineering Structures*, 48:442–457, 2013.
- S. Marjanishvili and E. Agnew. Comparison of various procedures for progressive collapse analysis. *Journal of Performance of Constructed Facilities*, 20(4):365–374, 2006.
- S. M. Marjanishvili. Progressive analysis procedure for progressive collapse. *Journal of Performance of Constructed Facilities*, 18(2):79–85, 2004.
- H. Marzouk, M. Hossin, and A. Hussein. Crack Width Estimation for Concrete Plates. *ACI Structural Journal*, 107(3):282–290, 2010.
- Aldo McKay, Kirk Marchand, and Manuel Diaz. Alternate path method in progressive collapse analysis: Variation of dynamic and nonlinear load increase factors. *Practice Periodical on Structural Design and Construction*, 17(4):152–160, 2012.
- K. Menchell, T. J. Massart, Y. Rammer, and P. Bouillard. Comparison and Study of Different Progressive Collapse Simulation Techniques for RC Structures. *Journal of Structural Engineering-ASCE*, 135(6):685–697, 2009.
- Y. Mirzaei and M. Sasani. Progressive collapse resistance of flat slabs: modeling post-punching behavior. *Computers and Concrete*, 12(3):351–375, 2013.
- D. Mitchell and W. D. Cook. Preventing Progressive Collapse of Slab Structures. *Journal of Structural Engineering-ASCE*, 110(7):1513–1532, 1984.
- A. Miyamoto, M. W. King, and M. Fujii. Nonlinear Dynamic Analysis of Reinforced-Concrete Slabs under Impulsive Loads. *ACI Structural Journal*, 88(4):411–419, 1991.
- O. A. Mohamed. Progressive collapse of structures: Annotated bibliography and comparison of codes and standards. *Journal of Performance of Constructed Facilities*, 20(4):418–425, 2006.

REFERENCES

- A. Muttoni. Punching shear strength of reinforced concrete slabs without transverse reinforcement. *ACI Structural Journal*, 105(4):440–450, 2008.
- A. Naji and F. Irani. Progressive collapse analysis of steel frames: Simplified procedure and explicit expression for dynamic increase factor. *International Journal of Steel Structures*, 12(4):537–549, 2012.
- D. E. Newland and D. Cebon. Could the World Trade Center have been modified to prevent its collapse? *Journal of Engineering Mechanics-ASCE*, 128(7):795–800, 2002.
- US Department of Defense (DoD). United facilities criteria - design of buildings to resist progressive collapse: UFC 4-023-03, 2009.
- Office of the Deputy Prime Minister. The Building Regulations 2000 - structure: approved document A (2004 edition), 2006.
- H. Okamura and K. Maekawa. Nonlinear-Analysis and Constitutive Models of Reinforced-Concrete. *Computer Aided Analysis and Design of Concrete Structures, Vols 1 and 2*, pages 831–850, 1990.
- J. D. Osteraas. Murrah building bombing revisited: A qualitative assessment of blast damage and collapse patterns. *Journal of Performance of Constructed Facilities*, 20(4): 330–335, 2006.
- P. C. Pandey and S. V. Barai. Structural sensitivity as a measure of redundancy. *Journal of Structural Engineering-ASCE*, 123(3):360–364, 1997.
- T. W. Park. Inspection of collapse cause of Sampoong Department Store. *Forensic Science International*, 217(1-3):119–126, 2012.
- Paresh V. Patel and Digesh D. Joshi. Various approaches for mitigating progressive collapse of asymmetrical RC building. In *Structures Congress 2012, March 29, 2012 - March 31, 2012*, Structures Congress 2012 - Proceedings of the 2012 Structures Congress, pages 2084–2094. American Society of Civil Engineers (ASCE), 2012.
- C. Pearson and N. Delatte. Ronan point apartment tower collapse and its effect on building codes. *Journal of Performance of Constructed Facilities*, 19(2):172–177, 2005.
- K. Phuvoravan and E. D. Sotelino. Nonlinear finite element for reinforced concrete slabs. *Journal of Structural Engineering-ASCE*, 131(4):643–649, 2005.
- M. A. Polak. Ductility of reinforced concrete flat slab-column connections. *Computer-Aided Civil and Infrastructure Engineering*, 20(3):184–193, 2005.

REFERENCES

- A. J. Pretlove, M. Ramsden, and A. G. Atkins. Dynamic Effects in Progressive Failure of Structures. *International Journal of Impact Engineering*, 11(4):539–546, 1991.
- S. Pujol and J. P. Smith-Pardo. A new perspective on the effects of abrupt column removal. *Engineering Structures*, 31(4):869–874, 2009.
- K. Qian and B. Li. Slab Effects on Response of Reinforced Concrete Substructures after Loss of Corner Column. *ACI Structural Journal*, 109(6):845–855, 2012.
- K. Qian and B. Li. Experimental Study of Drop-Panel Effects on Response of Reinforced Concrete Flat Slabs after Loss of Corner Column. *ACI Structural Journal*, 110(2):319–329, 2013.
- E. Ramabhushanam and L. Marjorie. Structural Assessment of Bomb Damage for World Trade Center. *Journal of Performance of Constructed Facilities*, 8(4):229–242, 1994.
- J.N. Reddy. *Mechanics of laminated composite plates and shells: theory and analysis*. CRC Press, 2004.
- M. F. Ruiz, Y. Mirzaei, and A. Muttoni. Post-Punching Behavior of Flat Slabs. *ACI Structural Journal*, 110(5):801–811, 2013.
- P. Ruth, K. A. Marchand, and E. B. Williamson. Static equivalency in progressive collapse alternate path analysis: Reducing conservatism while retaining structural integrity. *Journal of Performance of Constructed Facilities*, 20(4):349–364, 2006.
- H. Saito, A. Imamura, M. Takeuchi, S. Okamoto, Y. Kasai, H. Tsubota, and M. Yoshimura. Loading Capacities and Failure Modes of Various Reinforced-Concrete Slabs Subjected to High-Speed Loading. *Nuclear Engineering and Design*, 156(1-2):277–286, 1995.
- M. Sasani. Response of a reinforced concrete infilled-frame structure to removal of two adjacent columns. *Engineering Structures*, 30(9):2478–2491, 2008.
- M. Sasani and J. Kropelnicki. Progressive Collapse Analysis of an Rc Structure. *Structural Design of Tall and Special Buildings*, 17(4):757–771, 2008.
- M. Sasani and S. Sagioglu. Progressive collapse resistance of Hotel San Diego. *Journal of Structural Engineering-ASCE*, 134(3):478–488, 2008.
- M. Sasani and S. Sagioglu. Gravity Load Redistribution and Progressive Collapse Resistance of 20-Story Reinforced Concrete Structure following Loss of Interior Column. *ACI Structural Journal*, 107(6):636–644, 2010.

REFERENCES

- M. Sasani, M. Bazan, and S. Sagioglu. Experimental and analytical progressive collapse evaluation of actual reinforced concrete structure. *ACI Structural Journal*, 104(6):731–739, 2007.
- M. Sasani, A. Kazemi, S. Sagioglu, and S. Forest. Progressive Collapse Resistance of an Actual 11-Story Structure Subjected to Severe Initial Damage. *Journal of Structural Engineering-ASCE*, 137(9):893–902, 2011.
- J. Schellhammer, N. J. Delatte, and P. A. Bosela. Another Look at the Collapse of Skyline Plaza at Bailey’s Crossroads, Virginia. *Journal of Performance of Constructed Facilities*, 27(3):354–361, 2013.
- H. Sharma, S. Hurlebaus, and P. Gardoni. Performance-based response evaluation of reinforced concrete columns subject to vehicle impact. *International Journal of Impact Engineering*, 43:52–62, 2012.
- Simulia. ABAQUS Inc. User Manuel, version 6.10, 2010.
- P. P. Smith, M. P. Byfield, and D. J. Goode. Building Robustness Research during World War II. *Journal of Performance of Constructed Facilities*, 24(6):529–535, 2010.
- Uwe Starossek. *Progressive collapse of structures*. Thomas Telford, 2009. Includes bibliographical references and index.
- Y. P. Su, Y. Tian, and X. S. Song. Progressive Collapse Resistance of Axially-Restrained Frame Beams. *ACI Structural Journal*, 106(5):600–607, 2009.
- N. Trivedi and R. K. Singh. Prediction of impact induced failure modes in reinforced concrete slabs through nonlinear transient dynamic finite element simulation. *Annals of Nuclear Energy*, 56:109–121, 2013.
- M. H. Tsai and T. C. Huang. Progressive collapse analysis of an RC building with exterior partially infilled walls. *Structural Design of Tall and Special Buildings*, 22(4): 327–348, 2013.
- M. H. Tsai and B. H. Lin. Dynamic Amplification Factor for Progressive Collapse Resistance Analysis of an RC Building. *Structural Design of Tall and Special Buildings*, 18(5):539–557, 2009.
- US General Services Administration (GSA). Alternate path analysis & design guidelines for progressive collapse resistance, 2013.
- A. S. Usmani, Y. C. Chung, and J. L. Torero. How did the WTC towers collapse: a new theory. *Fire Safety Journal*, 38(6):501–533, 2003.

REFERENCES

- H. R. Valipour and S. J. Foster. Finite element modelling of reinforced concrete framed structures including catenary action. *Computers & Structures*, 88(9-10):529–538, 2010.
- A. G. Vlassis, B. A. Izzuddin, A. Y. Elghazouli, and D. A. Nethercot. Progressive collapse of multi-storey buildings due to sudden column loss - Part II: Application. *Engineering Structures*, 30(5):1424–1438, 2008.
- A. G. Vlassis, B. A. Izzuddin, A. Y. Elghazouli, and D. A. Nethercot. Progressive collapse of multi-storey buildings due to failed floor impact. *Engineering Structures*, 31(7):1522–1534, 2009.
- R. L. Vollum, M. A. Eder, A. Y. Elghazouli, and T. Abdel-Fattah. Modelling and experimental assessment of punching shear in flat slabs with shearheads. *Engineering Structures*, 32(12):3911–3924, 2010.
- W. Y. Wang and S. Teng. Modeling cracking in shell-type reinforced concrete structures. *Journal of Engineering Mechanics-ASCE*, 133(6):677–687, 2007.
- W. Y. Wang and S. Teng. Finite-Element Analysis of Reinforced Concrete Flat Plate Structures by Layered Shell Element. *Journal of Structural Engineering-ASCE*, 134(12):1862–1872, 2008.
- Robin Whittle. *Failures in concrete structures : case studies in reinforced and prestressed concrete / Robin Whittle*. CRC Press, 2013. Includes bibliographical references and index.
- J. G. M. Wood. Pipers Row car park collapse: Identifying risk. *Concrete (London)*, 37(9):3, 2003.
- S. X. Wu, X. D. Chen, and J. K. Zhou. Tensile strength of concrete under static and intermediate strain rates: Correlated results from different testing methods. *Nuclear Engineering and Design*, 250:173–183, 2012.
- O. Yagob, K. Galal, and N. Naumoski. Progressive collapse of reinforced concrete structures. *Structural Engineering and Mechanics*, 32(6):771–786, 2009.
- B. Yang and K. H. Tan. Experimental tests of different types of bolted steel beam-column joints under a central-column-removal scenario. *Engineering Structures*, 54:112–130, 2013.
- S. L. Yap and B. Li. Experimental Investigation of Reinforced Concrete Exterior Beam-Column Subassemblages for Progressive Collapse. *ACI Structural Journal*, 108(5):542–552, 2011.

REFERENCES

- W. Yi, F. Zhang, and S Kunnath. Progressive Collapse Performance of RC Flat Plate Frame Structures. *Journal of Structural Engineering*, 140, 2014.
- W. J. Yi, Q. F. He, Y. Xiao, and S. K. Kunnath. Experimental study on progressive collapse-resistant behavior of reinforced concrete frame structures. *ACI Structural Journal*, 105(4):433–439, 2008.
- J. Yu, T. Rinder, A. Stolz, K. Tan, and W. Riedel. Dynamic Progressive Collapse of an RC Assemblage Induced by Contact Detonation. *Journal of Structural Engineering*, 140(6): 04014014, 2014.
- Y. X. Zhang, M. A. Bradford, and R. I. Gilbert. A layered shear-flexural plate/shell element using Timoshenko beam functions for nonlinear analysis of reinforced concrete plates. *Finite Elements in Analysis and Design*, 43(11-12):888–900, 2007a.
- Y. X. Zhang, M. A. Bradford, and R. I. Gilbert. A layered cylindrical quadrilateral shell element for nonlinear analysis of RC plate structures. *Advances in Engineering Software*, 38(7):488–500, 2007b.
- Y Zheng, D Robinson, S Taylor, D Cleland, and A Shaat. Analysis of compressive membrane action in concrete slabs. *Bridge Engineering*, 161(BE1):21–31, 2008.
- M. Zineddin and T. Krauthammer. Dynamic response and behavior of reinforced concrete slabs under impact loading. *International Journal of Impact Engineering*, 34(9): 1517–1534, 2007.

Experiment Design Calculations

This appendix chapter provides the calculations used to design the Reinforced Concrete (RC) slabs used during the experimental programme in Chapter 3. The approach is based on EN 1991-1 (2002) and EN 1992 (2004). Finally, a comparison between the fully sized prototype design and the scaled model is presented.

A.1 Model slab details

Total Dimensions: 4.1 metres by 2.1 metres by 80mm deep

Imposed dead load: $5.0kN/m^2$

Imposed live load: $2.5kN/m^2$

Total imposed load: $5.0 + 2.5 = 7.5kN/m^2$

Self weight: $0.08 \times 25 = 2kN/m^2$

Applying Ultimate Limit State (ULS) load factors from EN 1990 (2002) Eq. 6.10a and 6.10b:

$$1.25 \times (5 + 2) + 1.5 \times 2.5 = 12.5kN/m^2$$

A.2 Moment calculations

Treating slab as an equivalent beam, effective width 1 meter for the long direction with 3 simple supports and Uniformly Distributed Load (UDL) of 12.5kN/m gives a bend-

ing moment diagram shown in Fig A.1.

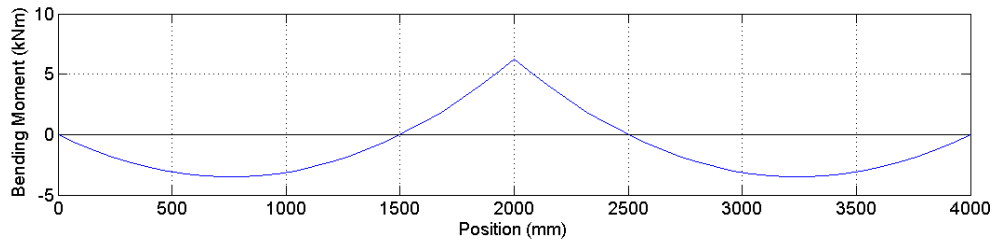


Figure A.1: Equivalent Bending Moment Diagram for Long direction under ULS loading

Therefore Max Hogging moment = 6.24 kNm

Using equivalent beam theory, 75% of moment is in column strip:

Design Hogging Moment = $0.75 \times 6.24 / 1 \text{ metre} = 4.68 \text{ kNm/m}$

and Max Sagging moment = 3.51 kNm

for sagging, 55% of moment considered in column strip

Sagging Moment = $0.55 \times 3.51 / 1 \text{ metre} = 1.93 \text{ kNm/m}$

Similarly, the short direction has effective width 2m along its midline and 2 simple supports with UDL of 25 kN/m . This gives the bending moment diagram shown in A.2.

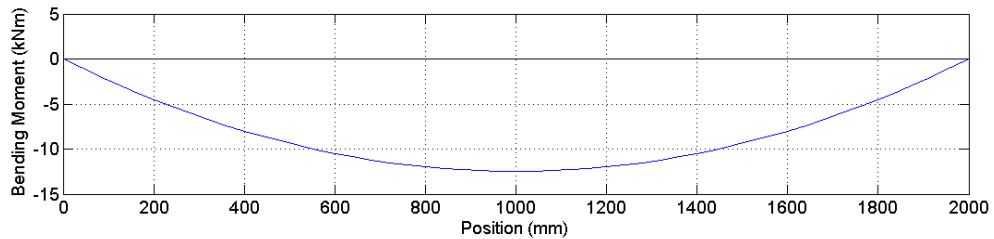


Figure A.2: Equivalent Bending Moment Diagram for Short direction under ULS loading

So Max Sagging Moment = 12.5 kNm

with 55% of moment in column strip:

Design Sagging Moment = $0.55 \times 12.5 / 2 \text{ metres} = 3.43 \text{ kNm/m}$

A.3 Reinforcement calculations

Characteristic Concrete Cube Strength: $f_{ck,cube} = 30N/mm^2$

Characteristic Concrete Cylinder Strength: $f_{ck} = 25N/mm^2$

Mean Axial Tensile Strength: $f_{ctm} = 2.6N/mm^2$

Characteristic Steel Strength: $f_{yk} = 500N/mm^2$

Design Steel Strength: $f_{yd} = \frac{f_{yk}}{1.15} = 435N/mm^2$

Area of required reinforcement:

$$A_{s,req} = \frac{M_d}{f_{yd}z} \quad (A.3.1)$$

where M_d is the design moment and z is the lever arm given by Equation A.3.2

$$z = \frac{d}{2}(1 + \sqrt{1 - 3.53K}) \quad (A.3.2)$$

and Equation A.3.3 gives K

$$K = \frac{M_d}{bd^2f_{ck}} \quad (A.3.3)$$

b and d are the width and effective depth of the section respectively

Therefore for top steel $A_{s,req} = 158.24mm^2/m$

and bottom steel $A_{s,req} = 115.3mm^2/m$

Additionally, minimum reinforcement is controlled by Equation A.3.4

$$A_{s,min} = \frac{0.26f_{ctm}bd}{f_{yk}} \quad (A.3.4)$$

so $A_{s,min} = 0.26 \times 2.6 \times 1000 \times 70/500 = 94.64mm^2/m$

Therefore provide H6@200 steel mesh top and bottom both ways ($A_{s,prov} = 142.37mm^2/m$) except over central columns where provide H6@150 ($A_{s,prov} = 188.5mm^2/m$)

A.4 Shear checks

Shear stress, v_{Ed} , around a column is given by Equation A.4.1.

$$v_{Ed} = \beta \frac{V_{Ed}}{u_i d} \quad (\text{A.4.1})$$

Where V_{Ed} is the design shear force and u_i is the control perimeter being considered. β is a factor to account for eccentricity in the loading.

For an example, the corner case is presented.

Corner Column Shear force: $V_{ed} = 7287N$

Basic control perimeter at $2d$ from column face: $u_1 = 490mm$

Reduced basic control perimeter: $u_1^* = 355mm$

$$\beta = u_1 / u_1^* = 1.38$$

Therefore, the design shear stress at the basic control perimeter is:

$$v_{Ed} = 1.38 \times 7287N / (490mm \times 70mm) = 0.28N/mm^2$$

The shear resistance of the concrete, without shear reinforcement, $v_{Rd,c}$, is given by Equation A.4.2.

$$v_{Rd,c} = C_{Rd,c} k (100 \rho_l f_{ck})^{(1/3)} \quad (\text{A.4.2})$$

Where $C_{Rd,c}$ is taken as 0.12 in the UK, k is a factor related to the depth, taken as 2.0 for this case and ρ_l is the tensile flexural reinforcement ratio. Therefore $v_{Rd,c} = 0.39N/mm^2$.

However, $v_{Rd,c}$ should be greater than v_{min} , given by A.4.3.

$$v_{min} = 0.035 k^{(3/2)} \sqrt{f_{ck}} \quad (\text{A.4.3})$$

Therefore $v_{Rd,c} = 0.495N/mm^2$ which is greater than v_{Ed} .

Therefore no shear reinforcement is required.

A.5 Scaling comparison

Figure A.3 shows the different values and ratios from a full sized prototype design to the scaled model used for the experimental testing. The scaling ratios are also presented to allow a comparison into which factors are influenced by scaling the geometry. As the aim of the scaled model is to represent the same demand to capacity response as a full structure, the M_d/M_y and deflection over span ratios are of primary interest. Both these ratios are close to 1, indicating a suitable comparison. Additionally, it can be seen that changing the geometry by a factor of 3 requires increasing the applied load, to account for the change in selfweight.

APPENDIX A: EXPERIMENT DESIGN CALCULATIONS

				Scale				Scale	
<u>Geometry</u>		Prototype	Model	Factor	<u>Loading (kN/m²,kN)</u>		Prototype	Model	Factor
Span (mm)		6000	2000	3	Slab SW		6	2	3
Depth (mm)		240	80	3	Applied DL		1	5	0.2
Cover to centroid (mm)		45	15	3	Applied LL		2.5	2.5	1
Total Length (mm)		12000	4000	3					
Total Width (mm)		6000	2000	3	Charterstic UDL		9.5	9.5	1
Span/Eff depth (mm)		30.8	30.8	1	ULS UDL		12.5	12.5	1
<u>Mass</u>									
Mass/area (kg/m ²)		969	969	1	Total Charteristic Load		684	76	9
ULS Mass/area (kg/m ²)		1276	1276	1	Total ULS Load		900	100	9
Total Mass (Tonne)		69.80	7.76	9					
Total ULS Mass (Tonne)		91.84	10.20	9					
					<u>Reinforcement (mm²/m)</u>		Scale		
<u>Bending Moments (kNm/m)</u>							Prototype	Model	Factor
ULS Max Hogging		42.09	4.68	9	As,Req		513.76	171.25	3.00
					As,Prov		523.60	188.00	
					H10@150		H6@150		
ULS Max Sagging Long Side		17.38	1.93	9	As,Req		207.83	69.28	3.00
					As,Prov		392.70	141.37	
					H10@200		H6@200		
ULS Max Sagging Short Side		30.92	3.44	9	As,Req		373.81	124.60	3.00
					As,Prov		392.70	141.37	
					H10@200		H6@200		
As,min (mm ² /m)		294.06	98.02	3					
ρ,min		0.0012	0.0012	1	<u>ULS</u>				
ρ,Prov,Hog		0.0022	0.0024	1	Md/My Hog		0.998	0.927	1.08
					Sag		0.978	0.905	1.08
My,Hog (kNm/m)		42.1725	5.0474	8.36					
My,Sag/Min (kNm/m)		31.6293	3.7955	8.33					
<u>Deflections (mm)</u>									
<u>SLS</u> Full		6.98	2.33	3	deflection / span		0.0012	0.0012	1.00
Column Loss		38.99	13.00	3			0.0065	0.0065	1.00
<u>Periods (sec)</u>									
		<u>1st Mode</u>			<u>2nd Mode</u>				
<u>SLS</u>	Full	0.1520	0.0861	1.77	0.1476	0.0836	1.77		
	Column Loss	0.3089	0.1749	1.77	0.1476	0.0836	1.77		

Figure A.3: Summary and comparison of slab prototype and model design